TO MY WIFE

RATE-DEPENDENT MECHANICS OF SUPERPLASTIC PROCESSES

RATE-DEPENDENT MECHANICS OF SUPERPLASTIC PROCESSES

By

ABDEL-RAHMAN ABDEL-FATTAH RAGAB, M.Sc.

A Thesis

Submitted to the School of Graduate Studies
in Partial Fulfillment of the Requirements
for the Degree
Doctor of Philosophy

McMaster University
June, 1973

DOCTOR OF PHILOSOPHY (1973)
(Mechanical Engineering)

MCMASTER UNIVERSITY
Hamilton, Ontario.

TITLE: Rate-Dependent Mechanics of Superplastic Processes

AUTHOR: Abdel-Rahman A.F. Ragab, B.Sc. (Cairo University)
M.Sc. (Université de Sherbrooke)

SUPERVISOR: Dr. J.L. Duncan

NUMBER OF PAGES: XXV, 246

ABSTRACT

Superplasticity is a hot-working phenomenon exhibited by many metallic alloys and observed above a temperature of about 40% of the absolute melting point. It is characterized by an ultra-fine grain microstructure, an unusually high rate dependence and very low resistance to deformation at low strain rates.

The plasticity theories and constitutive equations used in the analysis of secondary creep in structures are shown to be formally applicable to the study of superplastic deformation. A non-linear viscous model, with certain limitations, is employed to analyze superplastic deformation problems.

This thesis presents three separate and independent pieces of work. These problems namely; (a) analysis of post-necking geometry in tensile-forming processes, (b) creep testing of superplastic material in sheet form and (c) reverse-extrusion of rate-dependent materials, represent in the author's opinion three most important problems relating to the use of superplastic alloys in industry.

In tensile forming processes of superplastic alloys the deformation is unstable and it is shown that geometric non-uniformities develop continuously. The features of such deformation system are illustrated by the numerical analysis of initially non-uniform tensile bars and thin-walled tubes expanded by internal pressure. Experimental results obtained from testing zinc-aluminum alloy are compared with the numerical

results and satisfactory correlation is observed.

A technique is presented for obtaining creep data for superplastic sheets using a test in which a strip or indeed the whole sheet is arranged as a cantilever loaded by its own weight. Theory is given for deriving stationary creep parameters from measured deflection rates and for determining a stress, strain-rate curve using the skeletal point method. Tensile and bending creep tests were performed on superplastic zinc-aluminum sheets at room temperature and the creep data from both types of tests are compared.

In bulk forming of rate-dependent materials the load requirements are highly dependent on the forming speed. In the present work the traditional analytical method of slip-line field analysis has been extended to accommodate the extrusion of rate-sensitive materials such as superplastic alloys. The volume of the deformation zone and the effective mean strain-rate identified by the slip-line field solutions were incorporated to define a geometric factor which permits the extrusion pressure to be determined for a non-linear viscous material. Experimental results on reverse-extrusion of both as-cast and superplastic zinc-aluminum agree well with theoretical analysis.

SOMMAIRE

La superplasticité est un phénomène qui se manifeste lors due façonnage à chaud de nombreau alliages métalliques à une température à peu près égale à la moitié de la température de fusion exprimée en degrés absolus. L'état superplastique est caractérisé par une microstruture très fine et une très grande sensibilité de la contrainte à la vitesse de déformation.

Les théories sur la plasticité et les équations de comportement utilisées pour analyser le fluage secondaire sont applicables à l'étude de la déformation des matériaux superplastiques.

Cette thèse présente trois problèmes indépendants:

a) l'analyse de la géométrie d'échantillons superplastiques lors des procédés de formage en traction au-delà de la limite d'écoulement plastique uniforme;

b) des essais de fluage de matériaux superplasticques en forme de plaquettes;

c) des essais de refoulage de matériaux caractérisés par une grande sensibilité à la vitesse de déformation. Ces problèmes sont du point de vue de l'auteur, les plus importants pour les utilisations industrielles des matériaux superplastiques.

Au cours des procédés de formage lorsque les contraintes sont essentiellement en traction, l'écoulement superplastique est toujours instable et l'irrégularité des sections croît continuellement. Les caractéristiques

de ce régime de déformation sont illustrées par l'analyse numérique de deux exemples. Le premier est la déformation d'une éprouvette de traction ayant une irrégularité initiale de section. Le second est l'expansion d'un tube à paroi mince, initialement non-uniforme, au moyen de l'application d'une pression intérieure. Les résultats expérimentaux obtenus relatifs à l'allongement des éprouvettes d'une alliage superplastique Zn-Al confirment d'une manière satisfaisante les prévisions théoriques.

Une technique permettant d'obtenir des informations sur le comportement en fluage des matériaux superplastiques en forme de plaque est décrite. Cette technique consiste en la déformation d'une plaque encastrée à un bout soumise à son propre poids. Une théorie est élaborée permettant de déterminer les paramètres de comportement en fluage secondaire. Grâce à la méthode analytique de "skeletal point", il est de plus possible de déduire des essais de flexion, la courbe de contrainte par rapport à la vitesse de fluage. Des essais de fluage en flexion et en traction ont été réalisés sur un alliage superplastique de Zn-Al à la température ambiante. Les résultats expérimentaux démontrent qu'un essai de fluage en flexion peut être considéré comme un essai de contrôle de qualité pour les matériaux superplastiques.

Lors du refoulage des matériaux superplastiques, on constate que la charge est fonction de la vitesse de mise en forme. Au cours de notre travail, les méthodes analytiques traditionnelles tel que le "slip-line field" ont été adoptées et étendues pour permettre d'analyser la déformation des matériaux superplastiques. Le volume de la zone de déformation et la moyenne effective de la vitesse de déformation, défines par la théorie du "slip-line field" ont été utilisés pour identifier un nouveau paramètre géométrique. Ce paramètre permet de calculer la pression d'extrusion d'un matériau à comportement visqueux non-Newtonien. Les résultats expérimentaux obtenus lors d'essais d'extrusion à rebours confirment les analyses théoriques proposées.

ACKNOWLEDGEMENTS

The author wishes to express his appreciation to his supervisor Dr. John L. Duncan whose continuous guidance and encouragement made this thesis possible.

The author is indebted to Dr. M.A. Dokainish, Dr. G.AE. Oravas, Dr. G.F. Round and Dr. R. Sowerby for their valuable assistance.

Thanks are also due to Mrs. S. Thompson for her expert typing of the manuscript.

The scholarship awarded by McMaster University, Mechanical Engineering Department is gratefully acknowledged.

The author also extends his gratitude to Mechanical Engineering Department, Cairo University, Egypt for awarding a study-leave to pursue graduate studies in Canada.

TABLE OF CONTENTS

LIST OF SYMBOLS

A, A_o	Current and original cross-sectional area of a tensile test-piece.
δA, δA_o	Current and original nonuniformity of area in a tensile test-piece, $A_{max} - A_{min}$.
A_2, A_1	Maximum and minimum cross-sectional area of extrusion punch.
b, b_o	Current and initial extrusion billet height.
b_c	Width of cantilever cross-section.
D, D_o	Current and original diameter of a tensile bar.
δD, δD_o	Current and original nonuniformity of diameter in a tensile bar, $D_{max} - D_{min}$.
E	Elongation percentage.
F	Extrusion load.
h, h_o	Current and original thickness of a thin-walled tube.
h_c	Depth of cantilever cross-section.
H	Parameter of nonuniformity of the thickness of a thin-walled tube, $(h_{max} - h_{min}) / h_{av}$.
J_1, J_2, J_3	Invariants of the stress deviation tensor.
k	Shear yield stress of rigid, perfectly plastic material.
ℓ, ℓ_o	Current and original length of a tensile test-piece.
ℓ_c	Length of cantilever.
L	Grain size.
m	Strain-rate sensitivity index.
M	Bending moment.

n	Strain-hardening index.
N	Stress resultant in a shell.
p	Pressure.
P	Tensile load.
$\bar{P}$	Average extrusion pressure.
q	Distributed load intensity.
r	Extrusion ratio.
$r_m, r_{m,o}$	Current and original radius of a thin-walled tube.
R_e	Diametral expansion of a thin-walled tube.
R_n	Coefficient of normal anisotropy.
s, s_o	Current and original thickness of a tensile test-strip.
S_{ij}	Stress deviation tensor.
t	Time.
t_R	Rupture time.
Δt	Time increment.
T	Temperature.
(x,y,z)	System of cartesian co-ordinates.
(x_s, y_s)	Skeletal point co-ordinates
v	Cantilever beam deflection in y-direction.
v_o	Cross-head speed in a tensile test.
v_e	Extrusion velocity.
V	Volume.
$\dot{V}$	Volume rate.
Y	Yield stress.

w, w_o	Current and original width of a tensile test strip.
Δw	Nonuniformity parameter of the width of tensile test-strip, $(w_{max} - w_{min}) / w_{av}$.
w_c	Reverse-extruded cup wall thickness.
$\dot{W}$	Rate of dissipation of energy.
σ	Stress.
σ_e	Representative stress.
σ_o, σ_o'	Material stress parameters.
ε	Strain.
ε_e	Equivalent strain.
$\dot{\varepsilon}$	Strain-rate.
$\dot{\varepsilon}_e$	Representative strain-rate.
$\dot{\varepsilon}_o$	Strain-rate constant in creep power law.
λ	Creep exponent.
α	Extrusion punch profile angle.
θ	Angular displacement.
δ	Cantilever beam free-end deflection.
$\dot{\delta}$	Cantilever beam free-end deflection rate.
Δ	Extension of tensile test-piece in creep.
$\dot{\Delta}$	Tensile test-piece extension rate in creep.
ν	Poisson's ratio.

LIST OF FIGURES

PAGE

PAGE

PAGE

PAGE

PAGE

CHAPTER I

THE PHENOMENON OF SUPERPLASTICITY

1.1 The Superplastic Behaviour

Superplasticity is the name given to the behaviour of some metals and alloys which exhibit very low resistance to flow and extremely high ductility when deformed at certain conditions of temperature and strain-rate. Superplastic deformation is characterized by an unusually high-rate dependence approaching that of viscous materials such as molten glass and heated thermoplastics. Superplasticity is most dramatically displayed in a tensile test where the material undergoes very large elongations, sometimes close to 2000% with a surprisingly low flow stress.

1.2 Historical Background

In 1920, an unusual behaviour in the cold rolled Zn-Cu-Al tertiary eutectoid alloy was noticed by Rosenhain [1.1] who observed that this alloy "behaved differently from ordinary crystalline materials such as aluminum but very similarily to ...pitch, glass, etc". Subsequently in 1934, Pearson published a paper [1.2] showing a photograph of a tensile specimen of a lead-based alloy which had been elongated by some 1900%. In his work, Pearson related these enormous elongations to the strain-rate sensitivity, commented on the maintenance of the fine grain structure of these alloys and proposed a deformation mechanism. However, at that time, this phenomenon seems to have been regarded as a laboratory curiosity and was largely forgotten.

Later, the term superplasticity came into general use from 1945 onwards originating in the work of Bochvar et al [1.3] as a description of the exceptionally ductile behaviour of various non-ferrous eutectic and eutectoid alloys. Further work appeared in the Russian literature between 1945 and 1960 [1.4] and [1.5]. Bochvar and Sviderskaia introduced the eutectoid Zn-Al alloy to the superplastic group and this has become the most widely used and studied of all the alloys.

A review by Underwood in 1962 [1.6] revived the interest of Western workers and by 1965 a series of papers by Backofen and his co-workers [1.7] to [1.9] led to the formulation of basic rules for superplastic behaviour.

During the last decade the number of published articles on the subject increased rapidly but, in the main, these have been concerned with evolving a theoretical explanation for the mechanism of superplastic deformation. Very recently, however, published articles have started to discuss the technological implications of superplasticity but these only represent a small fraction of the published literature on superplasticity.

1.3 Types of Superplasticity

Superplastic behaviour can broadly be divided into two types:

i) Environmental Superplasticity [1.10] and [1.11]

Environmental superplasticity occurs in certain alloys which are thermally cycled about a phase transformation temperature; these materials appear to become "spontaneously plastic" due to intergranular stresses. Also, the very large elongations obtained under the action of small stresses in the presence of cyclic temperature changes for thermally anisotropic alloys or some metals subjected to neutron irradiation, is often termed environmental superplasticity. It should be noted that large tensile elongations are not, by themselves, indications of superplasticity. If necking is suppressed artificially in a tensile test, elongations of several hundred percent can be obtained in many alloys even in mild steel at room temperature [1.12].

ii) Isothermal Superplasticity

This type of superplastic behaviour, known sometimes as "micrograin superplasticity", is associated with alloys in which a particular ultra-fine grain structure (< 10 microns) can be induced and retained in a stable form at temperatures about half the absolute melting point.

Most investigations of superplastic behaviour have been concerned with alloys that show isothermal superplasticity. The reason is obviously that if superplasticity is to be applied to commercial forming of metals, it would seem more feasible to have the equipment operating at a single temperature than to cycle it repeatedly over a range of temperatures. In this present work only isothermal superplastic deformation is studied and the other phenomenon of environmental superplasticity is excluded.

1.4 Requirements for Isothermal Superplasticity

Whilst the theoretical explanations for isothermal superplasticity remain controversial, certain generalized rules appear to be necessary for a metal to exhibit this phenomenon. These rules are discussed below.

i) Ultra-fine equiaxed grain structure

Superplastic alloys all have an ultra-fine grain structure; the grain diameter is always less than 10 microns (10^{-6} m) and generally less than 2 microns. It may be seen from Table 1-1 [1.13] that superplastic grain sizes are at least an order of magnitude smaller than those in conventional "fine-grain" materials. Another unusual aspect of the microstructure in superplastic alloys is the morphology. In normal alloys, individual grains are elongated in the direction of extension or, if the temperature is high enough, grain growth occurs. In superplastic alloys, the grains usually do not elongate even though the material may be extended many hundred percent; during deformation the grains very often become more equiaxed and develop a rounded appearance.

For superplastic alloys, at constant strain-rate and temperature, the stress σ follows the relation

$$\sigma \propto L^{b} \tag{1-1}$$

where L is the grain size. The exponent b in equation (1-1) has been reported in the literature as lying between 0.7 to 1.2 [1.14]. This relation, equation (1-1), is quite different from that governing the deformation of conventional metals in cold working. They follow the Hall-Petch relation

$$\sigma \propto \frac{1}{\sqrt{L}} \tag{1-2}$$

which implies that plastic strength is increased as grain size becomes smaller [1.15].

TABLE 1:1 GRAIN SIZE CLASSIFICATION

ASTM NO.	GRAIN SIZE MICRON	RANGE FOR COMMERCIAL STEELS
1	254	
2	180	
3	127	COARSE
4	90	
5	64	MEDIUM
6	45	
7	32	FINE
8	22.5	
9	16	
10	11	
11	7.9	
12	5.6	
13	4	
14	2.8	SUPERPLASTIC ALLOYS

(ii) Temperature above 0.4 Tm

Superplastic deformation occurs at temperatures above about 0.4 of the absolute melting point. The flow stress would normally decrease with increasing temperature unless some phase transformation occurs to inhibit superplasticity. The superplastic zinc-aluminum eutectoid alloy for instance, shows a marked decrease in flow stress as temperature rises till about 250°C after which it starts increasing as shown in Figure 1.1 [1.16].

iii) Appropriate strain-rate

A typical stress, strain-rate characteristic of a superplastic alloy is shown in Figure 1.2. It is seen that the strain-rate sensitivity, m (the slope of the logarithmic stress, strain-rate curve) is highest in the strain-rate range of 10^{-6} to 10^{-2} per sec. Full benefits of superplastic behaviour such as high necking resistance, are obtained at these strain rates. Table 1-II indicates the comparative position of superplastic forming strain-rates among other strain-rates achieved in other forming processes [1.13].

(See next page for TABLE 1-II)

1.5 Production and Retention of Ultra-Fine Grain Structure

The ultra-fine grain structure required for superplasticity can be obtained by a variety of mechanical and thermal treatments.

Other methods such as powder compaction, electro-deposition or pack rolling of thin foils have been studied in the laboratory [1.17] and [1.18].

Three different alloys, the zinc-aluminum eutectoid, the lead-tin eutectic

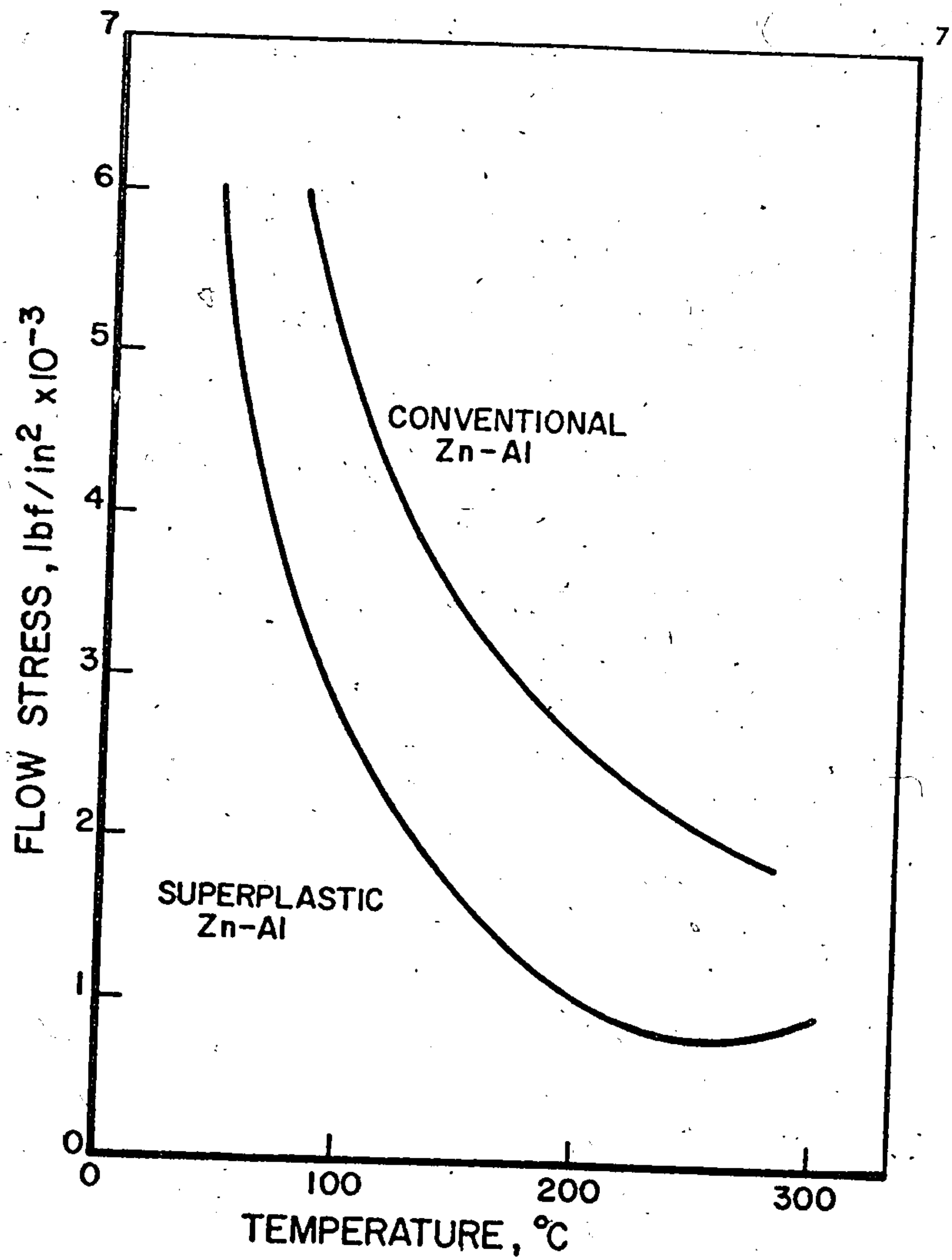

Fig. 1.1 Variation in flow stress with temperature for superplastic eutectoid zinc-aluminum alloy at a strain rate of .01 per second [Ref. 6.15].

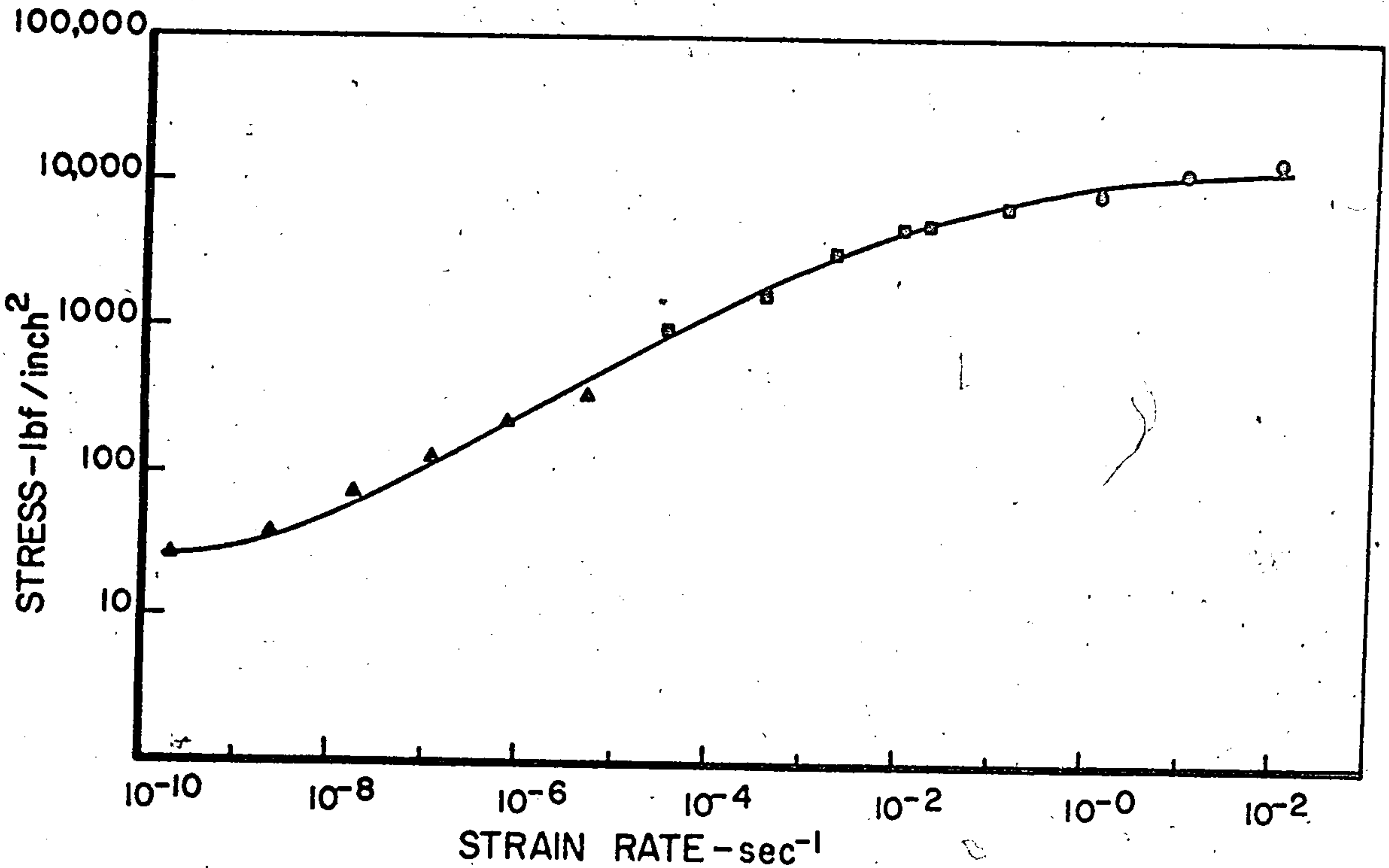

Fig. 1.2 Typical stress, strain-rate characteristic of a superplastic alloy. The material is eutectic tin-lead alloy of grain size 5μ. The experimental points are collected from the following references: Ref. 1.8, Ref. 1.27 and Ref. 2.4.

TABLE 1 - II: Strain-Rates in Metalworking Processes

PROCESS	STRAIN-RATE (per sec.)
Superplastic deformation	10^{-4} to 10^{-1}
Creep	10^{-10} to 10^{-5}
Normal hotworking processes	1 to 10^{2}
Machining (cutting speed 80 ft/sec.)	10^{4}
Explosive forming	10 to 10^{2}
Explosive welding	10^{5}

and the nickel-chromium-iron system are considered below to demonstrate the various thermo-mechanical processes used.

i) Zinc-aluminum eutectoid

In the Zn - 22 Al eutectoid alloy, the ultra-fine structure can be obtained directly by thermal treatment only. The phase diagram, Figure 1.3 shows that when the eutectoid alloy is heated above 275°C, the invariant temperature, it is transformed from a two phase mixture to a single solid phase. If this heated alloy is suddenly cooled to 0°C it results in a supercooled, unstable solid solution which, when brought up to room temperature, decomposes into the equilibrium two-phase state with the required micro-duplex structure, Figure 1.4(a). The same alloy, however, if cooled slowly from above the invariant temperature yields a typical lamellar eutectoid structure as shown in Figure 1.4(b) [1.19].

ii) Lead-tin eutectic

This alloy can be given a micro-duplex structure by drastic mechanical working such as extrusion. As the grain is squeezed, its length is initially increased to maintain constant volume. The energy put into the system by extrusion is then dissipated to a large extent by recrystallization. Recrystallization breaks up the individual long, narrow and heavily strained grains into several short strain-free ones.

iii) Nickel-chromium-iron system

These alloys fall in the class where superplasticity is produced by techniques involving appropriate combinations of mechanical working and

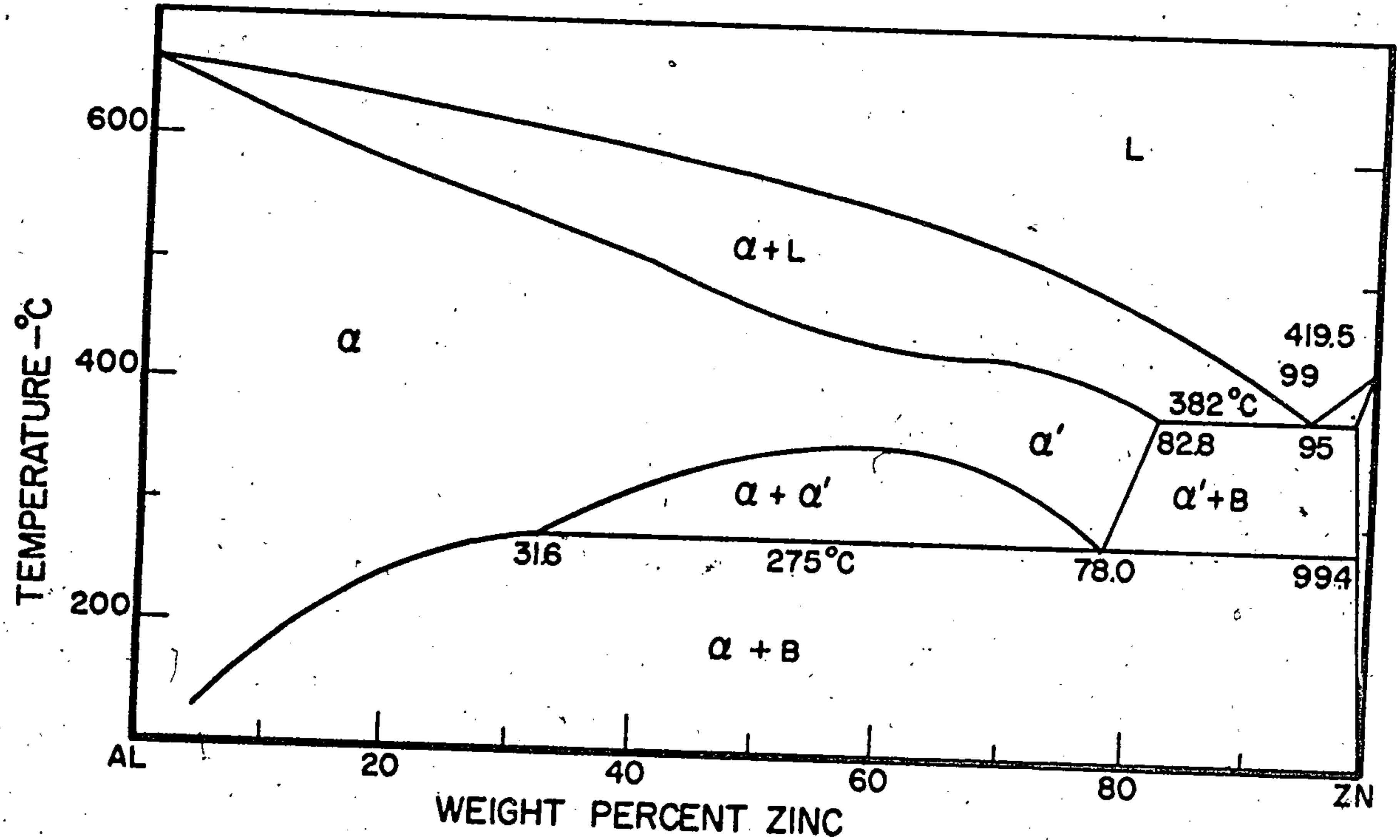

Fig. 1.3 Zinc-aluminum phase-diagram.

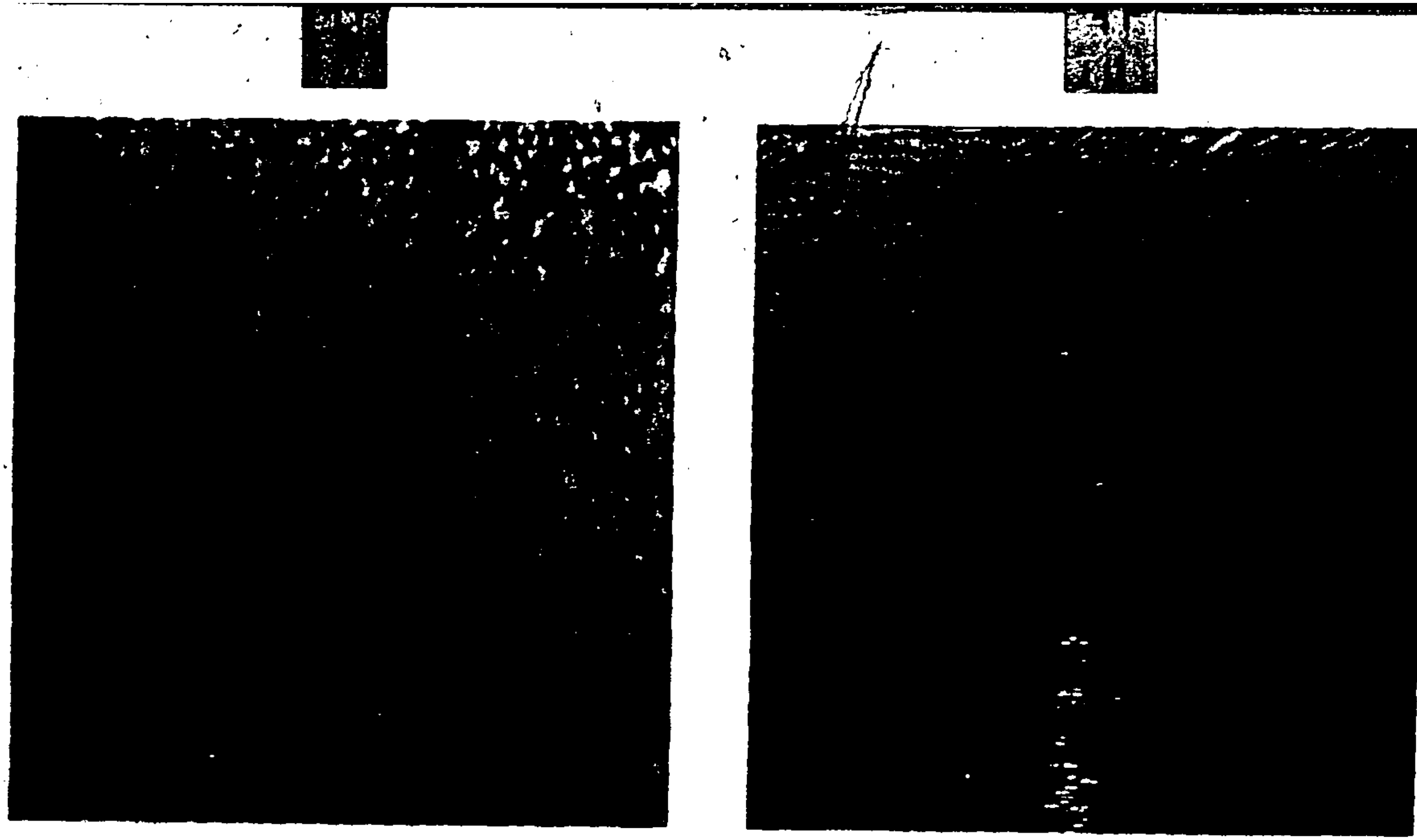

(B) SUPERPLASTIC MICROSTRUCTURE OF QUENCHED ALLOY (A) LAMELLAR MICROSTRUCTURE OF SLOW COOLED ALLOY

FIG. 1.4 - MICROSTRUCTURE OF ZINC-ALUMINUM EUTECTOID ALLOY
[REF. 1.19]

thermal treatment. The alloy is heated into the single phase region and then hot worked by rolling or forging till the temperature of the work-piece decreases well into the two phase region. During deformation and cooling, there is simultaneous occurrence of recrystallization and precipitation.

Most of the alloys that have been observed to behave superplastically are two-phase alloys where the presence of a finely dispersed second phase could inhibit the growth of grains in a major matrix phase. If the chemical composition of each phase is very different, grain growth can only occur by massive diffusion of solute atoms and even in micron size grains this is a slow process [1.19]. Thus it seems that a prerequisite to obtaining superplasticity is to successfully produce a micro-duplex structure.

Pure metals cannot be superplastic since, although a fine grain size can be achieved, it is unstable at high temperatures and the grains grow rapidly before superplastic deformation can be obtained.

1.6 Commercial Superplastic Alloys

Various lists of superplastic alloys appear in the literature and Table 1-III is an example [1.20]. Most of these materials have been made in the laboratory only, but a few have been produced industrially.

i) Eutectoid zinc-aluminum

The eutectoid zinc-aluminum alloy is, perhaps, the most attractive superplastic alloy known today. It is relatively easy to cast and roll into sheet and simple heat treatment produces the required fine grain size in a stable microstructure. Its strain-rate sensitivity is not greatly strain-rate

TABLE 1-III: ALLOYS IN WHICH ISOTHERMAL SUPERPLASTICITY HAS BEEN OBSERVED

Base Metal	Alloy wt%	Temp. °C	Grain size (microns = 10^{-6} metres)	"m"
Aluminium	33 Cu	440-530	1-2	0.9
	12 Si 4 Cu	500	-	0.4
Cadmium	26 Zn	20	1-2	0.5
Chromium	27.5 Co	1200	-	-
Cobalt	10 Al	1200	0.4	0.3
Copper	10 Mg	700	-	-
	10-12 Al	500	-	-
	10 Al 4 Fe	800	10	0.6
	38-50 Zn	450-550	3	0.5
Iron	0.14 C 1.2 Mn 0.1 V	900	2	0.6
	0.34 C 0.47 Mn 2.0 Al	900	2	0.5
	0.42 C 1.9 Mn	730	1-2	0.6
	26 Cr 6.5 Ni) 30 Cr 6.0 Ni)	870-980	2	0.5
Lead	20 Sn	20	3	0.5
	5 Cd	0	4	0.3
Magnesium	0.5 Zr	500	20	0.3
	6 Zn 0.6 Zr	270-310	0.5	0.5
	23 Ni	450	-	-
	30 Cu	450	-	-
	33 Al	400	-	-
Nickel	nil	820	8	-
	39 Cr 8 Fe 2 Ti	980	2	0.5
Tin	5 Bi	20	1	0.5
	2-38 Pb	20	1-2	0.5
	33 Cd	20	1-2	0.5
Titanium	6 Al 4V	900-980	6	0.9
	5 Al 2.5 Sn	1000	18	0.7
Zinc	nil	0-20	1-2	-
	0.5 Al	20	1-2	-
	5 Al	200-360	1-2	0.7
	22 Al	200-260	1-2	0.5
	40 Al	250	1-10	0.5
Zirconium	-	900	12	0.5

dependent and remains at a reasonably high level to strain-rates up to 0.1 per sec., which are within a technologically useful range. Maximum, m, for this material is observed in the range of 250°C - 270°C which is above normal service temperatures and yet not high enough to present any difficulty in actual forming.

The binary zinc-aluminum eutectoid alloy has low creep resistance at room temperature; however, this problem has been successfully reduced,[1.16] and [1.21], with small additions of other metals which reduce creep rates to acceptable levels without affecting the superplastic behaviour.

Its room temperature strength is comparable to that of 70/30 brass. The alloy may be joined by soldering and spot welding, and its resistance to corrosion under atmospheric conditions and in steam is much better than that of mild steel.

Considerable academic and industrial attention is focused on this alloy, and it is the most common superplastic material available commercially. It presently sells for 75¢/lb in North America in the superplastic state. In England, Imperial Smelting Corp. Ltd. and its associates have been producing commercial alloys of this type for some years.

ii) Aluminum-Bronzes

Some superplastic aluminum-bronzes have recently been placed on the market. Two such alloys, CDA 619 and CDA 638 have room temperature yield strength of 20-25 tons per square inch. After a simple heat treatment, CDA 619 has a yield strength of 50 - 60 tons per square inch. Their corrosion, oxidation and wear resistance and electrical conductivity at room temperature are very good.

iii) High temperature alloys

Micro-duplex, 26 Cr-6 Ni, stainless steel and wrought Ti - 6Al - 6V titanium alloy show good superplastic properties at about 1000°C and have been used to produce commercial components [1.22].

1.7 Industrial Usage of Superplasticity

Recent literature contains many examples of components formed experimentally from superplastic alloys [1.22] and [1.23]. Industrially, some of the components today being manufactured from superplastic alloys include jet engine turbine and compressor discs, Concorde passenger amenities panels, air to air heat exchanger cores and pulleys and gears used in electronic equipment, Figures 1.5 and 1.6.

Because superplastic properties tend toward those of heated thermoplastics, the industrial objective has frequently been to produce superplastic metal parts using the inherently cheaper and simpler forming processes employed in the plastics industry [1.25]. The advantages claimed are:- lower cost of forming equipment, greater uniformity of thickness than in conventional pressing and greater elongation or expansion than would be possible with a conventional metal.

In certain structural components the superplastic part may be more economical than a plastic part because of the better creep resistance and higher strength of superplastic alloys compared with plastics at room temperature.

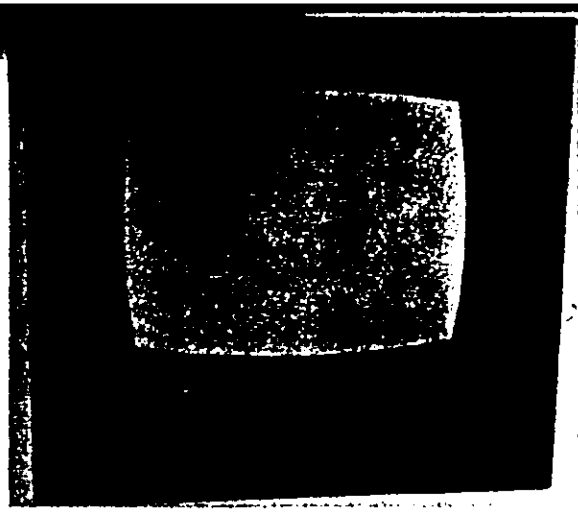

(A) PROTOTYPE CATHODE-RAY TUBE BEZEL, THERMOFORMED FROM SUPERPLASTIC ZN-AI EUTECTOID SHEET (I.B.M., ENDICOTT, N.Y.)

(B) PRESSURE - AUGMENTED DEEP DRAWN CUP OF SUPERPLASTIC LEAD-TIN ALLOY (REF. 1.23)

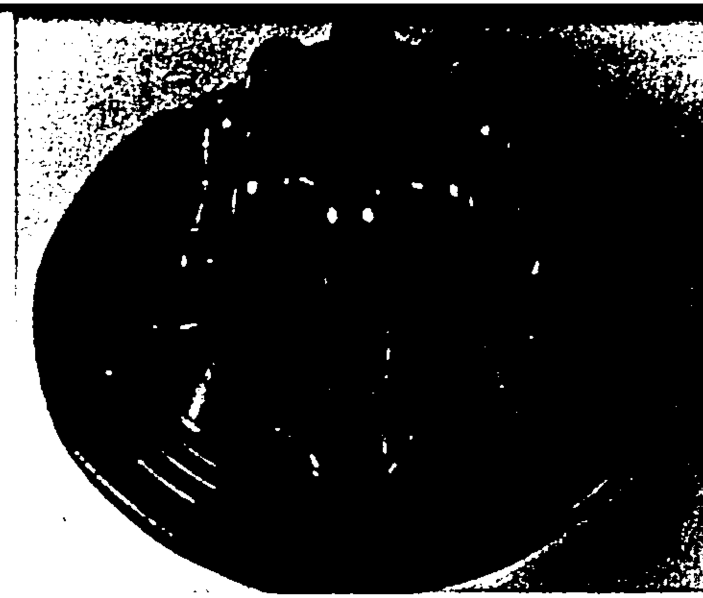

(C) DISH FORMED BY HYDROSTATIC PRESSURE FROM SUPERPLASTIC PB-SN ALLOY (REF. 1.23)

(D) CEILING TILES FORMED FOR SUPERPLASTIC ZN-AI EUTECTOID SHEET BY INTERNAL PRESSURE INTO A FEMALE DIE (COMINCO LIMITED, SHERIDAN PARK, ONT.)

FIG. 1.5 - APPLICATIONS OF SUPERPLASTICITY

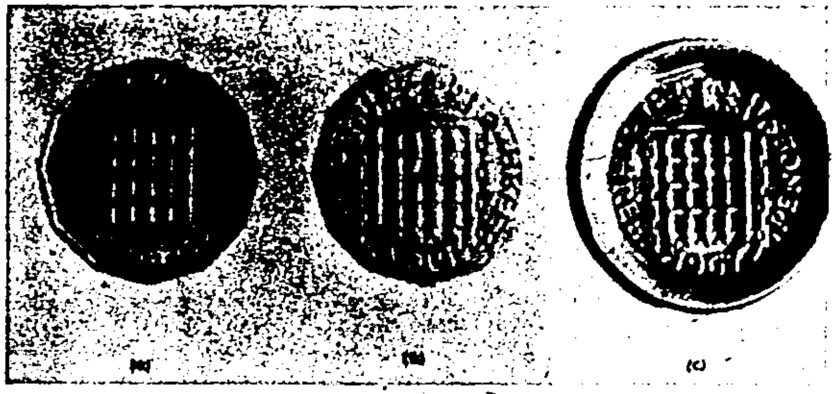

(A) STAMPING DIE MADE FROM SUPERPLASTIC ZN-AL EUTECTOID; IN ORDER FROM THE LEFT, COIN USED AS PATTERN, SUPERPLASTIC DIE, IMPRESSION STRUCK IN COPPER IN THE DIE (REF. 1.27)

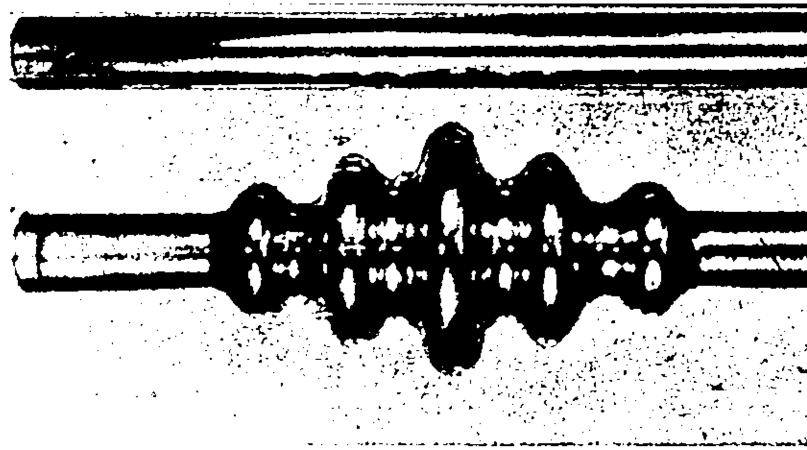

(B) CORRUGATED SUPERPLASTIC PB-SN TUBE FOUND IN A SINGLE OPERATION INTO A FEMALE DIE BY INTERNAL PRESSURIZATION (REF. 1.23)

(C) DEVELOPMENT OF THE FORMING PROCESS OF A SUPERPLASTIC ZN-AL CUP; IN ORDER FROM THE LEFT, EXTRUSION BILLET, REVERSE-EXTRUDED CUP, PRESSURE FORMED CUP (REF. 6.15).

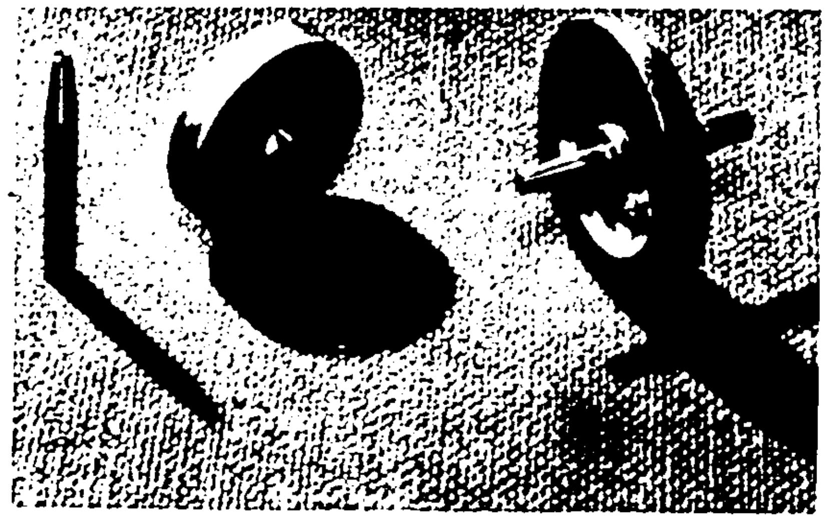

(D) FLYWHEEL FORMED FROM SUPERPLASTIC ZN-AL EUTECTOID ALLOY IN ONE OPERATION (IBM, LEXINGTON - KENTUCKY)

FIG. 1.8 - APPLICATIONS OF SUPERPLASTICITY

Moreover, in the aircraft industry and other advanced areas of manufacturing, there is an increasing requirement for normally difficult to form metals. A good example is the titanium alloys presently being introduced in supersonic aircraft. For such projects, the slow forming rate of superplasticity is not a factor limiting its application provided it replaces otherwise complex and expensive fabrication techniques.

If the superplastic temperature for an alloy is low and service temperatures are likely to be high, a grain-coarsening treatment may have to be applied after processing to ensure that superplasticity does not return back during use. This treatment could be one means of substantially improving the creep resistance of the material. However, in case of high melting point materials, the service temperatures are well below the superplasticity range, and the fine-grained structure can be retained to provide excellent mechanical properties in the finished product. The small grain size is also advantageous in that it leads to the production of very smooth surfaces; ideal for polishing or plating.

The applicability of various forming processes to superplastic metals is briefly discussed below

i) Rolling

In rolling, any reduction in the roll force would be advantageous and in theory superplasticity would allow this if the strain rate during rolling were not too high. The rolling of uncommon, and difficult to work alloys which are fortuitously superplastic under rolling conditions could be carried out to advantage. The Ti/6Al /4V alloy, commonly used in the aircraft industry is such an example. It has been suggested that reductions of 10:1 can be effected in roll separating forces during plastic deformation [1.26].

ii) Forging

Low flow stresses required for superplastic flow permit lower loads in press forging. This is particularly beneficial in parts in which intricate detail and sharp corners must be obtained. In these parts high forging loads are required with conventional materials to achieve complete die filling. With superplastic alloys the material will continuously flow into the interstices under a moderate load applied for a longer period and excellent detail is obtained. Saller and Duncan [1.27] demonstrated this by making an excellent Zn-Al stamping die using a coin as pattern. They then used this die at room temperature to strike an impression on a copper slug, Figure 1.6(a). The dynamic strength of Zn-Al at room temperature is higher than that of copper and the die was found satisfactory for short production runs.

The superplastic copper alloy CDA 638 is being used on an experimental basis for computer memory discs [1.28]. These can easily be forged from this material with little or no subsequent machining.

iii) Drawing processes

In conventional cold-working of sheet where deep-shaped parts are required, it is usual to start with a sheet considerably larger than the plan area of the final part. The material is drawn into the die and deep parts are produced without excessive thickness variation. The ram presses on the bottom of the cup and the forming force is transmitted through the cup wall in order to deform the flange and draw it inwards. It can be shown that the stress required to cause yielding in the flange is much less than that required in the cup wall so that the flange can be deformed inwards while the cup wall remains rigid. But in superplastic alloys, deformation occurs under the action of any stress and the cup wall deforms and progressively thins if drawing is attempted [1.28]. Al Naib and Duncan [1.23] have however, used a pressure-augmented deep drawing process to 'draw' deep cups as shown in Figures 1.5(b) and 1.7.

iv) Extrusion

Since extrusion is another compressive process, most of the discussion on rolling and forging would apply here as well.

Furthermore, alloys which are difficult to extrude in the normal coarse-grained state may possibly become extrudable in the fine-grained superplastic condition.

v) Die-less drawing and 'roll-less' rolling

The resistance to necking of superplastics alloys has been used to devise a method of die-less drawing [1.25].

On applying tension, size reduction may be achieved in a locally heated region (induction heating is used) which is at the superplastic temperature, Figure 1.8. A good degree of conformity to the original shape is possible and reproducibility to within .0005 inch can sometimes be achieved. There is obviously no die wear or die lubrication. This method can also be used to produce controlled tapered or stepped lengths of complex shapes.

A process of "roll-less rolling" based on the same principle can be envisaged.

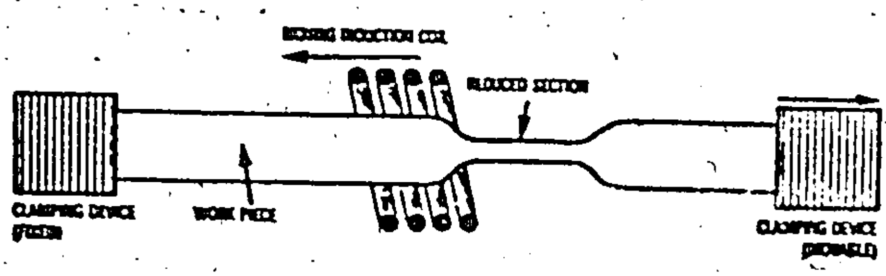

Fig. 1.8 Die-less wire drawing process.

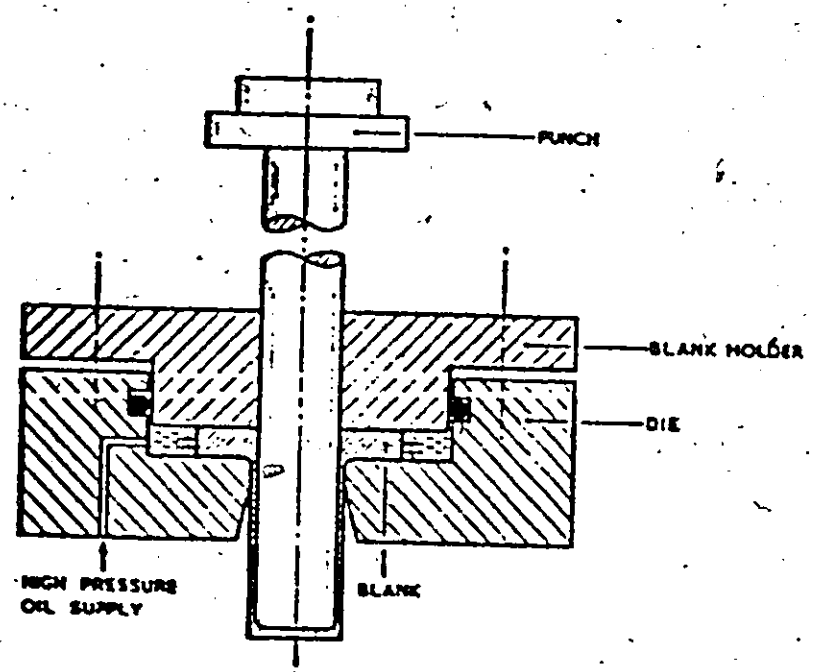

Fig. 1.7 Pressure-augmented deep drawing equipment [Ref. 1.23].

vi) Stretching processes

Superplastic alloys in the form of sheet or thin-walled tube can be stretch-formed to produce useful components. Normally this is achieved by air or gas pressure applied to one side of the sheet or tube. In order to complete the process in an acceptable time, say 10 to 30 seconds, the pressures are usually in the range of 50 to a few hundred pounds per square inch. This would be a high pressure compared with those used to stretch-forming of plastics but is a low pressure for a metal forming process.

The British car industry has investigated the possibility of using Zn-Al sheet for producing automobile body panels. Normally a large number of different panels are individually pressed-many of them requiring complicated sequences of operations - and then assembled together. With zinc-aluminum, quite complicated panels can be vacuum-formed in one operation.

The advantage of superplastic alloys in these processes is that much larger surface strains can be achieved before failure and also that, for a given change in shape, the variation in thickness across the part will be less for the superplastic alloy than for the conventional alloy [1.28]. Employing superplastic alloys in stretch forming operations may result in reduction of tooling and labour costs and elimination of interstage annealing.

CHAPTER II

BEHAVIOUR OF SUPERPLASTIC ALLOYS

2.1 Phenomenological classification

Superplasticity is a hot-working phenomenon observed above a temperature of about 40% of the absolute melting point. The most important aspect of superplasticity can be observed by comparing the stress, strain-rate characteristic of an alloy in its normal "coarse" grain state with that of the same alloy in the ultra-fine grain, superplastic state, as in Figure 2.1. At conventional forming speeds, both materials have a similar rate-sensitivity and flow stress. At very low deformation rates - creep forming - the rate-sensitivities are similar but the flow stress of the superplastic alloy is extremely low. There exists a transition range, often regarded as the "superplastic range" where the strain rate sensitivity, for a metal, is unusually high. This range may extend over two or three decades of strain rate. The index m, which is the slope of this line in a logarithmic diagram of σ-$\dot{\varepsilon}$, is frequently called the strain-rate sensitivity index and may be defined by

$$m = \frac{d\ (\ln \sigma\ )}{d\ (\ln \dot{\varepsilon}\ )} \qquad (2\text{-}1)$$

In hot-working, conventional alloys have a definite yield point and their flow stress is dependent on strain as well as strain-rate. Superplastic alloys, on the other hand, have no identifiable yield stress * ; they deform

---

* See section 2.3.5

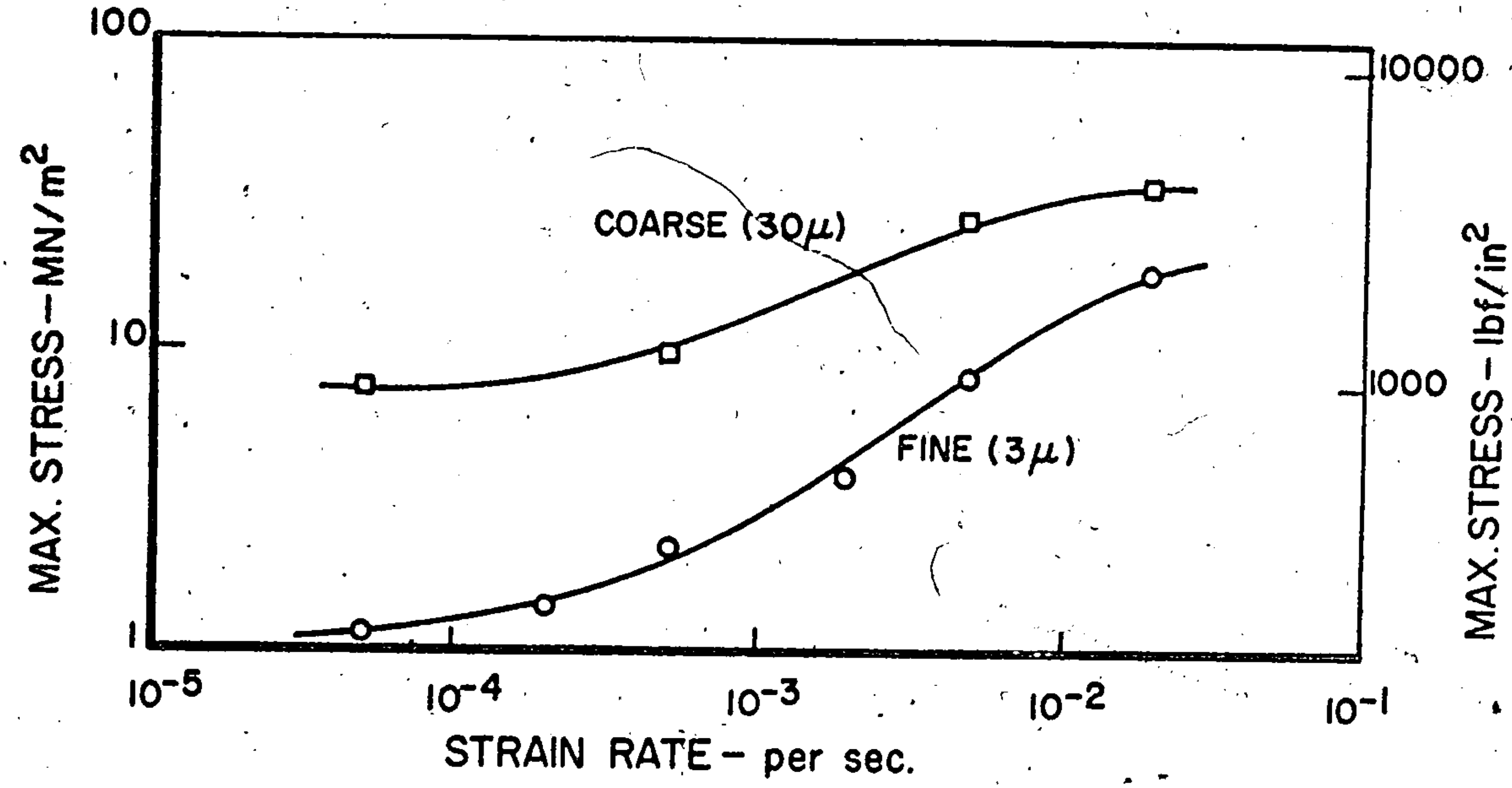

Fig. 2.1 Stress, strain-rate characteristic of superplastic 60/40 brass tested at 600°C, compared with that of the same alloy in its conventional state [From Ref. 2.34].

under any stress, however small, and their properties are surprisingly insensitive to strain. Their microstructure is virtually unchanged by large deformations and this, in itself, is an unusual characteristic for polycrystalline materials.

The classification of superplastic alloys presents some difficulties. They could be considered as fluids and, because their strain rate dependence is non-linear with an index in the range $0.25 < m < 0.8$, they would be classed as non-Newtonian fluids. Within this classification the absence of a measurable yield stress required to initiate deformation, precluded their classification as Bingham plastics. Within the superplastic range, they fit the category of pseudo-plastic fluids, but this does not fit their behaviour at very low strain-rates. In asmuchas these alloys have a basically crystalline structure and can be handled in an apparently solid state, they are best regarded as solids. The term "viscous solid" may be a good description even if, in a strict sense, the words are contradictory [1.13].

A more useful classification can be made by comparing superplastic alloys with other materials which are hot-worked. Figure 2.2 shows, schematically, the stress, strain-rate characteristic for steel during forging and for a polymer in a thermoforming operation. The superplastic alloy is typically formed at a lower strain-rate than either of the other two, but it may be seen that the level of stress and the strain-rate sensitivity are both in between those of the typical metal and the thermoplastic.

Superplasticity is often regarded as an extension of normal creep behaviour in metals. There are, in fact, many affinities between creep

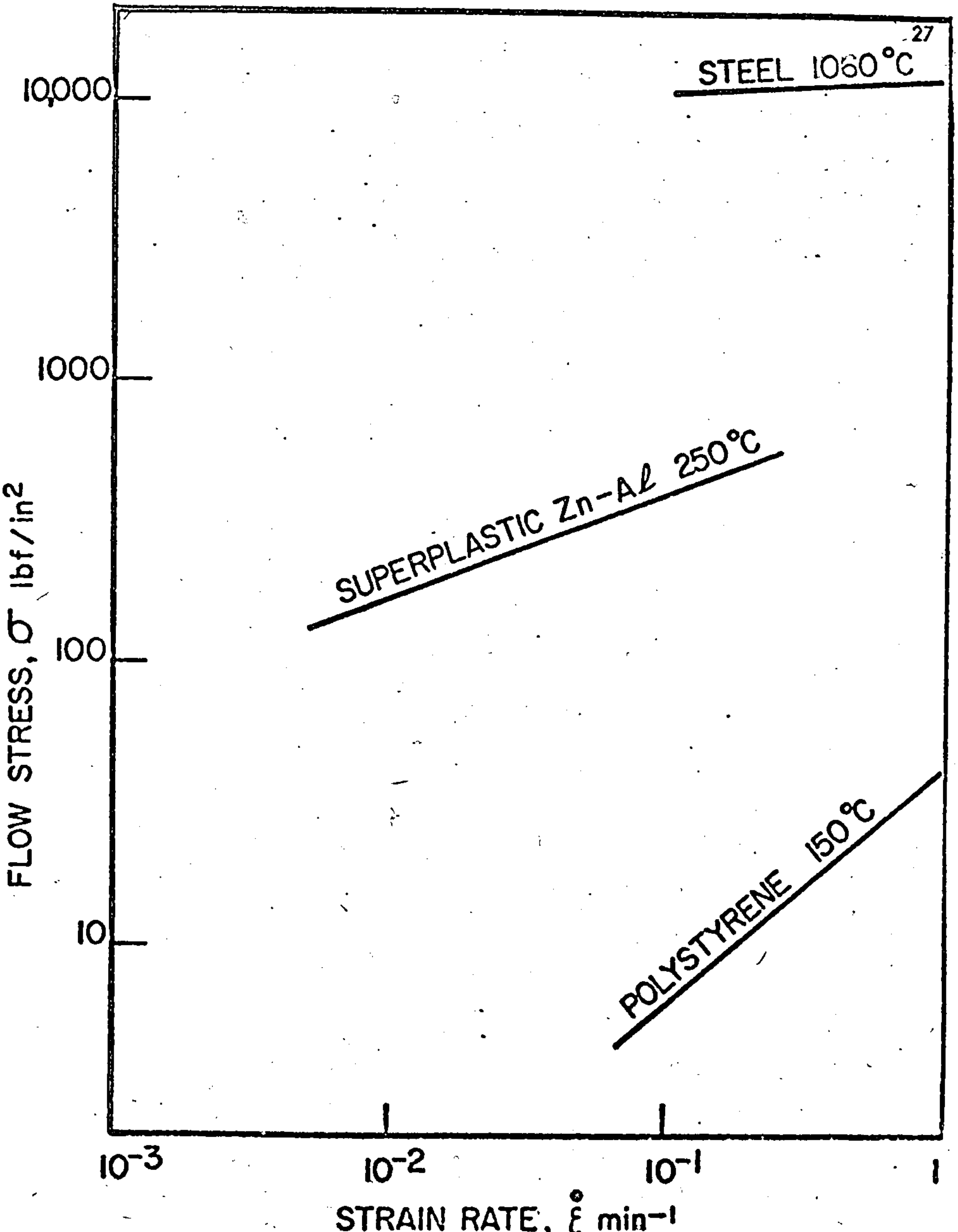

Fig. 2.2 Comparison of hot-working stress, strain-rate characteristic for different materials [From Ref. 1.13].

and superplasticity, for instance, in being both rate-dependent phenomena prevailing at elevated temperatures. Metal physicists also show similarity between the mechanism of superplastic deformation and that of creep particularly at low strain rates. Figure 2.3, however shows that typical deformation rates at which superplasticity occurs differ by many orders of magnitude than those of creep.

In summary, the overall phenomenological behaviour of superplastic alloys can be easily described as follows. At low strain rates, superplastic alloys deform under the action of small stresses -- a few hundred pounds per square inch -- compared with a few thousand pounds in normal alloys. At higher-strain rates, up to the lower limit of conventional hot-working speeds, superplastic alloys have a high strain rate-sensitivity -- typically 0.5 compared with 0.1 in most metals. This behaviour is sufficiently unusual and distinct, but is probably best regarded as one region of the overall spectrum of the behaviour of deformable solids. Hence much of the theory used to describe rate-dependent deformation can be applied to superplastic forming processes.

2.2 Mechanisms of Superplastic Deformation

Metal physicists tend to agree on the basic deformation processes which could operate in superplastic flow, however they disagree on the relative importance of each process. The principal processes which have been assumed to occur during the microscopic deformation of superplastic alloys are:

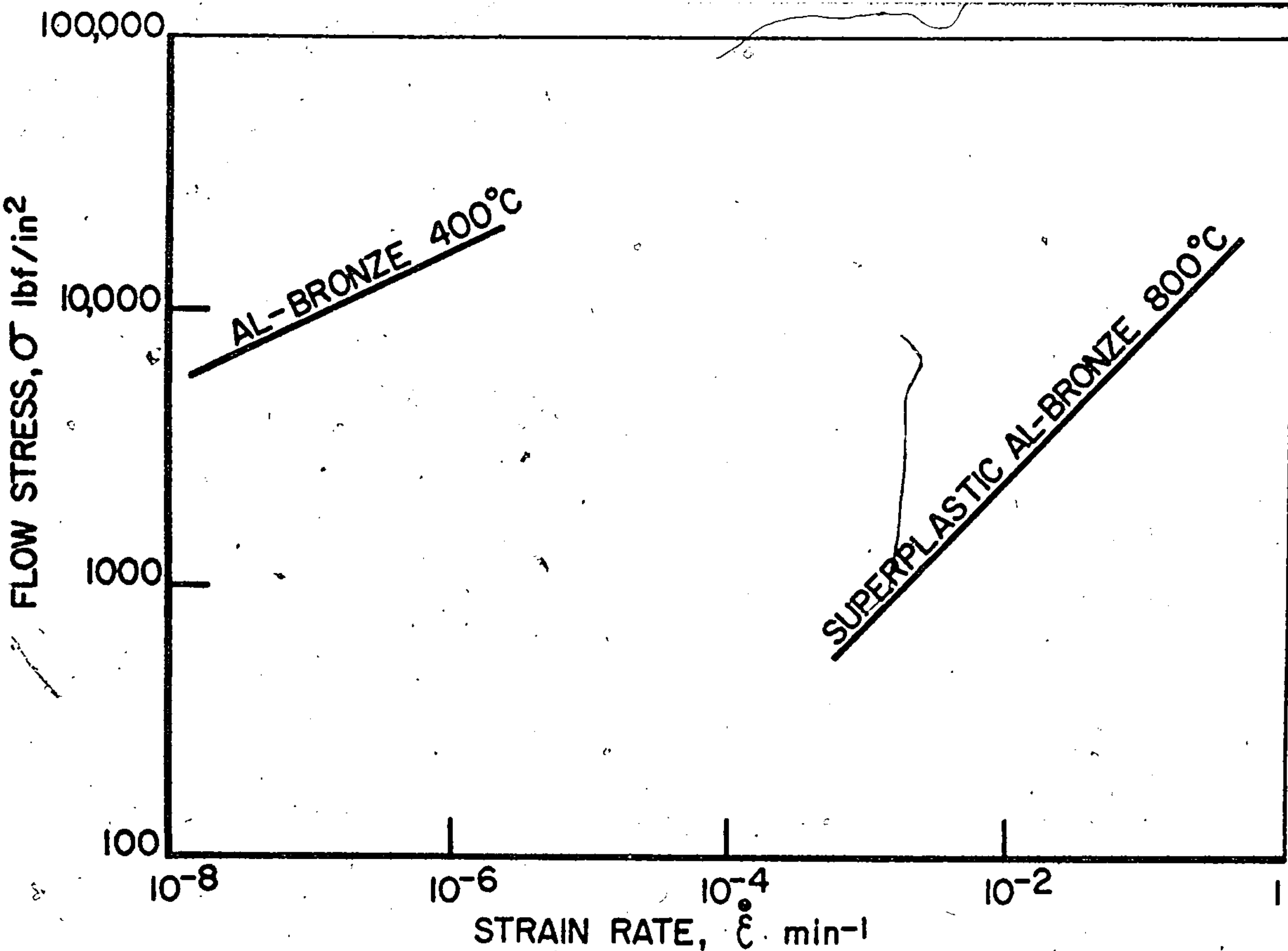

Fig. 2.3 Creep and superplastic deformation in aluminum-bronze [From Ref. 1.13].

(i) Diffusion creep

(ii) Grain-boundary sliding

(iii) Dynamic recovery

(iv) Dislocation creep

Several proposed deformation mechanisms are based essentially on one or other of the above mentioned processes. However, as controversy exists regarding these mechanisms, it is only intended to give here a brief account of their fundamental aspects and to comment on the influence each process may have on mechanical properties.

(i) Diffusion creep [1.8] and [2.1]

Figure 2.4(a) shows the mechanism of vacancy-diffusion creep. Under an applied tensile stress, the upper and lower grain boundary facets experience a tensile stress which aids formation of vacancies. Atoms may therefore diffuse or migrate as a result of these vacancies from regions of compressive stress in the grain to tensile regions. Vacancy migration may be either through the body of the grain, Nabarro-Herring diffusion, or along the grain boundary as proposed by Coble. The predicted strain-rate for Nabarro-Herring diffusion is,

$$\dot{\varepsilon} = C_1 \frac{\sigma}{L^2} \tag{2-2}$$

where L is the average grain size and C_1 is a constant and for Coble diffusion

$$\dot{\varepsilon} = C_2 \frac{\sigma}{L^3} \tag{2-3}$$

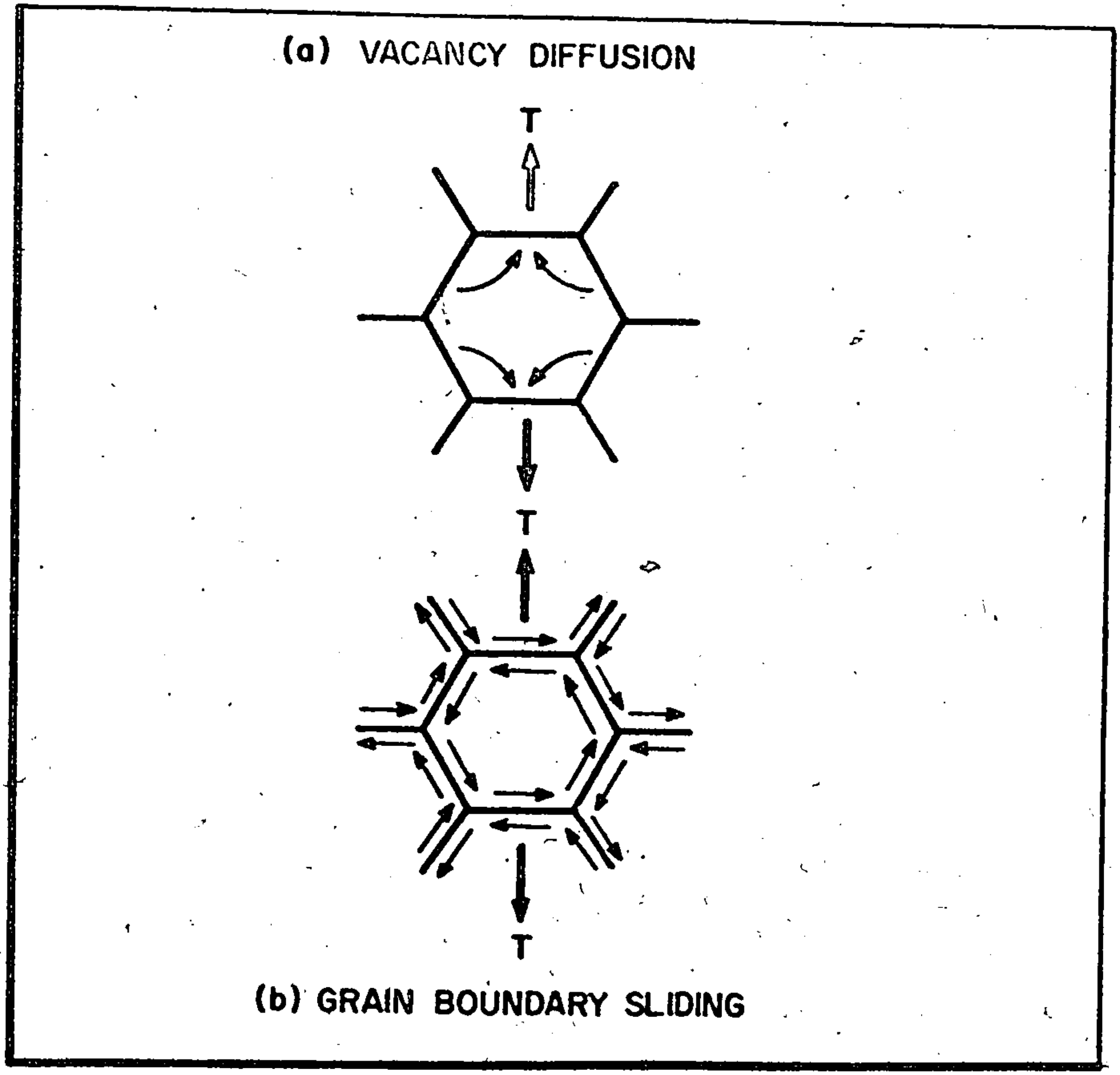

Fig. 2.4 Schematic representation of deformation mechanisms.

Vacancy creep mechanisms have several inadequacies as sufficient explanation for superplasticity :

- They predict a linear relation between stress and strain rate which is rarely observed.

- The predicted strain-rates are generally much lower than those observed experimentally.

- Both mechanisms predict grain elongation which is rarely observed after extensive superplastic deformation.

- The strain-rate sensitivity index is not unity as predicted but tends to be about 0.3 or less at the low strain-rates at which diffusion mechanisms might be expected to dominate.

Ashby [2.2] has shown that grain boundaries act as perfect vacancy sources and sinks (as required for N-H or Coble creep) only if dislocation-like line defects in them are free to climb. If these become pinned by precipitates on or near grain boundaries, they can no longer be perfect sources and sinks. This may support the theory that there is a "threshold stress" σ_0' required to initiate climb and hence diffusion creep in superplastic materials. This has been suggested by some investigators [1.18] and [2.3] to [2.8]. However, this argument appears to be contrived in order to permit a low rate-sensitivity index at low strain-rates as experimentally observed. Further research into the existence and nature of σ_0' is still needed.

(ii) <u>Grain-boundary sliding [1.9] and [2.6] to [2.8]</u>

Grain-boundary sliding is the relative movement of adjacent grains by a shear translation along their common interface, Figure 2.4(b). The fact that the grains remain unchanged in shape after deformation in most superplastic materials has led a number of workers to suggest that grain-boundary sliding is the chief mechanism in superplastic flow, with other accommodation processes. A large amount of evidence has been presented in favour of grain-boundary shear. Alden [2.7] for instance in his experiments on Sn-Bi eutectic superplastic alloy, has shown that scratches remaining from metallographic polishing are offset at grain boundaries and remain relatively straight within each grain. A few per-cent strain was found enough to transform an initially polished surface into one with an intense granular appearance. Further, the grains remained equiaxed after deformation.

Under conditions of pure grain-boundary sliding in small grain size systems, the rate of straining would be given by [2.13]

$$\dot{\varepsilon} = C_3 \frac{\sigma}{L} \tag{2-4}$$

where C_3 is a constant. Such an ideal situation is not possible as sliding cannot occur continuously on all boundaries without some accompanying deformation within the grains themselves [2.10]. Without this added deformation mode the polycrystalline aggregate as a whole cannot be plastically deformed to any appreciable degree without porosity, [2.6] which was found generally absent in superplastic elongation. However, Johnson [2.5] has suggested that the absence of voids, may not be such a serious problem facing models based on boundary sliding, as sintering mechanisms are known to occur faster than was once thought.

Grain-boundary sliding itself would lead to a low strain-rate sensitivity because grain boundaries are not smooth, and after some shear, sliding may be obstructed where ledges and such obstacles along the boundary interlock. Thus for highly strain-rate sensitive boundary-shear to occur, resistance to sliding must be lowered by smoothing out the ledges and making the stress concentration triple junctions mobile.

(iii) Dynamic recovery [2.5]

When strain-free grains are produced by recrystallization all signs of prior hardening are removed and ductility is restored. It would appear reasonable, to invoke a continuous version of suchaprocess, i.e. deformation with simultaneous annealing, to account for superplasticity. This idea is somewhat controversial since it presupposes that recrystallization is the main softening process during hot-working. There is much discussion [2.11] as to whether recrystallization does occur continuously and simultaneously during hot-working and regarding the alternative softening processes which otherwise has to operate. For example, it is contended that in some materials conventional recrystallization occurs only after straining ceases. Investigations which indicate that superplastic deformation involves processes of continuous recovery have been mainly qualitative and rely chiefly on metallographic evidence, and much work is still needed to understand the role of dynamic recovery processes in superplastic deformation.

(iv) Dislocation creep [2.12] and [2.13]

Under conditions of normal high-temperature deformation in coarse-grained materials, dislocations usually become entangled forming dislocation cells within each grain. Each dislocation cell consists of a region of almost perfect crystal bounded by a wall of tangled dislocations. The size of the cells is normally reciprocally related to the applied stress. Predictions of cell size in fine-grained materials suggested that even at rather high stresses the dislocation cells should be larger than grains as small as those in superplastic alloys. On the basis of these observations, Hayden et al [2.12] and [2.13] have formulated certain preconditions for any dislocation creep mechanism of superplasticity.

- Creep would occur without the formation of a dislocation cell structure.

- Dislocations are probably nucleated at grain corners or grain-boundary ledges. After traversing the grain, they are probably destroyed at suitable grain-boundary locations.

- Because of the low stresses and the great mobility of the grain boundaries for sliding and migration it is improbable that dislocation pile-ups would be formed.

Since dislocation cells and pile-ups inhibit creep their relative absence facilitates it and hence may provide an explanation of superplasticity. This model, however, has to be investigated further in order to account satisfactorily and quantitatively for the distinct stages of the sigmoidal shape of stress-strain rate curve as shown in Figure 1.2.

Avery and Backofen [1.8] explain superplasticity in terms of two competing processes. In accordance of this concept they developed an analytical expression of the form

$$\dot{\varepsilon} = \frac{A\,\sigma}{L^2} + B \sinh \beta\sigma \qquad (2\text{-}5)$$

where L is the grain size and A, B and β are constants at a given temperature. The first term in equation (2-5) is associated with Nabarro-Herring diffusional creep and the second term is attributed to dislocation climb. In such a case vacancy-migration creep dominates over dislocation climb at low rates of deformation and leads to a strain-rate sensitivity of unity at small stresses. Although this is observed in one or two isolated cases, the more general observation is that strain-rate sensitivity reaches a maximum of < 1 as the strain-rate falls and then decreases again. Packer and Sherby [1.14] have modified equation (2-5) to

$$\dot{\varepsilon} = \frac{A'\sigma^2}{L^3} + B\sigma^2 \sinh \beta'\sigma^{2.5} \qquad (2\text{-}6)$$

The first term is an empirically modified expression for grain-boundary vacancy-migration creep [2.5] and the second is based on dislocation glide and was derived by Weertman. The revised equation again failed to predict the decrease in strain-rate sensitivity at very low strain-rates.

A model for superplasticity in two phase materials involving crystallographic slip and continuous recovery by grain boundary migration or recrystallization has put forward by Johnson et al [2.14]

Lee [2.6] has proposed that at low strain-rates at least 50% of the deformation occurs by grain-boundary sliding whereas diffusion creep could account for the rest. In the intermediate strain-rate, where the strain-rate sensitivity is maximum, accommodation is achieved by grain deformation and recovery.

This brief account of the proposed mechanisms for superplastic deformation gives an idea of the existing controversy in the field. More work is required to gain complete understanding of what actually happens on microscopic scale during superplastic deformation.

2.3 Basic Phenomenological Model

In discussing mathematical models in general one can hardely improve on Drucker's suggestion [2.15] that "The best model to use is the simplest one which will exhibit the characteristics of greatest interest". These mathematical models are usually abstracted from experimental results and the constitutive equation most widely used to describe superplastic behaviour in a tensile test is

$$\left(\frac{\sigma}{\sigma_o}\right) = \left(\frac{\dot{\varepsilon}}{\dot{\varepsilon}_o}\right)^m \tag{2-7}$$

where σ and $\dot{\varepsilon}$ are the stress and strain-rate respectively and σ_o and m are material parameters. σ_o indicates the strength of the material at a particular strain-rate, $\dot{\varepsilon}_o$ is a constant customarily taken as unity and m is frequently called the strain-rate sensitivity index. In order to avoid the risk of oversimplification, the limitations imposed on the use of this non-linear viscous model (such as strain, time, anisotropy, etc) are indicated and discussed below.

2.3.1 Strain-rate sensitivity

Over an extended range of strain-rates, the $\sigma/\dot{\varepsilon}$ curve in a logarithmic diagram, such as Figure 1.2, is typically sigmoidal for a superplastic alloy. If m is assumed constant, equation (2-7) will only fit this curve over a limited range of strain-rate. It is customary therefore to present curves showing the variation of m with $\dot{\varepsilon}$. These are derived either by differentiating a smooth curve drawn through σ, $\dot{\varepsilon}$ points calculated from many tests, or, alternatively from a single test in which a number of step changes are made in the strain-rate. The latter method was first suggested by Backofen et al [1.7] and is always referred to as "the velocity step-change method". Figure 2.5 is a schematic diagram of the load-time record of a tensile test covering a change of velocity at time t from v_0 to v_0'. The extrapolation of the lower curve v_0 is carried to establish a common strain for both speeds. By assuming only slow variation of m with strain-rate over the experimental range, an m value could then be calculated from

$$m = \ln (P_A / P_B) / \ln (v_0 / v_0') \qquad (2\text{-}8)$$

Backofen found the m value to be reproducible (for zinc-aluminum eutectoid) and independent of strain-history, being determined only by temperature and the particular strain-rates associated with a given velocity change. The advantage of the procedure of Backofen et al, besides the fact that it needs only one test specimen, is that the flow stresses are compared at constant strain, however the extrapolation of a load-time curve will introduce some error [2.16].

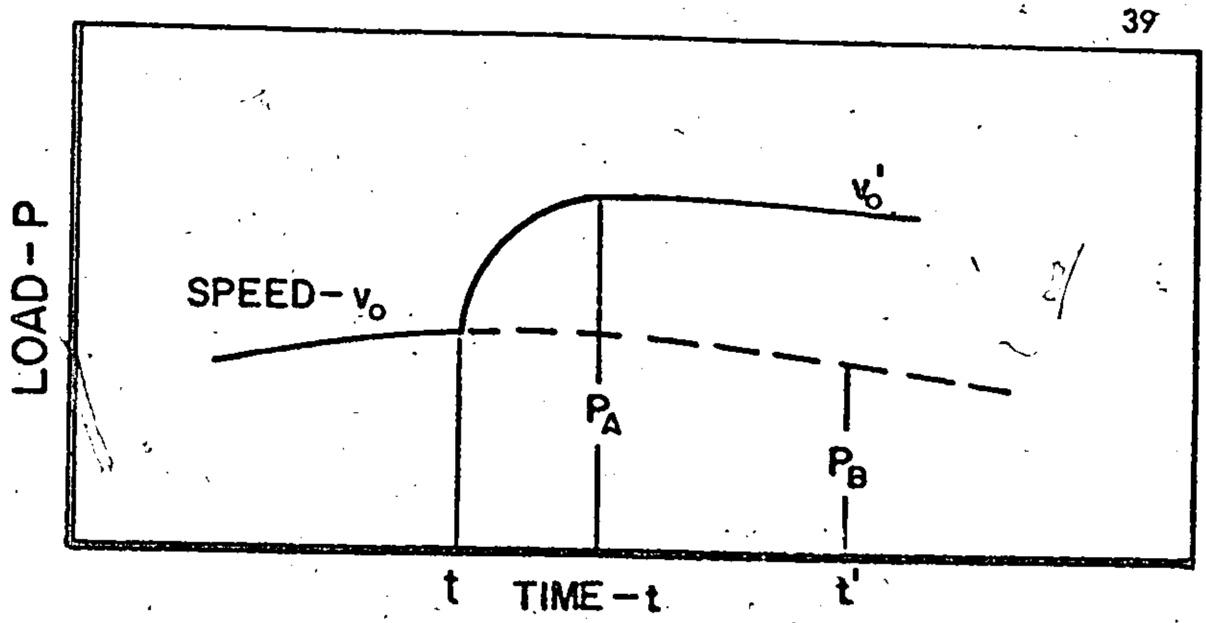

Fig. 2.5 Schematic diagram showing the velocity step-change method. P_A and P_B are tensile loads at the same strain.

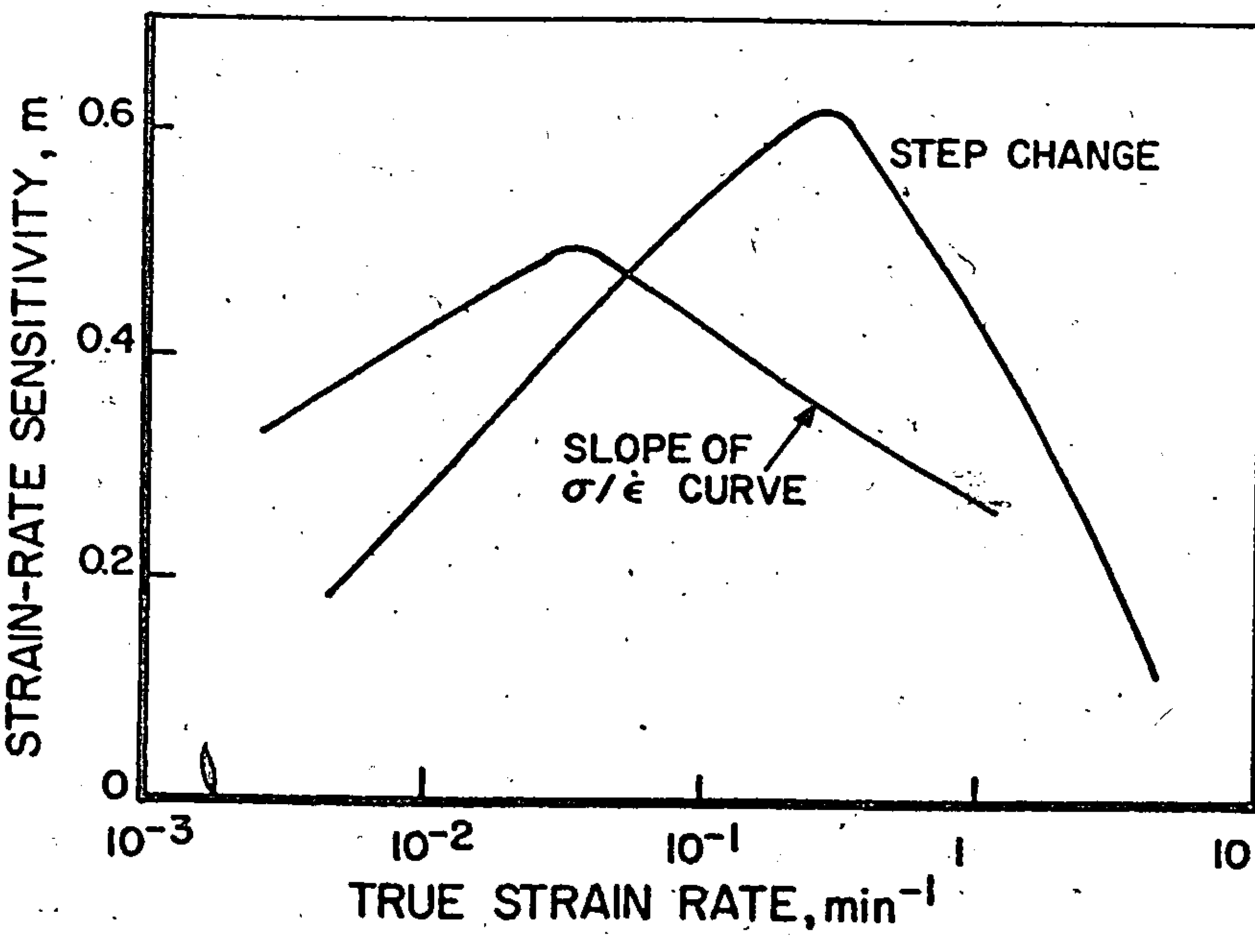

Fig. 2.6 Variation of strain-rate sensitivity with strain-rate as determined by two different methods for Cu - 9.5% Al - 4% Fe bronze [From Ref. 2.24].

In Figure 2.6, m versus $\dot{\varepsilon}$ curves determined from the two methods namely; $\sigma/\dot{\varepsilon}$ slope and velocity change are compared and in general the results do not agree [2.17]. The discrepancy in these curves is significant and may be attributed mainly to grain-coarsening during superplastic deformation and/or uncertainties in both local true strain-rate and stress state which arise as a result of non-uniform elongation occurring beyond the plastic instability limit [2.17].

In technological superplastic processes, abrupt changes in strain-rate are unlikely and therefore the determination of m from the slope of the $\sigma-\dot{\varepsilon}$ curve is the preferred method. In general, these processes will be carried out at strain-rates where m is greatest and the error introduced by assuming m to be constant in, for example, the range $10^{-2} < \dot{\varepsilon} < 10^{-1}$ min^{-1} for the material in Figure 2.6 will not be great. In certain very stable alloys, this range could be extended to two or three orders of magnitude.

2.3.2 Hardening

In a constant cross-head speed tensile test, the strain-rate diminishes as the test-piece extends. Assuming a known, constant value of m, a constant true strain-rate curve can be derived. Nicholson [2.18] fitted an equation

$$\sigma = f(\dot{\varepsilon})\ \varepsilon^{n} \qquad (2-9)$$

to such a curve and obtained a value of the strain-hardening index, n, of 0.06 for eutectoid zinc-aluminum.

Baudelot [2.19] and Suéry investigated the superplastic deformation of the eutectic alloy of lead-tin at various temperatures, and found that the flow stress is only a function of the true strain-rate, the temperature and the initial size of the alloy grain. In their careful experiments, large uniform elongations were achieved and neither grain growth nor strain-hardening were observed. On the other hand, Newbury and Joy [2.20] observed an apparent stress increase with strain in testing the same Pb-Sn alloy, but this was shown by Baudelet et al [2.19] to result from a systematic error due to neglecting the amount of deformation within the grips in calculating the stress-strain diagram.

Watts and Stowell [2.21] carried out constant true strain-rate tests on copper-aluminum eutectic and found results to be well fitted by an equation

$$\frac{\sigma}{\sigma_o} = 1 + f(\dot{\varepsilon})\,\varepsilon \qquad (2\text{-}10a)$$

The degree of linear strain-hardening was appreciable and was attributed to microstructural coarsening. This grain coarsening appeared in some of their tests to be governed by time at temperature and not strain. They also observed that a change from a banded to a more equiaxed microstructure occurred during superplastic deformation.

Linear strain-hardening as given by equation (2-10a) was also observed by Taplin and Dunlop [2.17] in superplastic aluminum-bronze, even in the absence of appreciable grain growth. They concluded that the apparent rise in flow stress is partially due to strain-induced hardening and also partially due to the development of a triaxial stress state in the specimens following necking.

The deformation of as-extruded copper 7% phosphorus alloy was studied by Baudelet et al [2.22] and the stress was related to strain by

$$\sigma = \sigma_o(\dot{\varepsilon}) + \eta\,\varepsilon \qquad (2\text{-}10b)$$

where η is a constant. The true stress-strain characteristic of uniformly elongated specimens showed a transition range which is associated with the transformation of the as-extruded and homogenized state to the superplastic state. In the superplastic range the strain-hardening coefficient was negligible, and the stress increase during the deformation was related to the increase of the phase size. This growth of grain size was found to be an increasing function of the deformation in the superplastic range. Same results were obtained by the same authors in studying the deformation of 60/40 Brass.

In all tests where hardening occurred, the undeformed material had marked directionality. Its microstructure showed banding phases along either extrusion or rolling directions. Consequently, these materials do not immediately possess an equiaxed grain-structure, a characteristic of superplasticity, and the test results showing an increase in apparent stress with deformation should be viewed bearing this in mind. For materials of equiaxed grain-structure in its undeformed state, grain growth may take place and this can influence the properties as is evident from equations (2-2) to (2-6) but this cannot be shown incontrovertibly to be only strain dependent. It may be time dependent as well. The difficulty of introducing a time function is well known in creep [2.23], and in superplasticity until more data are available, a simple model as indicated by equation (2-7) appears justified.

2.3.3 Anisotropy

Recently, few workers [2.24] and [2.25] have studied the anisotropic

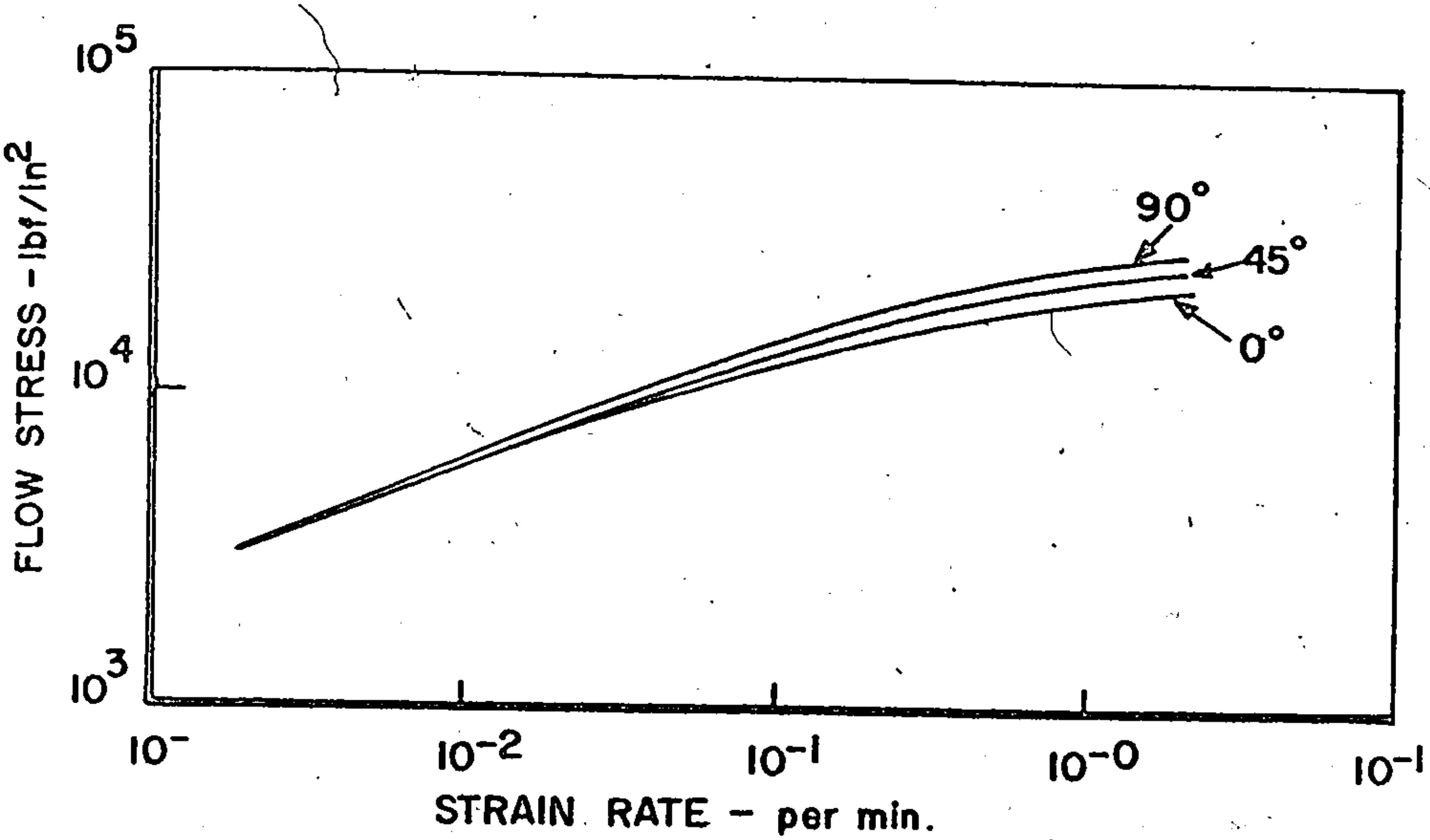

Fig. 2.7 Stress, strain-rate characteristic of superplastic Zn-0.4% Al tensile specimens cut at 0,45 and 90° to the rolling direction [From Ref. 2.25].

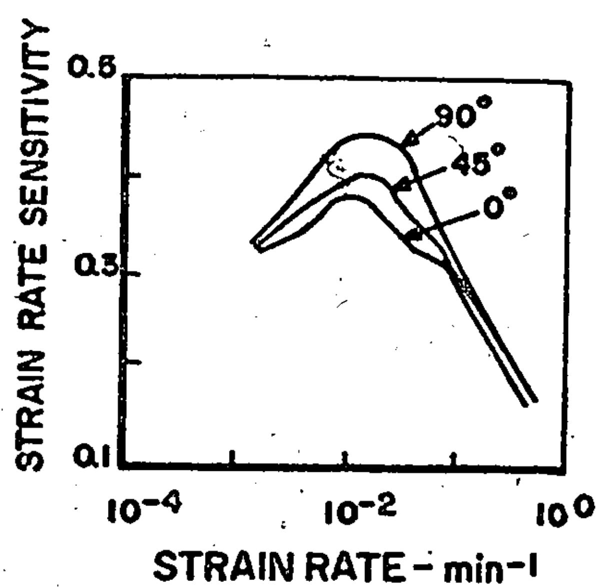

Fig. 2.8 Strain-rate sensitivity index of superplastic Zn-0.4% Al tensile specimens cut at 0,45 and 90° to the rolling direction [From Ref. 2.25].

effects in superplastic material produced in sheet form by rolling. The metallographic examination of these materials revealed fibrous microstructures and elongated grains parallel to the rolling direction in the undeformed condition. During uniaxial tests of specimens cut from these rolled sheets, anisotropy has been reported; this is manifested by unequal transverse strains and a dependence of total elongation on the orientation of the test-piece with direction of rolling. The stress strain-rate curves obtained from test-pieces of different orientations are shown in Figure 2.7. Similarily Figure 2.8 shows the variation of strain-rate sensitivity m in the planes of the sheet at different strain-rates. Phenomenologically, the level of the stress, strain-rate curves are very similar and in any analysis should not introduce serious error.

2.3.4 Temperature

The variation of flow stress with temperature in zinc-aluminum eutectoid is shown in Figures 1.1 and 2.9. The results of Naziri and Pearce [2.25], Figure 2.9 were obtained from a number of isothermal tests at constant cross head speed. The curve of Fields et al [2.26] is from a single test in which the temperature was gradually increased and finally exceeded the transformation temperature. The difference in the level of the two curves before transformation may be due to a difference in the grain size of the materials tested.

The dependence of the strain-rate sensitivity on temperature is shown in Figure 2.10 for the zinc-aluminum eutectoid [1.7]. It is seen that m attains high values (0.45 - 0.55) which is typical for superplastic behaviour in the temperature range of (475 - 550 Tm) ^{o}k.

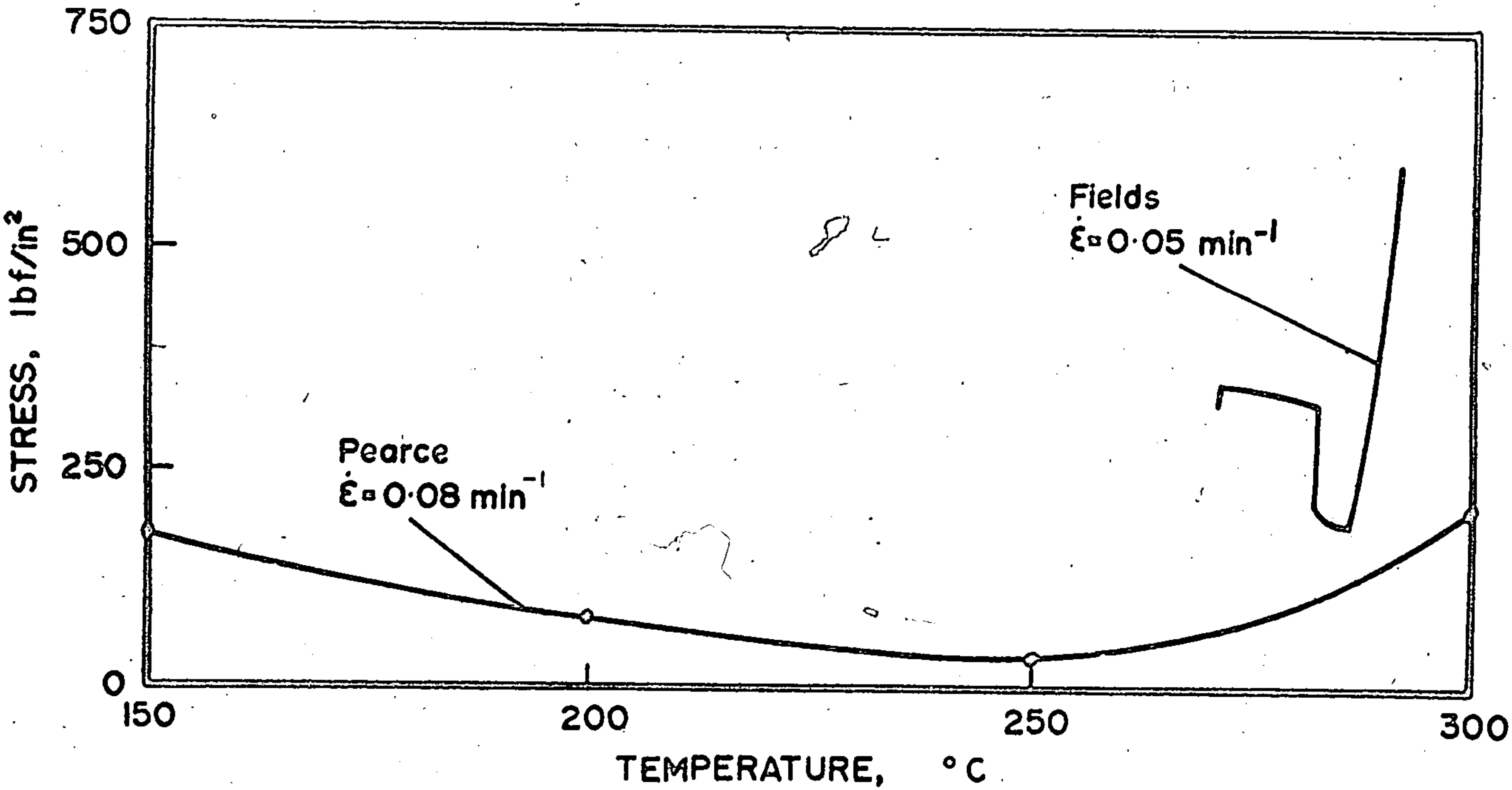

Fig. 2.9 Variation of flow stress with temperature for superplastic Zn-Al eutectoid alloy [From Refs. 2.25 and 2.26].

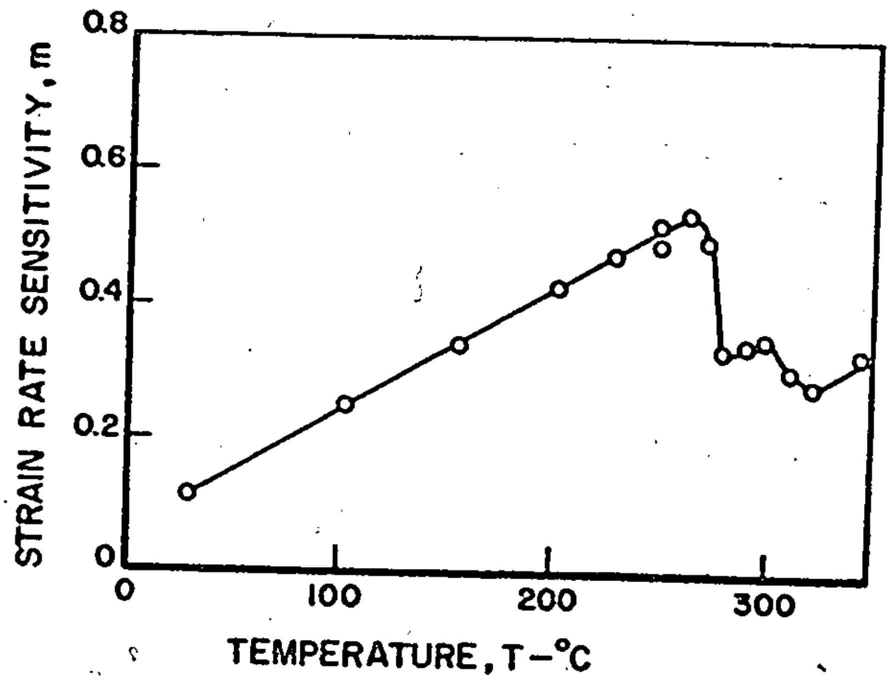

Fig. 2.10 Variation of strain-rate sensitivity with temperature for superplastic Zn-Al eutectoid alloy [From Ref. 1.7].

2.3.5 Creep yield stress

In an attempt to explain the low strain-rate sensitivity at low strain-rates Johnson [2.5] suggested the presence of a back-stress or "creep yield" stress. Quantitative investigations which measure the back-stress in superplastic deformation are almost non-existent in literature. The only exception is tests formed by Burton [2.4] on the lead-tin eutectic alloy at very low strain-rates as shown in Figure 1.2. The lowest strain rate in these tests was in fact the limiting sensitivity of the creep apparatus. By plotting the low stress results on a linear scale a distinct onset-stress for the deformation was obtained (= 25 psi). This back stress is very low and it only represents 2% of a typical flow stress for the lead-tin alloy. This may be not surprising since at elevated temperatures, diffusion is rapid and only a very small stress is necessary to cause a metal to creep by atomic diffusion at very small strain-rates [2.27].

2.4 Empirical Constitutive Equations

The power law given by equation (2-7) represents the stress, strain-rate characteristic of superplastic alloys over a limited range of strain-rate, Figure 1.2. Other consitutive equations could be used especially where the logarithmic $\sigma/\dot{\varepsilon}$ diagram is non-linear in the strain-rate range of interest. Two examples of these constitutive equations are given below.

2.4.1 Power law with m & σ_o as functions of $\dot{\varepsilon}$

At constant temperature the strain-rate sensitivity m depends on the strain-rate $\dot{\varepsilon}$ and grain size L of the superplastic alloy. The power law given by equation (2-7) can be thus modified to have the form

$$\sigma = \sigma_o(\dot{\varepsilon}, L) \quad \dot{\varepsilon}^{m(\dot{\varepsilon}, L)} \qquad (2\text{-}11)$$

where σ_o and m are functions of $\dot{\varepsilon}$ and L. Expressions for the dependence of σ_o and m on strain-rate can be arbitrarily chosen using conventional curve fitting procedures applied to experimental data.

Padmanbhan and Davies [2.28] have presented a numerical method for analyzing superplasticity data determined by conventional testing procedures. They fitted equation (2-11) to experimental data obtained by Holt and Backofen [1.9] for superplastic aluminum-copper alloys of different grain sizes. It was assumed that the actual values of m and σ_o could be represented by polynomials of the form

$$m = \sum_{r,s=0}^{r+s=i} a_{rs} \, (-\log_{10} \dot{\varepsilon})^r \, L^s$$

$$\sigma_o = \sum_{r,s=0}^{r+s=i} b_{rs} \, (-\log_{10} \dot{\varepsilon})^r \, L^s \qquad (2\text{-}12)$$

The numerical values of the coefficients a_{rs} and b_{rs} were determined by multi-dimensional regressional analysis. Table 2-I gives the predicted values of stresses using equation (2-11) at different strain-rates and grain sizes.

2.4.2 Hyperbolic-sine law

Another appropriate equation for the situation in which the strain-rate sensitivity decreases with increasing strain-rate is

$$\dot{\varepsilon} = \dot{\varepsilon}_o \sinh \left(\frac{\sigma}{\sigma_o}\right) \qquad (2\text{-}13)$$

This law originally suggested by Prandtl has been used in the analysis of creep. This empirical law appears to be rooted in the mechanism of deformation in the atomic lattices in polycrystalline materials and responsible for the generally viscous behaviour prevalent in the ductile metals at high temperatures. Although, so far, no generally satisfactory mechanism of superplasticity has been proposed, a number of investigators [1.8] and [1.14] have expressed the deformation mechanism by $\sigma/\dot{\varepsilon}$ relationships similar to equation (2-13).

In order to account for the observed low strain-rate sensitivity, Johnson [2.5] has suggested introducing a back-stress in the superplastic consitutive equation. The existence and nature of this "threshold stress" has been discussed in section 2.3.5. Assuming back stress σ_o' , equation (2-13) becomes

$$\dot{\varepsilon} = \dot{\varepsilon}_o \sinh \frac{\sigma - \sigma_o'}{\sigma_o} \qquad (2\text{-}14a)$$

or

$$\sigma = \sigma_o' + \sigma_o \sinh^{-1} \left(\frac{\dot{\varepsilon}}{\dot{\varepsilon}_o} \right) \qquad (2\text{-}14b)$$

In the above equation $\dot{\varepsilon}_o$, σ_o and σ_o' are only functions of the grain size L (measured in μm). Further, from numerical analysis it was found that dependence of $\dot{\varepsilon}_o$ on the grain size has the form

$$\dot{\varepsilon}_o = \alpha / L^{\beta} \qquad (2\text{-}15)$$

where α and β are constants . The constants in equations (2-14a), (2-14b) and (2-15) were found using a numerical optimization technique [2.30]. The predicted stresses using equations (2-14) are given in Table 2-I for different strain-rates and grain sizes. For comparison, Table 2-I shows also stresses predicted by a power law of constant m and σ_o fitted to the same experimental data.

TABLE 2-I: Fitting empirical laws to superplastic data

L (μm)	σ (observed) [Ref. 1.9]	σ (Davies et al)	σ (sinh-law)	σ (power-law)	$\dot{\varepsilon}$ observed [Ref. 1.9]
7.7	210	205	210	214	5×10^{-5}
	510	507	541	528	2×10^{-4}
	1000	1051	1089	958	5×10^{-4}
	2100	1986	2100	1960	1.5×10^{-3}
	2900	2379	2624	2733	2.5×10^{-3}
	3300	4103	3116	3712	4×10^{-3}
5.5	320	328	320	385	1.5×10^{-4}
	810	714	710	728	5×10^{-4}
	1100	1144	1078	993	9×10^{-4}
	1750	2014	1750	1515	2×10^{-3}
	2150	2483	2412	2185	4×10^{-2}
	3050	1636	3317	3545	1×10^{-2}
4.6	205	249	205	224	1×10^{-4}
	405	414	349	388	2.3×10^{-4}
	900	859	834	811	7×10^{-4}
	2600	2583	2600	2568	4×10^{-3}
	3100	3041	3102	3357	6×10^{-3}
	4750	3977	3744	4706	1×10^{-2}
3.8	200	71	200	203	1×10^{-4}
	520	597	520	550	5×10^{-4}
	905	903	888	844	1×10^{-3}
	2100	2013	2260	1988	4×10^{-3}
	3100	3030	3122	3050	8×10^{-3}
	4200	5467	3927	4500	1.5×10^{-2}
2.8	105	156	105	110	6×10^{-5}
	600	748	644	657	1×10^{-3}
	1000	895	911	849	1.5×10^{-3}
	1500	1358	1777	1452	3.5×10^{-3}
	4000	3603	3906	3650	1.5×10^{-2}
	5100	6056	5100	5896	3.2×10^{-2}
1.7	110	116	110	118	2×10^{-4}
	320	270	246	318	9×10^{-4}
	600	552	455	538	2×10^{-3}
	1020	1096	969	981	5×10^{-3}
	2050	2460	2064	2015	1.5×10^{-2}
	2900	2191	2900	3175	3×10^{-2}

It is seen that the hyperbolic-sine law provides a better agreement between the experimental and the predicted stresses than the other two empirical relations. The mean percentage error using the hyperbolic law is 6% rising to 15% when Davies equations are employed. Davies numerical anlaysis, although possessing generality, fails to predict the stresses at points in the periphery of the strain-rate range. The forms of the expressions for m and σ_o given by equations (2-12) are obviously not amenable to analytical solutions of superplastic deformation problems and thus seem to be of little practical value. Hence it may be preferable to represent the superplastic data over a wide range of strain rate by a simpler form such as the hyperbolic-sine law.

2.5 Mathematical theory of Superplasticity

The deformation of superplastic material under a multiaxial stress system is assumed to be governed by the same laws as those originally proposed for steady-state creep by Odqyist and Baily [2.23]. Since the derivation of these laws has been given many times in the literature it deserves only the barest outline in the present work.

Our fundamental assumption is that superplastic deformation takes place without volumetric deformation, i.e. in the usual cartesian tensor notation

$$\dot{\varepsilon}_{kk} = \dot{\varepsilon}_{11} + \dot{\varepsilon}_{22} + \dot{\varepsilon}_{33} = 0 \qquad (2\text{-}16)$$

According to experimental evidence the strain rate $\dot{\varepsilon}_{ij}$ will not be influenced by imposing a hydrostatic pressure upon the stress system σ_{ij}. This implies the introduction of stress deviation tensor

$$S_{ij} = \sigma_{ij} - \frac{1}{3}\,\delta_{ij}\,\sigma_{kk} \qquad (2\text{-}17)$$

where δ_{ij} the Kronecker's delta, is equal to unity when $i = j$ and to zero when $i \neq j$.

The rate of dissipation of energy per unit volume is

$$\dot{W} = \sigma_{ij} \; \dot{\varepsilon}_{ij} = S_{ij} \; \dot{\varepsilon}_{ij}$$

and thus

$$\dot{\varepsilon}_{ij} = \frac{\partial \dot{W}}{\partial \sigma_{ij}} = \frac{\partial \dot{W}}{\partial S_{ij}} \tag{2-18}$$

If we now introduce the hypothesis that $\dot{W}$ be a flow potential which is dependent on some scalar quantity of the stress system σ_{ij}, then

$$\dot{W} = f\,(J_1 \,,\; J_2 \,,\; J_3) \tag{2-19}$$

Where J_1, J_2 and J_3 are the stress invariants of the stress deviation tensor. They are given by

$$\begin{aligned} J_1 &= S_{kk} \\ J_2 &= \frac{1}{2} \; S_{ij} \; S_{ji} \\ J_3 &= \frac{1}{3} \; S_{ij} \; S_{jk} \; S_{ki} \end{aligned} \tag{2-20}$$

In particular if incompressibility is assumed and the influence of J_3 is considered negligible [2.31] equation (2-19) reduces to

$$\dot{W} = f\,(J_2) \tag{2-21}$$

If we limit this treatment to isotropic materials we may introduce the quantity σ_o as

$$\sigma_o^{\;2} = \frac{3}{2} \; S_{ij} \; S_{ji} = \frac{1}{3} \; J_2 \tag{2-22}$$

The quantity σ_o is known as the effective or equivalent stress and taken as the positive square root of $\sigma_o^{\;2}$. The numerical constants in equation (2-22) are chosen so that σ_o reduces to σ_{11} in the special case of uniaxial stress system.

Therefore equation (2-21) becomes

$$\dot{W} = f(\sigma_e) \tag{2-23}$$

Carrying out the differentiation in equation (2-18) we obtain

$$\dot{\varepsilon}_{ij} = \frac{\partial \dot{W}}{\partial S_{ij}} = \frac{\partial \dot{W}}{\partial \sigma_e} \frac{\partial \sigma_e}{\partial S_{ij}} = \frac{3}{2} \frac{d\dot{W}}{d\sigma_e} \frac{S_{ij}}{\sigma_e} \tag{2-24}$$

Equation (2-24) shows that the tensors of strain-rate and stress are coaxial.

In the special case of uniaxial creep we require that equation (2-24) reduces to Norton's creep law

$$\left(\frac{\dot{\varepsilon}_{11}}{\dot{\varepsilon}_o}\right) = \left(\frac{\sigma_{11}}{\sigma_o}\right)^{\lambda} \tag{2-25}$$

where $\lambda = \frac{1}{m}$. Therefore

$$\frac{\dot{\varepsilon}_{11}}{\dot{\varepsilon}_o} = \frac{3}{2} \frac{d\dot{W}}{d\sigma_e} \frac{2\sigma_{11}/3}{\sigma_{11}} = \left(\frac{\sigma_{11}}{\sigma_o}\right)^{\lambda} \tag{2-26}$$

and the body relations take the form

$$\dot{\varepsilon}_{ij} = \frac{3}{2} \dot{\varepsilon}_o \left(\frac{\sigma_e}{\sigma_o}\right)^{\lambda-1} \frac{S_{ij}}{\sigma_o} \tag{2-27}$$

If now, we introduce the effective creep strain-rate $\dot{\varepsilon}_e$ by means of

$$\dot{\varepsilon}_e^2 = \frac{2}{3} \dot{\varepsilon}_{ij} \dot{\varepsilon}_{ij} \tag{2-28}$$

equation (2-26) yields

$$\left(\frac{\sigma_e}{\sigma_o}\right) = \left(\frac{\dot{\varepsilon}_e}{\dot{\varepsilon}_o}\right)^{\frac{1}{\lambda}} = \left(\frac{\dot{\varepsilon}_e}{\dot{\varepsilon}_o}\right)^{m} \tag{2-29}$$

It should be noted that the above analysis can be applied to other empirical uniaxial stress, strain-rate relations such as equations (2-13) and (2-6). In these cases the generalized forms [2.32] are given by

$$\dot{\varepsilon}_o = \dot{\varepsilon}_o \sinh \left(\frac{\sigma_e}{\sigma_o}\right) \tag{2-30}$$

$$\dot{\varepsilon}_{ij} = \frac{3}{2} \left[\frac{A}{L^3} \sigma_e + B \sigma_o \sinh (\beta \sigma_e^{2.5}) \right] S_{ij} \tag{2-31}$$

Experiment to verify the above theory of superplastic deformation under multi-axial stress systems has not been carried out. Perhaps the reason for this is the reliance of investigators on the experimental evidence existing in creep literature. The only demonstration of the validity of equation (2-29) as applied to superplastic deformation is due to Duncan and Ghosh [2.33]. In their work they have tested superplastic lead-tin eutectic under tension, compression and torsion and correlated the results using equation (2-29) as shown in Figure 2.11. It will be appreciated that the correlation between the results is satisfactory. Further experimental work is still suggested to verify the applicability of mathematical creep theory to different superplastic materials subjected to different stress systems.

2.6 Conclusions

Superplasticity is the viscous behaviour of most alloys which have an ultra-fine grain structure when they are deformed slowly at an elevated temperature. Their mechanical behaviour can be described simply and with reasonable accuracy but the micro-mechanical mechanisms giving rise to this behaviour are not entirely clear.

The present theory used in analyzing superplastic processes owes a considerable amount to existing mathematical theory of creep. In isothermal

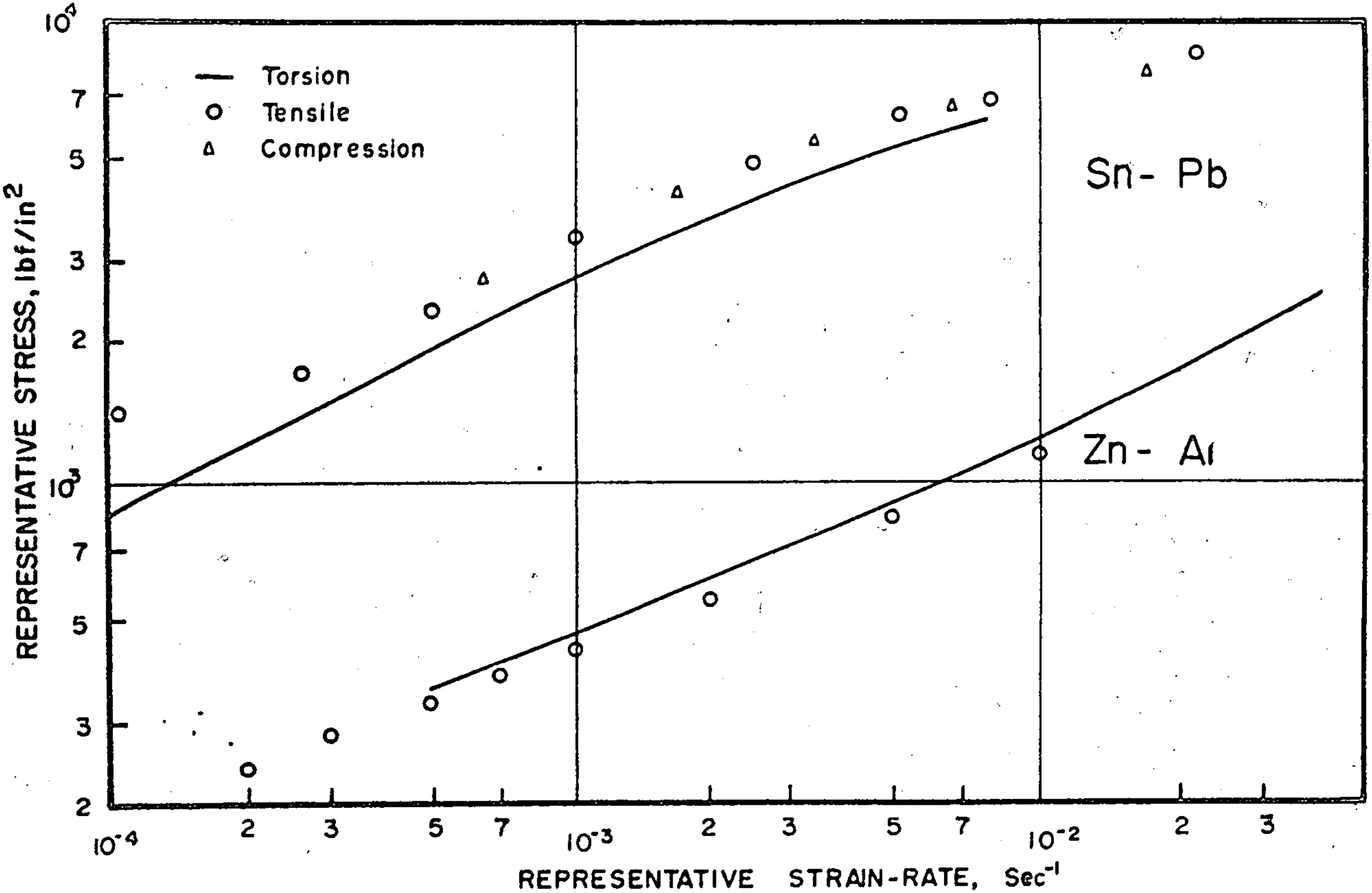

Fig. 2.11 Representative stress, strain-rate curves derived from uniaxial and torsion tests on two superplastic alloys. [From Refs. 2.33 and 2.35].

superplastic forming processes in which there are no abrupt changes in strain-rate and where the total variation of strain-rate does not greatly exceed one order of magnitude, a generalized constitutive equation of the form

$$\left(\frac{\sigma_e}{\sigma_o}\right) = \left(\frac{\dot{\varepsilon}_e}{\dot{\varepsilon}_o}\right)^m$$

may be employed. The material parameters σ_o , $\dot{\varepsilon}_o$ and m should be derived from a $\sigma/\dot{\varepsilon}$ curve obtained from steady-state uniaxial or torsion tests in the appropriate strain-rate range.

CHAPTER III

REVIEW OF PLASTIC INSTABILITY IN THE TENSILE TEST

3.1 Introduction

Plastic instability is identified when a state of uniform plastic strain gives way to one in which deformation is more or less localized. Necking in a tensile test bar is the most familiar and widely analyzed example.

By recognizing that the stress σ is a function of many variables, including strain, ε, strain-rate, $\dot{\varepsilon}$, and temperature, T; then

$$\sigma = \sigma \; (\varepsilon, \dot{\varepsilon} \; , T) \tag{3-1}$$

Therefore the net rate of the strain-induced hardening is

$$\frac{d\sigma}{d\varepsilon} = \left(\frac{\partial\sigma}{\partial\varepsilon}\right) + \left(\frac{\partial\sigma}{\partial\dot{\varepsilon}}\right) \left(\frac{d\dot{\varepsilon}}{d\varepsilon}\right) + \left(\frac{\partial\sigma}{\partial T}\right) \left(\frac{dT}{d\varepsilon}\right) \tag{3-2}$$

Any one term on the right hand side could represent the source of instability if it becomes sufficiently negative. Usually, however, only $\frac{\partial\sigma}{\partial T}$ has the right sign for this, which suggests immediately that the least tendency toward adiabatic deformation contributes to unstable flow. In case of isothermal test equation (3-2) reduces to

$$\frac{d\sigma}{d\varepsilon} = \left(\frac{\partial\sigma}{\partial\varepsilon}\right) + \left(\frac{\partial\sigma}{\partial\dot{\varepsilon}}\right) \left(\frac{d\dot{\varepsilon}}{d\varepsilon}\right) \tag{3-3}$$

The condition for initiating unstable flow after any amount of prior straining is that, somewhere in the material, the next increment of strain-induced hardening be cancelled out by an accompanying strain-induced softening. This strain-induced softening can be due to material defect and /or geometrical perturbation.

3.2 Derivation of Instability Condition in Simple Tension

There is no one single criterion of tensile instability. If the component is considered as a load carrying structure the criterion is generally a maximum in the applied load. This may coincide with a change from a state of uniform plastic straining in which small perturbations in strain do not develop rapidly to one in which straining becomes progressively more non-uniform.

The onset of instability has been related, theoretically, to the material behaviour in a tensile test. It is assumed that at the onset of instability the load carrying capacity of the test-piece starts to decrease. The load P, during the uniform deformation region is given by

$$P = \sigma A \qquad (3\text{-}4)$$

Where A is the current cross sectional area of the tensile test specimen. Thus at the onset of instability

$$dP = 0 = A\, d\sigma + \sigma\, dA \qquad (3\text{-}5)$$

but since $-\dfrac{dA}{A} = d\varepsilon$,

therefore the condition

$$\frac{d\sigma}{d\varepsilon} = \sigma \qquad (3\text{-}6)$$

determines the onset of instability without any particular reference to the material behaviour.

In a tensile test, for homogeneous deformation at constant volume

$$\varepsilon = -\ln \frac{A}{A_o} \qquad (3\text{-}7)$$

The strain-rate in the bar is by definition,

$$\dot{\varepsilon} = \frac{d\varepsilon}{dt} = -\frac{1}{A}\frac{dA}{dt} = -\frac{\dot{A}}{A} \qquad (3\text{-}8)$$

Therefore $$\frac{\partial\dot{\varepsilon}}{\partial\varepsilon} = \left(\frac{d\dot{A}}{dA} - \frac{\dot{A}}{A}\right) = \left(\frac{d\dot{A}}{dA} + \dot{\varepsilon}\right) \qquad (3\text{-}9)$$

Substituting equation (3-9) into equation (3-3) yields

$$\frac{d\sigma}{d\varepsilon} = \frac{\partial\sigma}{\partial\varepsilon} + \frac{\partial\sigma}{\partial\dot{\varepsilon}}\left(\frac{d\dot{A}}{dA} + \dot{\varepsilon}\right) \qquad (3\text{-}10)$$

As proposed by Hart [3.1], the deformation stays uniform if the magnitude of any cross-section difference along the test-piece does not increase, i.e. $d\dot{A}/dA < 0$. Therefore, instability will start to occur when $(d\dot{A}/dA)$ becomes zero and hence equation (3-10) reduces to

$$\frac{d\sigma}{d\varepsilon} = \frac{\partial\sigma}{\partial\varepsilon} + \dot{\varepsilon}\frac{\partial\sigma}{\partial\dot{\varepsilon}} \qquad (3\text{-}11)$$

If we consider that the material behaviour can be represented for isothermal process by

$$\sigma = \sigma_0\, \varepsilon^n\, \dot{\varepsilon}^m \qquad (3\text{-}12)$$

where σ_0 is a strength constant, n is a strain-hardening coefficient and m is the strain-rate sensitivity index, then from equation (3-12)

$$\frac{\partial\sigma}{\partial\dot{\varepsilon}} = m\frac{\sigma}{\dot{\varepsilon}}$$

and $$\frac{\partial\sigma}{\partial\varepsilon} = n\frac{\sigma}{\varepsilon} \qquad (3\text{-}13)$$

Substituting equations (3-13) into equation (3-11) yields the instability condition

$$m + n/\varepsilon = 1 \qquad (3\text{-}14)$$

For strain hardening materials with negligible rate dependence, equation (3-14) clearly reverts to the Considère condition. For non-strain hardening materials the deformation would be stable only for linear viscous (Newtonian) materials in which m = 1.

3.3 Post-necking Geometry of Tensile Test-pieces

In an attempt to predict the post-necking geometry of a tensile test-piece, different investigators have always assumed that the undeformed profile of the specimen has some kind of geometric perturbation. The following sections review the development of the geometry of tensile test-pieces for different classes of material behaviour.

3.3.1 Rigid, perfectly-plastic material (n=m=0)

A tensile bar of a rigid, perfectly-plastic material is obviously at the point of instability as soon as plastic flow occurs. The transformation from uniform tensile to localized flow begins immediately at the weakest cross-section of the bar.

Thomason [3.2] provided an analysis based on the assumption that the non-uniform flow will cause the load carrying capacity of the specimen to decrease at the maximum rate with continued extension. On this basis, the theoretical profiles for tensile specimens were determined using an upper bound solution at the neck.

3.3.2 Strain-hardening material ($m = 0,\ n \neq 0$)

The post-instability deformation of tensile specimens of strain hardening material does not lend itself to simple analysis. With continuing plastic flow the strain hardening rate is gradually reduced to the point where the rate of decrease in load, due to decreasing cross-sectional area, exceeds the rate of increase in load due to strain-hardening. At this point the maximum load is reached and the subsequent flow can become unstable with uniform plastic flow transforming to a localized neck and the elastic parts of the specimen undergoing recovery under decreasing load.

An experimental investigation was carried out by Lubahn [3.3] to correlate the occurrence of a maximum in the external load with a change in the strain condition from a uniform to a local one. Tensile strips of aluminum alloy were tested at very small extension rates. The gradual change in shape of the strain distribution along the specimen, as the test proceeded, showed that the strains were nearly constant with position along the length of the test-piece up to strain of about 8%. With further strain increase, small non-uniformities appeared. Lubahn did not consider them as local necks in the sense of an instability effect because they did not represent points where the strain continued to increase in the absence of strain at other points. There was, however, a certain maximum strain which has been denoted as the necking strain above which the strains continued to increase in only one localized region. This necking strain was about 18.5%.

In the necked portion of a tensile test bar, a triaxial state of stress exists and the precise evaluation of stresses and strains and thus the profile shape of the bar becomes complicated. Useful approximate calculations of the stress distribution in the neck of a tensile test bar was given by Siebel and

Davidenkov et al [2.29]. Their analyses were based on the assumption that the axial strain across the narrowest section was uniform. Bridgman [3.4] approximated the contour of a tension specimen at the neck by a circular arc and thus obtained a set of semi-empirical formulas to determine the stresses in the necked portion. These investigations involve certain approximations and do not account for the various experimental shapes of the profiles of the necked portions of tensile specimens tested at different conditions.

Recently, Chen [3.5] has carried out a theoretical investigation in the problem of necking of a bar made of isotropic, elastic-plastic and strain-hardening material. The tension specimen considered in the analysis was an imperfect bar of which the lateral surfaces deviate slightly from the straight surfaces of the perfect bar. The initial radius R was given by

$$R = R_o \left(1 - \beta e^{-\alpha x^2} \right) \qquad (3\text{-}15)$$

where R_o is the end radius, x is the axial coordinate and α and β are constants. The constitutive equation was formulated such that plastic unloading was taken into account. The strain-rate was assumed to depend not only on the current stress rate but also on the whole stress and deformation histories.

A numerical iterative technique was employed to solve the rather complex, governing field equations. The displacements, the strains and the stresses were calculated in the whole loading history. The predicted load-displacement diagrams indicated that the maximum value of the total load of an imperfect bar agrees well with that of the perfect bar. It was also found that the plastic unloading (which started at the ends of the bar) did begin slightly after the total load starts to decrease. From knowledge of the displacement, the shapes of the necked specimen at different stages of deformation were calculated and presented. However no precise comparison between theory and experiment was made in this analysis.

3.3.3 Linear viscous material ($m = 1, n = 0$)

In the analysis of predicting the subsequent profiles of a bar during the last portion of a tension test, Nadai and Manjoine [3.6] assumed the original shape of the bar such that the areas at the end are only slightly bigger than the minimum area. The area along the bar was assumed to vary according to the relation

$$A = A_1 \left(1 - \frac{\beta}{1 + \alpha x^4}\right) \qquad (3\text{-}16)$$

where A_1 is the maximum area at the ends, x is the axial coordinate in the undeformed geometry and α & β are constants. The profiles of the necked bars were predicted for linear viscous material deforming according to the relation

$$\sigma = \sigma_o \dot{\varepsilon} \qquad (3\text{-}17)$$

The analysis demonstrated that a bar of a linear viscous material will be pulled out quite gradually under tension forces until it becomes a fine filament in the manner reminiscent of the pulling of glass bars in hot flame.

3.3.4 Bingham solid

A Bingham solid is characterized by the constitutive relation

$$\sigma = \sigma_o' + \sigma_o \dot{\varepsilon} \qquad (3\text{-}18)$$

Nadai and Manjoine [3.6] worked out a one-dimensional theory of neck development of a bar made of this material. Evidently, till the stress reaches σ_0^* in the maximum sections, no further deformation takes place according to the material law. The other sections of the bar where the stress is higher than σ_0^* will start to contract first at slow rate. After a certain finite time the portion near the minimum cross-section will start to contract rapidly and the deformation will be localized.

Ilyushin and Ishlinsky [3.7] by means of two-dimensional theory of visco-plasticity, studied the stability of the flow in a thin strip made of Bingham material under tension. They found the interesting result that specimens having an undeformed profile with shallow waves may or may not neck farther down in the narrowest sections. This was found to depend on the rates with which the specimens are stretched.

3.3.5 Non-linear viscous material ($m < 1$, $n=0$)

For a material with negligible strain-hardening but rate-dependence with $m < 1$, equation (3-14) indicates that the deformation is immediately unstable. It is of importance to determine how the initial geometric inhomogeneities develop during the unstable flow.

A physical picture can be obtained qualitatively if we consider bars of two materials having a different rate-sensitivity index, m, but at some instant the same non-uniformity in cross-sectional area as shown in Figure 3.1(a). In the narrow portion the stress in each bar is increased by the same amount of $\delta\sigma_1$ but from Figure 3.1(b) it may be seen that

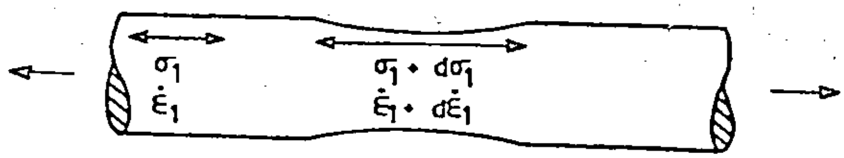

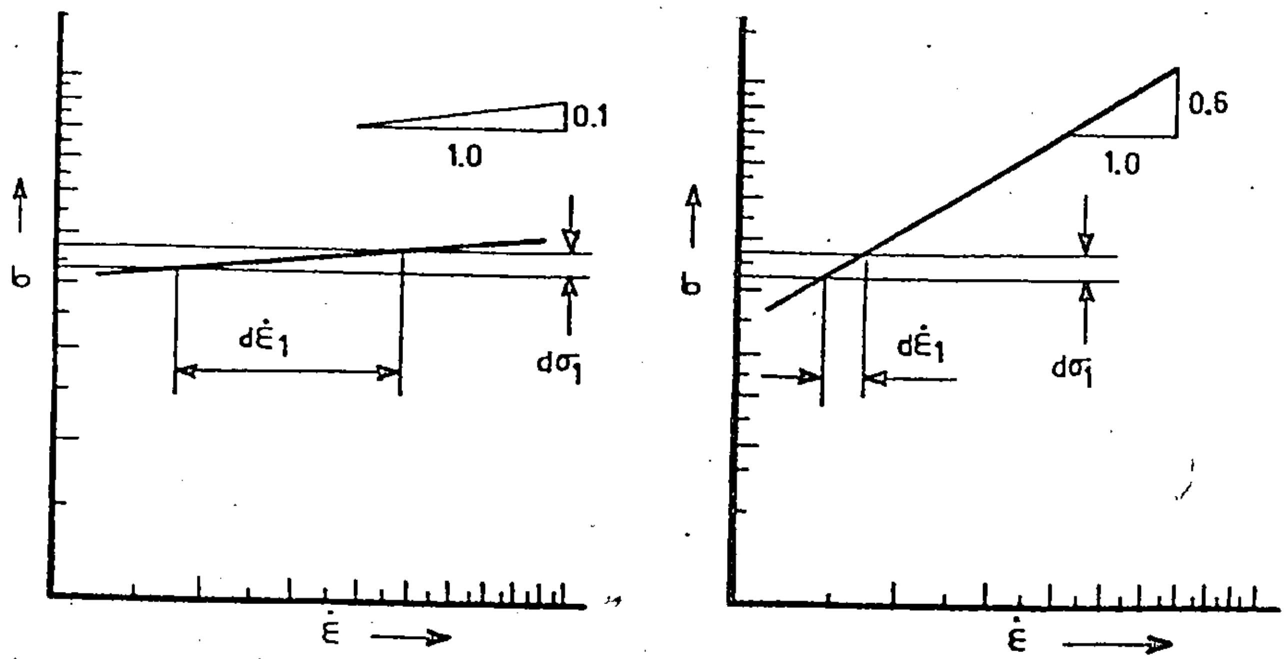

Fig. 3.1 Schematic diagram illustrating the dependence of the rate of growth of a geometrical non-uniformity in a tensile test-piece on the strain-rate sensitivity.

the difference in strain rate $\delta\dot{\varepsilon}_1$ for the material with low m is much greater. Therefore the non-uniformity in this will grow at a faster rate.

The progress of necking for a non-linear viscous material (m=0.1) was calculated by Hoff [3.8]. It was assumed that the cross-sectional area of the bar was 1% greater at the two ends than in the middle and the area varied along the bar according to a sine law. A state of one-dimensional stress was assumed through the analysis. The theoretical rupture times for intrinsic plastic failure were then calculated and found to correlate with experimental results.

An approximate relation describing the growth of a geometrical inhomogeneity in a tensile test of a non-linear viscous material was developed by few investigators. In analysis given below reference is made to that given by Duncan et al [1.23].

A tensile test strip of superplastic material is considered to have initially a uniform cross-sectional area, A_o, except for a short length in which the cross-section area differs by a small positive quantity δA_o. It is assumed that in the small inhomogeneity the material strains in uniaxial tension, i.e. triaxiality of stress is neglected.

At any instant the stress and strain rate σ and $\dot{\varepsilon}$ respectively in the bar and $(\sigma + \delta\sigma)$ and $(\dot{\varepsilon} + \delta\dot{\varepsilon})$ within the inhomogeneity and the cross-sectional area is A and $A + \delta A$.

By definition:

$$\dot{\varepsilon} = -\frac{1}{A}\frac{dA}{dt} \tag{3-19}$$

and

$$\dot{\varepsilon} + \delta\dot{\varepsilon} = -\frac{1}{\delta A + A}\frac{d(A + \delta A)}{dt} \tag{3-20}$$

From equilibrium

$$P = \sigma A = (\sigma + \delta\sigma)\ (A + \delta A) \tag{3-21}$$

The constitutive equation

$$\sigma = \sigma_o\ \dot{\varepsilon}^m$$

applied at the cross-sectional area $(A + \delta A)$ yields

$$(\sigma + \delta\sigma) = \sigma_o (\dot{\varepsilon} + \delta\dot{\varepsilon})^m \tag{3-22}$$

Combining equations (3-19) to (3-22) and neglecting the higher orders of δ, we arrive at

$$\frac{d\ (\delta A)}{dt} = (1 - \frac{1}{m}) \quad \frac{\delta A}{A}\ \frac{d\ A}{dt}$$

Integrating yields

$$\delta A = (\frac{A}{A_o})^{(1 - \frac{1}{m})} \quad \delta A_o \tag{3-23}$$

Equation (3-23) states that the growth of an original cross-section irregularity at certain value of strain is very sensitive to the value of m. If m = 1, equation (3-23) tells that the cross-section irregularities or incipient necks are simply preserved during pulling and hence if there are no disturbances there can be no necking.

Recently valuable experimental observations have been made by Wray [3.9] on the tensile plastic instability at an elevated temperature and its dependence upon strain-rate. The tests were conducted on tensile specimens made of indium-lead alloy at room temperature (0.69 Tm). This alloy at room temperature is strain-sensitive, non-strain hardening and exhibits an almost viscous behaviour especially at moderate strain-rates. The initial undeformed specimens had no significant deviations from the cylindrical shape. The change in specimen shape as tensile deformation proceeds was determined experimentally and the general features of the change of shape of deformed cylinders were as follows:

-- the deformation becomes non-uniform even at small strains,

-- not only one, but several necks may form along the length of the specimen.

The necks present along the cylinder were separated into active necks and dormant necks and accordingly, Wray was able to distinguish between two types of plastic instability. The first type is the formation of several active necks in a specimen previously deforming in a uniform manner. The second type involves the unstable situation that develops when a number of active necks are growing concurrently, almost at the same rate, and one neck becomes more active at the expense of the others until eventually intrinsic plastic failure takes place at this neck.

CHAPTER IV

POST-INSTABILITY TENSILE DEFORMATION OF SUPERPLASTIC ALLOYS

4.1 Introduction

In most tensile cold-working operations where the material is regarded as strain-hardening but not time-dependent, the deformation process is a stable one; the load generally rises continuously and initial non-uniformities in the workpiece do not develop catastrophically. The onset of instability is generally regarded as the end point of the process and this frequently coincides with the cessation of strain in certain regions and the rapid concentration of strain in an unstable or "necked" region.

Tensile superplastic forming operations on the other hand are unstable throughout the process; the load continually decreases and, of more importance, initial non-uniformities develop continuously from the start. Useful products can however be formed in these unstable processes [1.22] to [1.24] because the rate of growth of non-uniformities is slow and large deformations can be achieved before the thickness variation becomes technologically unacceptable.

A complete anlysis of the unstable tensile deformation of superplastic test-pieces does not appear to have been presented in the literature. In the work presented in this chapter, the material is assumed to follow the simple non-linear viscous model described by equation (2-29) [4.1]. Initial non-uniformities are assumed to be solely geometric in nature. Material parameters are those for common superplastic alloys and the size of non-uniformities are typical of those which would inevitably be present in commercially produced work-pieces.

Geometrical changes in two simple components loaded in tension are theoretically analyzed. One part is a slightly tapered tensile test-piece and the other is a non-uniform thin-walled tube expanded by internal pressurization. Experimental evidence supporting the theory is also given.

4.2 Theoretical Analysis

4.2.1 Uniaxial Tension of a Perfectly Uniform Test-Piece.

When a uniformly distributed tensile load is applied to the ends of a perfectly cylindrical bar of homogeneous material, the state of stress is one-dimensional and the bar deforms uniformly. Consider a tensile test-piece made of superplastic material which has a constitutive equation in the form

$$\left(\frac{\sigma_e}{\sigma_o}\right) = \left(\frac{\dot{\varepsilon}_e}{\dot{\varepsilon}_o}\right)^m \tag{4-1}$$

where σ_e is the representative stress

$\dot{\varepsilon}_e$ is the representative strain-rate

$\dot{\varepsilon}_o$ is a constant taken customarily as unity

σ_o is a material strength parameter

m is the strain-rate sensitivity index which is generally a function of $\dot{\varepsilon}$.

If P is the applied tensile load, which may vary throughout the test, the equilibrium equation is

$$P = A\,\sigma_e = \frac{\pi}{4}\,D^2\,\sigma_e \tag{4-2}$$

where A and D are the current cross-sectional area and current diameter of the specimen respectively.

The representative strain-rate, at any time t, is

$$\dot{\varepsilon}_e = \frac{1}{A}\frac{dA}{dt} = -\frac{2}{D}\frac{dD}{dt} \tag{4-3}$$

Combining equations (4-1), (4-2) and (4-3) yields

$$\frac{dD}{dt} + \frac{\dot{\varepsilon}_o}{2}\left(\frac{4P}{\pi\sigma_o}\right)^{\frac{1}{m}} D^{1-\frac{2}{m}} = 0 \tag{4-4}$$

If instead of equation (4-1) the experimental stress, strain-rate characteristic of the material is fitted by the hyperbolic-sine law,

$$\frac{\sigma}{\sigma_o} = \sinh^{-1}\left(\frac{\dot{\varepsilon}}{\dot{\varepsilon}_o}\right) \tag{4-5}$$

a similar analysis yields the following differential equation

$$\frac{dD}{dt} + \frac{\dot{\varepsilon}_o}{2}\sinh\left(\frac{4P}{\pi D^2\sigma_o}\right) D = 0 \tag{4-6}$$

Neither equations (4-4) nor (4-6), in this general form, are amenable to analytical integration. However, for most superplastic alloys, the values of the material parameters m and σ_o are usually constant over a limited range of strain-rate. Therefore, the equilibrium equation (4-4) can be integrated such that

$$\int_{t_o}^{t} - \left(\frac{\dot{\varepsilon}_o}{2}\right) \left(\frac{4P}{\pi \sigma_o}\right)^{\frac{1}{m}} dt = \frac{m}{2} D^{\frac{2}{m}} + C$$

where C is a constant of integration.

(a) Case of constant load test

Considering the case of a constant load test, $P(t) = P_o$, the diameter at any time t is determined by integrating equation (4-6) which yields

$$D = \left[D_o^{\frac{2}{m}} - \frac{\dot{\varepsilon}_o t}{m} \left(\frac{4P_o}{\pi\sigma_o}\right)^{\frac{1}{m}} \right]^{\frac{m}{2}} \tag{4-7}$$

where Do is the initial diameter of the test-piece. Following Hoff's definition [3.8], the rupture time t_R is the time needed to reach zero cross-section area and for the perfect bar this corresponds to infinite elongation. Hence from equation (4-7)

$$t_R = \frac{m}{\dot{\varepsilon}_o} \left(\frac{\pi\sigma_o D_o^2}{4 P_o}\right)^{\frac{1}{m}} \tag{4-8}$$

A plot of expression (4-7) is shown in Figure 4.1, for cylindrical bars made of the same superplastic material (m = 0.5) but for different initial diameters. The abscissa in this Figure represents a non-dimensional time which is equal to time t divided by the rupture time of a perfect

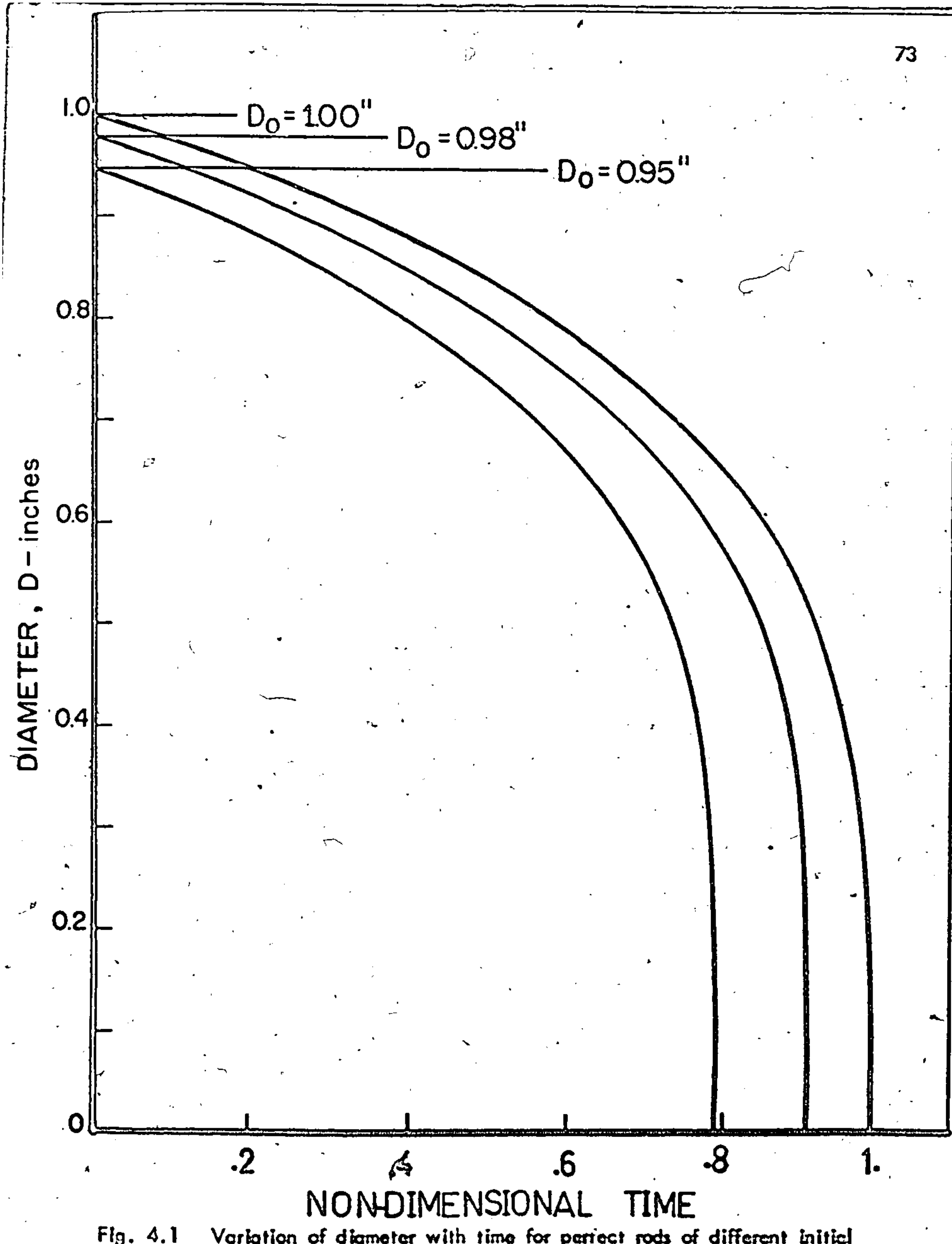

Fig. 4.1 Variation of diameter with time for perfect rods of different initial diameters under the action of a constant load. (P = 200 lbf, σ_o = 10,000 lbf/in^2 and m = 0.5).

bar of diameter Do = 1 inch. It is seen that a difference of 5% in the initial diameter of a test-piece would reduce its rupture time by about 20%.

An interesting result pertains to the effect of the strain-rate sensitivity in a constant load test. Figure 4.2 shows the variation of diameter with time calculated for perfect bars each having different values of m. The load on each bar was different and so chosen that the "rupture times" were all equal to, say, the rupture time of the specimen for which m = 0.5. Conventional alloys will have a value of m < 0.25 [1.13] and Figure 4.2 indicates that rapid acceleration of straining is to be expected in constant load tests after modest reductions of 10-20% in diameter. In superplastic alloys however where 0.5 < m <1.0 , much larger deformations are possible before the strain-rate accelerates appreciably and constant load test may therefore be quite appropriate for testing these alloys.

(b) <u>Controlled-rate tests</u>

The ordinary engineering tensile test is usually carried out with constant cross-head speed v_o. In this case

$$\dot{\varepsilon} = \frac{1}{\ell}\frac{d\ell}{dt} = \frac{v_o}{\ell} = -\frac{2}{D}\frac{dD}{dt} \tag{4-9}$$

$$\frac{dD}{dt} + \left(\frac{v_o}{2\ell_o D_o^2}\right) D^3 = 0 \tag{4-10}$$

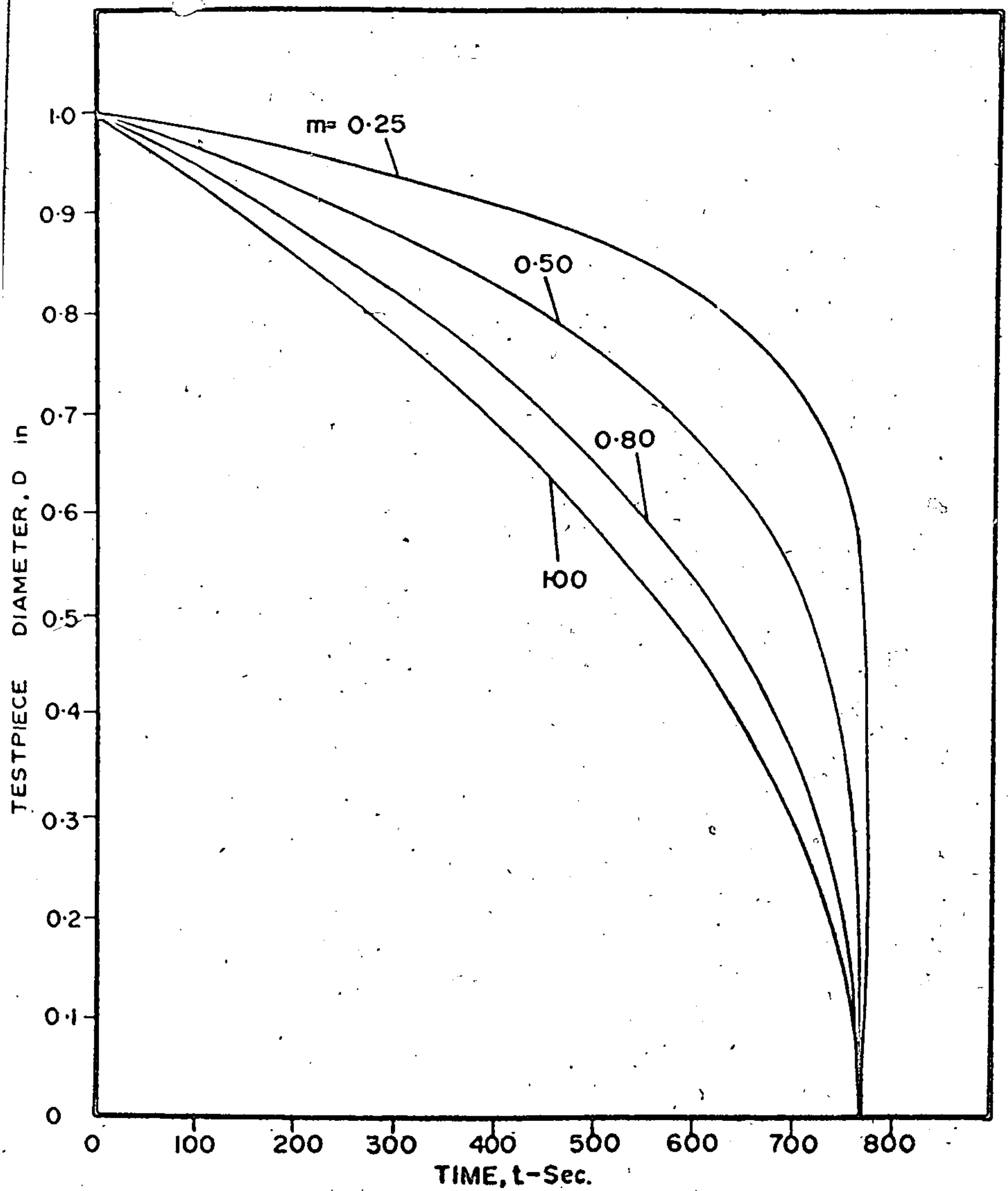

Fig. 4.2 Variation of diameter with time for perfect rods of different strain-rate sensitivity, m, under the action of a constant load.

where ℓ_o is the initial length of the specimen.

Integrating (4-10) yields an expression for the diameter D, at any time t, as

$$D = D_o \left(\frac{\ell_o}{\ell_o + v_o t}\right)^{\frac{1}{2}} \tag{4-10a}$$

Applying the equilibrium condition, the load-time relation is

$$P = \frac{\pi\sigma_o D_o^2}{4} \cdot \frac{\ell_o \quad v_o^{\ m}}{(\ell_o + v_o t)^{1+m}} \tag{4-10b}$$

Similarily, a constant strain-rate tensile test may be analyzed to arrive at the relations

$$D = D_o \exp(-\dot{\varepsilon}_c t/2) \tag{4-11a}$$

and

$$P = \frac{\pi \sigma_o D_o^2}{4} \dot{\varepsilon}_c^{\ m} \exp(\dot{\varepsilon}_c t) \tag{4-11b}$$

where $\dot{\varepsilon}_c$ is the constant strain-rate at which the test is performed. For the same initial strain-rate , $(\dot{\varepsilon})_{t=o}$ = .001 sec^{-1} the diameter-time curves of the three different cases of, constant load, constant cross-head speed and constant-strain-rate tests are illustrated in Figure 4.3

4.2.2 Tension of a Non-uniform Test-piece

In the following section, the growth of a slight geometrical non-uniformity present in axially loaded tensile test-pieces is theoretically investigated throughout the deformation process. The behaviour of the material of the test-piece is governed by equation (4-1).

The undeformed test-piece is considered as a straight-sided tapered bar of circular cross-section, Figure 4.4(a). The taper is assumed to be small and deformation to occur under a uniaxial stress state throughout. Neglecting the

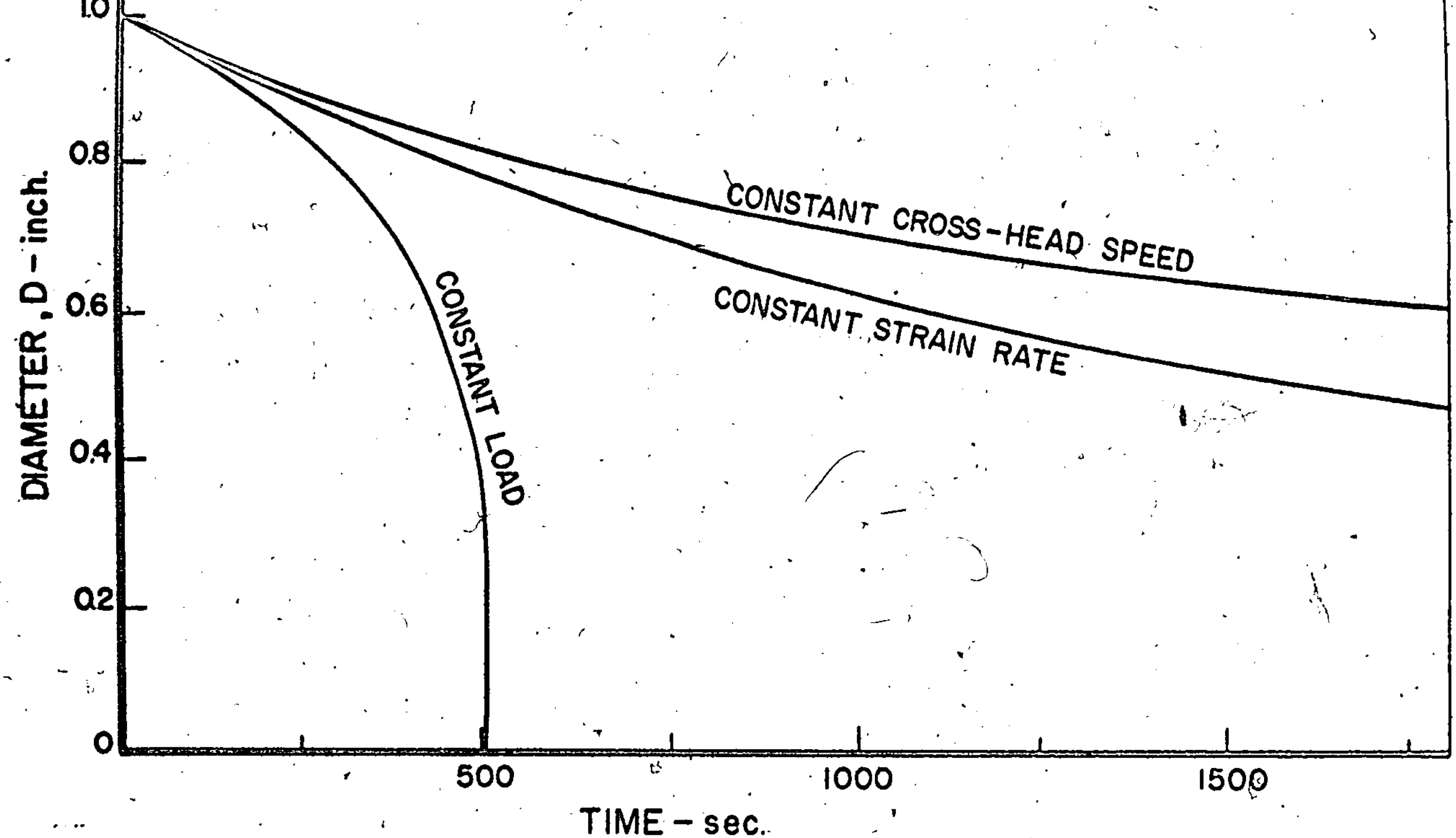

Fig. 4.3 Variation of diameter with time for perfect rods of superplastic material, m=0.5, stretched in different processes with the same initial strain-rate.

triaxiality of stress during the progress of the deformation process has been assumed by several other investigators [3.1], [3.6] and [3.8]. This assumption is justified since the experimental results of superplastic rods tested in tension show no localized reduction in area at any point along the rod, even at very large elongations.

The bar is divided into j elements of equal initial length $\Delta\ell$, Figure 4.4(b) which after the application of a load P for time Δt has deformed as shown in Figure 4.4(c). Assuming the volume of each element is constant, we obtain for the i^{th} element, at time $t = t_1$

$$\Delta\ell_{i,o}\,(D^2_{i,o} + D^2_{i+1,o} + D_{i,o}\,D_{i+1,o}) \qquad (4\text{-}12a)$$

$$= \Delta\ell_{i,1}\,(D^2_{i,1} + D^2_{i+1,1} + D_{i,1}\,D_{i+1,1})$$

The overall length is

$$\ell_1 = \sum_{i=1}^{j} \Delta\ell_{i,1} \qquad (4\text{-}12b)$$

and the percentage elongation is

$$E = \frac{\ell_o - \ell_1}{\ell_o} \times 100\% \qquad (4\text{-}12c)$$

(a) <u>Constant load test</u>

The equilibrium equation of the i^{th} cross section of the bar under load P_o was given before as

$$\frac{dD_i}{dt} + \left(\frac{\dot{\varepsilon}_o}{2}\right)\left(\frac{4\,P_o}{\pi\sigma_o}\right)^{\frac{1}{m}} D_i^{\,1-\frac{2}{m}} = 0 \qquad (4\text{-}13)$$

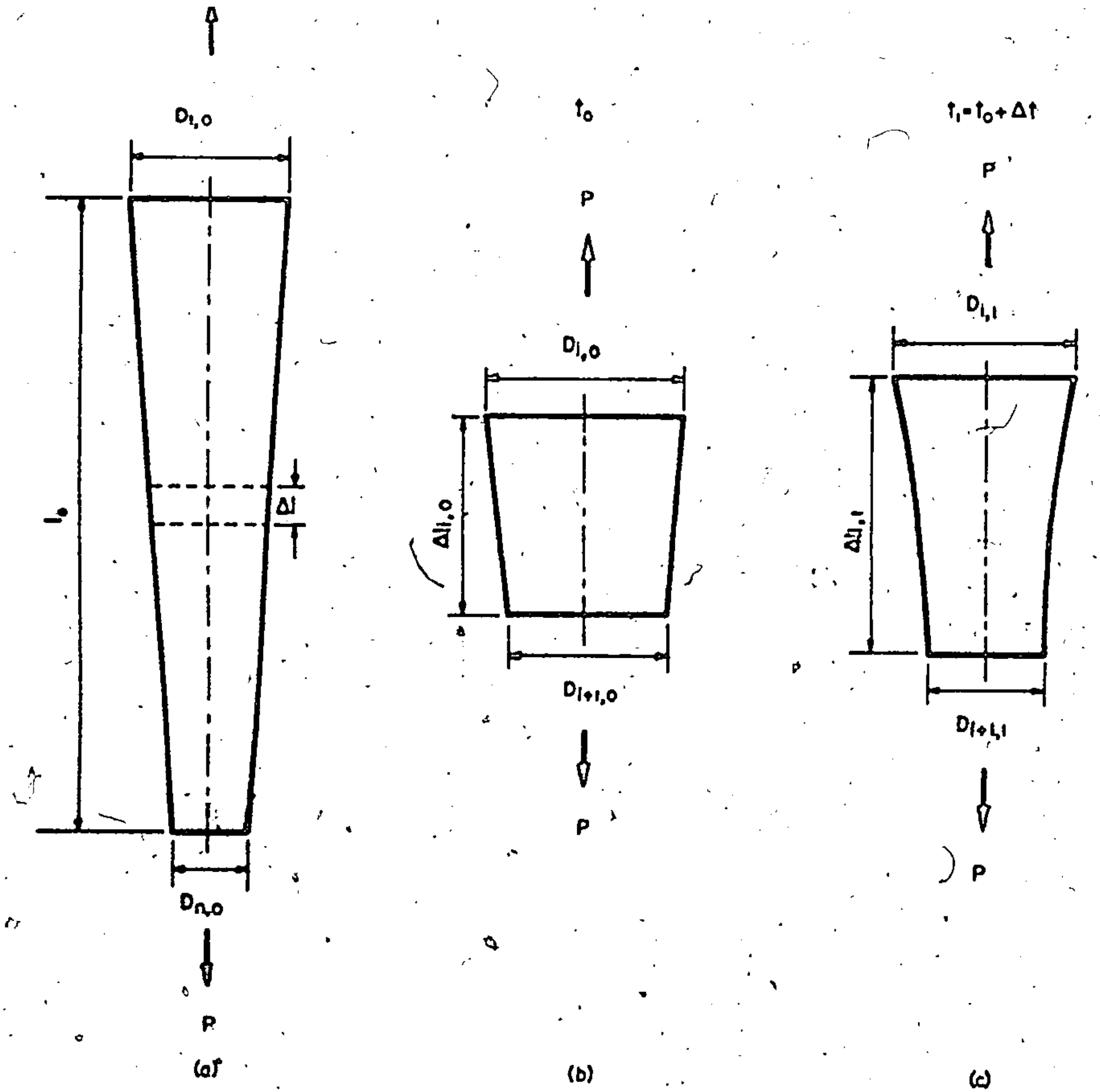

Fig. 4.4 Schematic diagram of (a) initial non-uniform tensile rod, (b) undeformed element, (c) deformed element.

In the case where the material parameters m and σ_o are assumed constant the integration of equation (4-13) yields for the i^{th} diameter at time t,

$$D_{i,t} = [D_{i,o}^{\frac{2}{m}} - \frac{\dot{\varepsilon}_o t}{m} (\frac{4 P_o}{\pi \sigma_o})^{\frac{1}{m}}]^{m/2} \qquad (4-14)$$

Both equations (4-12) and (4-14) define the deformed geometry of the bar at any instant, i.e. at any given total elongation E. In the case where m and σ_o are not constant throughout the deformation process, equations (4-13) may be solved numerically to obtain the deformed diameters. A computer program was written to handle the more general problem of uniaxial deformation of a non-uniform tensile test-piece with any form of initial geometrical inhomogeneity and whose material properties may be represented by constitutive equations other than the power law given by equation (4-1). This program is given in Appendix A-1.

(b) <u>Controlled-rate test</u>

In either constant cross-head speed or constant average strain-rate tests, the specimen length ℓ, is a simple prescribed function of time. The manner in which the specimen deforms may also be calculated from equation (4-13) except that for each time increment the appropriate value of P to give the prescribed length increase must be found by an iterative method.

The effect of the strain-rate sensitivity index m on the development of a non-uniformity is shown schematically in Figure 4.5. The undeformed bar was 1 inch diameter by 5 inch long with a difference in diameter of .01 inch. The difference in diameters for different m is shown for bars extended to approximately 500% elongation. (The width scale is exaggerated in this Figure). For the linear viscous material, m=1, the absolute difference in cross-section area from one end to the other does not alter and this agrees with an earlier analytical result [3.1], the proportional non-uniformity $\delta D/D_{max}$ will however increase as D_{max} becomes smaller. Figure 4.6 also shows similar results over a wider range and indicates the very rapid growth of a non-uniformity in non-superplastic materials i.e., for $m < 0.25$. On the other hand the same Figure shows that large elongations can be achieved with the least amount of non-uniformity if m is kept as high as possible i.e., $m > 0.6$. Figure 4.7 shows the strain-rate distribution along the length of the test-piece for different elongations. It is seen that the strain-rate at a given cross-section of the bar, increases continuously as the deformation proceeds. This, of course, is due to the viscous behaviour of the material as described by equation (4-1). It also explains the large elongations usually achieved in superplastic tensile processes, since at any stage of the process, each part of the test-piece contributes continuously and considerably to the final elongation. In non-superplastic materials after certain point, the deformation becomes localized in a small part, the neck, and virtually ceases in the adjacent parts; thus

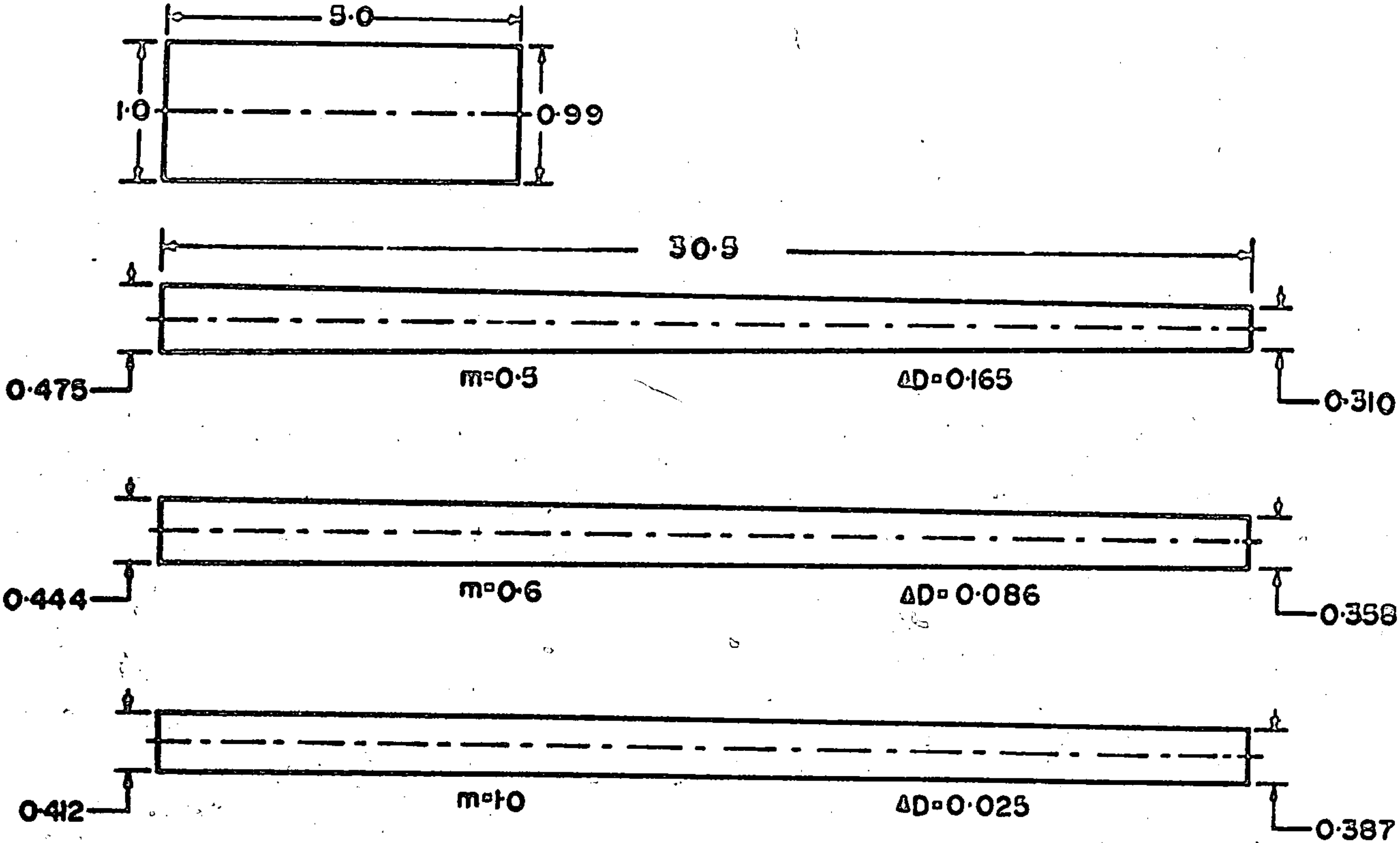

Fig. 4.5 Schematic diagram of tapered tensile rods of different strain-rate sensitivity elongated to 510% in simple tension.

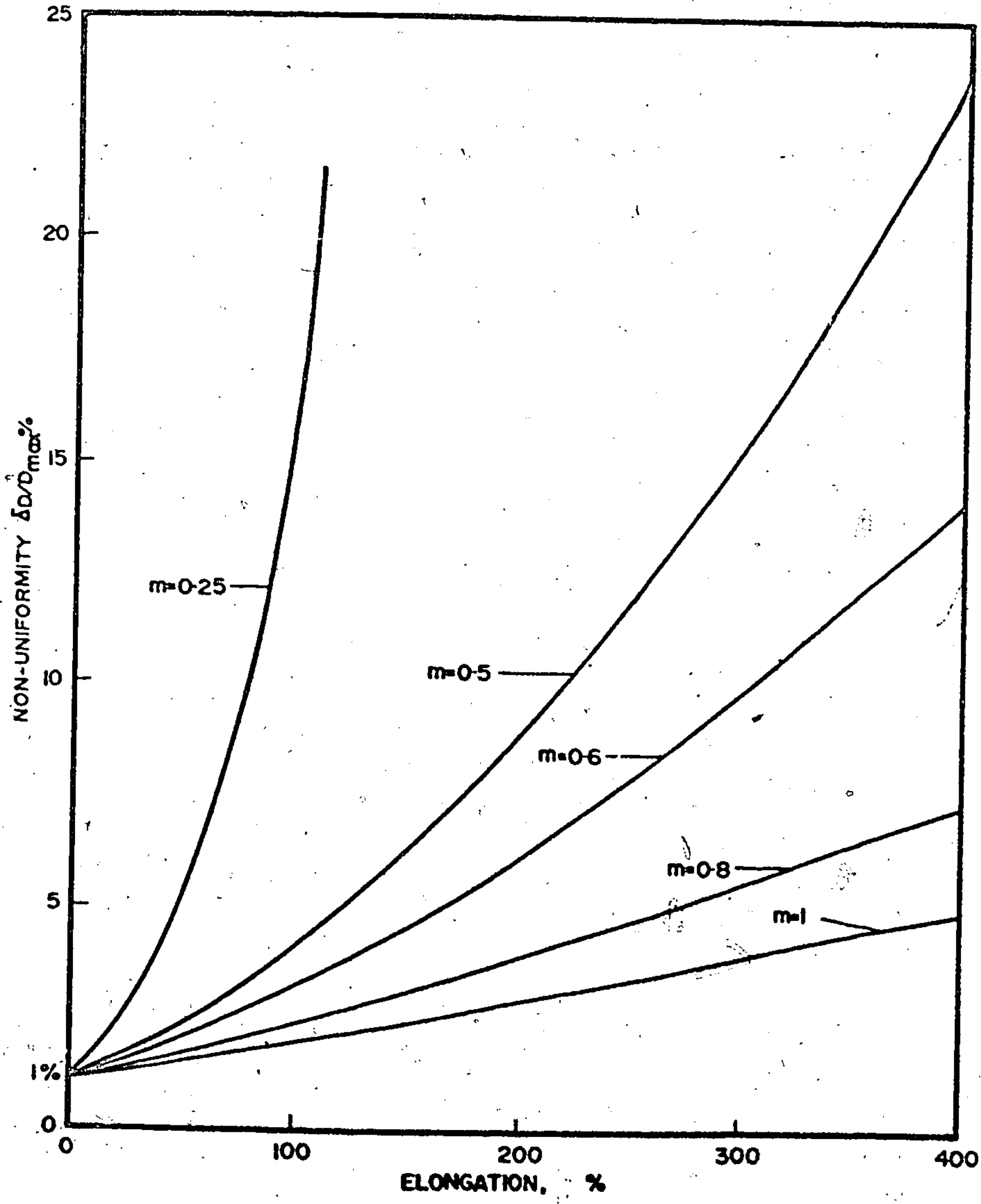

Fig. 4.6 Growth of non-uniformity, $(D_{max}-D_{min}) / D_{max}$, with total elongation for test-pieces having an initial non-uniformity of 1% and deformed under constant load.

rupture occurs at low elongations. The strain-rate distribution shown in Figure 4.7 demonstrates also the incorrectness of the statement that the increase in the flow stress at an incipient neck in superplastic material will cause the deformation to slow down in this region.

The rate at which different non-uniformities will develop as the bar elongates is shown in Figure 4.8 for a material having a strain rate sensitivity index, $m = 0.5$. The rate at which small non-uniformities develop is not large and it should be noted that the smallest value shown, 0.5%, is equivalent to an initial discrepancy of 1 thousandth of an inch in a bar of initial diameter of 0.2 inch. In general, the discrepancy in machined test-pieces would not exceed this value and may often be much smaller. The average strain-rate during the tensile deformation of a non-uniform test-piece is plotted versus elongation in Figure 4.9 for the three types of tests. It is easily seen that the average strain-rate in a constant load test increases by less than one order of magnitude for large elongations (250%) which again suggests that constant load test may be suitable for testing these materials.

4.2.3 Free Expansion of a Thin-Walled Concentric Tube by Internal Pressure.

Consider a perfectly-thin walled concentric tube made of superplastic material which deforms according to the power law given by equation (4-1). Assuming that thin-shell theory holds, the equations of equilibrium will suffice to determine the state of stress in the tube due to an internal pressure p, as follows:-

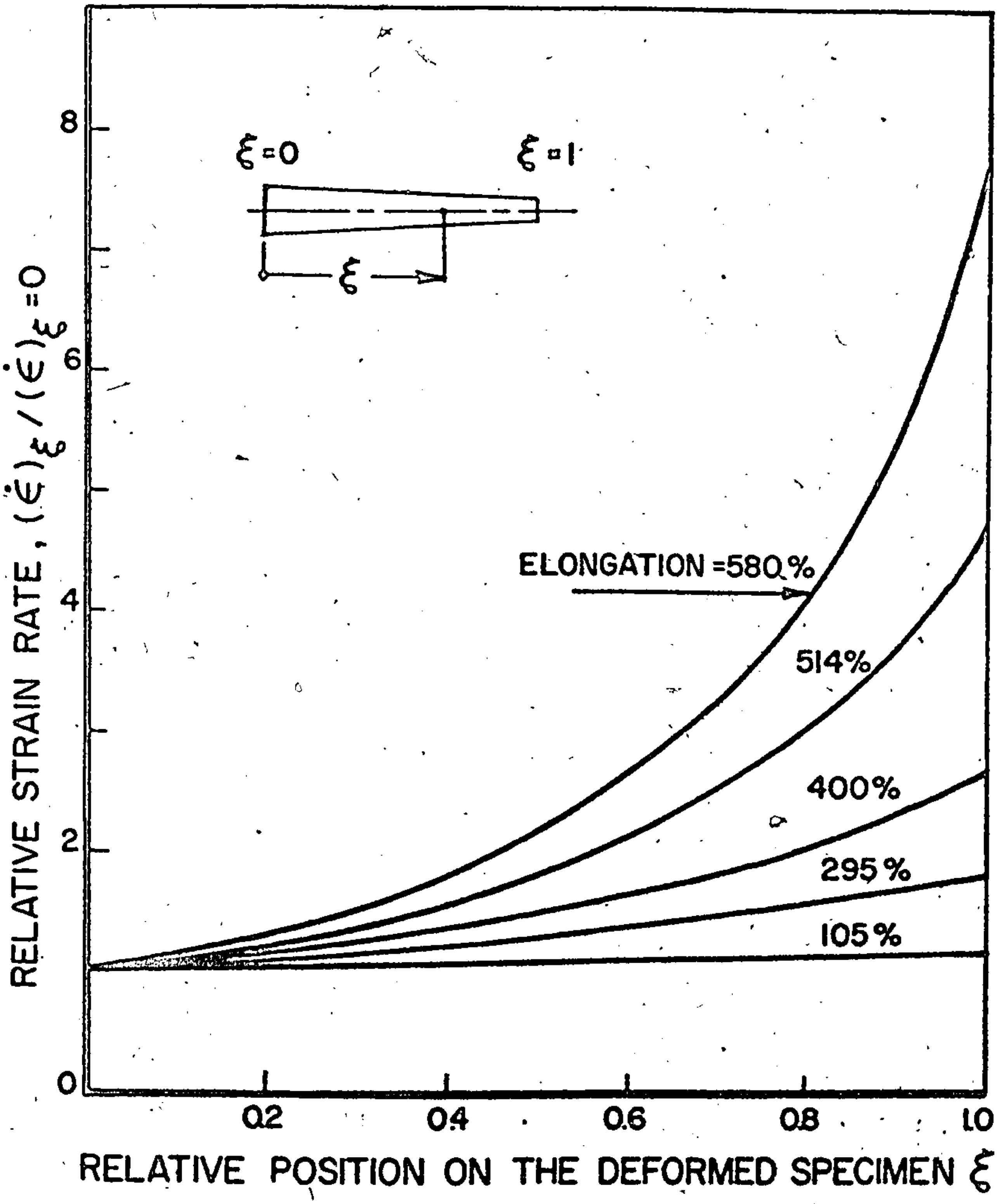

Fig. 4.7 Strain-rate distribution along the length of a superplastic tensile test-piece, m = 0.5, under the action of a constant load. The initial non-uniformity is 1%.

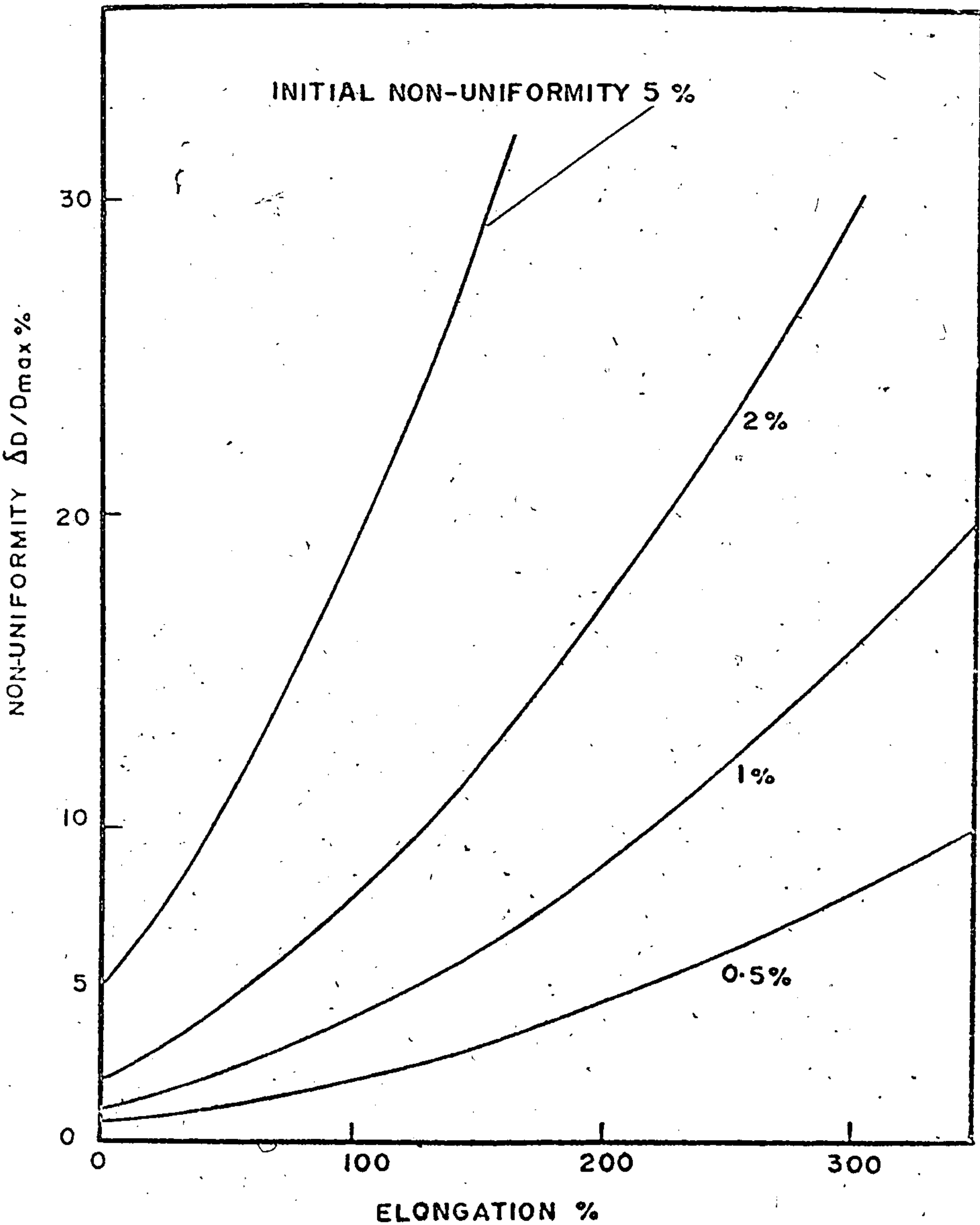

Fig. 4.8 Variation of non-uniformity with elongation under constant loads for bars of the same material, m = 0.5, but having different initial non-uniformity.

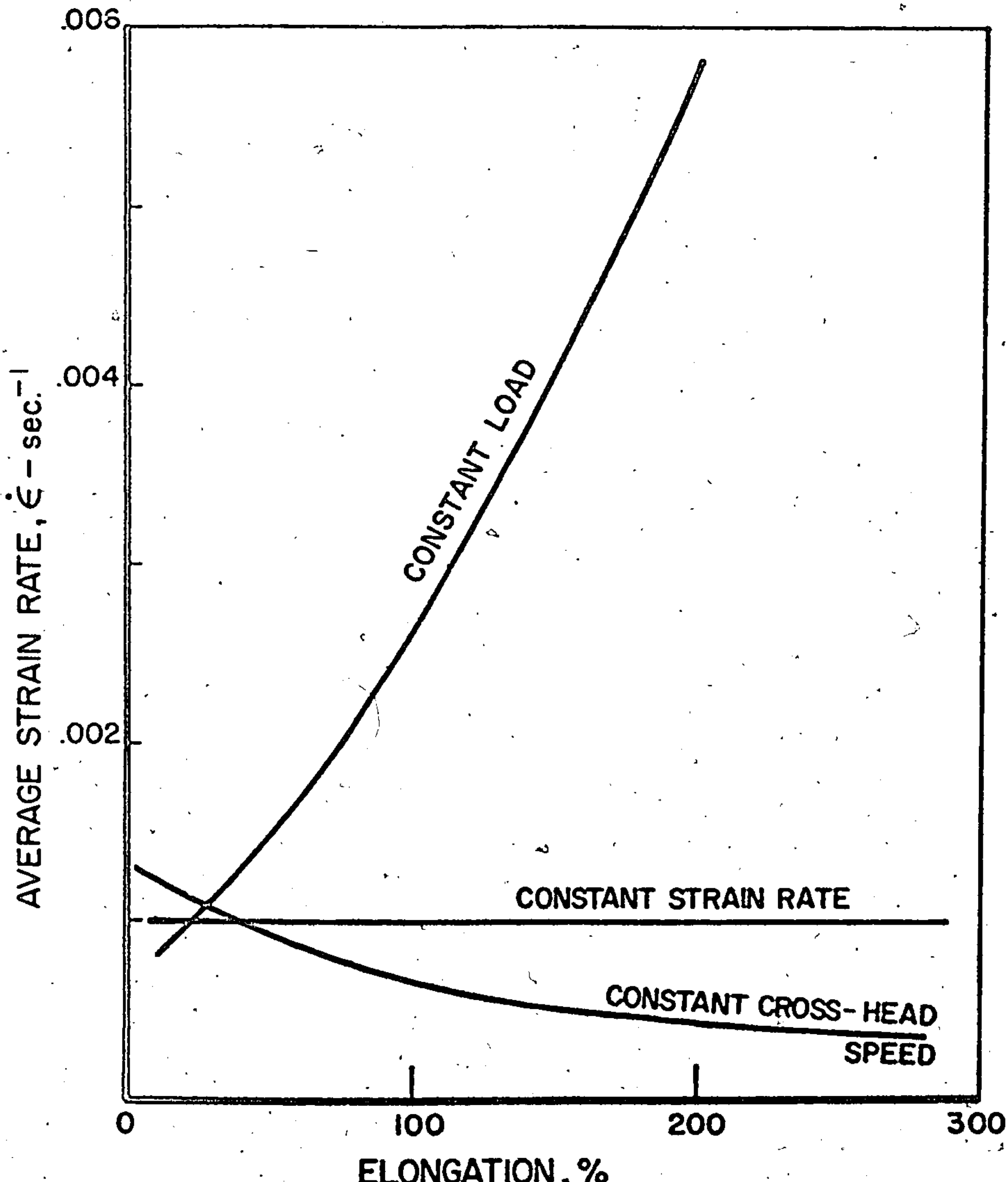

Fig. 4.9 Variation of average strain-rate with elongation for superplastic bars, $m = 0.5$, having the same initial non-uniformity 1% but stretched in different processes.

the hoop stress resultant is,

$$N_\theta = p r_m \tag{4-15a}$$

and the axial stress resultant is,

$$N_a = p r_m / 2 = N_\theta / 2 \tag{4-15b}$$

where r_m is the current mean radius of the tube. The representative stress σ_e is thus, given by

$$\sigma_e = \frac{\sqrt{3}\, N_\theta}{2\, h} = \frac{\sqrt{3}\, p r_m}{2\, h} \tag{4-16}$$

where h is the current thickness of the tube. For a long tube, the deformation is plane strain and the axial strain-rate $\dot{\varepsilon}_a = 0$. Therefore the volume constancy condition is

$$\dot{\varepsilon}_\theta + \dot{\varepsilon}_h = 0 \tag{4-17}$$

where $\dot{\varepsilon}_\theta$ is the hoop strain rate and $\dot{\varepsilon}_h$ is the thickness strain-rate. The representative strain-rate $\dot{\varepsilon}_e$ is

$$\dot{\varepsilon}_e = \frac{2}{\sqrt{3}}\, \dot{\varepsilon}_h = -\frac{2}{\sqrt{3}}\, \frac{1}{h}\, \frac{dh}{dt} \tag{4-18}$$

Substitution of equation (4-16) and equation (4-18) into the constitutive equation (4-1) yields the differential equation

$$\frac{\sqrt{3}\, \dot{\varepsilon}_o}{2} \left(\frac{\sqrt{3}\, p r_m}{2\, h\, \sigma_o} \right)^{\frac{1}{m}} + \frac{1}{h}\, \frac{dh}{dt} = 0 \tag{4-19}$$

Using the incompressibility condition

$$r_m = r_{m,o} \frac{h_o}{h} \tag{4-20}$$

where $r_{m,o}$ is the undeformed mean radius of the tube, equation (4-19) takes the form

$$\frac{dh}{dt} - \dot{\varepsilon}_o \left(\frac{\sqrt{3}}{2}\right)^{1+\frac{1}{m}} \left(\frac{p r_{m,o} h_o}{2\sigma_o}\right)^{\frac{1}{m}} h^{1-\frac{2}{m}} = 0 \tag{4-21}$$

The solution of the above equation in conjunction with equation (4-20) defines the deformed geometry (the mean radius and the thickness) of the tube at any time t. For cases where m and σ_o are constants, the solution of equation (4-21) is obtained analytically but otherwise a numerical technique must be employed.

(a) Case of constant pressure

For the case of constant internal pressure $p = p_o$, the solution of equation (4-21), assuming constant m and σ_o is

$$h = h_o \left[1 - \frac{\sqrt{3}\, t}{m} \left(\frac{\sqrt{3}\, r_{m,o} p_o}{2 h_o \sigma_o}\right)^{\frac{1}{m}}\right]^{m/2} \tag{4-22}$$

The theoretical rupture time, assuming complete ductile failure, is determined by setting $h=0$ in equation (4-22)

$$t_R = \frac{m}{\sqrt{3}} \left(\frac{2 h_o \sigma_o}{\sqrt{3}\, r_{m,o} p_o}\right)^{\frac{1}{m}} \tag{4-23}$$

Obviously the rupture time decreases as the strain-sensitivity index m decreases.

(b) Case of constant strain-rate

An equivalent differential form of equation (4-16) is

$$\frac{d\,\sigma_e}{\sigma_e} = \frac{dp}{p} + 2\,\frac{dr}{r} \tag{4-24}$$

If the tube expands at constant strain-rate, σ_e will remain constant and thus $d\sigma_e = 0$. Hence integration of (4-24), making use of the initial condition, yields

$$p = p_o\,\left(\frac{r_{m,o}}{r_m}\right)^2 = p_o\,\left(\frac{h}{h_o}\right)^2 \tag{4-25}$$

where p_o is the initial pressure. Substituting equation (4-25) into equation (4-21) and integrating gives

$$h = h_o \exp\left[-\left(\frac{\sqrt{3}}{2}\right)^{1+\frac{1}{m}} \left(\frac{p_o\, r_{m,o}}{2\,\sigma_o\, h_o}\right)^{\frac{1}{m}} t\right] \tag{4-26}$$

Figure 4.10 shows the variation of the thickness with time in the two processes of constant load and constant strain-rate expansion of a tube of superplastic material of m = 0.5.

4.2.4 Free Expansion of a Thin-Walled Eccentric Tube by Internal Pressure.

A thin-walled tube of a superplastic alloy can be expanded by internal pressure to many times its initial diameter [1.23] as shown in

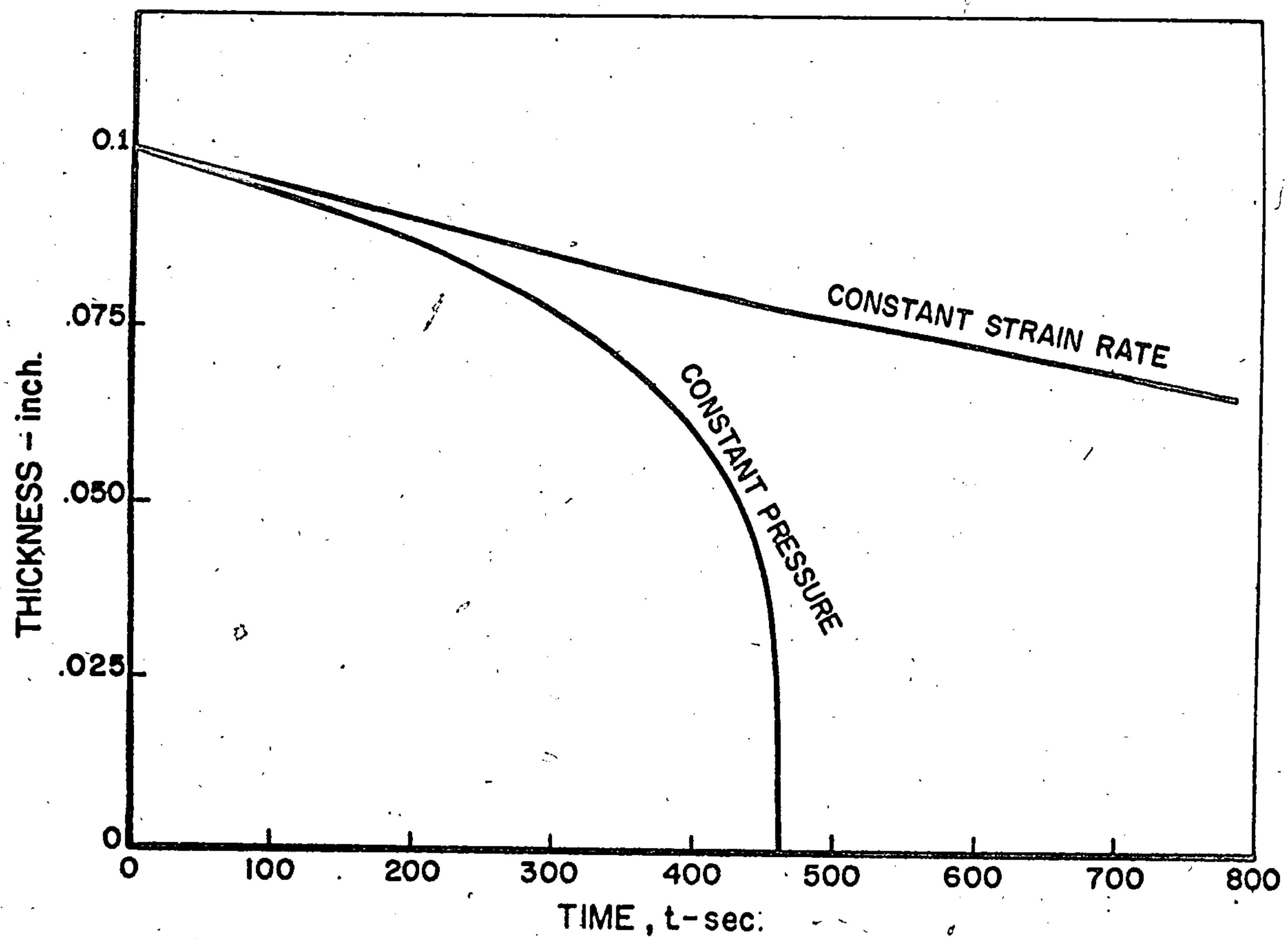

Fig. 4.10 Variation of thickness with time for perfect superplastic tubes, m=0.5, expanded by internal pressure in two different processes.

Figure 4.11. One type of non-uniformity is evident in the photograph, namely the variation in diameter along the length of the tube. A tube of strain-hardening material will, up to a point, remain cylindrical during expansion whereas in the superplastic tube a section where the diameter is slightly greater than elsewhere will expand faster and the bulbous shape will gradually develop. A second type of non-uniformity can be observed on a normal section of such a tube; regions which are locally thin will strain faster and non-uniformities in the wall thickness will develop around the circumference.

Extreme expansions as shown in Figure 4.11 are not attempted industrially but diameter increases of 2-3 times may be required and the variation of wall thickness is a technologically important consideration.

The initial geometry of the tube analyzed in this work is shown schematically in Figure 4.12. The mid wall line of the tube section is assumed to be of radius $r_{m,o}$. The wall thickness at any point is easily calculated from the other gemetrical quantities shown in Figure 4.12. In addition to the assumptions mentioned throughout the analysis of the concentric tube, the following assumptions are made:-

— the cross-section is initially uniform axially and remains so during expansion.

— the mid-wall line is, at any instant, a circle of radius r_m. Experimental evidence indicates that this assumption is valid up to reasonably large diametral expansions.

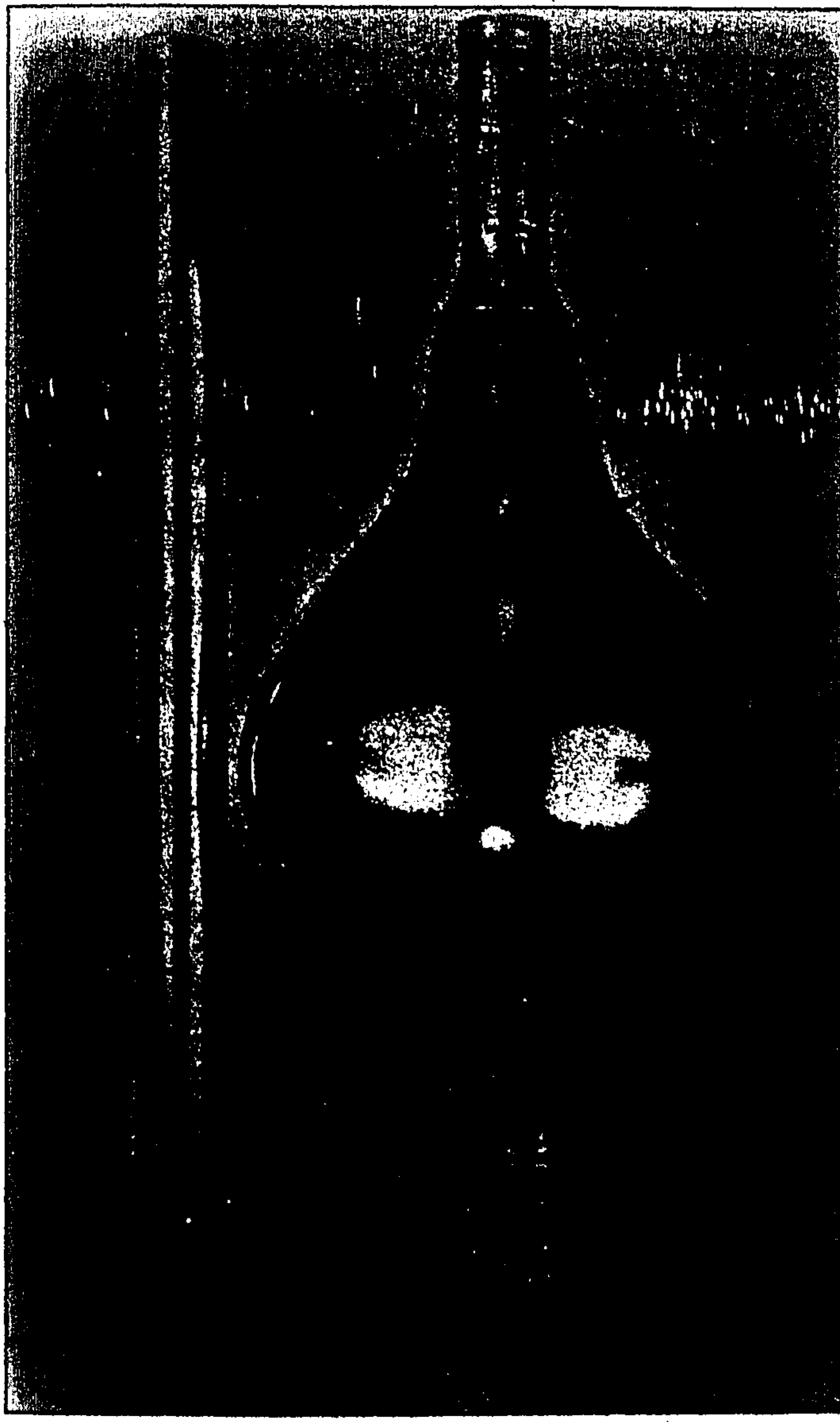

FIG. 4.11 - FREE EXPANSION OF LEAD-TIN SUPERPLASTIC TUBE BY INTERNAL PRESSURIZATION [REF. 1.23]

— The eccentricity is small with respect to the mean radius so that bending and shear stresses are negligible [1.22].

The plasticity theories given in section 2.4 and constitutive equation (4-1) are employed and a numerical analysis is performed by considering the deformation of a large number of elements each subtending an equal angle $\Delta\theta$ initially. The initial thickness of each element h_o is readily determined from the initial geometry, Figure 4.12. Assuming the volume of each element remains constant, we obtain at time $t_1 = t_o + \Delta t$, the condition,

$$\frac{h_{i,o} + h_{i+1,o}}{2} r_{m,o} \cdot \Delta\theta_{i,o} = \frac{h_{i,1} + h_{i+1,1}}{2} r_{m,1} \cdot \Delta\theta_{i,1} \tag{4-27}$$

With the above assumptions, the circumferential and axial stress resultants are

$$N_\theta = p\, r_{m,1} \tag{4-28}$$

$$N_a = N_{\theta/2} \tag{4-29}$$

where N_θ is constant around the circumference at any instant. The equilibrium equation for the i^{th} thickness is

$$\frac{dh_i}{dt} - \left(\frac{\sqrt{3}}{2}\right)^{1+\frac{1}{m}} \dot{\varepsilon}_o \left(\frac{p r_{m,o} h_o}{2\sigma_o}\right)^{\frac{1}{m}} h_i^{1-\frac{2}{m}} = 0 \tag{4-30}$$

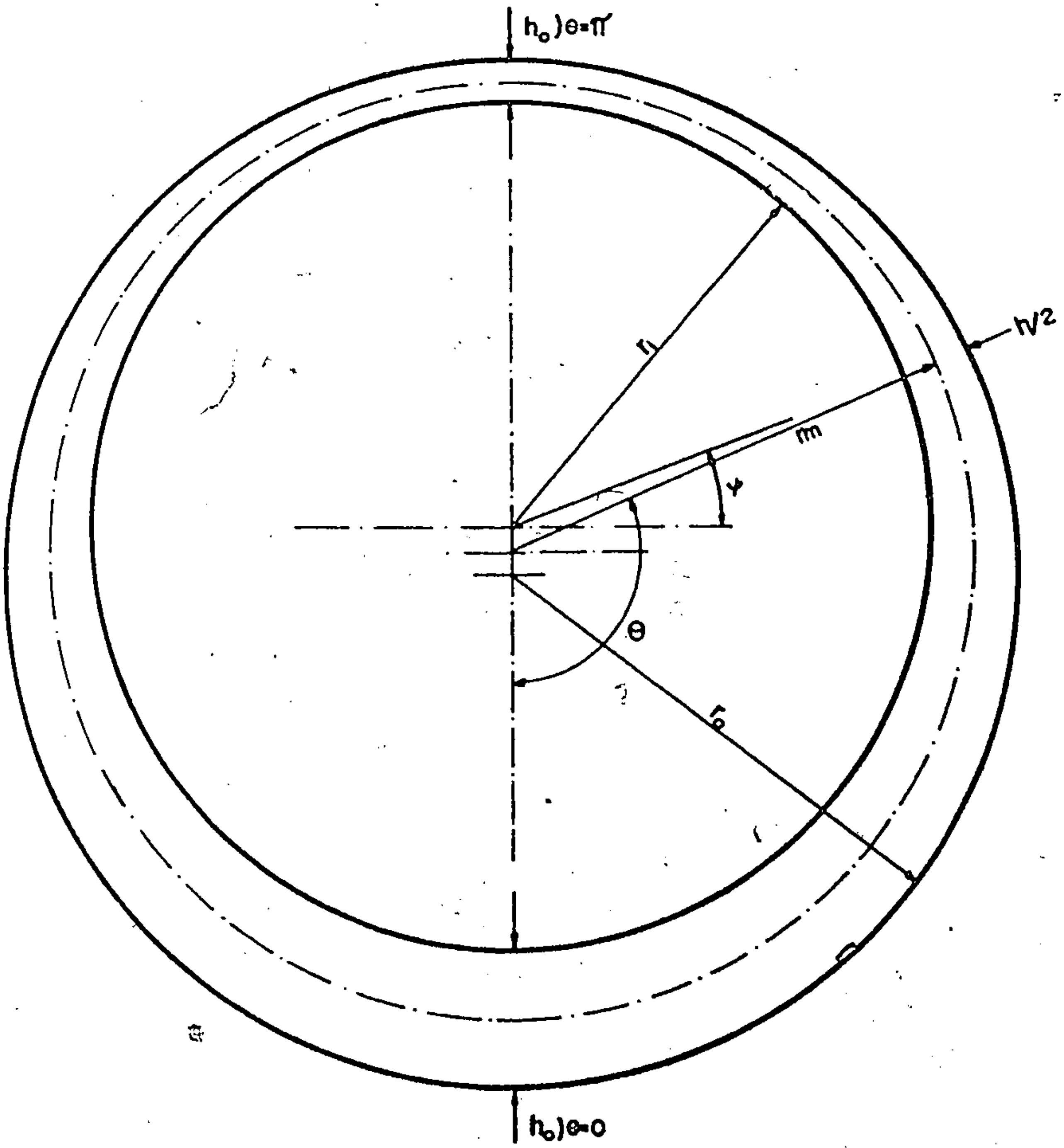

Fig. 4.12 Schematic section of the undeformed non-uniform tube.

To solve equations (4-27) and (4-30), in a general case, an increase in the mean radius is assumed for a given pressure p applied for a time Δt. Values of $h_{1,1} \ldots h_{j+1,1}$ and $\Delta\theta_{1,1} \ldots \Delta\theta_{j,1}$ are obtained and the solution is considered correct if $\sum_{i=1}^{j} \Delta\theta_i = \pi$

If this condition is not satisfied the correct value for $r_{m,1}$ is found by an iterative method. This method of solution is suitable in cases where the pressure p is an unknown function of time or when the material parameters m and σ_0 are functions of the strain-rate. However in the case of constant pressure expansion of a tube made of superplastic alloy of constant material parameters, the current thickness h_i is simply given by

$$h_{i,t} = h_{i,o} \{1 - \frac{\sqrt{3}t}{m} (\frac{\sqrt{3} r_{m,o} P_o}{2h\sigma_o})^{\frac{1}{m}}\}^{m/2} \tag{4-31}$$

The result of a typical calculation is shown schematically in Figure 4.13. The wall thickness is shown to an exaggerated scale and the case analyzed is a tube of 4 in. diameter by 0.1 in wall thickness expanded to a final diameter of 8 in. The thickness variation is defined by

$$H = (h_{max} - h_{min}) / h_{av} \ \%$$

which in this example was initially 10%. The diametral expansion, defined by, $R_e = (r_{m,t} - r_{m,o}) / r_{m,o}$ % was 100%. The prescribed process in this example was one of constant mean strain-rate; the value of m for the material was 0.5 and the initial and final wall thickness is shown for various points around the tube. It will be observed that except for points on the axis of symmetry, the trajectory of a point has both a radial and tangential component.

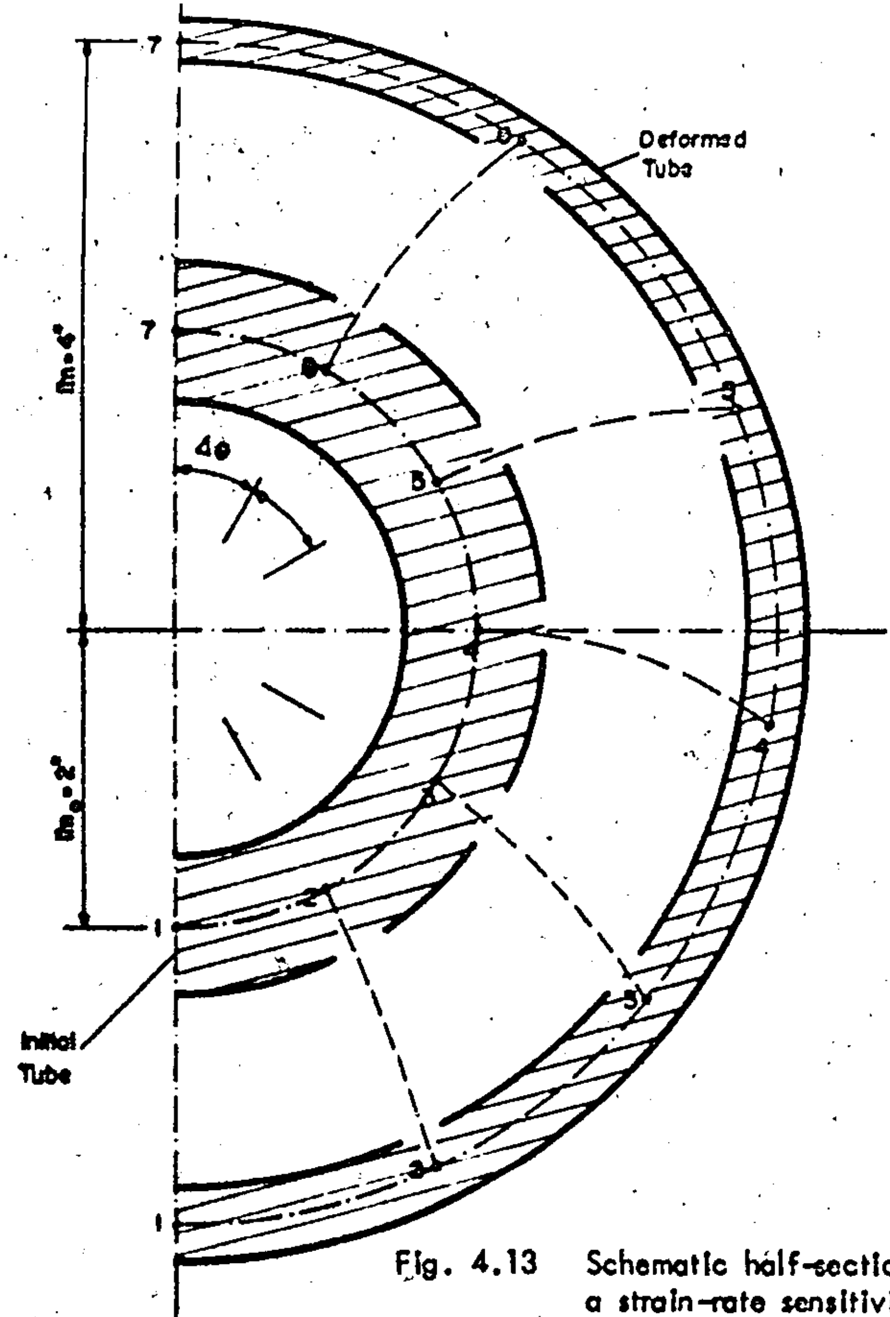

	h_o	h
1	0·105	0·060
2	0·104	0·059
3	0·103	0·056
4	0·100	0·051
5	0·098	0·046
6	0·096	0·041
7	0·095	0·040

Fig. 4.13 Schematic half-section of the initial and deformed tube. The material has a strain-rate sensitivity of m=0.5, and the initial non-uniformity is 10% (the thickness is shown to an exaggerated scale).

In the examples considered the geometry of the tube was not dependent on the type of loading process chosen and for convenience a constant pressure loading process was chosen for subsequent examples rather than constant strain-rate or constant-rate of diametral expansion. In Figure 4.14, the wall thickness variation is shown for different values of m. The initial thickness variation was 10% and this doubles after only 15% expansion for the non-superplastic tubes, $m < 0.25$. For a superplastic tube, $m = 0.8$, an expansion of 70% can be achieved for the same increase in non-uniformity. The influence of initial thickness variation in a tube having $m = 0.5$ is shown in Figure 4.15. In commercially produced tube, the initial thickness variation would probably be between 2 and 5% and the example shows that this would increase by a factor of about three for an expansion of 100%.

Similar to the results obtained in a tensile test of a non-uniform test-piece, the thickness strain-rate becomes higher at the thin points of the tube than that at the thick ones. Figure 4.16 illustrates the thickness strain-rate variation around the tube for different diametral expansions. This justifies the statement that, unlike conventional metals, straining does not become concentrated in the incipient neck; it merely proceeds at a higher rate and large deformations occur in all parts of the deforming body before rupture takes place.

Figure 4.17 shows the variation of the non-dimensional average thickness strain-rate $\dot{\varepsilon}_h$ during a constant pressure expansion process. It

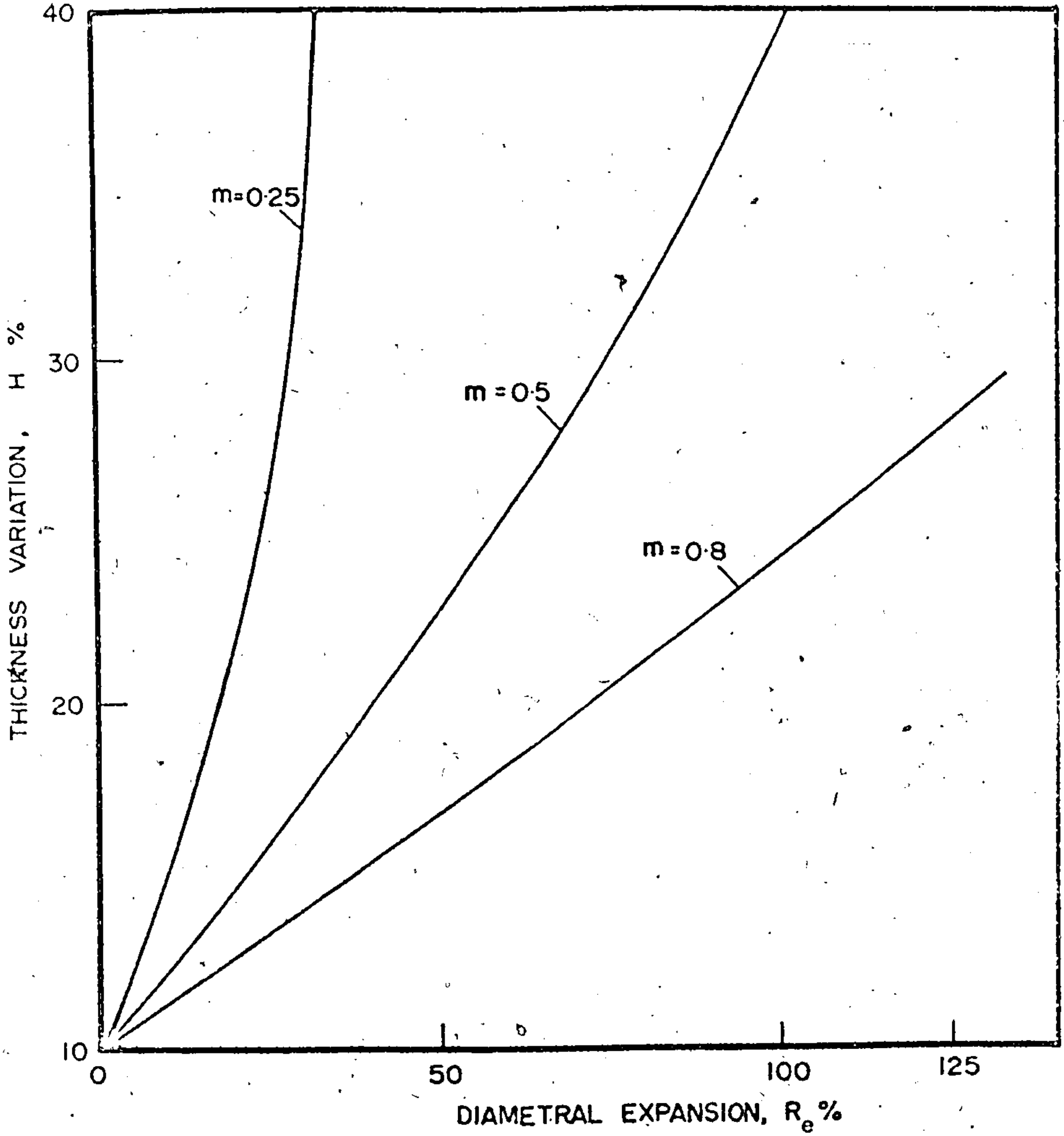

Fig. 4.14 Diagram showing the effect of strain-rate sensitivity, m, on the increase of non-uniformity of wall thickness during expansion.

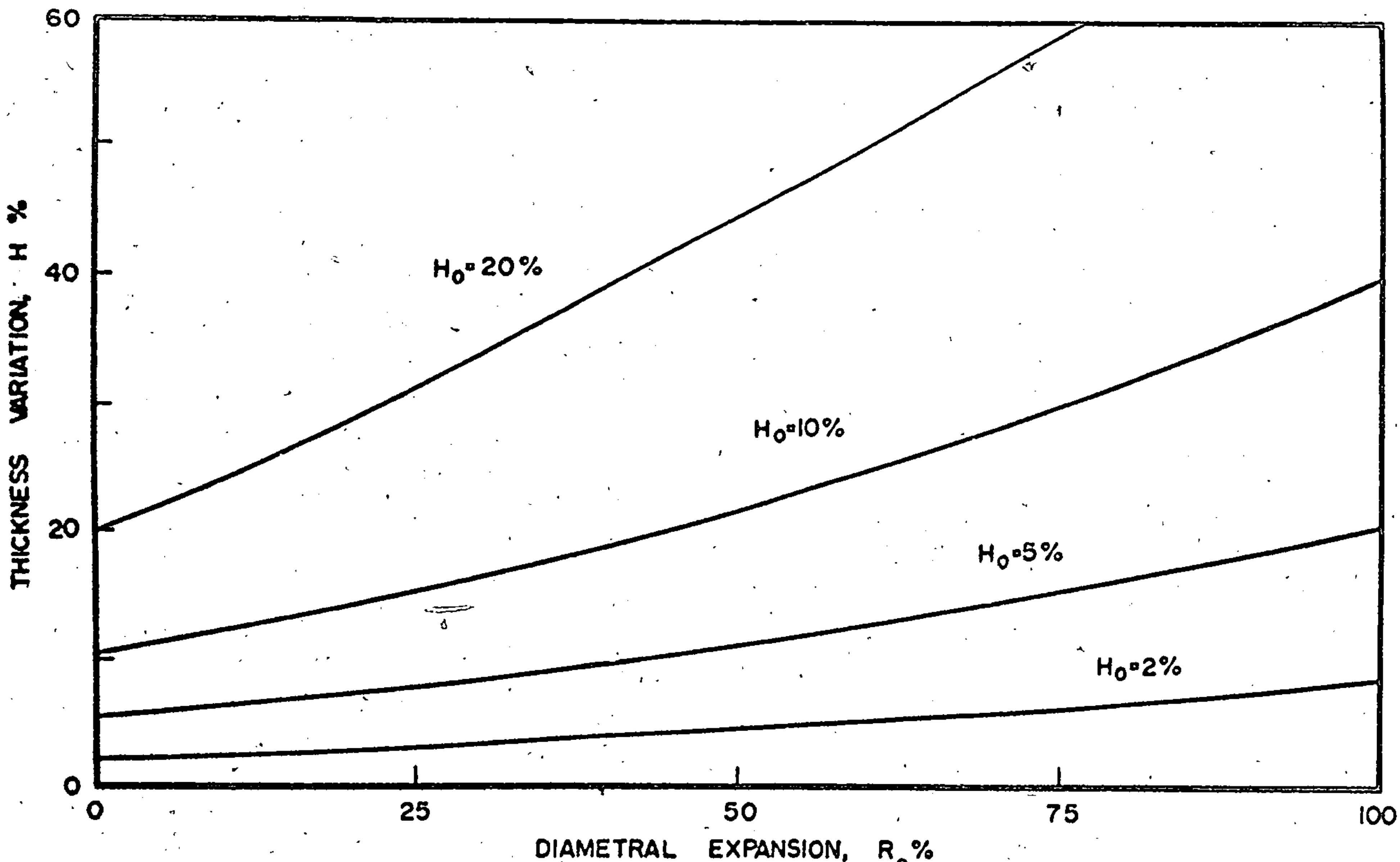

Fig. 4.15 Increase in non-uniformity with expansion for tubes of the same material, m=0.5, but different initial non-uniformity.

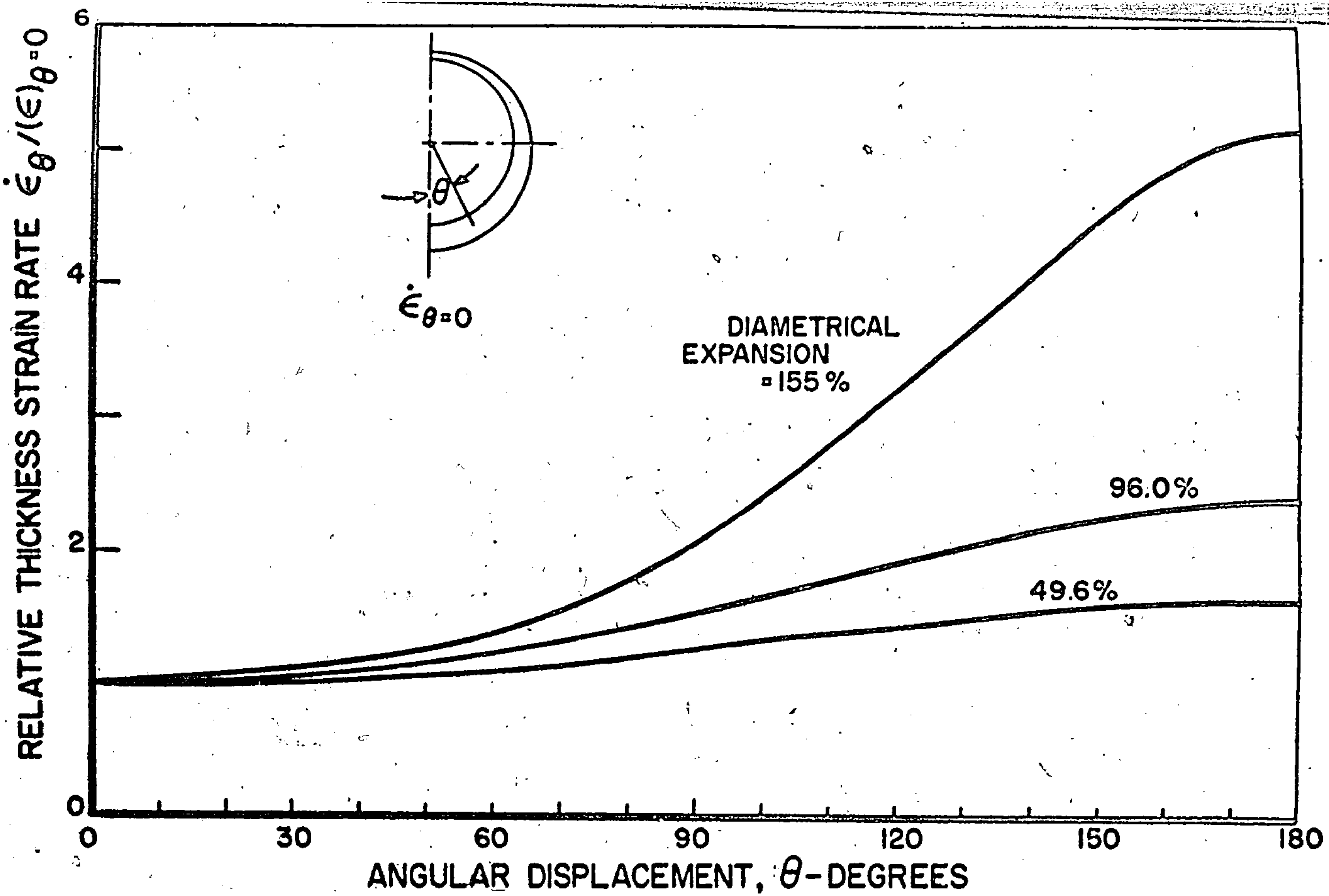

Fig. 4.16 Thickness strain-rate distribution around thin superplastic tube, m=0.5, expanded by constant internal pressure. The initial thickness non-uniformity is 10%.

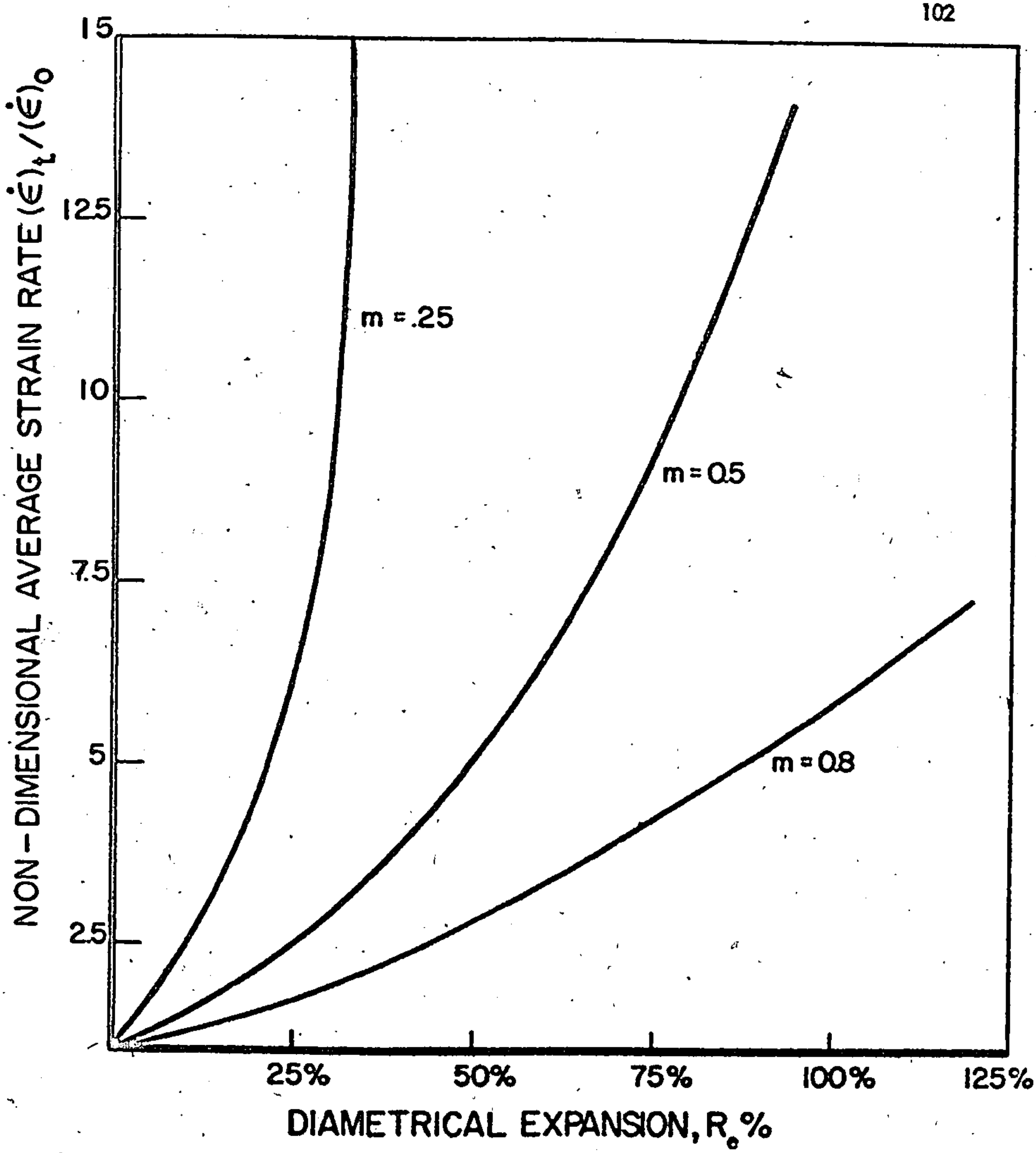

Fig. 4.17 Diagram showing the effect of strain-rate sensitivity, m, on the increase of average thickness strain-rate during the expansion of a thin non-uniform tube of internal pressure.

is seen that the change in $\dot{\varepsilon}_h$ does not exceed one order of magnitude up to diametral expansions of 75% for a typical superplastic alloy ($m = 0.5$).

4.3 Experimental Work

4.3.1 Constant Cross Head Speed Tensile Tests of Uniform Test-Pieces.

This section describes the results of experiments performed to determine the behaviour of the Zinc-Aluminum eutectoid alloy. The material parameters σ_o and m in the power law

$$\left(\frac{\sigma}{\sigma_o}\right) = \left(\frac{\dot{\varepsilon}}{\dot{\varepsilon}_o}\right)^m \qquad (4\text{-}1)$$

were obtained from constant cross-head speed tests. The determination of these material parameters is essential in investigating the tensile deformation of non-uniform tensile test specimens.

(a) Material and specimen preparation

The material tested was an eutectoid zinc-aluminum alloy (78% Zn - 22% Al). In order to produce the ultra-fine grain structure required for superplasticity [4.2], cast slabs were homogenized at 360°C for a minimum of 8 hours. They were then hot-rolled at a temperature above 280°C to about 90% reduction. The resulting sheets were solution-treated at 340°C for about 2 hours and quenched for 30–40 seconds in agitated ice-cold water. The sheets were then cold-rolled to the final dimensions of 3 foot square by .085 inch thickness.

Tensile test specimens were accurately machined by milling from the superplastic sheets. Small cuts and adequate coolant were used in the milling process to ensure that the material properties remained unaltered. The dimensions of the test specimens are shown in Figure 4.18 (a). The specimen wide shoulders were necessary to minimize the deformation within the grips during the tensile test. Three sets of specimens were prepared and the first set was tested in the as-received condition while the second set was annealed and the last set quenched. The annealing process was performed by keeping the specimens in a heated furnace at 360°C for 6 hours and then allowing them to cool down, in the furnace, to room temperature. The quenching process consisted of the same homogenizing procedure followed by quenching in agitated ice-cold water for about 30 seconds. The microstructures of three material conditions are shown in Figure 4.20. A gauge length of 1.25 inch was scribed on all the specimens and measurements of the thickness and width were recorded.

(b) Test procedure

In order to determine the material parameters, constant cross-head speed tests were performed using an Instron machine. The testing

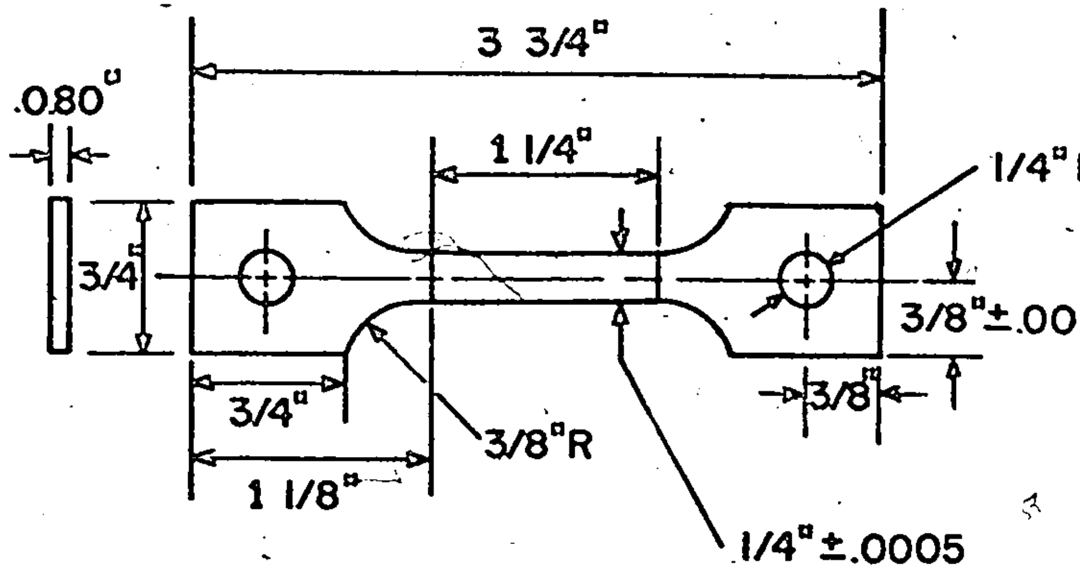

Fig. 4.18(a) Tensile test-piece

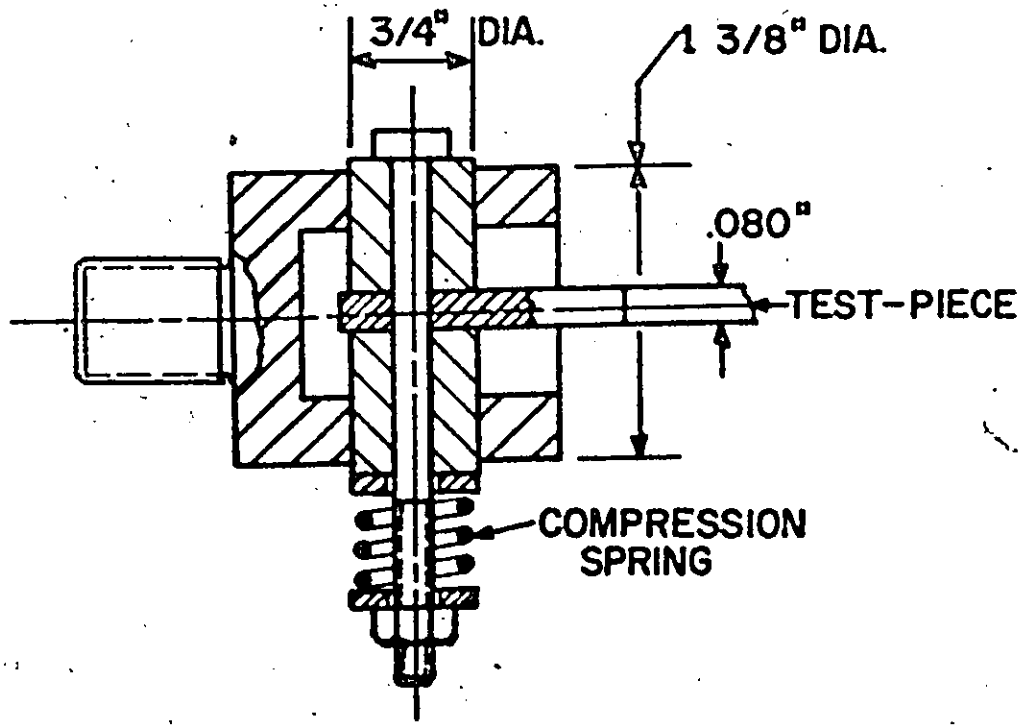

Fig. 4.18(b) Tensile grips for superplastic material testing

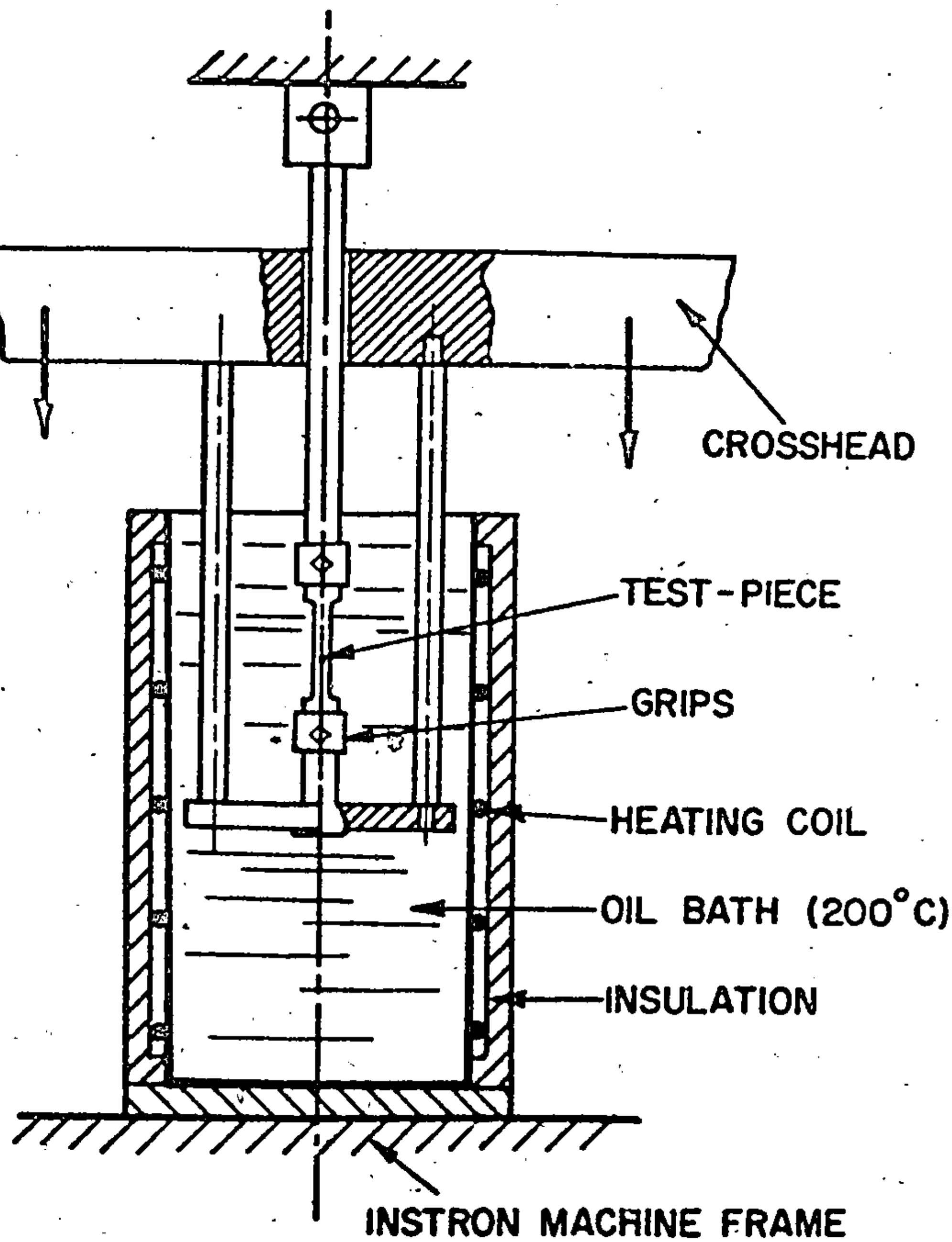

Fig. 4.19 Experimental arrangement for constant cross-head speed test of Zn - Al eutectoid alloy.

(A) AS-RECEIVED

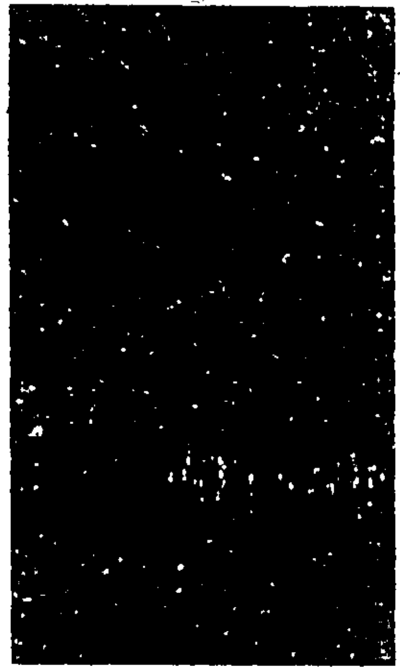

(B) QUENCHED

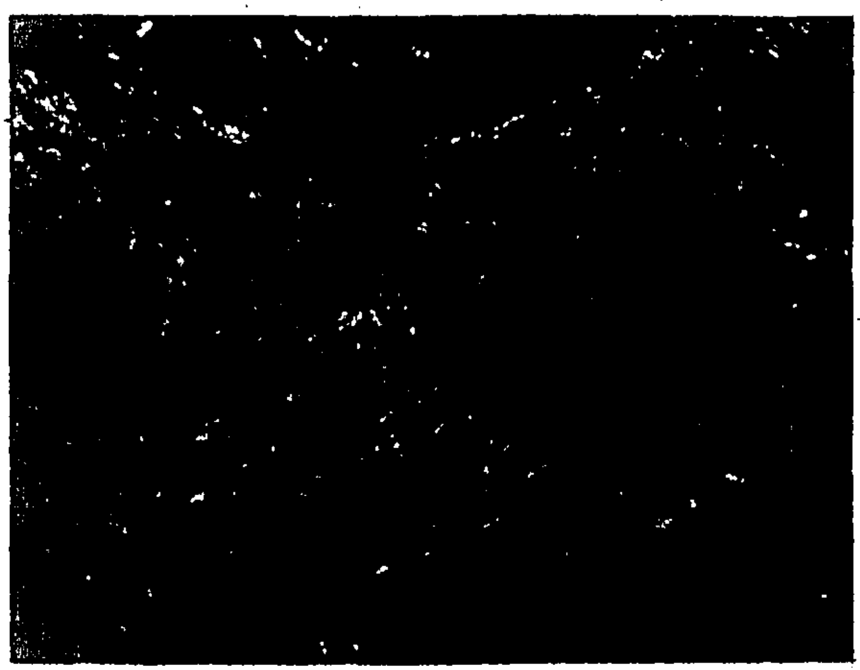

(C) ANNEALED

FIG. 4.20 - MICROSTRUCTURE OF ZINC-ALUMINUM EUTECTOID ALLOY (X 1600)

arrangement is shown schematically in Figure 4.19. The test specimen was fixed in specially designed grips which provide both positive and frictional gripping action, Figure 4.18(b). A compression coil spring, was used to compensate for the loss of the frictional gripping force due to any thinning of the specimen within the shoulders.

Most of the tensile tests were conducted atatemperature of 200°C. The as-received material was also tested at 150°C. The media used to provide these high temperatures was an electrically heated oil bath. The depth of the oil bath was enough to enclose the gripped specimen up to 400% elongation.

The test started by immersing the gripped specimen in the oil bath which was at about 140°C. The oil was then heated up to the required temperature. An intermittent stirring process kept the oil temperature uniform. After applying a very slight tension on the specimen, both the extension dials and the load cross-head travel chart were set to zero.

A preliminary tensile test was first conducted. The test was interrupted at different stages and the current distance between the gauge marks was measured, thus providing the actual extension of the gauge length. By knowing the chart speed the extension was also calculated from the load cross-head travel chart. Comparison between the two methods of estimating the extension showed a negligible difference. Consequently it was decided to use the load cross-head travel chart to calculate the current length of the specimen.

The tensile tests were performed at constant cross-head speed within the range of 0.002 - 2.0 inch/minute. A typical load cross-head travel chart is shown in Figure 4.21.

(c) Determination of material parameters

Stress/Strain-rate characteristic

The interpretation of the constant cross-head speed test results shown typically by Figure 4.21, was based on the assumption that the cross-sectional area of the test specimen, remained uniform during the test. Thus the uniaxial stress σ , and the strain-rate $\dot{\varepsilon}$ were calculated using the expressions,

$$\sigma = \frac{P}{A} = \frac{P}{A_o}\frac{\ell}{\ell_o} \qquad (4\text{-}32)$$

$$\dot{\varepsilon} = \frac{v_o}{\ell} \qquad (4\text{-}33)$$

where v_o is the constant cross-head speed at which the test was conducted. For the purpose of calculating the $\sigma/\dot{\varepsilon}$ characteristic, the load P and the length ℓ in equations (4-32) and (4-33) are taken to correspond to the maximum load point on the load-cross-head travel chart. For most of the tests performed on the as-

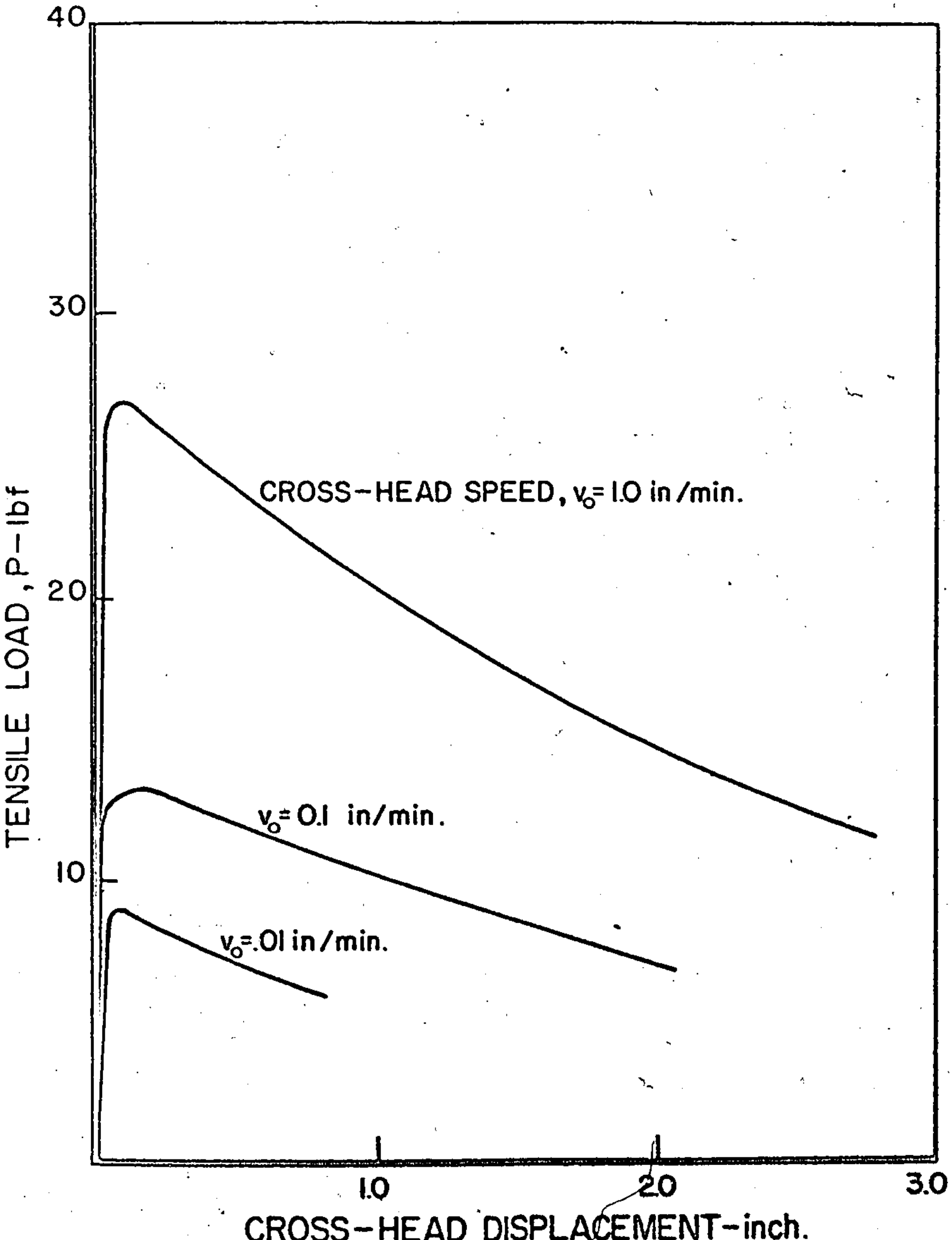

Fig. 4.21 A typical load, cross-head travel diagram obtained from testing superplastic Zn - Al alloy at constant speed.

received and quenched material, the maximum load occurred at strains in the vicinity of .075. Table 4-I shows a typical set of data for tests conducted at different speeds on the quenched material.

TABLE 4-I: Constant cross-head speed test results

A_o = .0294 inch^2	ℓ_o = 1.25 inch	Material condition: quenched			Testing Temp. = 200°C
v_o inch/min	ℓ inch	P lbf	A inch^2	$\dot{\varepsilon}$ per sec	σ lbf/inch^2
.002	1.320	6.37	.0223	2.25×10^{-5}	286
.010	1.335	8.92	.022	1.25×10^{-4}	406
.050	1.300	12.17	.0226	6.40×10^{-4}	538
.100	1.325	13.77	.0222	1.26×10^{-3}	620
.500	1.325	22.02	.0222	6.30×10^{-3}	992
2.00	1.350	31.97	.0218	$2.47 \quad 10^{-2}$	1465

The stress-strain-rate characteristics of the as-received, quenched and annealed materials are shown in Figures 4.22 and 4.23. A straight line fit of log σ or versus log $\dot{\varepsilon}$ does not appear to be a good representation of the material behaviour over the whole strain-rate range. Hence the two points corresponding to the lower strain-rates were excluded and the power law

$$\left(\frac{\sigma}{\sigma_o}\right) = \left(\frac{\dot{\varepsilon}}{\dot{\varepsilon}_o}\right)^m \qquad (\dot{\varepsilon}_o = 1)$$

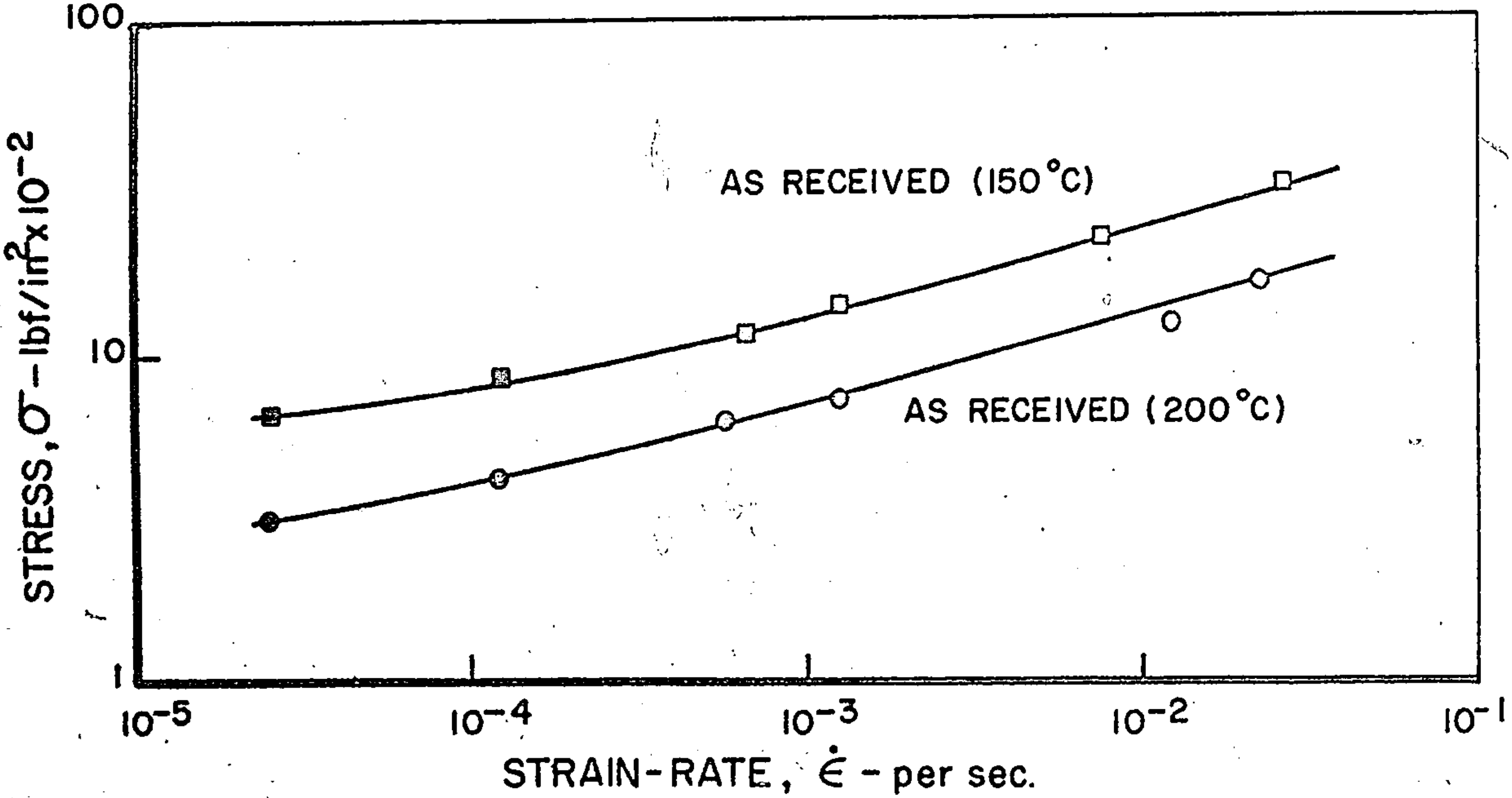

Fig. 4.22 Stress, strain-rate characteristic of as-received Zn - Al eutectoid alloy at two different temperatures

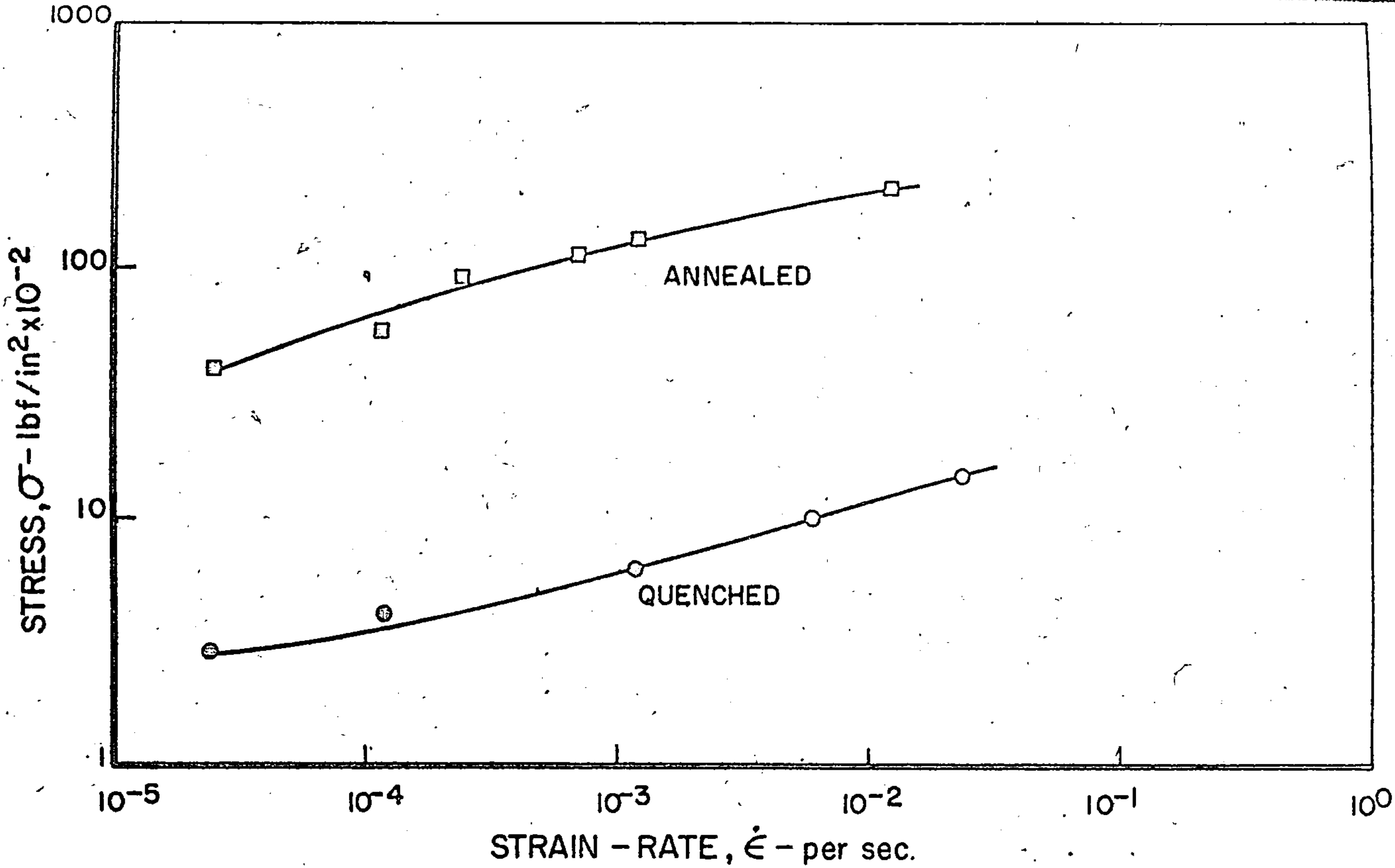

Fig. 4.23 Stress, strain-rate characteristic of quenched and annealed Zn-Al eutectoid alloy at 200°C.

was fitted to the rest of the $\sigma/\dot{\varepsilon}$ points. The least square fitting method was used to determine the material parameters σ_o and m as given in Table 4-II.

Strain-rate sensitivity index

The strain-rate sensitivity index m at constant temperature is defined by $m = (d \ln \sigma) / d (\ln \dot{\varepsilon})$.

It may be determined by two different methods. The first method uses the stress-strain rate diagram derived from tensile tests of different specimens, each pulled at different cross-head speed. Numerical differentiation of the logarithms of both the stress and strain-rate determines the variation of m with the strain-rate. The second method involves making sudden changes in the cross-head speed during the tensile test of one specimen. According to this method, first suggested by Backofen [1.7], the value of m at a given value of strain and temperature is

$$m = \ln (P_A / P_B) / \ln (v_o/v_o^{\prime}) \qquad (4\text{-}34)$$

where P_A and P_B are the steady-state loads corresponding to the different velocities, $v_o^{\prime}$ respectively (see Figure 2.5). A typical set of data of the velocity-change method is given for the quenched material in Table 4-III. The variation of m vs. $\dot{\varepsilon}$ as determined by the two methods is also shown in Figures 4.24(a), (b) and (c) for the three different material conditions.

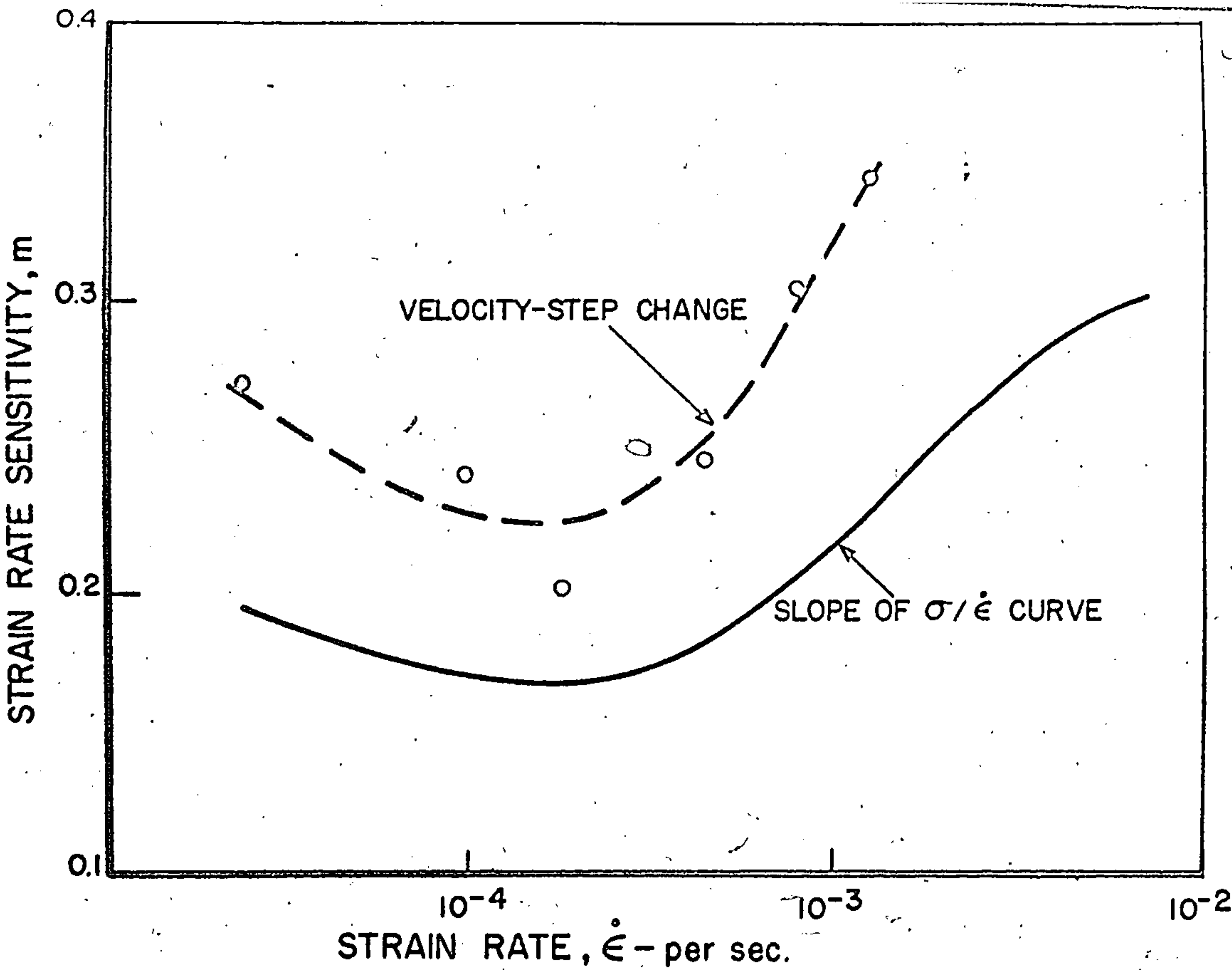

Fig. 4.24(a) Variation of strain-rate sensitivity with strain-rate for as-received Zn-Al eutectoid alloy at 200°C.

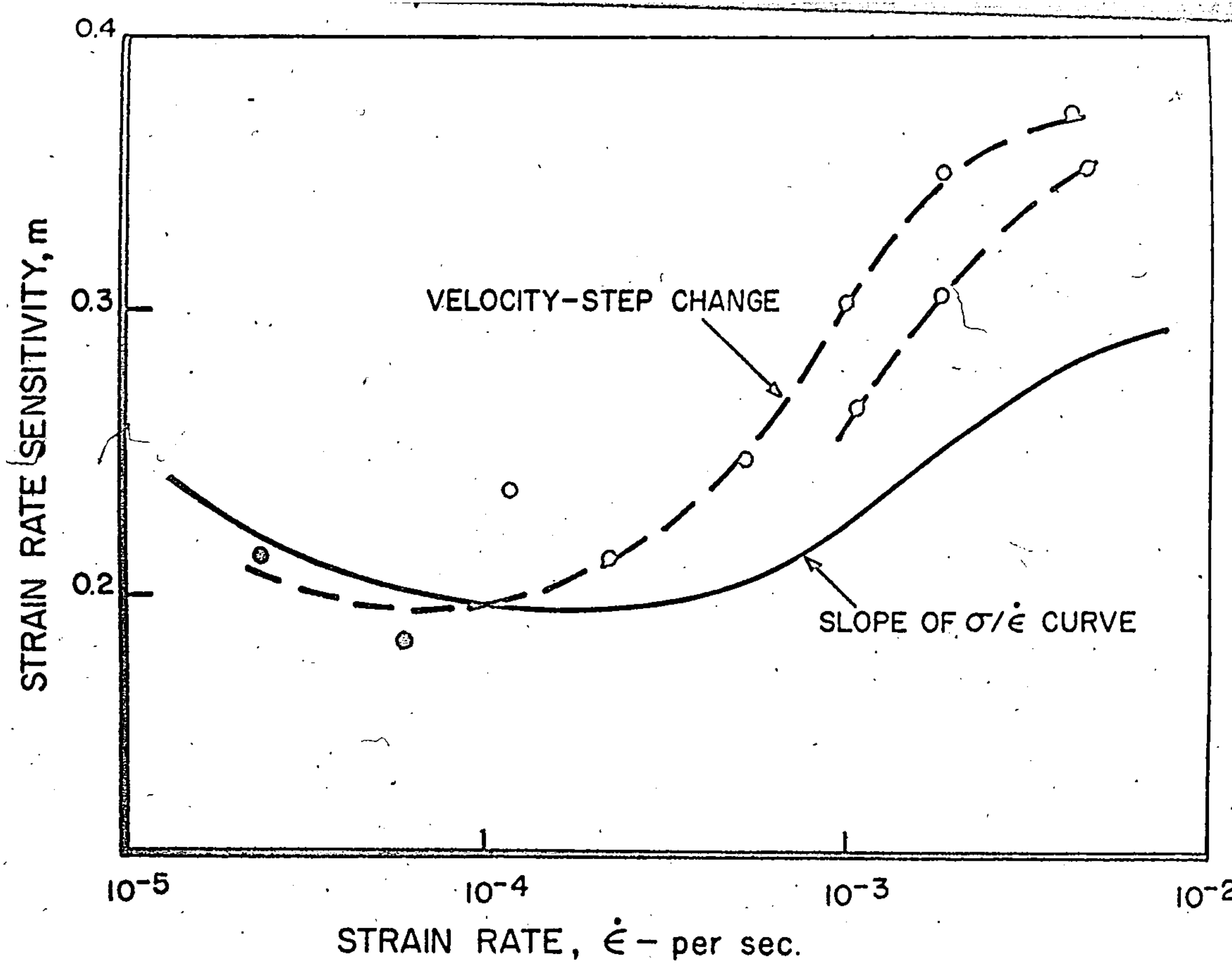

Fig. 4.24(b) Variation of strain-rate sensitivity with strain-rate for as-received Zn-Al eutectoid alloy at 150°C.

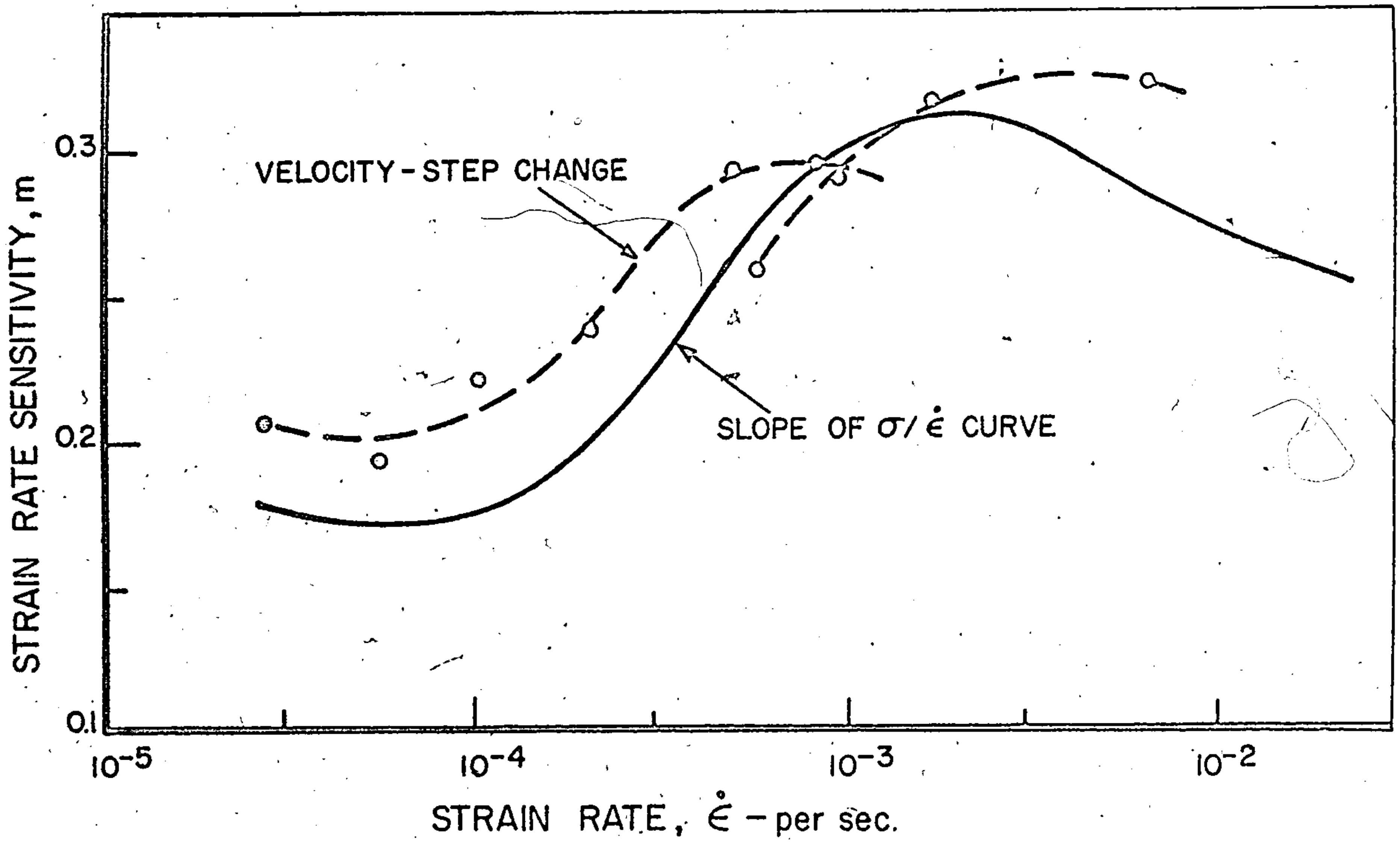

Fig. 4.24(c) Variation of strain-rate sensitivity with strain-rate for quenched Zn-Al eutectoid alloy at 200°C.

TABLE 4-II: Material parameters for Zn - Al eutectoid

Material Condition	Temperature °C of testing	m	σ_o, $lb_f/inch^2$
As-received	150	.280	8940
As-received	200	.315	5230
Quenched	200	.300	4080
Annealed	200	——	——

TABLE 4-III: Data obtained from the velocity-step change method

ℓ_o = 1.25 inch		material condition:quenched		Test Temperature:200°C
V_o inch/min	P_A/P_B	ℓ inch	$\dot{\varepsilon}$ sec^{-1}	m
.002	0.825	1.371	2.43 10^{-5}	.213
.005	0.855	1.376	6.05 10^{-5}	.183
.01	0.850	1.413	1.18 10^{-4}	.236
.02	0.825	1.493	2.23 10^{-4}	.212
.05	0.845	1.580	5.27 10^{-4}	.245
.10	0.815	1.670	1.00 10^{-3}	.300
.2	0.800	1.795	1.86 10^{-3}	.347
.5	0.775	1.940	4.28 10^{-3}	.367

The discrepancy between the values of m obtained from the two methods has been observed by other investigators [2.17]. It has been argued that the velocity step-change method is not reliable since a true steady-state within the material structure may not be always reached after changes of cross-head speed.

Material hardening

The load cross-head travel charts obtained from constant speed tests were used to calculate the $\sigma/\dot{\varepsilon}$ characteristics at different values of strain. Equations (4-32) and (4-33) were employed to obtain the stress, strain-rate curves represented by solid lines in Figure 4.25. Each curve is obtained from a single constant cross-head speed test and a point on the curve corresponds to a particular value of strain. It may be seen, particularly for the as-received material, that there is an apparent increase of stress with decrease of strain-rate. (In a constant speed test the strain-rate diminishes continuously with increasing elongation). The dashed line in Figure 4.25, joins the stress, strain-rate points corresponding to the maximum load. A plot of σ-$\dot{\varepsilon}$ curves obtained from a number of constant speed tensile tests for the as-received material, is shown in Figure 4.26 for different values of strain. It is seen that the slope of σ-$\dot{\varepsilon}$ curves remains almost the same although the stress level at a given strain-rate increases with

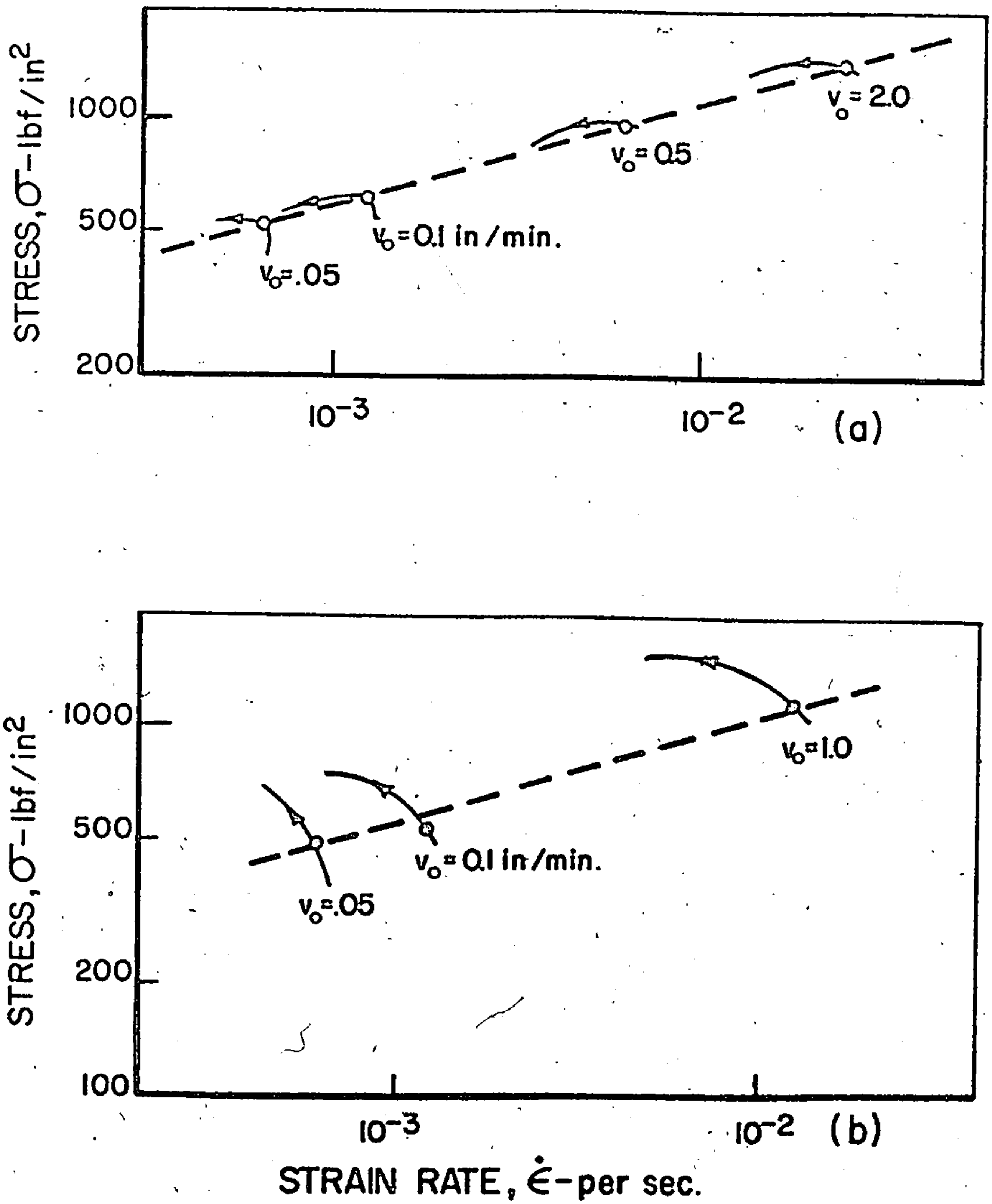

Fig. 4.25 Stress, strain-rate characteristic of Zn-Al eutectoid, derived from constant cross-head speed tensile tests at 200°C (a) Quenched material, (b) as-received material.

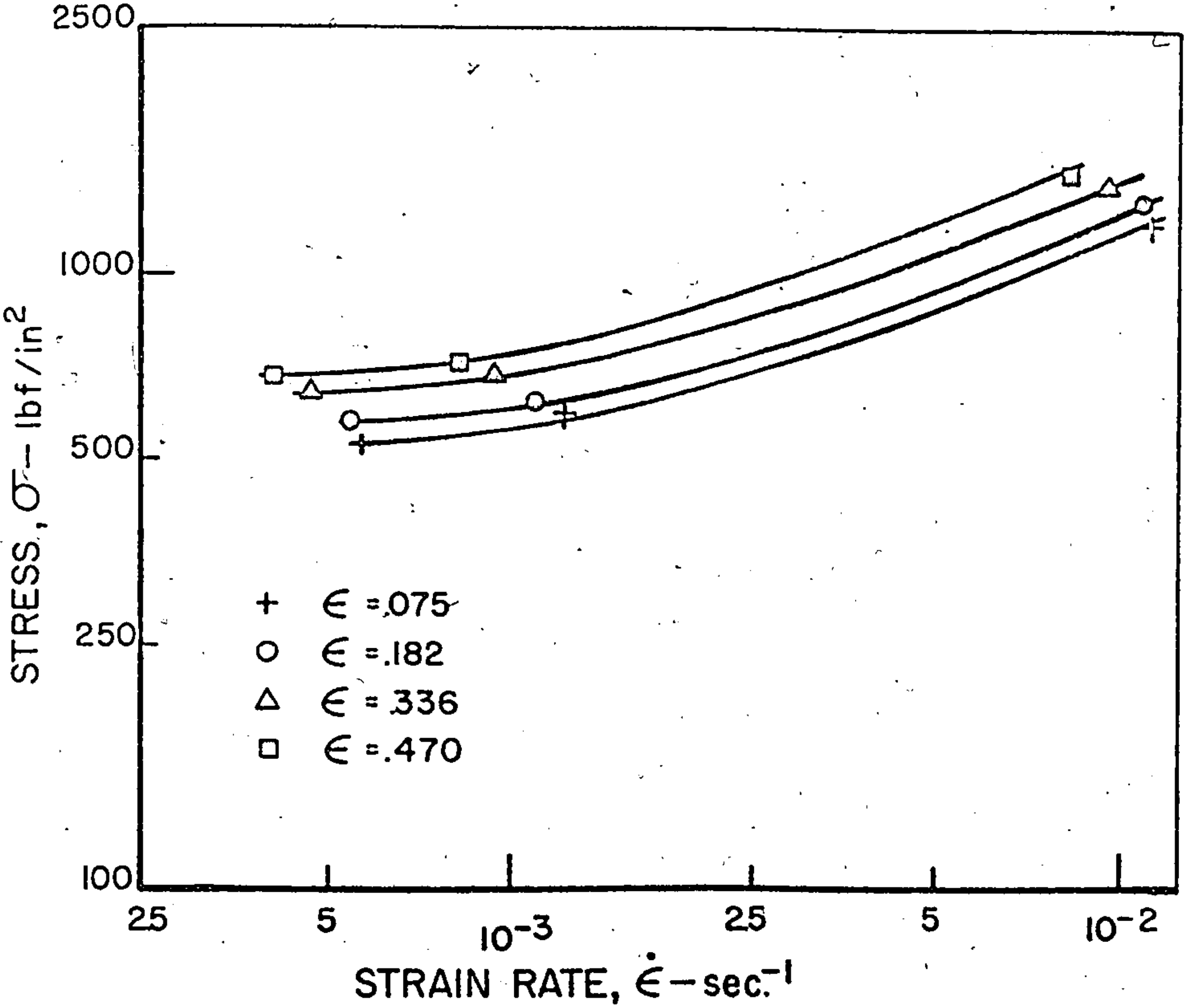

Fig. 4.26 Stress, strain-rate characteristic of as-received Zn-Al eutectoid at different values of strain.

increase of strain. This material behaviour differs from the strain-hardening phenomena observed in the deformation of conventional alloys in the following aspects:

-- The increase of stress during superplastic deformation occurs during the unstable flow régime, i.e. beyond the maximum load point. The state of deformation is then a non-uniform one.

-- In a constant cross-head speed tensile test the strain-rate diminishes as the specimen elongates. For a rate-sensitive material this means a decrease in the resistance to flow and this obviously introduces a difficulty in interpreting the test results.

-- The increase of stress during superplastic deformation could be considered asafunction of the deformation time rather than strain and this obviously complicates the mathematical modelling of the material behaviour [2.23].

-- Another reason which may contribute to the increase of stress during superplastic deformation, is the grain coarsening [2.21] which may take place during the test. This is however a controversial matter and concerns the mechanism of superplastic deformation.

The isolation of each of the above factors and the assessment of its influence on the apparent rise of stress with strain is necessary in understanding this material behaviour. This is obviously a difficult task. Some work analyzing this material behaviour has been reported in the literature, however the data available is not yet conclusive and use of a model which neglects strain-hardening appears to be justified at the present time.

4.3.2 Constant Load Tests of Non-Uniform Specimens

(a) Specimen preparation

The material tested was in the as-received condition in the form of sheets 3 foot square by .095 inch thickness. The method used to produce the ultra-fine grain structure required for superplasticity was described in Section 4.3.1(a). The test specimens were machined from the superplastic sheet, to the dimensions shown in Figure 4.27(a). The specimens had uniform width of 0.400 $\pm .001$ inch and thickness of 0.095 inch over a gauge length of 2 inches. The gauge length was scribed in the central portion of the specimen as remote as

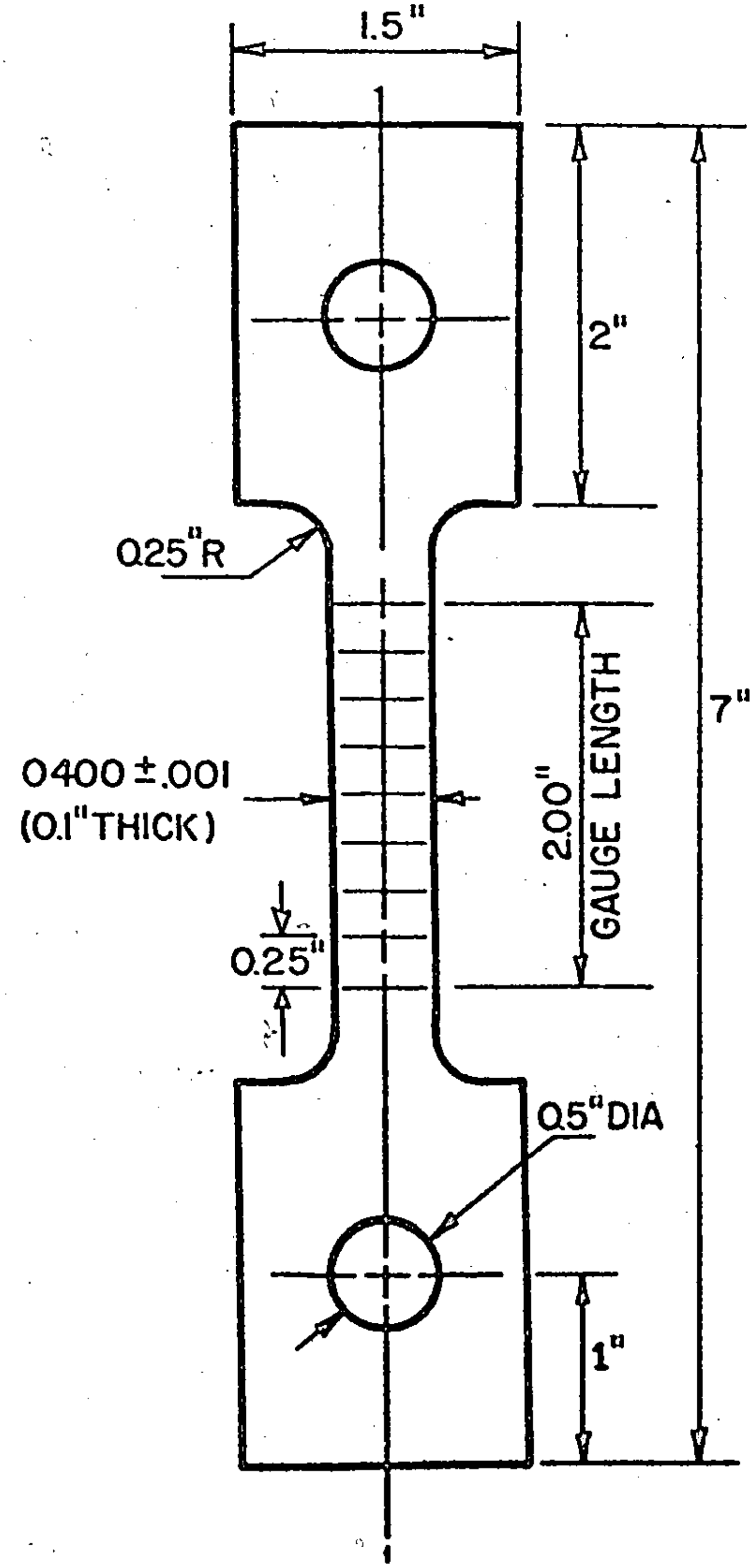

Fig. 4.27(a) Tensile test-piece

possible from the specimen shoulders so that any constraining effect on the deformation within the gauge length was avoided.

The specimens were divded to three batches and each one was remachined to produce a specific nominal width-taper, as given by

$$\Delta W_o = \left(\frac{W_2 - W_1}{W_{av}}\right)_{t=0} \qquad W_2 > W_1 \qquad (4\text{-}35)$$

where w_1 and w_2 are the widths at the extreme marks of the gauge length, and w_{av} is the average width over the gauge length. The values of the initial taper were chosen to be 2%, 4% and 7.5% over the gauge length. The 2 inch gauge length was then scribed cross-wise at equal distances of 0.25 inch as shown in Figure 4.27(a). The thickness of the specimen was measured at different points and found to be uniform within $\pm$ .0005 inch. Using a tool maker's microscope with least reading of 0.0001 inch, width measurements at the different marked stations of the gauge length were taken and recorded.

(b) Experimental equipment and test procedure

Constant load tests of tapered specimens were conducted in an oven with a loading arrangement as illustrated in Figure 4.27(b). The oven was fabricated from asbestos boards of 1/8 thickness and had the inside dimensions of 2 x 2 x 2 feet. Heat is generated by three strip-heaters with fins each of capacity 15 kw. The power supplied to the heaters was controlled by means of three

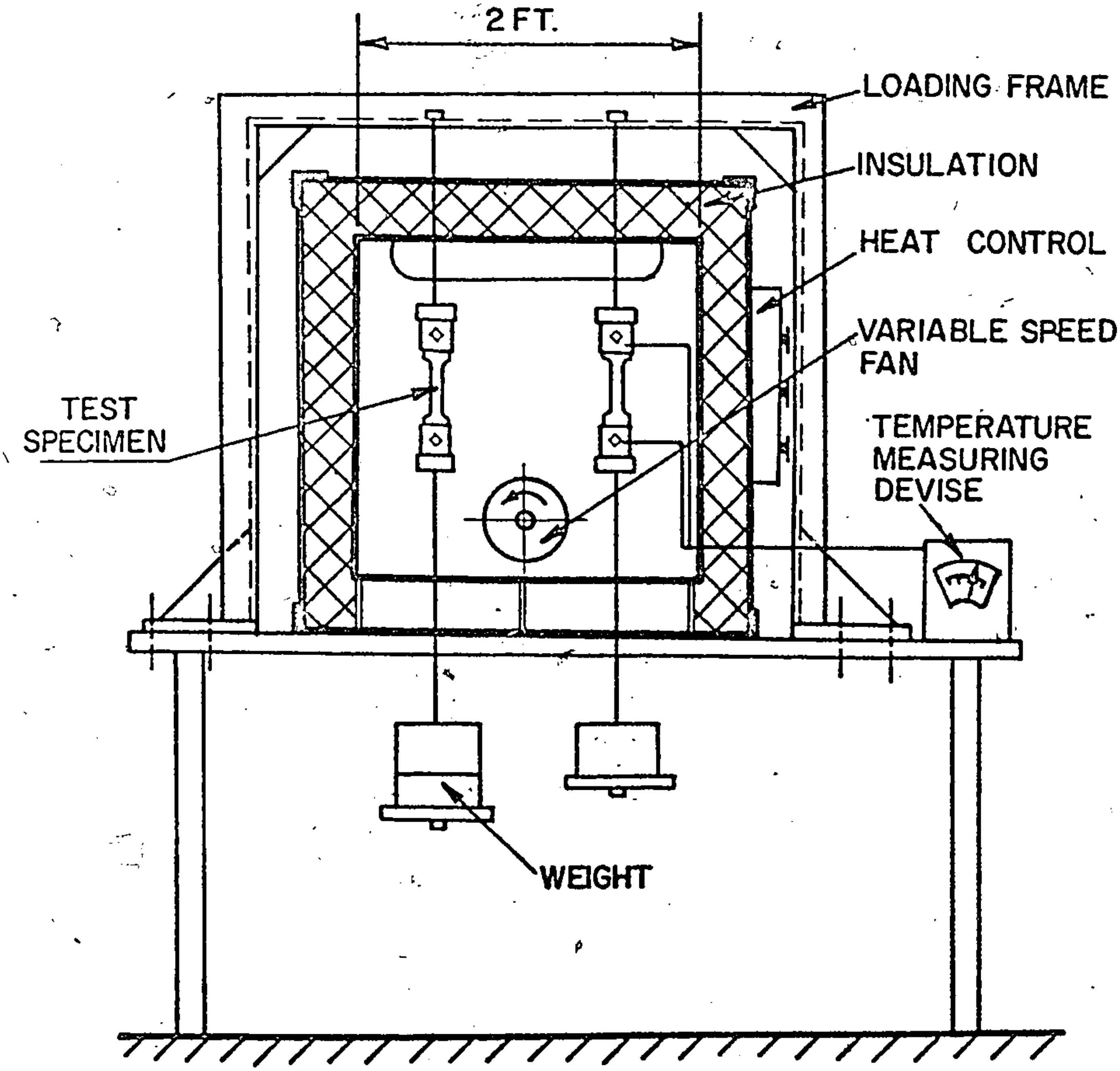

Fig. 4.27(b) Equipment for testing non-uniform tensile specimens under the action of constant load at 200°C.

multiple position switches. The air circulation inside the oven was assisted by fixing a 6 inch variable speed fan at the back panel as shown in Figure 4.27(b). The tensile test specimen was vertically held inside the oven using self-aligning grips. Two thermo-couple wires, one connected to the top grip and the other to the bottom one were used to measure the temperature along the specimen length.

Two non-uniform specimens were mounted vertically in the oven and care was taken to obtain coaxiality of loading. The oven was heated up to the testing temperature 200°C. The specimens were then loaded by means of dead weights and the test continued until each specimen had extended certain amount.

Temperatures at different points along the length of the specimen were measured throughout the test. Difficulties were experienced in obtaining uniform temperature distribution within the oven and few preliminary experiments were conducted in order to gain experience in controlling the temperature gradient. The use of a wide aluminum plate as a heat shield between the specimens and the oven door improved the uniformity of the temperature distribution. Also by proper adjustment of the heat input and the speed of the fan, the temperature variation was brought to a minimum of $\pm$ 2°C over length a of about 10 inches.

Specimens were tested under constant load conditions. The loads acting on the specimens were so chosen to produce strain-rates within the linear part of the $\sigma/\dot{\varepsilon}$ curve shown in Figure 4.22. Elongations ranging from 30% to 200% were obtained as shown in Figure 4.28.

(c) Experimental results

Tests were performed on superplastic tapered strips in the as-received condition, in order to study the growth of the geometrical non-uniformity during deformation. The initial and current geometrical non-uniformities are defined in terms of cross-sectional areas as

$$\delta A = \frac{A_{max}-A_{min}}{A_{av}} \qquad (4\text{-}36)$$

Typical test results are given in Table 4-IV. Appendix B includes all the experimental results of constant load tensile tests performed on non-uniform specimens. In Table 4-IV, the undeformed and deformed areas of the test specimen are calculated from thickness and width measurements at the marked stations along the gauge length. The normal anisotropy coefficient

$$R_n = \frac{\ln (W/W_o)}{\ln (S/S_o)} \qquad (4\text{-}37)$$

was also calculated and given in Table 4-IV. Figures

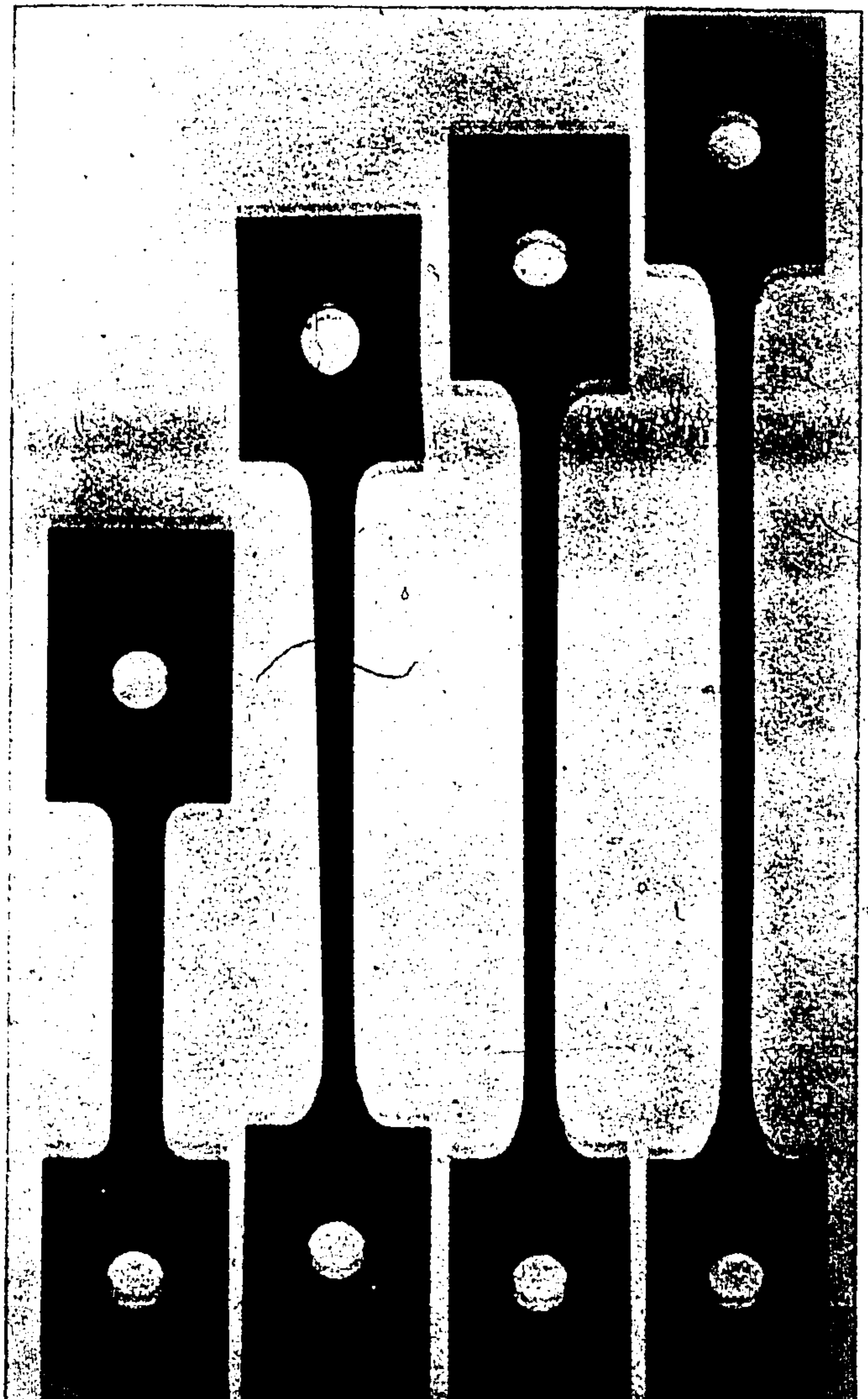

FIG. 4.28 - INITIALLY TAPERED TENSILE SPECIMENS OF SUPERPLASTIC ZN-Al ALLOY TESTED UNDER CONSTANT LOAD CONDITION

TABLE 4.IV: EXPERIMENTAL DATA OBTAINED FROM CONSTANT LOAD TESTS OF TAPERED TENSILE STRIPS OF AS-RECEIVED Zn-Al ALLOY AT 200°C

DIMENSIONS OF UNDEFORMED SPECIMEN				DIMENSIONS OF DEFORMED SPECIMEN				
Width w_o	Thickness s_o	Area A_o	Distance between marked stations	Width w	Thickness s	Area A	Distance between marked stations	$\frac{\ln(w/w_o)}{\ln(s/s_o)}$
.3899		.03665		.3199	.0701	.0223	-----	.6746
.3869		.03637		.3140	.0691	.0216	.4100	.6783
.3844		.0361		.3100	.0687	.0212	.4150	.6860
.3818		.0358		.3080	.0680	.0209	.4200	.6635
.3796	.0940	.0357	.2500	.3050	.0674	.0205	.4250	.6577
.3770		.0354		.3017	.0670	.0202	.4300	.6580
.3753		.0352		.2989	.0660	.0197	.435	.6436
.3740		.0351		.2913	.0643	.0187	.4400	.6581
.3716		.0349		.2852	.0629	.0179	.4742	.6587

4.29(a) to 4.29(g) show the deformed areas of the tapered specimens plotted versus the measured current lengths between the marked stations along the gauge length. The solid lines in these Figures represent the theoretical profiles of the deformed specimens as predicted by the numerical solution, described in Section 4.2.2. Both the experimental and theoretical results correspond to the same amount of total elongation. The average strain-rates determined theoretically are also indicated on these Figures. The growth of area non-uniformity versus total elongation for the three different initial tapers 2%, 4% and 7.5%, is demonstrated both theoretically and experimentally in Figures 4.30(a) to 4.30(c).

4.4 Comparison Between Theory and Experiment

Figures 30(a), 30(b) and 30(c) show that the theory tends to over-estimate the value of the current non-uniformity at a given elongation. Nevertheless the experimental results generally follow the trend predicted by the theory. Discrepancies between theory and experiment are greater at large elongations for high initial geometrical non-uniformity as seen from Figure 30(c). The discrepancies may be attributed to, firstly the lack of validity of the assumption of negligible triaxial stresses for high degrees of taper and secondly to the material inhomogeniety. Neglect of any strain or time-hardening in the empirical law used to represent the material properties may also affect the

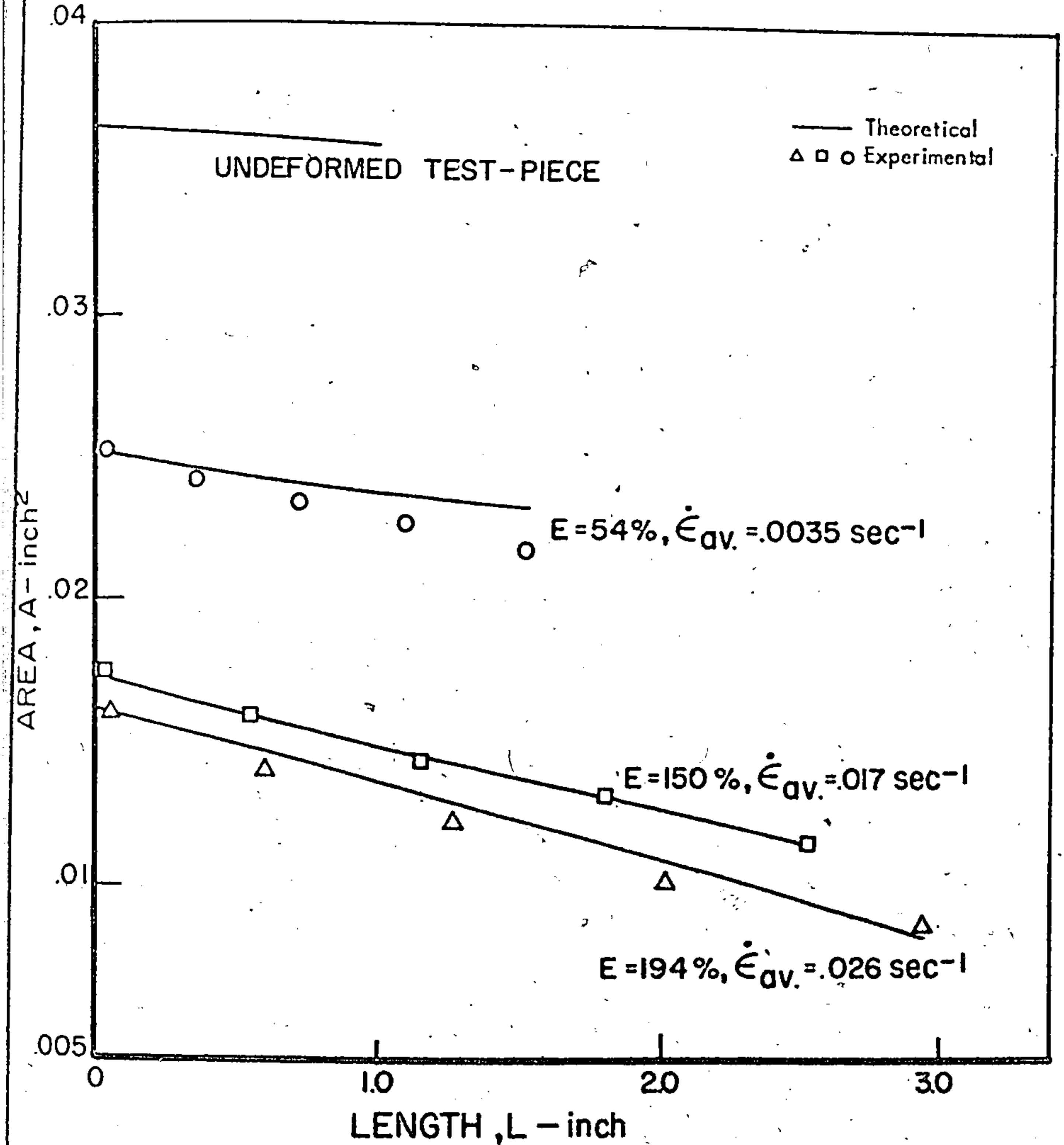

Fig. 4.29(a) Distribution of areas along the length of a test-piece with initial non-uniformity, $A_{max} - A_{min}$, of 2%.

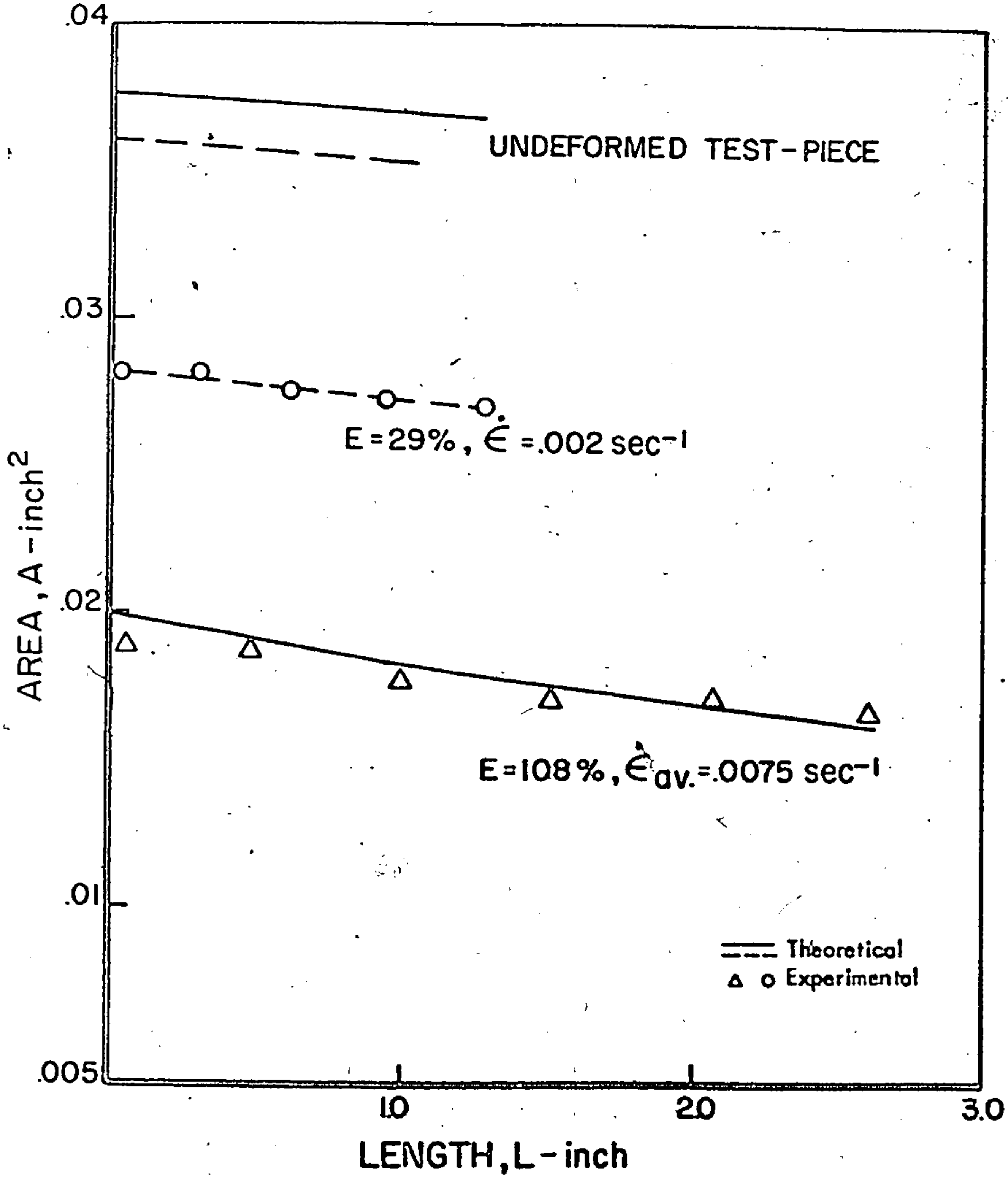

Fig. 4.29(b) Distribution of areas along the length of test-pieces of initial non-uniformity $A_{max} - A_{min}$ of 2%.

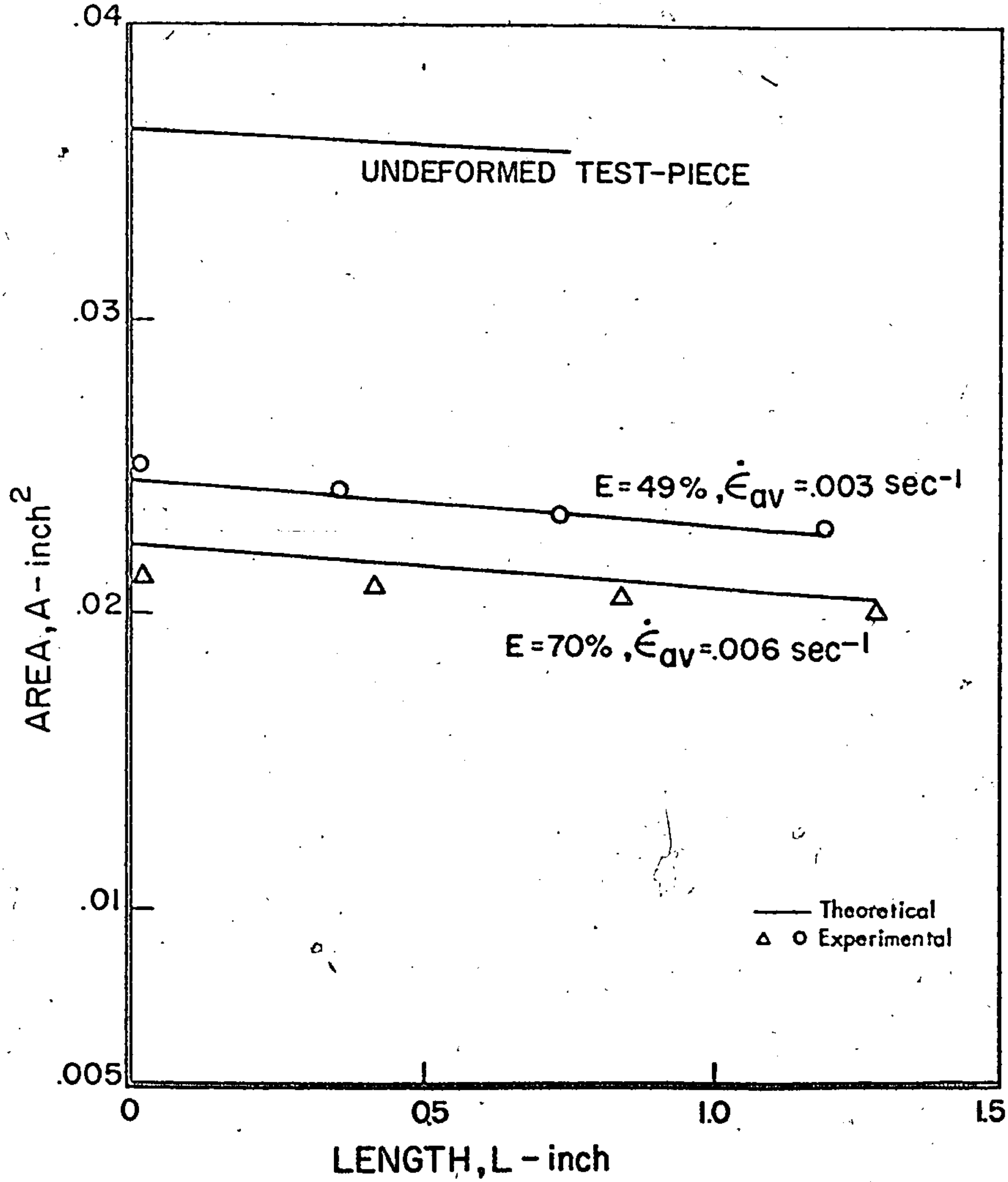

Fig. 4.29(c) Distribution of areas along the length of a test-piece with initial non-uniformity, $A_{max} - A_{min}$, of 2%.

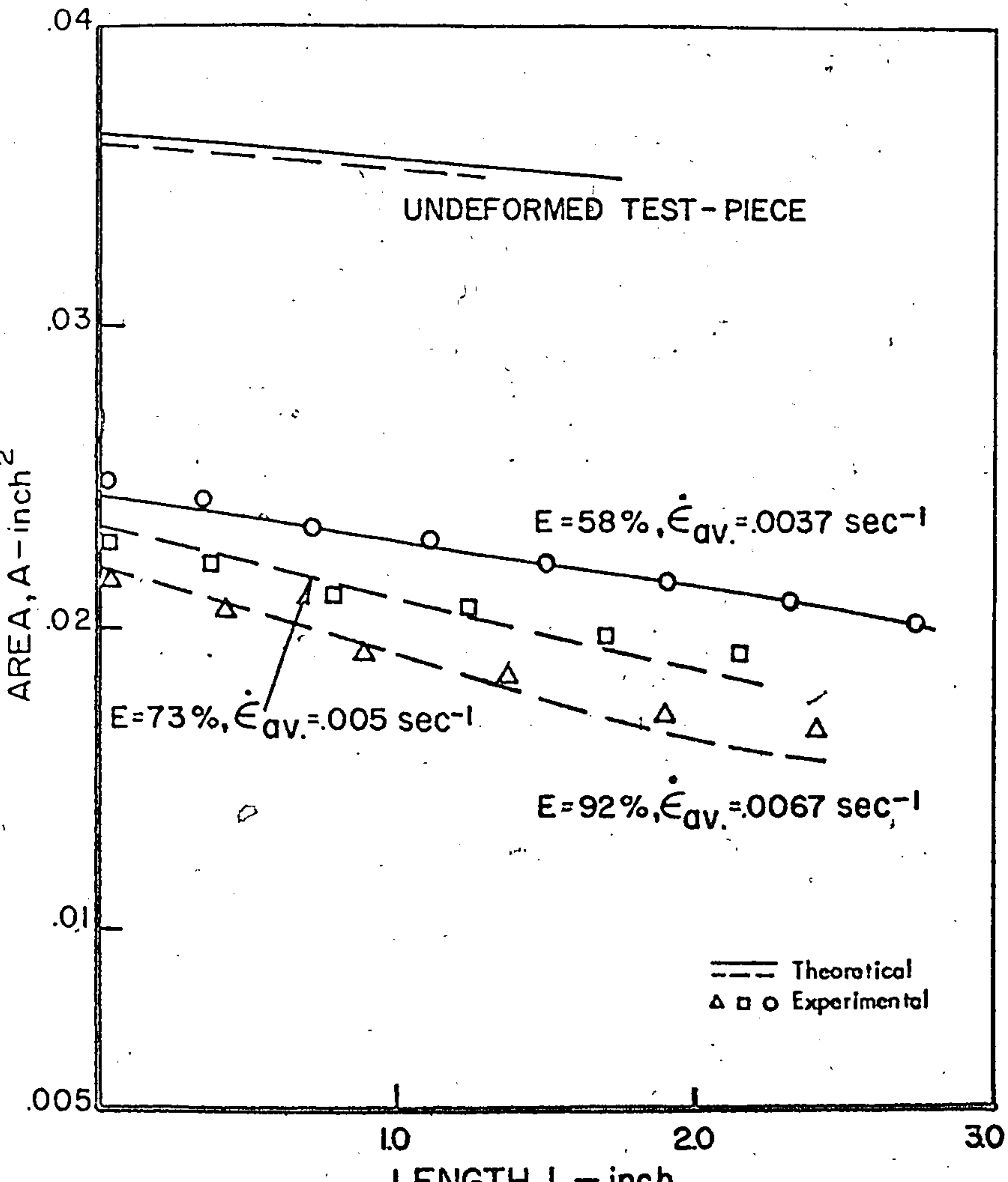

Fig. 4.29(d) Distribution of areas along the length of test-pieces of initial non-uniformity, $A_{max} - A_{min}$, of 4%.

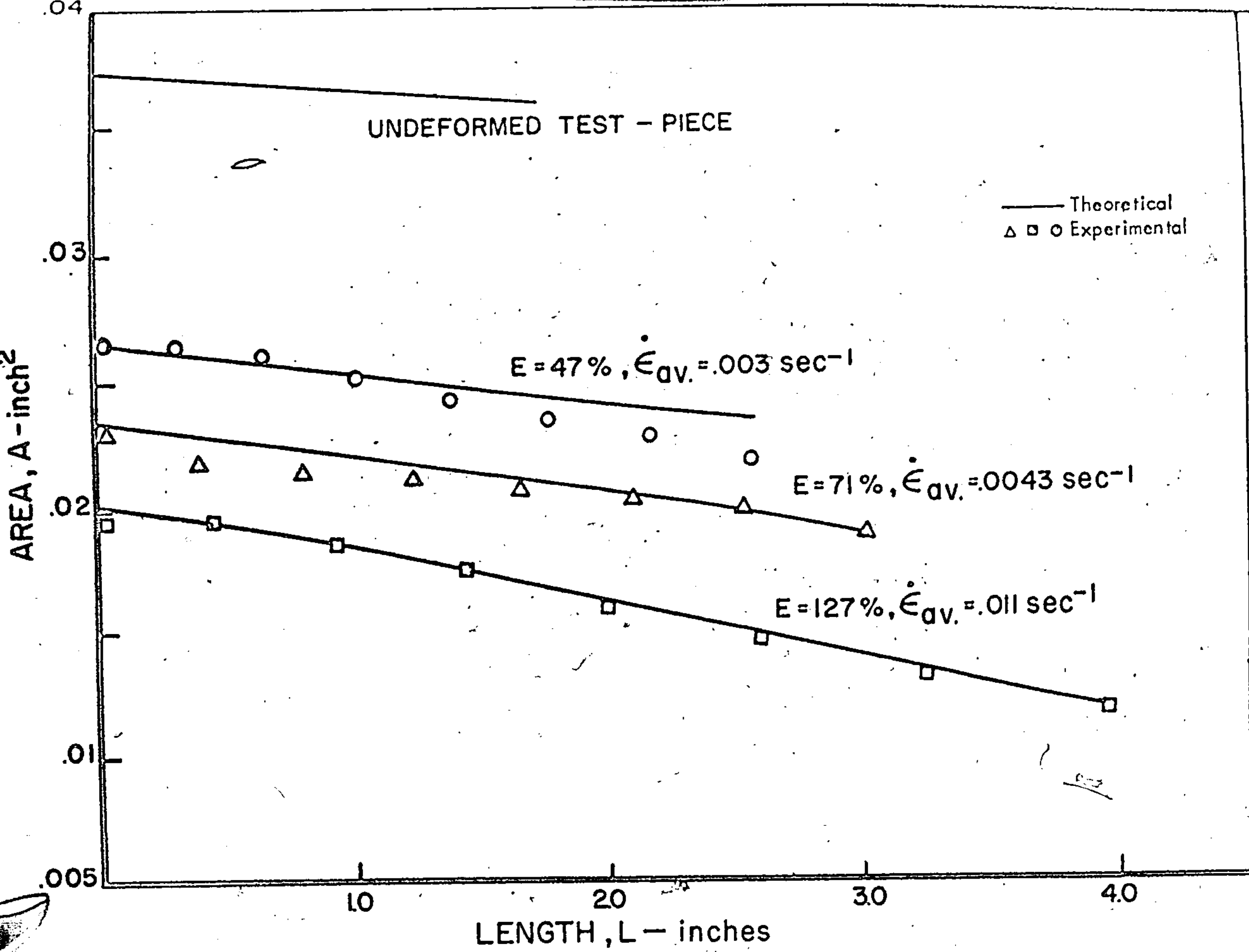

Fig. 4.29(a) Distribution of areas along the length of a test-piece of initial non-uniformity, $A_{max}-A_{min}$, of 4%.

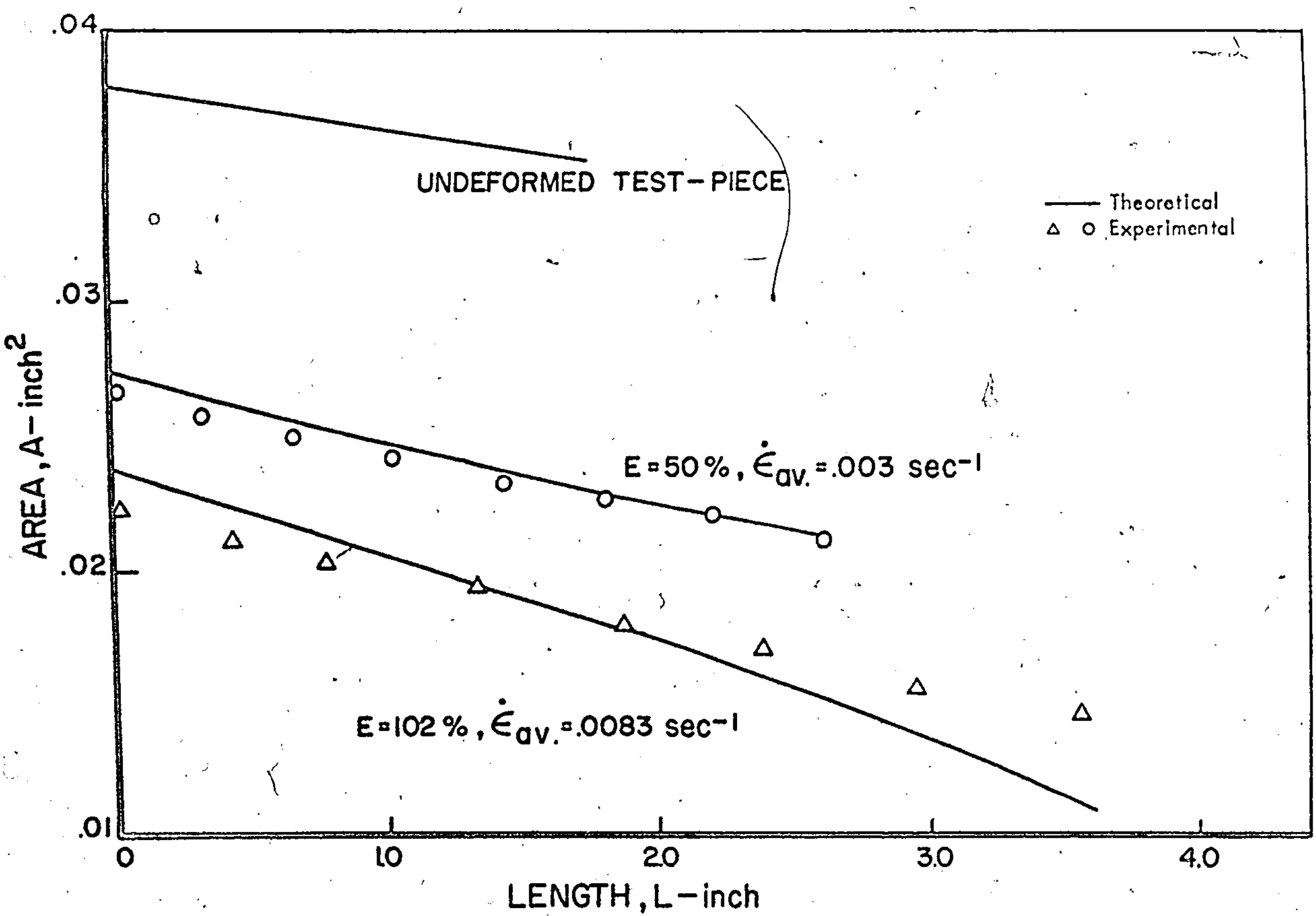

Fig. 4.29(f) Distribution of areas along the length of a test-piece of initial non-uniformity A_{max}-A_{min}, of 7.5%

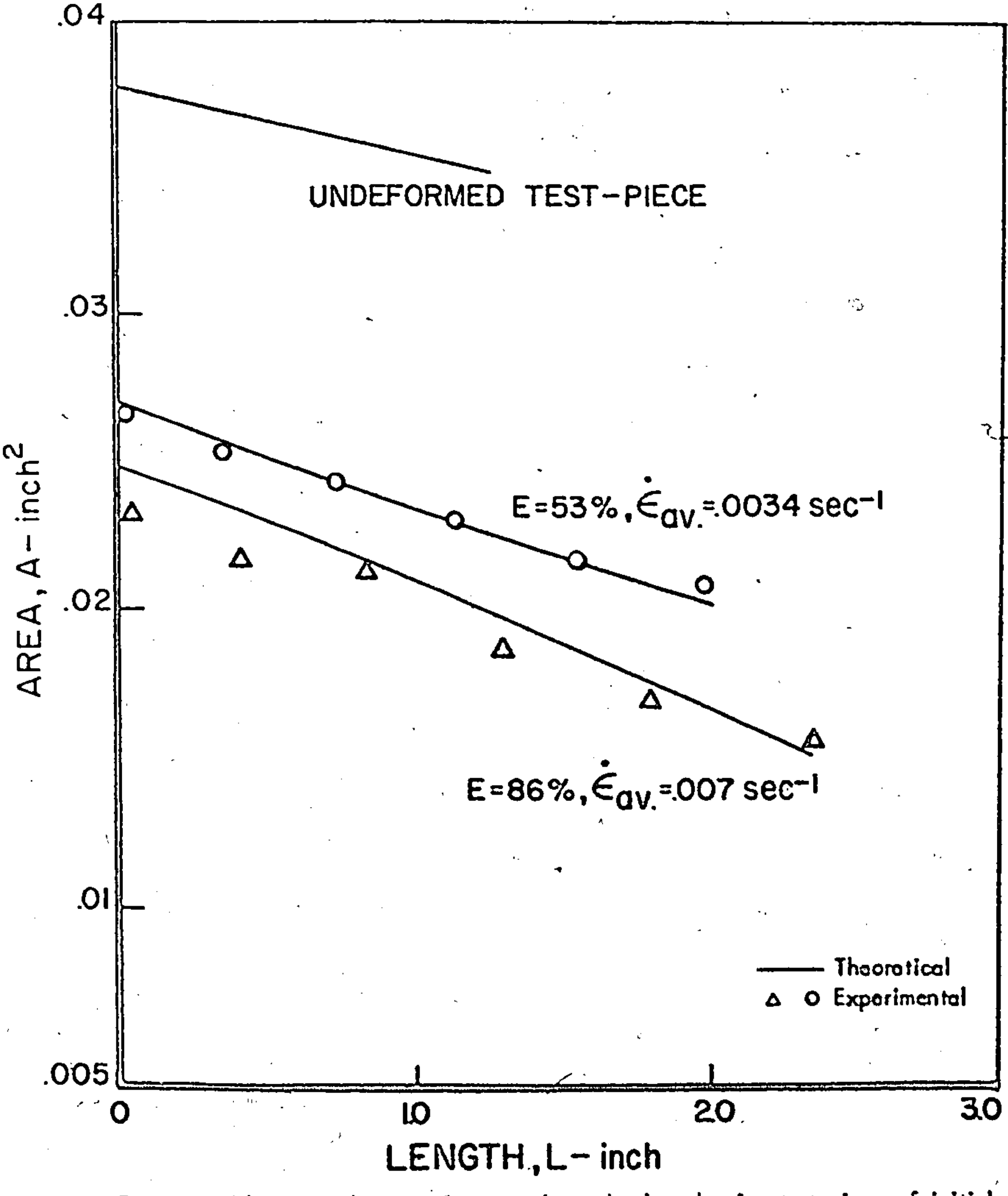

Fig. 4.29(g) Distribution of areas along the length of a test-piece of initial non-uniformity, A_{max}-A_{min}, of 7.5%.

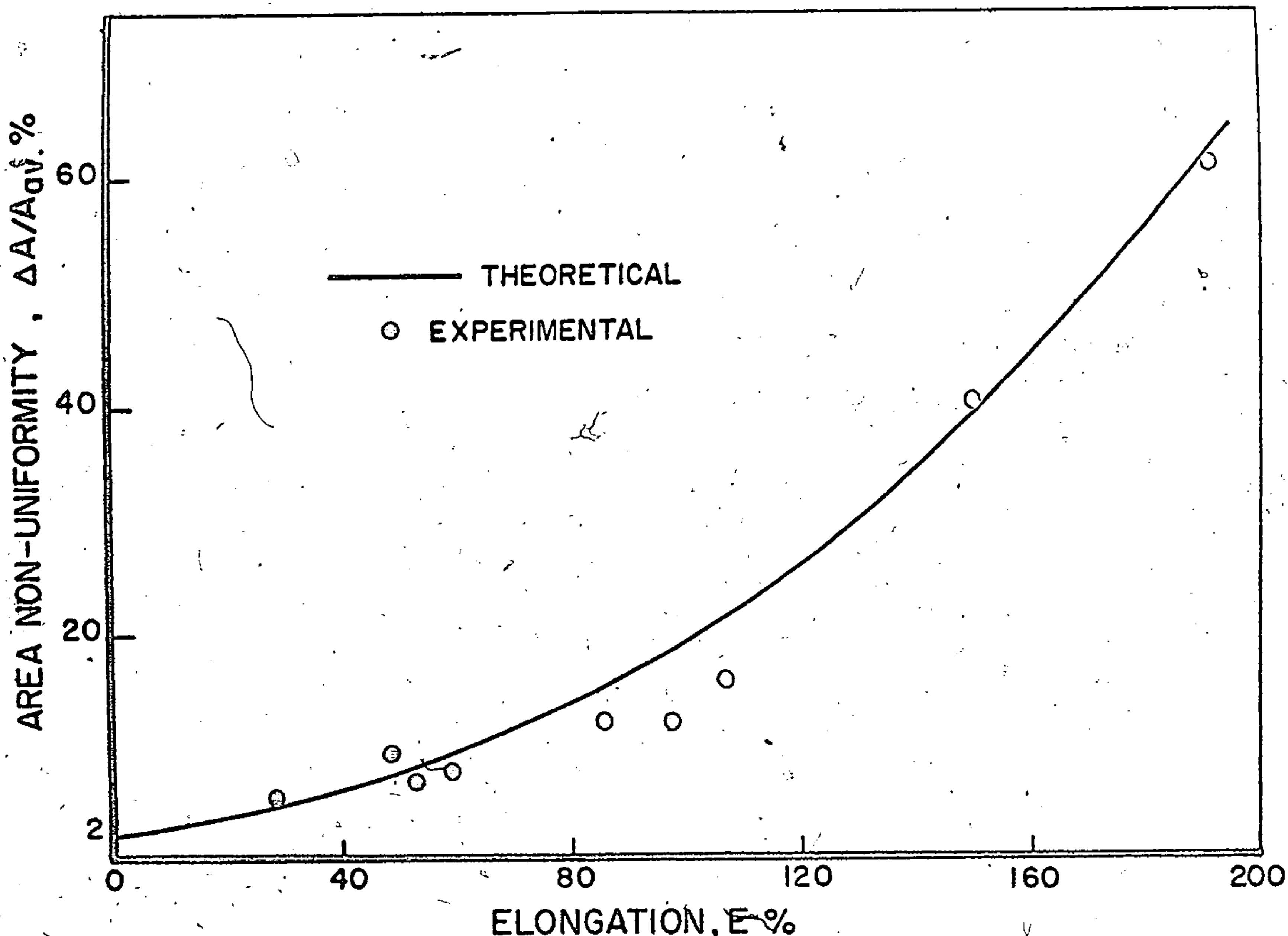

Fig. 4.30(a) Growth of area-nonuniformity with total elongation for test-pieces having an initial non-uniformity of 2%.

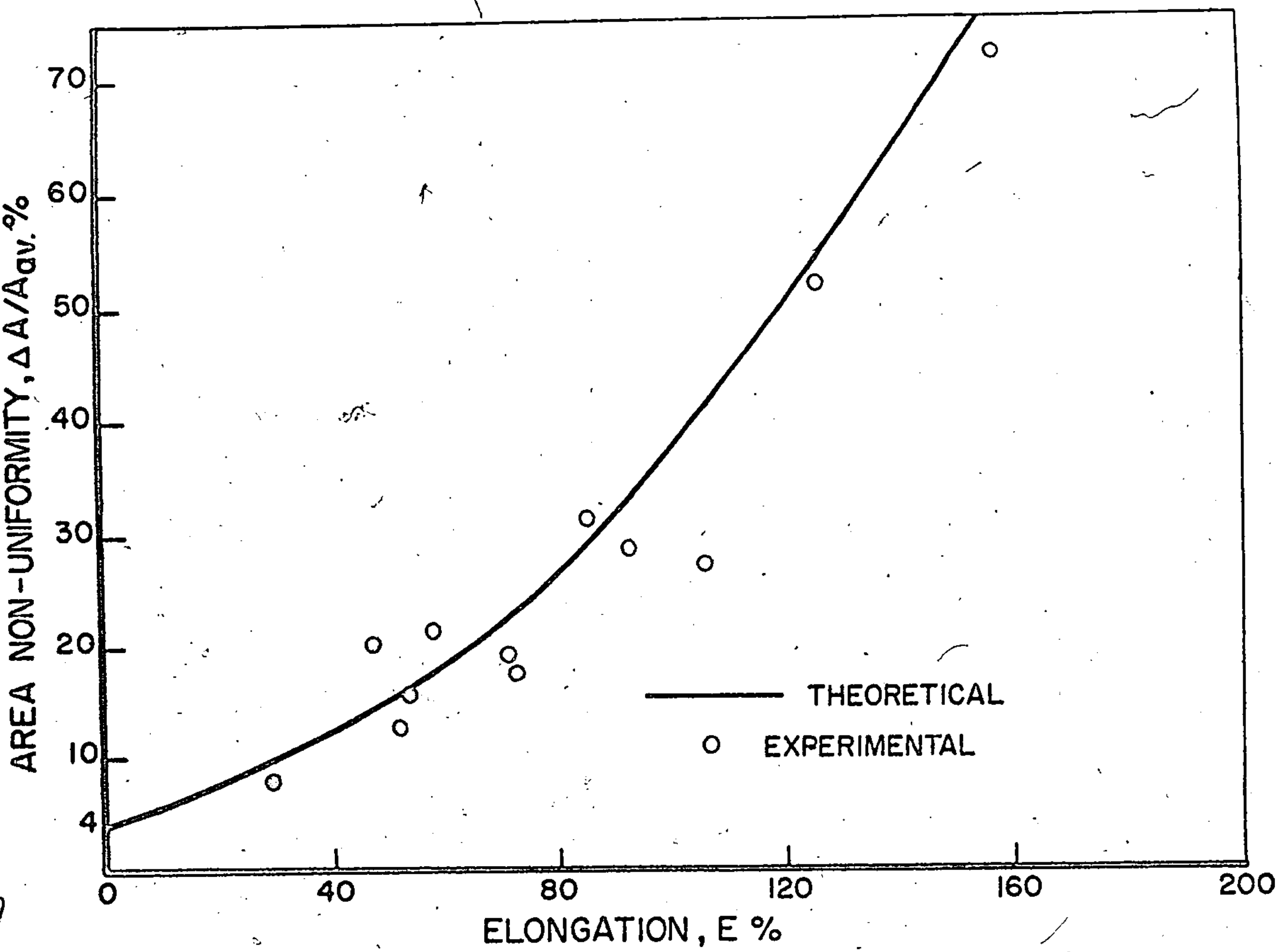

Fig. 4.30(b) Growth of area-nonuniformity with total elongation for test-pieces having an initial non-uniformity of 4%.

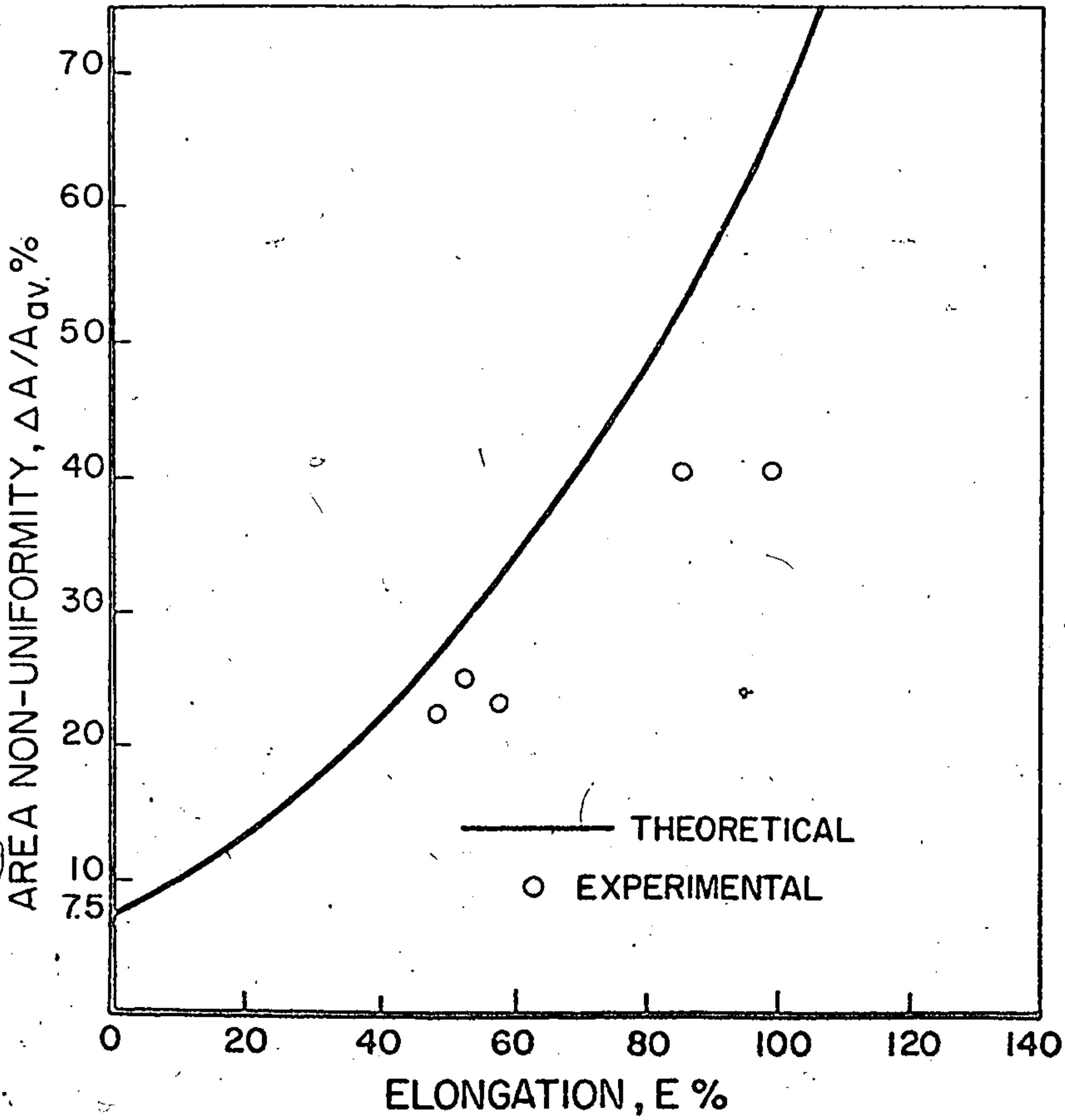

Fig. 4.30(c) Growth of area-nonuniformity with total elongation for test-pieces having an initial non-uniformity of 7.5%.

the correlation of theory and experiment. Nevertheless the results demonstrate that a technological theory, using a non-linear viscous material model, can be applied to estimate the growth of the geometrical non-uniformity in superplastic tensile forming processes.

4.5 Conclusions

Complete analytical solutions were produced for the deformation of a perfect test-piece or tube. The results were used as a guide in performing the numerical analysis for the superplastic non-uniform workpiece. Development of geometrical non-uniformities in axially-loaded rods and thin-walled tubes expanded by internal pressure were described.

A good correlation was found between theoretical and experimental results of uniaxial tension of non-uniform superplastic strips with slight initial taper. A detailed comparison between theoretical results presented here and other experimental work in the literature is not possible because authors have generally failed to present quantitative information on initial and final non-uniformities in the test-piece. It is reasonable to assume however that typical imperfections in an undeformed uniaxial test-pieces will be < 1/2% and the results here indicate that the nearly uniform elongation of such a specimen to 400% or more is consistent with the simple non-linear viscous model of material behaviour for values of material parameters typically found in superplastic alloys. Further, it is shown that such variations of cross-sectional area which do develop will be gradually distributed along the length of the specimen.

The theoretical results for the expansion of a non-uniform tube are in qualitative agreement with experimental observations [1.23]. Non-uniformity in wall thickness will always be present in commercially produced tubes and the results here indicate that for similar materials, non-uniformities grow more rapidly in expanding a tube than in drawing a rod. Within the limits of realistic tolerances however, diametral expansions of about 100% should be readily achieved in superplastic alloys.

Results obtained show that extensive overall tensile deformation can be achieved before initial inhomogenieties have developed to an unacceptable limit. Furthermore, the analysis presented here may be used to determine the tolerance required for industrial forming processes and may assist in understanding the behaviour of these alloys in the tension test.

CHAPTER V

DETERMINATION OF CREEP PROPERTIES IN SUPERPLASTIC SHEETS

5.1 Introduction

Superplastic alloys are considered ultra-fine grain alloys of common metals which can be hot-worked using very small loads and forged into intricate and decorative shapes. They also exhibit a high strain-rate sensitivity and can be stretch formed in processes resembling blow moulding and vacuum forming of thermoplastics [1.22 - 1.24]. However, if the fine-grain structure is retained after forming, these materials may suffer from poor creep resistance and although some information relating to creep properties in superplastic alloys is available, this is very limited [1.16] and [5.2]. This chapter describes methods of obtaining creep data from a bending test on superplastic sheet; the technique employs simple equipment and appears to be suitable for quality control testing of commercial sheet.

Creep bending tests have been used for many years, particularly for sheet plastics; the results are generally expressed in terms of bending deflections in a standardized test without attempting to derive the data in a more generalized form. It may not be widely appreciated that developments in creep theory permit tests under various stress systems to be correlated. Even if creep data is required in terms of parameters in a uniaxial test, these can still be derived from creep bending tests; this may be an advantage if the latter is a more convenient way of performing a test. Complex creep theory employs a number of assumptions about material behaviour which may not be true for all classes of material [2.23]. Experiments must be performed therefore to validate the theory for particular materials and in this work, the room temperature creep of a superplastic alloy sheet in bending and in simple tension is compared. The alloy, binary zinc-aluminum eutectoid, is known to obey Norton's creep law quite closely and has a large secondary creep range.

Creep data is required in many different forms. In some cases it is considered sufficient to indicate the stress required to produce a fixed creep strain in a specified time; this information is of limited value to the designer. Alternatively data may be presented in terms of the constants in an empirical stress, strain-rate relation; this is convenient analytically although the extent to which the material obeys the empirical law is not always known. A more complete representation of secondary creep behaviour can be given by a curve in a stress, strain-rate diagram; this is normally derived from measurement of secondary creep rates in a number of constant stress tests.

In this work a technique is presented for obtaining creep data for thin sheets using a test in which the whole sheet is arranged as a cantilever loaded by its own weight. Theory is given for deriving creep parameters from measured deflection rates in two tests and for deriving a stress, strain-rate curve from a number of bending tests using the skeletal point method.

Tensile and bending tests were performed on superplastic eutectoid Zn-Al sheet at room temperature and the creep information from both types of tests is compared.

5.2 Creep Bending Theory

Beams and wide plates subjected to time independent loading and undergoing creep deformation are analyzed using the elastic analogue. The elastic analogue hypothesis states that the solution of a problem of stationary creep is obtained as soon as the solution of the corresponding problem of non-linear elasticity is found [5.3].

A wide strip arranged as a cantilever loaded with a uniformly distributed load, q per unit length, is shown in Figures 5.1(a) and (b). The deflection of the neutral axis of the beam is defined by v(x, t) where the origin is at the moving end of the beam as shown in Figure 5.1(c). If the beam reaches a state of stationary creep, the rate of deflection of the moving end,

$$\dot{\delta} = \left[\frac{\partial}{\partial t} v\ (x,t)\right]_{x = \ell_c} \tag{5-1}$$

will become constant. Assuming that plane sections remain plane, the strain-rate at a height y from the neutral axis may be expressed in terms of the rate of change of curvature as follows:

$$(\dot{\varepsilon}_b)_y = -y\frac{\partial}{\partial t}\left(\frac{\partial^2 v}{\partial x^2}\right) = -y\dot{v}'' \tag{5-2}$$

where b denotes bending.

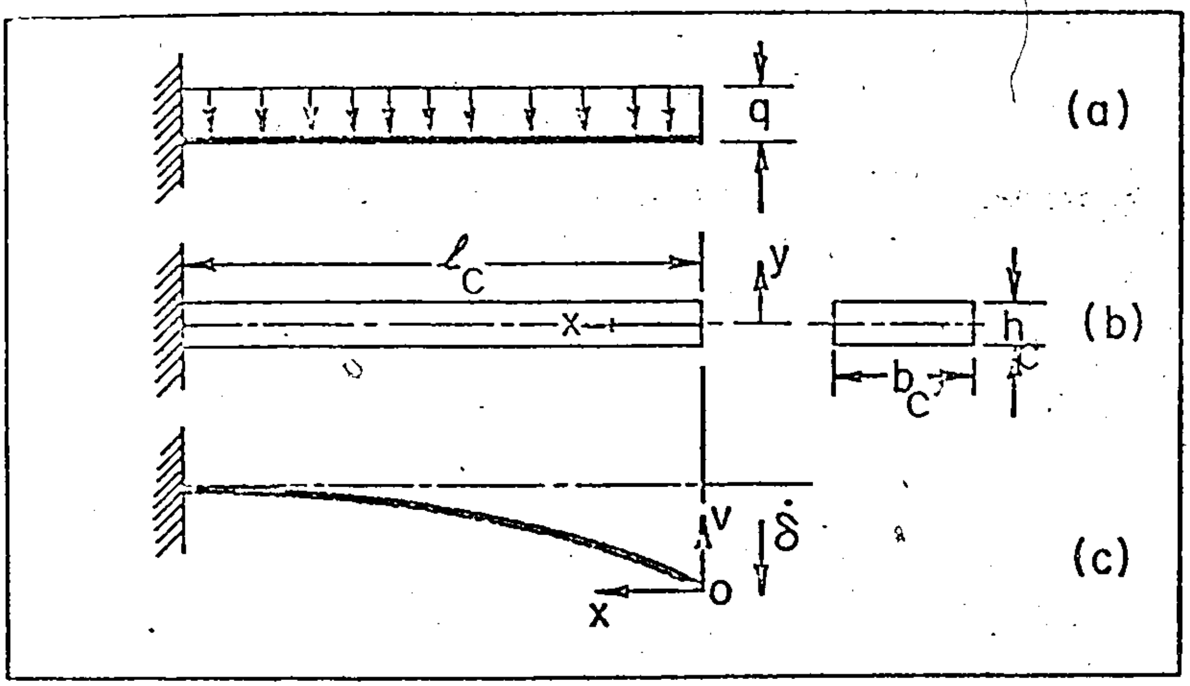

Fig. 5.1 Cantilever beam, showing co-ordinate system, loading and deflection.

For a wide strip, $b_c < h_c$, anticlastic curvature of the strip may be neglected so that bending is assumed to occur under conditions of plane strain, i.e.

$$\dot{\varepsilon}_z = 0$$

The incompressibility condition yields,

$$\dot{\varepsilon}_y = - \dot{\varepsilon}_b \qquad (5\text{-}3)$$

Thus the representative strain-rate is

$$\dot{\varepsilon}_e = \frac{2}{3} \dot{\varepsilon}_{ij} = \frac{2}{\sqrt{3}} \dot{\varepsilon}_b \qquad (5\text{-}4)$$

The representative stress is

$$\sigma_e = \frac{3}{2} S'_{ij} S'_{ij} = \frac{\sqrt{3}}{2} \sigma_b \qquad (5\text{-}5)$$

In secondary creep at constant temperature, many materials, including superplastic alloys, approximately obey the constitutive equation:

$$\left(\frac{\dot{\varepsilon}_e}{\dot{\varepsilon}_o}\right) = \left(\frac{\sigma_e}{\sigma_o}\right)^{\lambda} \qquad (5\text{-}6)$$

where $\dot{\varepsilon}_e, \sigma_e$ and λ are constants; generally an arbitrary value is prescribed for $\dot{\varepsilon}_o$; σ_o and λ are regarded as material parameters.

Substituting equations (5-4) and (5-5) into the constitutive equation (5-6) we obtain

$$(\sigma_b)_y = -\sigma_o \left(\frac{2}{\sqrt{3}}\right)^{\frac{\lambda+1}{\lambda}} \left(\frac{\dot{\varepsilon}_b}{\dot{\varepsilon}_o}\right)^{\frac{1}{\lambda}} \qquad (5\text{-}7)$$

where σ_b is the bending stress at a height y from the neutral axis.

Combining equations (5-2) and (5-7) yields

$$(\sigma_b)_y = -\sigma_o \left(\frac{2}{\sqrt{3}}\right)^{\frac{\lambda+1}{\lambda}} \left(\frac{y\dot{v}''}{\dot{\varepsilon}_o}\right)^{\frac{1}{\lambda}} \tag{5-8}$$

The equilibrium equation for the section shown in Figure 5.1(b) is

$$M = \int_A \sigma_b \; y \; dA = -\sigma_o \left(\frac{\dot{v}''}{\dot{\varepsilon}_o}\right)^{\frac{1}{\lambda}} I_\lambda \tag{5-9}$$

which yields

$$\dot{v}'' = -\dot{\varepsilon}_o \left(\frac{M}{\sigma_o I_\lambda}\right)^{\frac{1}{\lambda}} \tag{5-10}$$

where I_λ is a property of the section for a given value of λ.

For a rectangular cross-section of breadth b_c and depth h_c,

$$I_\lambda = \frac{2\lambda}{2\lambda+1} \left(\frac{b_c h_c^2}{4}\right) \left(\frac{h_c}{2}\right)^{\frac{1}{\lambda}} \left(\frac{2}{\sqrt{3}}\right)^{\frac{\lambda+1}{\lambda}} \tag{5-11}$$

(The resemblance between equations (5-10) and (5-11) and the well known bending equations

$$v'' = \frac{M}{EI} \quad \text{and} \quad I = \frac{b_c h_c^3}{12} \left(\frac{1}{1-\nu^2}\right)$$

for a linear elastic wide sheet is obvious).

For a cantilever strip with a uniformly distributed load intensity q, the bending moment at any section x, Figure 5-1(a) is

$$M = qx^2/2 \tag{5-12}$$

Substitution of equation (5-12) into (5-10) yields

$$\dot{v}'' = -\dot{\varepsilon}_o \left(\frac{qx^2}{2\sigma_o I_\lambda}\right)^\lambda \tag{5-13}$$

which upon integrating twice we obtain

$$\dot{v} = -\dot{\varepsilon}_o \left(\frac{q}{2\sigma_o I_\lambda}\right)^\lambda \frac{x^{2\lambda+2}}{(2\lambda+1)\quad(2\lambda+2)} + C_1 x + C_2$$

The boundary conditions $\dot{v}\ (0) = 0$ and $\frac{dv}{dx}\ (\ell_c) = 0$ give

$$C_1 = \dot{\varepsilon}_o \left(\frac{q}{2\sigma_o I_\lambda}\right)^\lambda \frac{\ell^{2\lambda+1}}{2\lambda+1} \text{ and } C_2 = 0$$

and therefore the deflection rate at the free end is

$$\dot{\delta}(\ell_c) = \dot{v}(\ell_c) = -\dot{\varepsilon}_o \left(\frac{q}{2\sigma_o I_\lambda}\right)^\lambda \frac{\ell_c^{\,2\lambda+2}}{(2\lambda+2)} \tag{5-14}$$

5.2.1 Determination of Creep Constants

If we consider two cantilevers of different lengths, ℓ_c then from equation (5-14) we obtain

$$\frac{\dot{\delta}_1}{\dot{\delta}_2} = \left[\frac{(\ell_c)_1}{(\ell_c)_2}\right]^{2\lambda+2} \tag{5-15}$$

where $\dot{\delta}_1$ and $\dot{\delta}_2$ are the deflection rates which may be measured for the spans(ℓ_{c_1}) and(ℓ_{c_2}) respectively. Therefore, the index λ can be obtained from equation (5-15) and σ_o is then found from equation (5-14).

Note that $\dot{\varepsilon}_0$ in equation (5-14) is a constant which, by convention, is chosen to have the value of 10^{-9} sec^{-1} or 3.6×10^{-6} hr^{-1}; following this, σ_0 may be described as the stress which will cause a constant creep rate of 10^{-9} sec^{-1} or about 3% strain in one year [5.3].

5.2.2 Determination of the Stress, Strain-Rate Curve.

If the material obeys equation (5-6) the shape of the stress distribution and the form of the deflection curve will depend on the index λ In simple structures however it is possible to find a point at which the stress and strain-rate are relatively insensitive to changes in λ within a fairly wide range. For example, in a rectangular beam, the stress distribution for a given bending moment for different values of λ in the range of $\lambda \geq 1$ is shown in Figure 5-2; it is a well known result that at a distance $y_s = \frac{h_c}{\sqrt{3}}$ from the neutral axis the stress is very nearly the same for all values of λ and can consequently be calculated using any value of λ arbitrarily selected within the given range. Similarly there exists some plane along the beam at a distance x_s where the rate of curvature, i.e.

$$\frac{\partial}{\partial t}\left(\frac{\partial^2 v}{\partial x^2}\right) = \dot{v}''$$

for a given end deflection rate is almost independent of λ within a given range. The strain-rate at a point in this section can therefore be determined directly from the measured end deflection rate without knowing precisely the value of λ. The point in this plane $x = x_s$ at a height from the neutral axis $y = y_s$ is known as the "skeletal point" [5.4] and [5.5]. With these

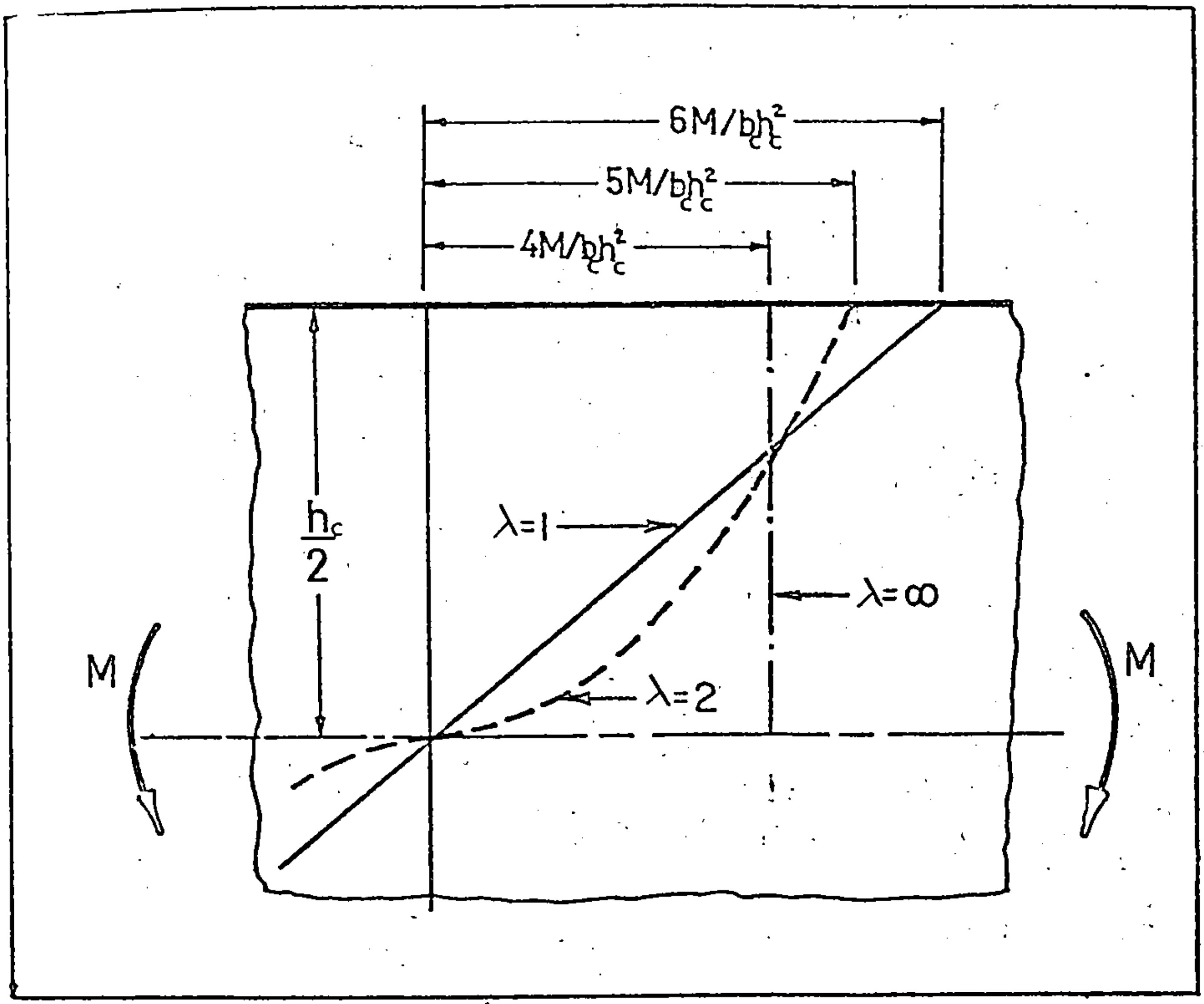

Fig. 5.2 Stress distribution for materials having different λ values.

assumptions we may state that the skeletal point is the only point in the beam where the stress and strain-rate are known explicitly from the beam configuration, the loading system and the measured end deflection rate. In the literature, it is often assumed that the stress and strain-rate at the skeletal point can also be determined in this way even if the material does not obey the power law form of equation (5-6). This is a hypothesis. The method of finding the skeletal point is given below; it follows methods stated elsewhere.

From equations (5-8) and (5-10) we can obtain a non-dimensional bending stress, namely

$$\left(\frac{\sigma_b}{M}\right) \cdot \left(\frac{b_c h_c^{\,2}}{4}\right) = \frac{1+2\lambda}{2\lambda} \left(\frac{2y}{h_c}\right)^{\frac{1}{\lambda}} \tag{5-16}$$

The L.H.S. of equation (5-16) is plotted against $(2y/h_c)$ for different values of λ in Figure 5.3(a). By inspection, we choose the value $(2y/h_c)=$ 0.636 where the non-dimensional stress is almost independent of λ. In Figure 5.3(b) the R.H.S. of equation (5-16) is plotted against λ for $(2y/h_c) = 0.636$. We find that this quantity varies only between 1.00465 and 1.00485 for $4 < \lambda \leq 6$, hence choosing a mean value of 1.00475, we obtain

$$(\sigma_b)_{y_s} = \frac{1.00475\ M}{b_c h_c^{\,2}/4} \tag{5-17}$$

for $y = y_s = 0.318h_c$

The strain-rate at the fiber y_s from the neutral axis is

$$\dot{\varepsilon} = -y\dot{v}''$$

and therefore it remains to determine that value of x for which $\dot{v}''$ is

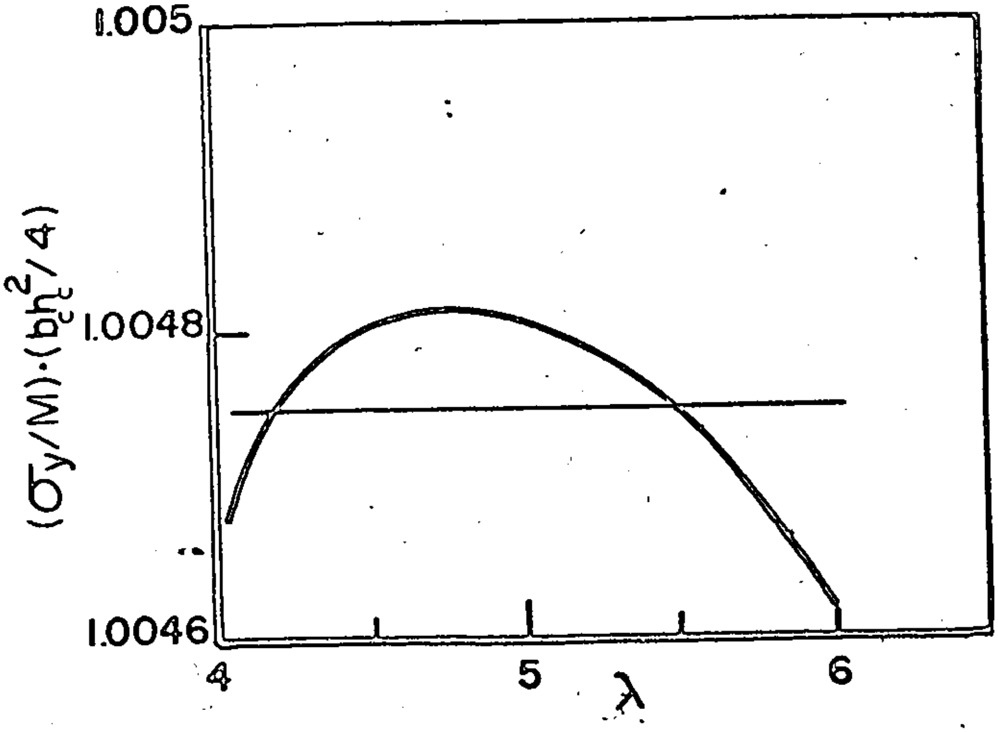

Fig. 5.3(b) Determination of the non-dimensional co-ordinate ($2y_s/h_c$) of the skeletal point.

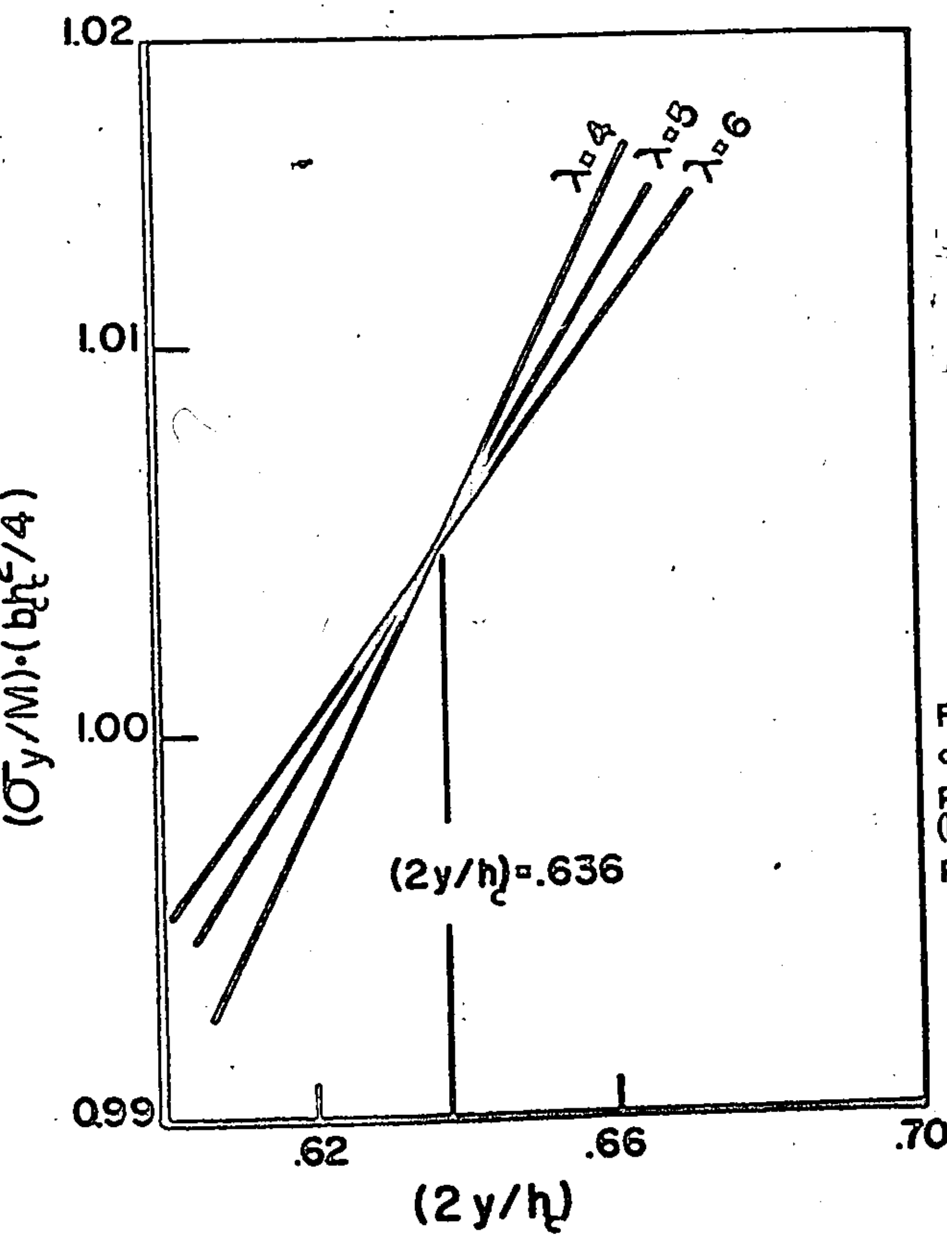

Fig. 5.3(a) Determination of the non-dimensional parameter (σ_y/M). ($b_c h_c^2/4$) at the skeletal point.

approximately the same function of the measured $\dot{\delta}$ regardless of the value of λ.

Following a similar method we can obtain from equations (5-13) and (5-14) a non-dimensional rate of change of curvature, namely

$$\frac{\dot{v}''}{\dot{\delta}/\ell_c^{\,2}} = (2\lambda+2) \left(\frac{x}{\ell_c}\right)^{2\lambda} \tag{5-18}$$

Plotting the L.H.S. of equation (5-18) versus (x/ℓ_c) for different values of λ, as shown in Figure 5.4(a) and choosing $(x/\ell_c) = 0.918$ we obtain from Figure 5.4(b) that the R.H.S. of equation (5-18) varies only between 5.02 and 5.10 for $4 \leqslant \lambda \leqslant 6$.

Therefore for $(x/\ell_c) = 0.918$ or $x_s = 0.918\ \ell_c$ it is sufficiently accurate to write

$$(\dot{v}'')_{x_s} = \frac{5.07\ \dot{\delta}}{\ell_c^2} \tag{5-19}$$

Thus, combining equations (5-2) and (5-19), the strain-rate at a distance y_s from the neutral axis at the section at x_s is

$$(\dot{\varepsilon}_b)_{x_s, y_s} = -y_s\ \frac{5.07\ \dot{\delta}}{\ell_c^2} = -\ 1.612\ \frac{\dot{\delta} h_c}{\ell_c^2} \tag{5-20}$$

Equations (5-17) and (5-20) thus permit the stress and strain-rate at a particular point to be determined explicitly from a cantilever test variables, geometry and loading, provided the index λ for the material is in the range $4 \leqslant \lambda \leqslant 6$.

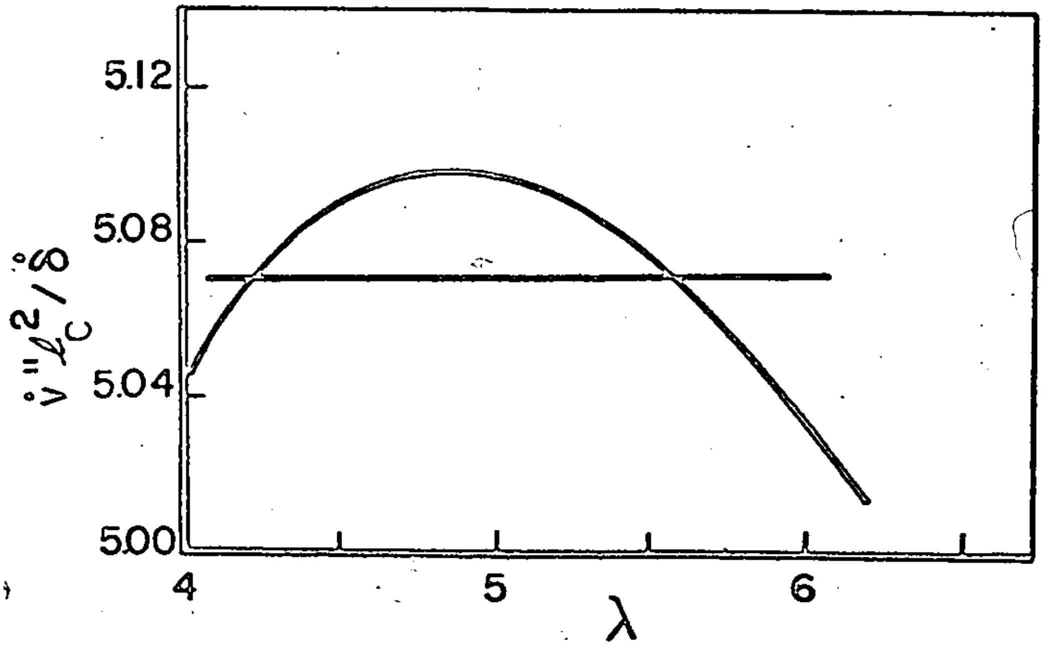

Fig. 5.4(b) Determination of the non-dimensional parameter ($\dot{v}''\ell_c{}^2/\mathring{\delta}$) at the skeletal point.

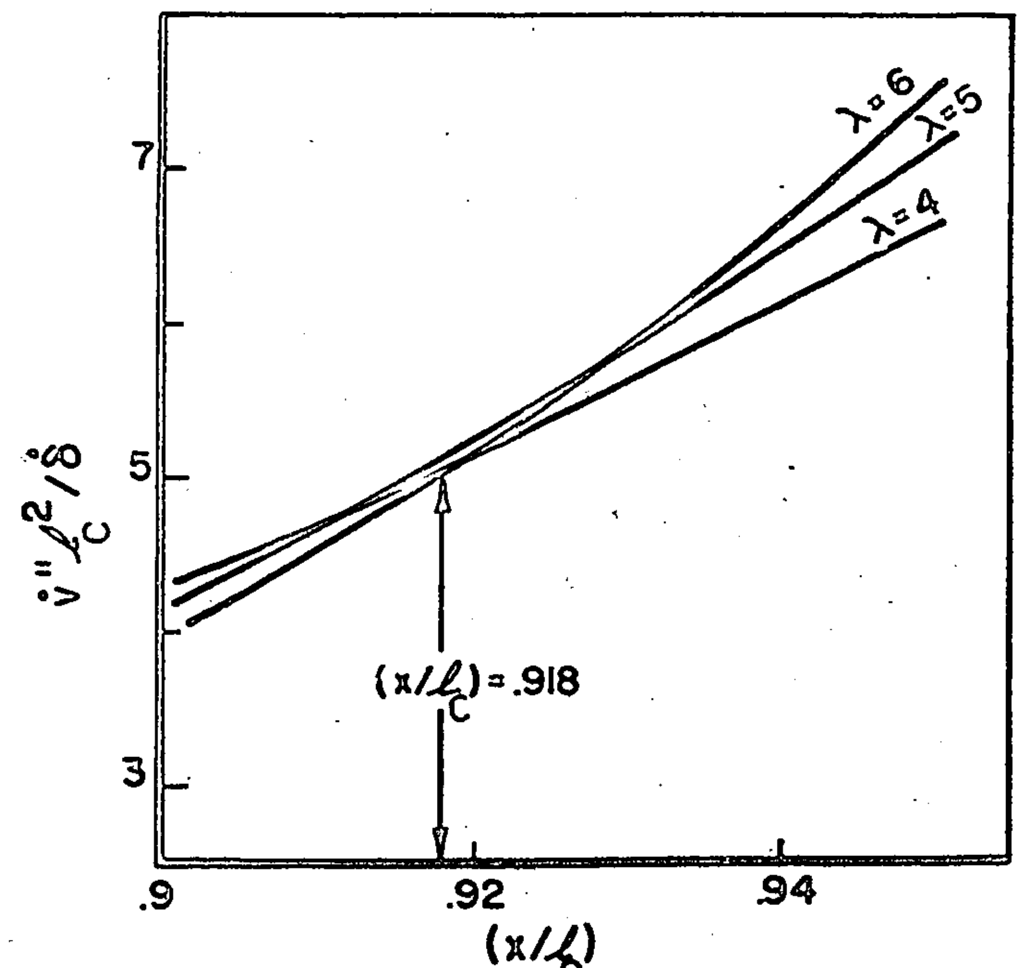

Fig. 5.4(a) Determination of the non-dimensional co-ordinate (x_s/h_c) of the skeletal point.

5.3 Creep Experiments

5.3.1 Material

The material used was 78%Zn -22%Al eutectoid alloy in the ultra-fine grain state, [4.2]. It was produced by homogenizing cast slabs at 360°C for a minimum of 8 hours, hot rolling to 90% reduction above 280°C, solution treating at 340°C, quenching in cold water for 30 to 40 seconds and finally cold rolling to 0.05 inches thickness.

5.3.2 Bending Test.

The sheet was set up as shown in Figure 5.5, so that two different cantilever lengths were obtained. It was clamped horizontally between straight pieces of timber to ensure a uniform grip and to prevent rotation at the point of support. The deflection was measured at the edge of the sheet with a vernier height gauge reading up to 0.001 inch. Three readings across the width of the sheet were taken each time and averaged. The tests were conducted at room temperature (28.0, ± 2°C).

Figure 5.6 shows deflection-time curves obtained for different cantilever lengths. Deflections were measured up to a total value of 20% of the span and the testing time ranged from 6 to 220 hours. It was observed that, after a transient period, the deflection rates become approximately constant. These constant deflection rates are presented in Table5.1.

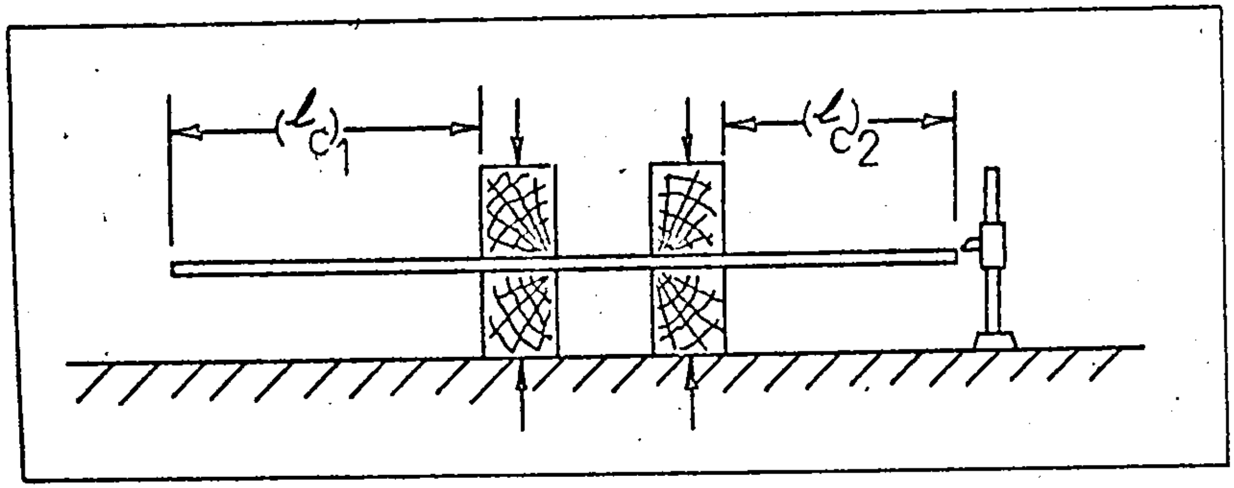

Fig. 5.5 Experimental arrangement for the two cantilever plate method.

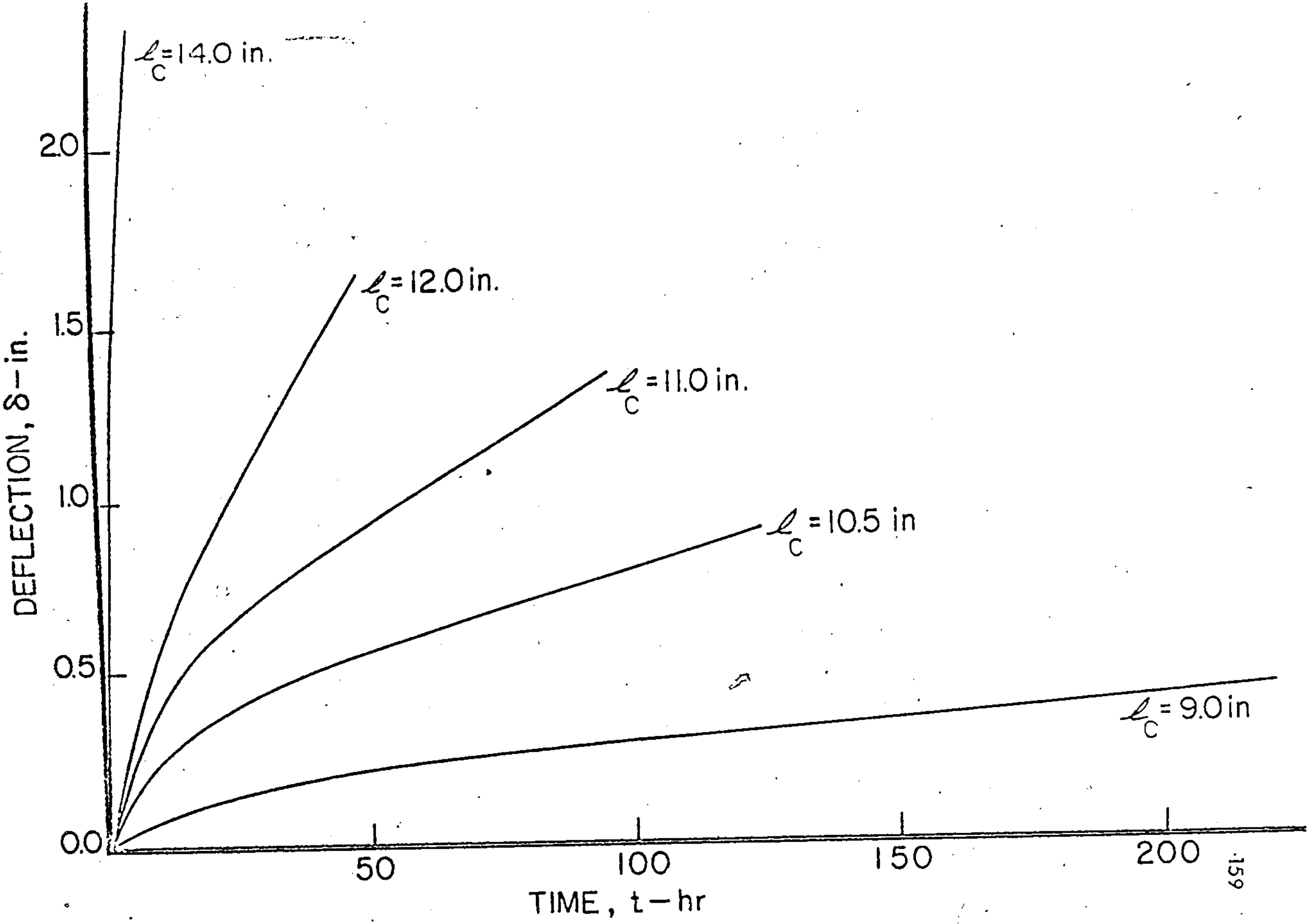

Fig. 5.6 Experimental deflection-time curve for superplastic Zn - Al sheet cantilever.

TABLE 5.I : Constant Deflection Rates for Different Cantilever Lengths

Cantilever length ℓ_c, inch	9	10.5	11	12	14
Deflection rate $\dot{\delta}$, inch/hr	0.0011	0.0053	0.0091	.0256	0.244

5.3.3 Tension Test .

Constant load tests were also carried out at the same temperature . Undeformed and tested specimens are shown in Figure 5.7. A 4 inch gauge length was scribed on the test-piece and current gauge lengths measured during the test using a cathetometer reading in divisions of 0.0005 inches.

Extension-time curves were obtained, as shown in Figure 5.8 for various tensile specimens each subjected to a different constant load. A secondary creep region, identified by a constant extension rate, was observed for all the tests. These rates are given in Table 5.II.

TABLE 5.II: Constant Creep Rates for Different Tensile Loads

Load, P lbs	25.30	27.80	33.03	42.85	62.94
Nominal Stress, σ lbf/in^2	1274	1399	1662	2134	3150
Creep rate $\dot{\Delta}$, inch/hr	7.82 10^{-5}	1.54 10^{-4}	1.47 10^{-3}	8.00 10^{-3}	4.06 10^{-2}

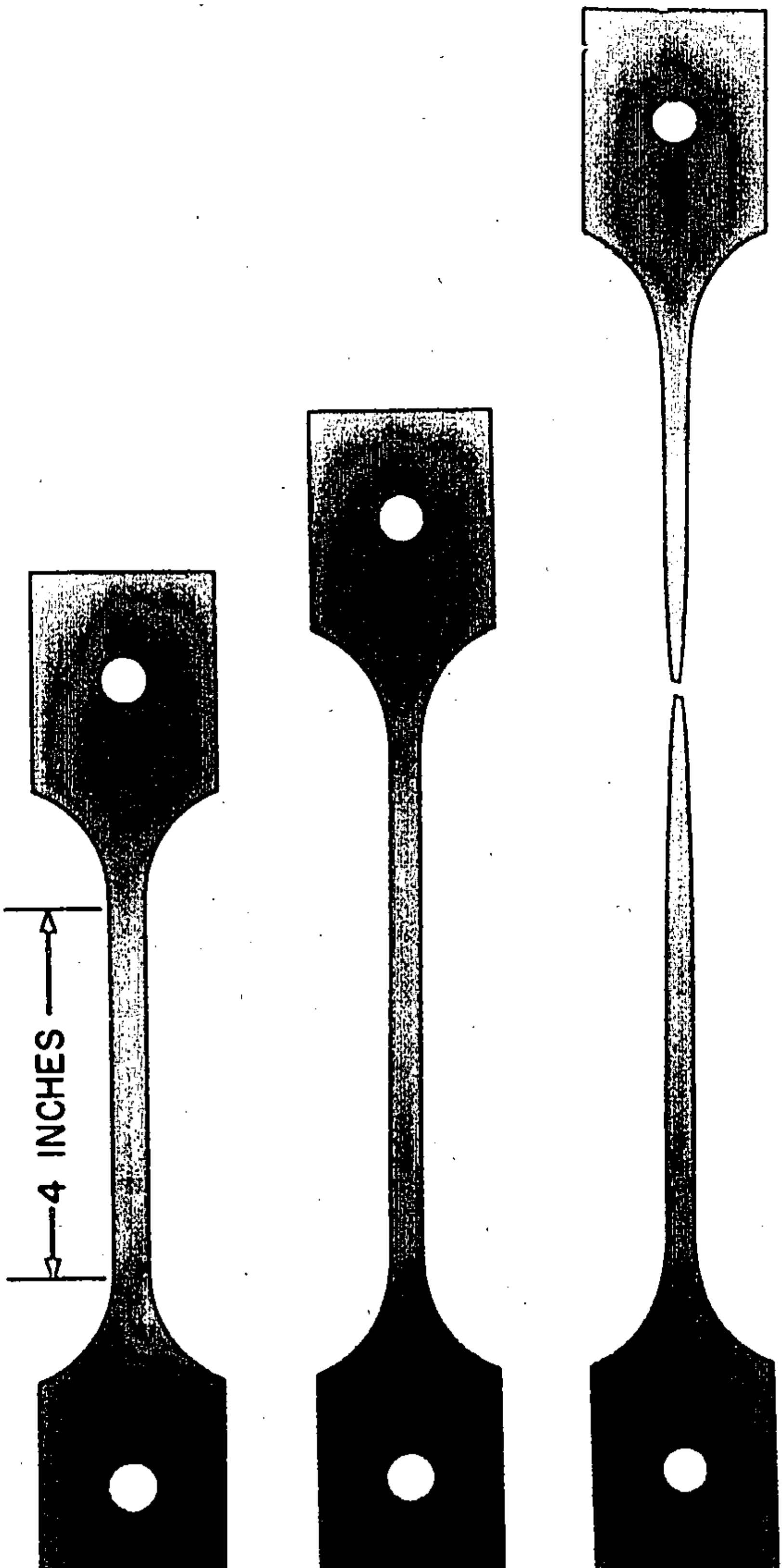

Fig. 5.7 Tensile superplastic Zn-Al specimens before and after creep testing

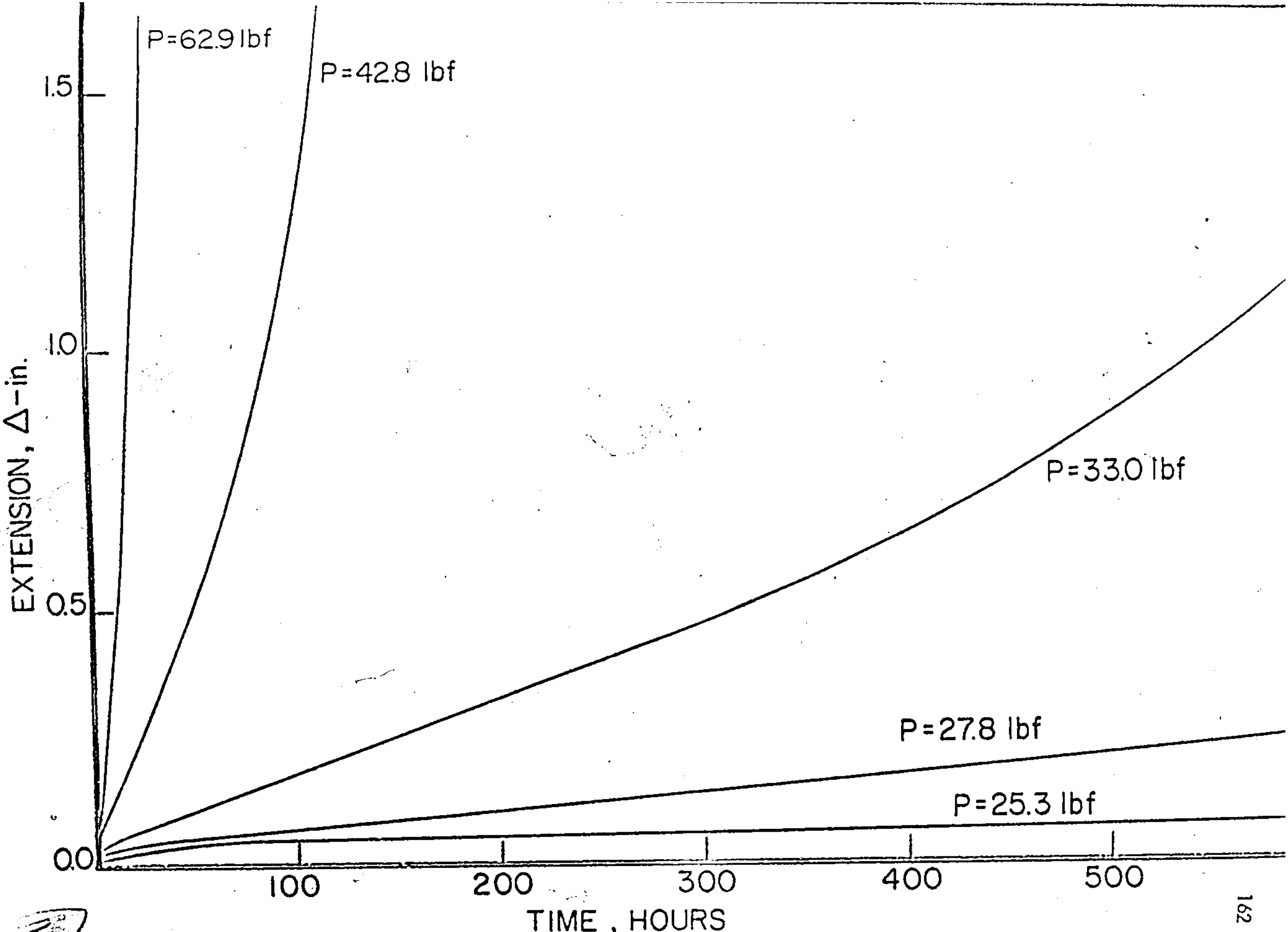

Fig. 5.8 Experimental extension-time curves for superplastic Zn - Al tensile specimens.

The nominal stress varied from 1200 to 3200 lbf/in^2 and the total testing time was between 30 to 600 hours respectively. Elongations up to 140% were reached before rupture as illustrated in Figure 5.7.

5.4 Calculation of Creep Data

Using the data in Table5.I and equation (5-15) the creep constants were determined from two pairs of tests and are presented in Table5.III.

TABLE5.III Creep constants determined from two pairs of bending tests.

$(\ell_c)_1 / (\ell_c)_2$	(14/9)	(12/10.5)
λ	5.11	4.89
σ_0 lbf/in^2	543	576

Again using the data in Table5.I and the skeletal point method (equations (5-17) and (5-20), the stress and strain-rate at the skeletal point (x_s, y_s) were calculated and plotted in Figure 5.9. (The load intensity, q, in this evaluation is equal to the weight per unit length of the strip.) A straight line was fitted by the method of least squares; this gave values for the creep constants of σ_0 = 674 lbf/in^2 and λ = 5.08.

From two tensile tests at different loads, the creep constants can be obtained using the equation,

$$\frac{\dot{\Delta}_1}{\dot{\Delta}_2} = \left(\frac{P_1}{P_2}\right)^{\lambda} \tag{5-21}$$

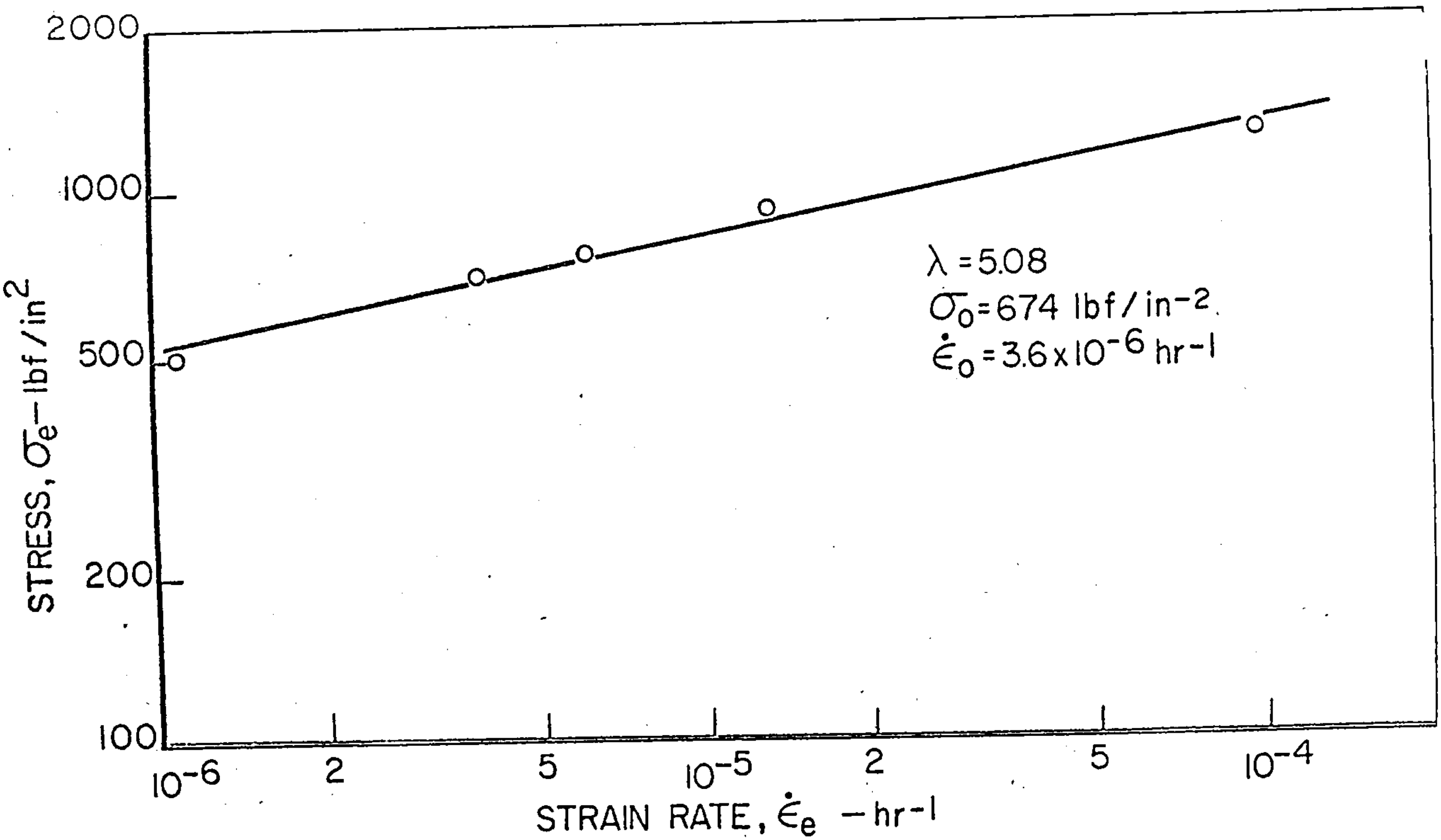

Fig. 5.9 Stress, strain-rate data obtained from cantilever bending tests of superplastic Zn-Al sheets

Table 5.IV gives the values of λ and σ_o as determined for arbitrarily chosen pairs of experiments.

TABLE 5.IV: Creep constants determined from two pairs of tensile tests.

P_1/P_2	$\frac{62.94}{25.30}$	$\frac{62.94}{33.03}$
λ	6.94	5.13
σ_o lbf/inch ^{2}	1070	716

True stress and strain-rate at an arbitrarily selected value of strain of 6% were calculated from tensile extension-time curves shown in Figure 5.8. The stress, strain-rate points are plotted in Figure 5.10 and these points are fitted by a line which gives values for the creep constants of $\sigma_o = 953$ lbf/in^2 and $\lambda = 6.67$. Figure 5.10 shows the stress and strain-rate points calculated from both the tensile and the bending tests. The least square fitting method is used again to obtain the creep constants of $\sigma_o = 702$ lbf/in^2 and $\lambda = 4.88$.

TABLE 5.V: Creep constants determined from stress, strain-rate points for different types of tests.

Type of test	λ	σ_o
Tensile Tests	6.67	953
Bending Tests	5.08	674
Tensile and Bending Tests Together	4.88	702

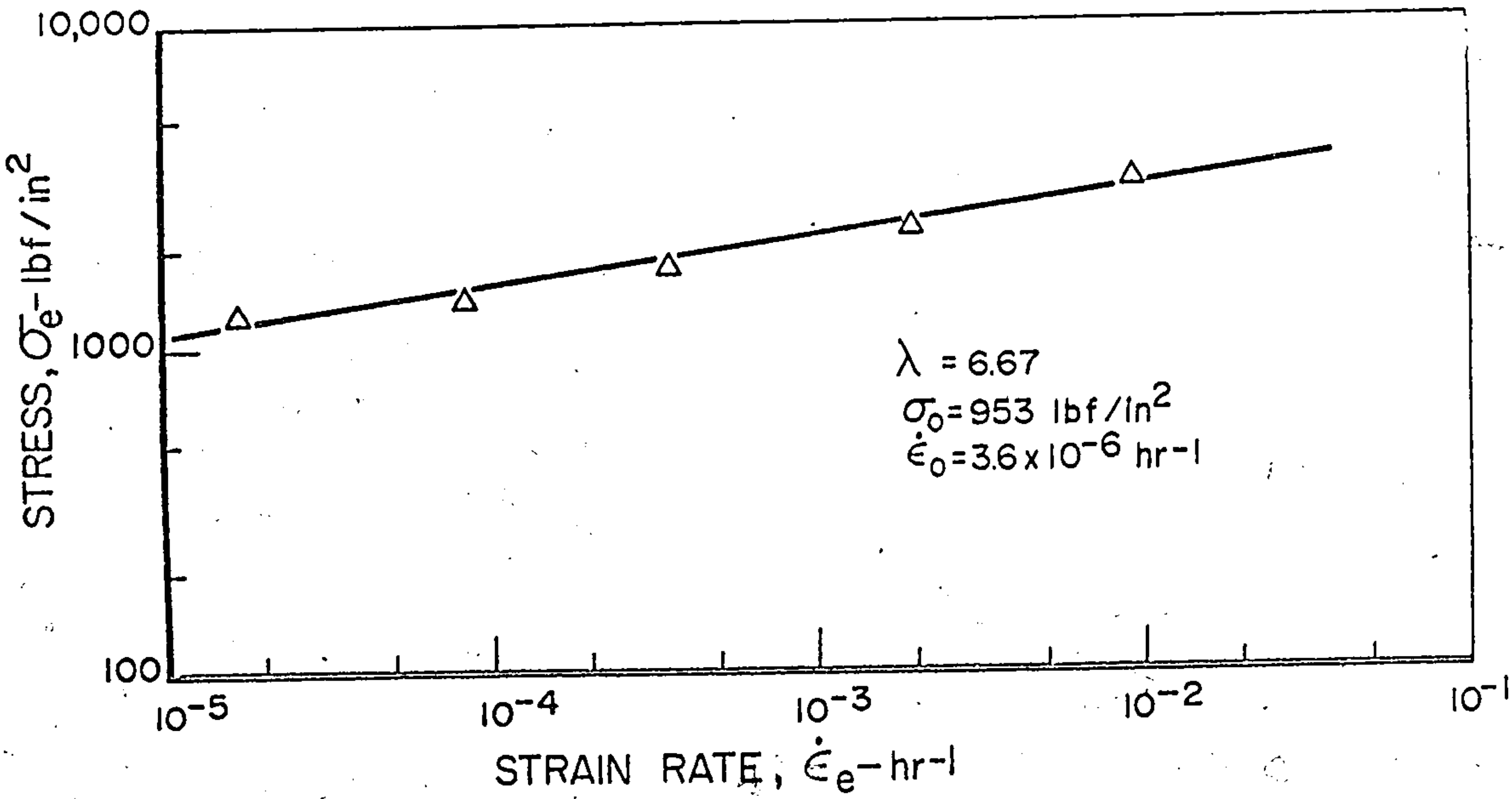

Fig. 5.10 Stress, strain-rate data obtained from tensile creep tests of superplastic Zn – Al specimens.

5.5 Comparison of Bending and Tension Test Results

The values of the creep constant σ_o and λ for the different tests in Tables 5.III and 5.IV show considerable discrepancy both between each type of test and between pairs of tests of the same kind. It has been observed elsewhere that there is generally some discrepancy between the results of different pairs of tests in the tension test.

The results in Figures 5.9 and 5.10 are shown together in Figure 5.11. Differences of the magnitude shown by this diagram are not unusual when tests conducted under different stress systems are compared [2.33]. The following factors may contribute to the discrepancy;

(i) multiaxial creep theory is employed to obtain equivalent stress and strain-rate from the bending test; it is unlikely that this theory will be obeyed exactly by the material [2.23;]

(ii) the uniaxial data refer to behaviour at a strain of 6% whereas the bending creep data indicates the behaviour of material at a considerably lower total strains, probably less than 1%;

(iii) the time scale of uniaxial and bending tests was different as may be seen from Figure 5.6 and 5.8 and although there is an overlap of strain-rates from the two tests, most of the bending tests gave a result for a lower strain-rate than in the tension tests;

(iv) although the bending stress and the axial stress in the tension test were both aligned in the direction of rolling

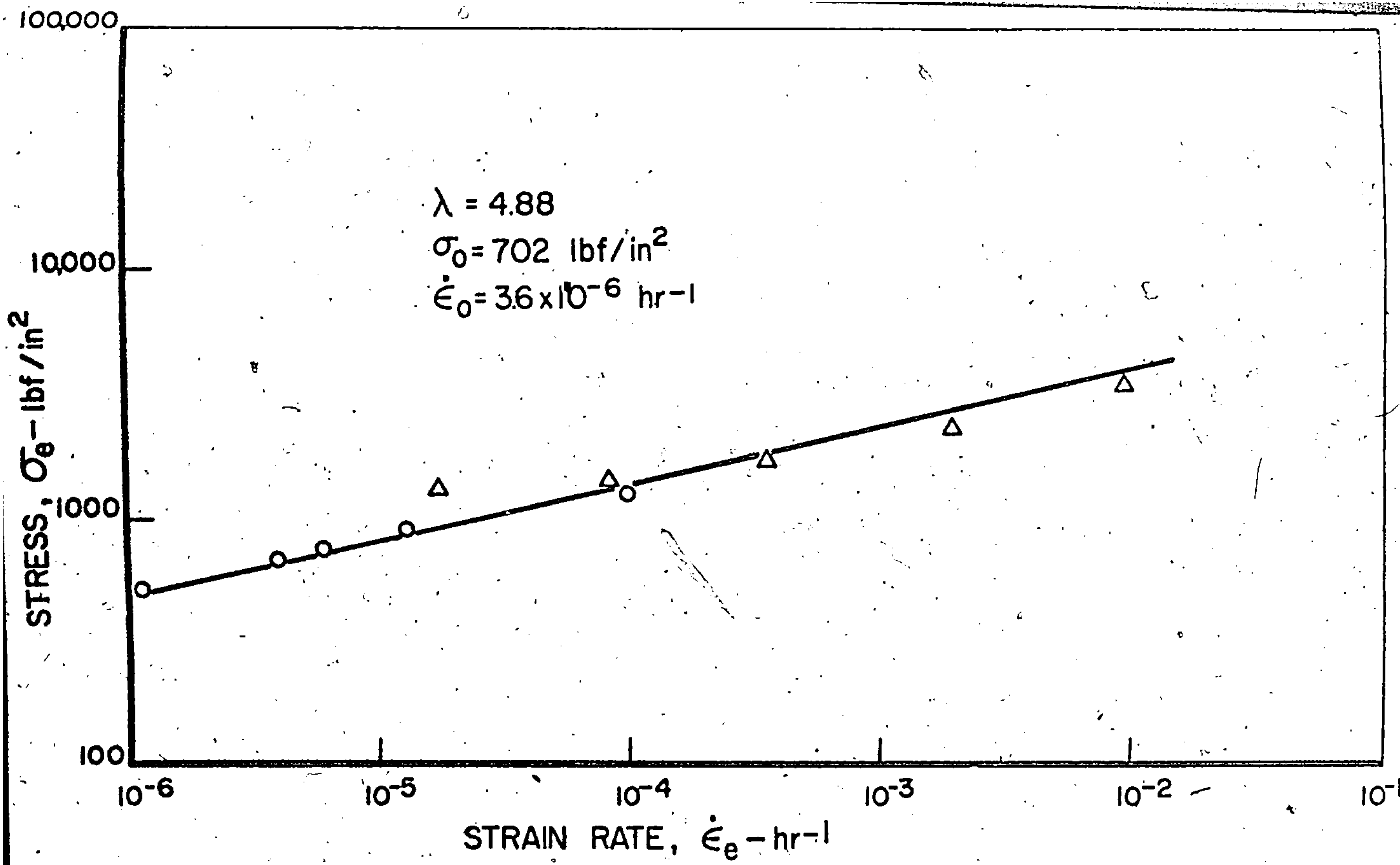

Fig. 5.11 Stress, strain-rate data obtained from tensile and bending creep tests together.

(0 - bending, Δ - tensile)

of the sheet, anisotropy and non-uniformity in the sheet could both lead to different results in each test.

5.6 Conclusions

For sheet material, creep data can be obtained from a test in which a wide strip is mounted as a horizontal cantilever loaded by its own weight. Data from this test can be expressed in the same form as the results of uniaxial tests.

Creep data in the form of constants in an empirical equation can be obtained from data from two bending tests but this method does not appear to give reliable results. A stress, strain-rate curve can be obtained from a number of bending tests by identifying the skeletal point for the beam.

Comparison of the results of bending and uniaxial tests indicates a significant difference between the two. This may well be due to deficiencies in the creep theory used to correlate the two results rather than attributing the discrepancy to defects in either test method. As creep data is used principally for design purpose and most design problems involve a multi-axial stress system, complex creep theory must be used inevitably to incorporate any test data into a real analysis. The criteria therefore for any test should not be whether it gives data which agrees well with uniaxial test data, but whether the data leads to reliable design predictions. Given the uncertainties which exist in the present creep theories, it is probable that the best test will be that in which the stress system resembles most closely the stress system in the real problem.

The bending test can be performed in a short time using simple measuring equipment. Also the results presented here indicate that it is a valid and economical test for superplastic sheet material. It is likely that further experiments would validate the method for other classes of material and the theory can readily be extended to cover tests in which higher stress levels are obtained by adding a point load (a weight) to the end of the cantilever. Developments of this kind could lead to substantial reduction in the cost of performing routine creep tests.

CHAPTER VI

REVERSE-EXTRUSION OF SUPERPLASTIC ALLOYS

6.1 Introduction

Bulk forming process such as extrusion, forging and hot rolling are compressive in nature and the analysis of forming loads is of technological importance. With rigid plastic materials, a value can be obtained for the forming load and this can generally be expressed in a non-dimensional form as a ratio between some applied pressure and the flow stress as in the extrusion parameter $\bar{P}/2k$ where k is the yield shear stress. With rate-dependent materials however, such as superplastic alloys, there is no single forming load, but rather a relationship between applied load and forming speed. Thus one must ensure that not only is the force capability of the machine sufficient but also that the speed of the operation is appropriate.

Comparatively little attention has been given to the problem of extrusion of rate-dependent materials [6.1] to [6.4]. Only a few investigators have considered the problem of forward extrusion of these materials, and all aimed at obtaining an average or mean value of the strain-rate. As pointed out by Jonas, the strain-rate in an element of material passing through a process could be averaged either with respect to time and/or with respect to some displacement parameter in the process; these averages could differ by as much as an order of magnitude. Differences of this magnitude in strain-rate determination however will not lead to such large differences in load if the material has a rate-sensitivity index of 0.2 or less as in hot working of metals.

Jonas' analysis [6.3] of rate-dependent extrusion is based on homogeneous work hypothesis, i.e. neglecting the redundant work. This obviously would result in an underestimation of the effective strain and strain-rate within the deformation zone.

Other analyses [6.4] consider conical flow with an element consisting of a spherical shell, velocity discontinuities at each end of the zone being neglected. Such analyses fail to deal with the important features of industrial extrusion processes where large reductions and square dies are frequently employed.

Another approach to this kind of problem has developed from visioplasticity methods [6.2] and [6.5] and employs digital computers to determine loads for rate-dependent materials as in the work of Shabaik and Kobayashi [6.5]. This approach however often fails to convey a generalized physical concept of important aspects of the process and can be extremely expensive in terms of computational costs.

Perhaps the most useful analytical techniques for studying extrusion have been the slip-line field and upper bound methods. These can only be conveniently applied to the analysis of plane strain rigid, perfectly plastic problems, but various techniques have been developed whereby solutions for general extrusion problems can be infered from plane strain solutions. Techniques have also been developed for accommodating strain-hardening behaviour, [6.6] and [6.7].

In the present work, the process considered is the reverse-extrusion of a cylindrical billet into a thin-walled cup as shown in Figure 6.1. Geometrically this operation resembles piercing or impact extrusion. Piercing of rigid, perfectly plastic materials was analyzed by Dipper [6.8] using a method first suggested by Siebel; the billet was assumed to deform in two homogeneous cylindrical zones and the radial stress was equated at the interface. Kudo obtained an upper bound solution to the same problem [6.9] assuming a central homogeneous cylinder and an outer ring in which tangential velocity discontinuities existed. Here, the effect of rate-sensitivity on the back-extrusion process is studied theoretically following the earlier approaches and considering separate deformation régimes; plane strain slip-line field solutions are employed to determine the average strain and pressure near the corner of the punch. It is shown that for a non-linear viscous material, a simple geometric factor, derived from the slip-line field, can be used to convert the solution for perfectly plastic material to one for a rate-sensitive material. The method appears to have a generality beyond the particular example of back-extrusion.

Theoretical results are compared with recently available experimental data on the back-extrusion of both as-cast and superplastic zinc-aluminum alloy.

6.2 Theoretical Analysis of Reverse-Extrusion

For the purpose of analysis, it is considered that there are four distinct régimes in the extrusion process as shown in the diagram in Figure 6.2. In zone I the material is compressed in an axisymmetric homogeneous process between frictionless surfaces. The material leaves I with an approximately uniform radially

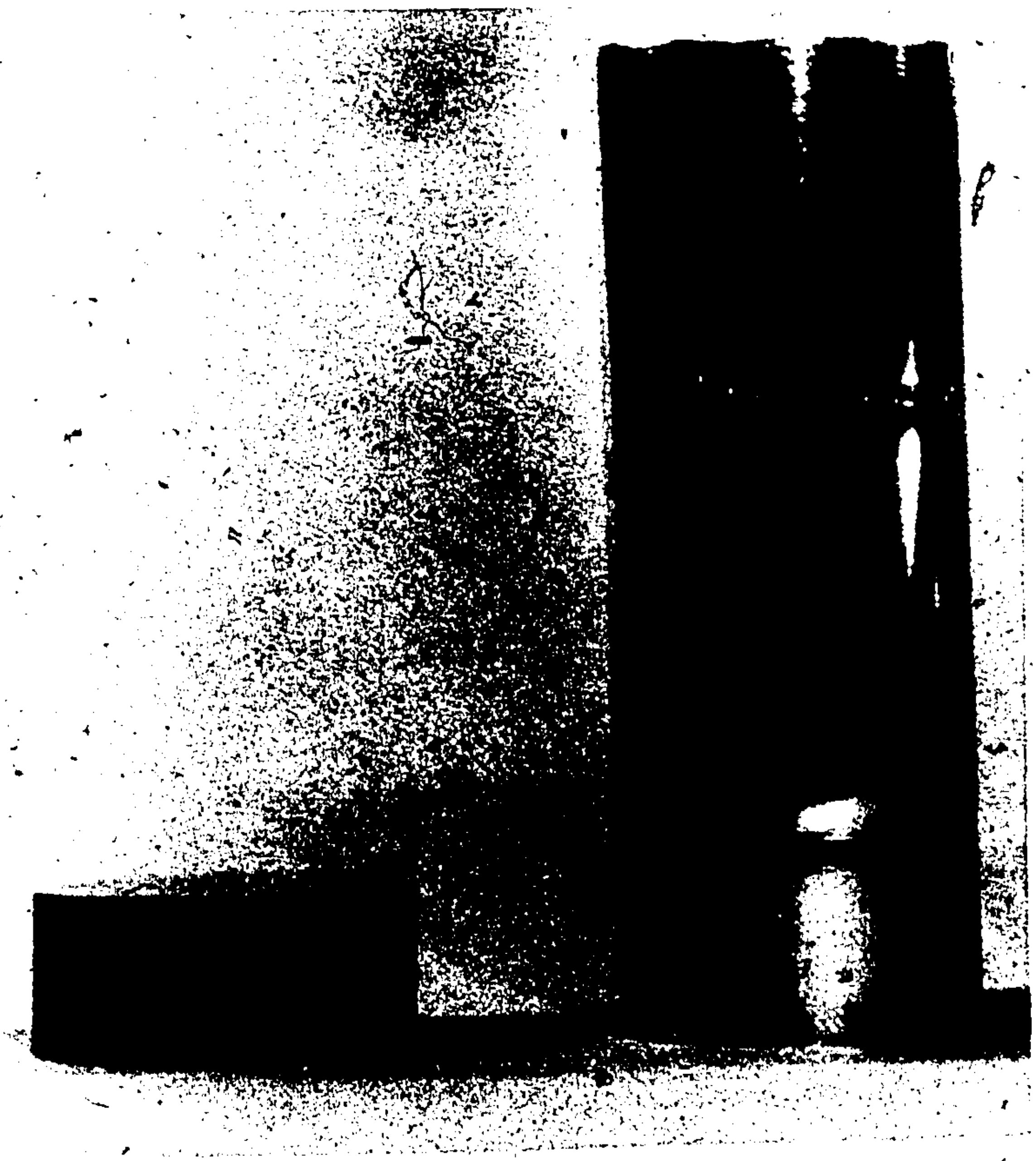

Fig. 6.1 Photograph of an eutectoid zinc-aluminum billet and a reverse-extruded cup [Ref. 6.15]

outwards velocity; the deformation in II is analyzed as a plane strain "side-extrusion" operation. The simplifying assumption of plane strain in this zone is defensible as the deformation occurs in a narrow annular region at the outer edge of the billet [6.10]. The material exits up the cup wall, IV, which is assumed rigid. Under certain conditions a dead metal zone, III, is considered to exist at the corners of the container.

It has been demonstrated that the geometry of deformation in extrusion processes is remarkably similar for a wide range of material behaviour, provided the tooling geometry and surface conditions are maintained constant, [6.2] and [6.10]. It is therefore assumed that the results of an analysis for a rigid, perfectly plastic material can be employed to establish mean values of strain-rate in the different zones for the extrusion of rate-dependent materials [6.11].

Superplastic alloys; over a few decades of strain-rate have a non-linear viscous behaviour which may be fitted by a power law,

$$\sigma = \sigma_0 \, \dot{\varepsilon}^m \qquad (6\text{-}1)$$

where the strain-rate sensitivity index m may have a value of about 0.5. In equation (6-1), the material parameter σ_0 has the dimensions [stress] [time]^m; this may lack mathematical elegance but is sanctioned by custom. The power law offers good limiting possibilities in theoretical analysis since for m = 1, the law describes Newtonian behaviour whereas the rigid, perfectly plastic material may be considered as a special case for which m = 0.

6.2.1 Rigid, Perfectly Plastic Analysis

The boundaries of the deformation zone II in Figure 6.2, are obtained from a slip-line field as shown in Figure 6.3. This slip-line field resembles the plane strain fields obtained for side extrusion [6.12]. In the reverse extrusion process, however, the depth of the billet, b, continuously diminishes and this is equivalent to a reduction in the "side extrusion ratio". The fields for different values of b are readily obtained as shown in Figure 6.3, and the mean radial pressure $\bar{P}_s$, can be derived, in the manner outlined in Appendix C, for each value of b. Figure 6.4 shows the gradual decrease of the parameter $(\bar{P}_s/2k)$ as b becomes smaller. The mean value of tool pressure on the inclined part of the punch, $\bar{P}_q$, can also be determined from this field.

In Zone I, Figure 6.2, if the uniaxial flow stress is σ_1, the pressure required to deform the material in the presence of a surrounding radial pressue $\bar{P}_s$, is

$$\bar{P}_r = \bar{P}_s + \sigma_1 \qquad (6\text{-}2)$$

This is based on the assumption that a hydrostatic stress does not affect yielding, even for rate-sensitive materials [2.23] and [4.1].

If the back-extrusion pressure is defined as

$$\bar{P} = \frac{\text{punch force}}{\text{punch c.s. area}} \qquad (6\text{-}3)$$

$$= \frac{F}{A_2}$$

then the equilibrium equation for the punch is

$$\bar{P}\ A_2 = \bar{P}_r\ A_1 + \bar{P}_q\ \cos\alpha.\ (A_2 - A_1) \qquad (6\text{-}4)$$

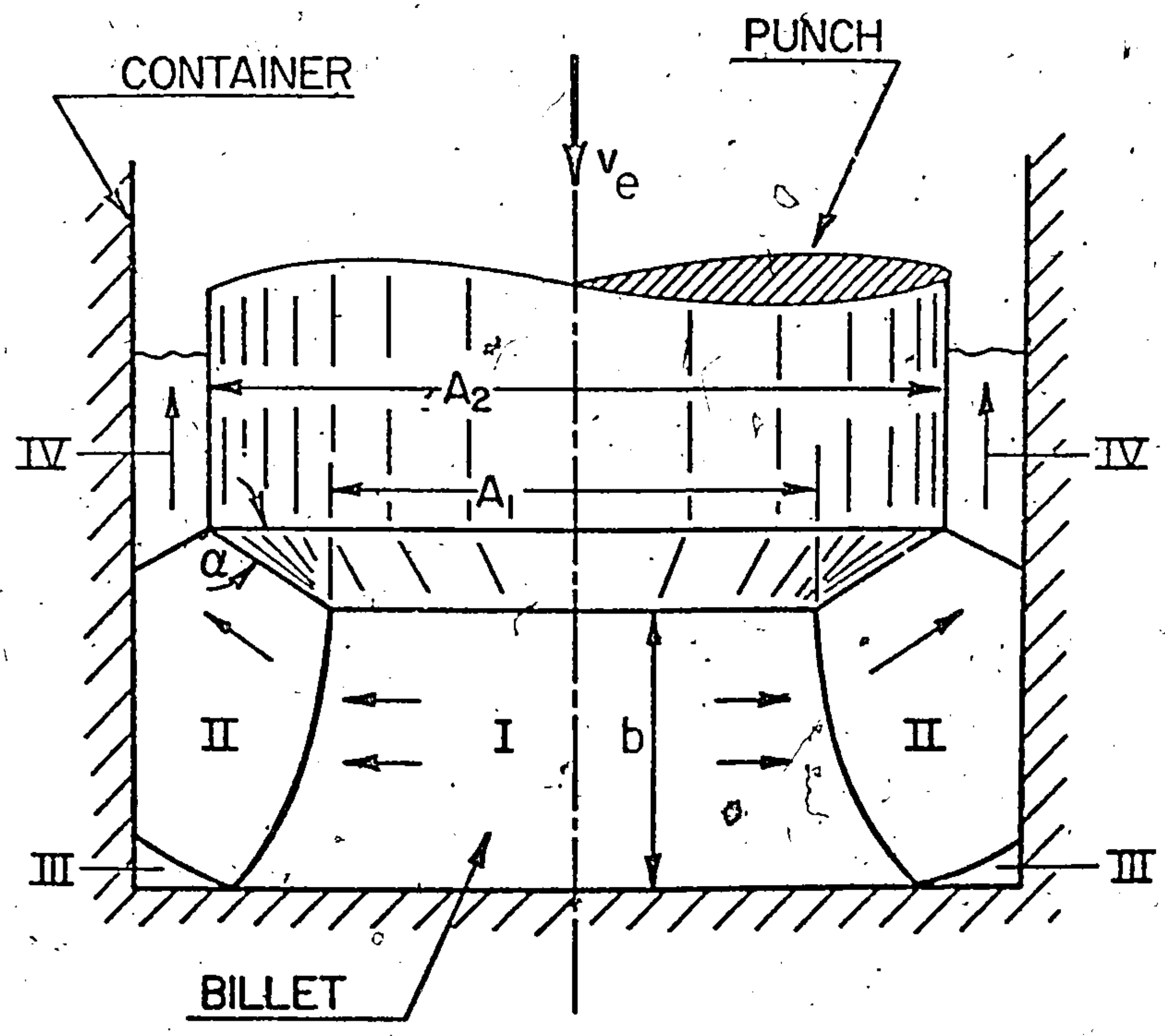

Fig. 6.2 Schematic diagram of axisymmetric reverse-extrusion showing the different deformation regions.

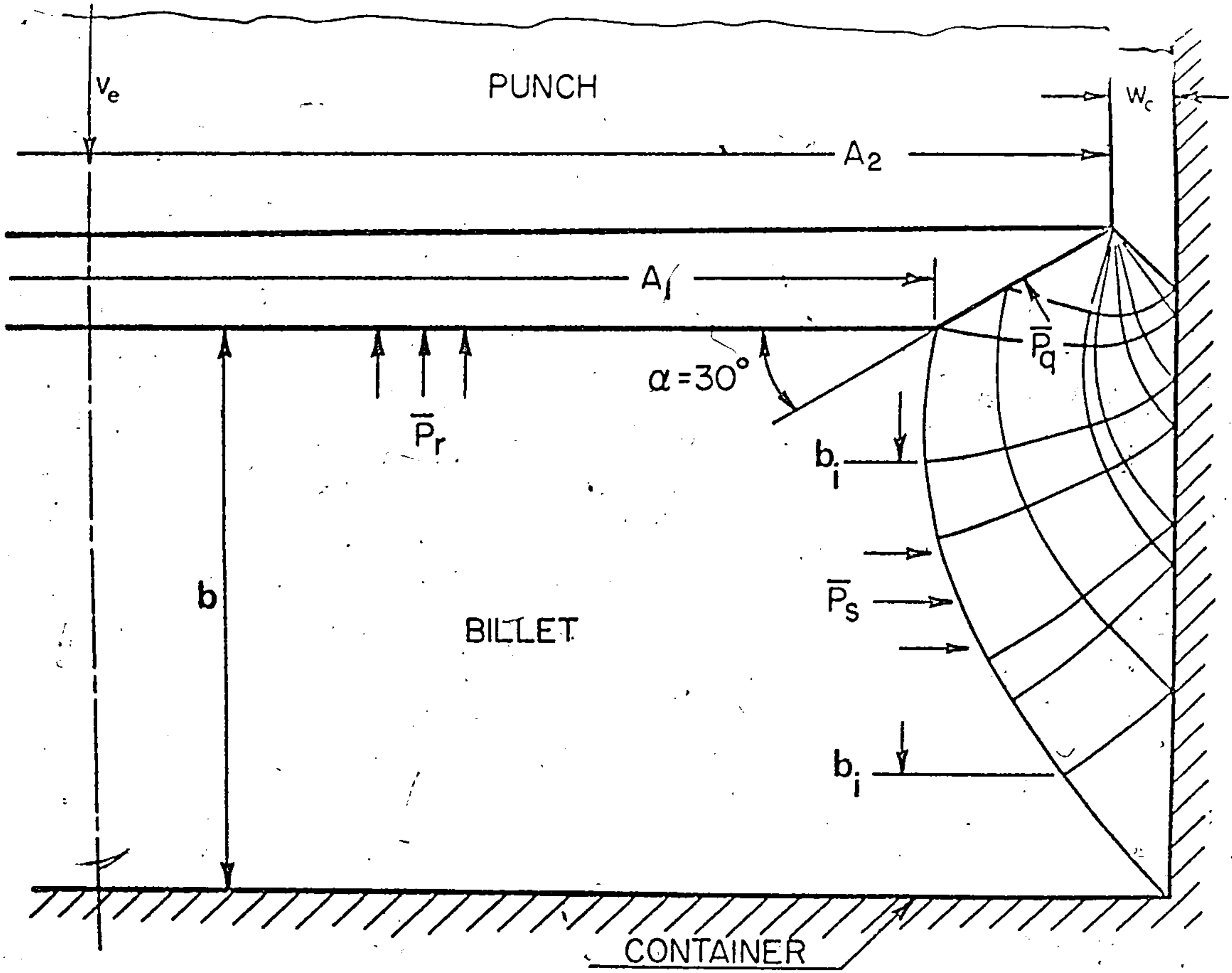

Fig. 6.3 Slip line field for the deformation in Zone II for a punch having a 30° chamfer angle.

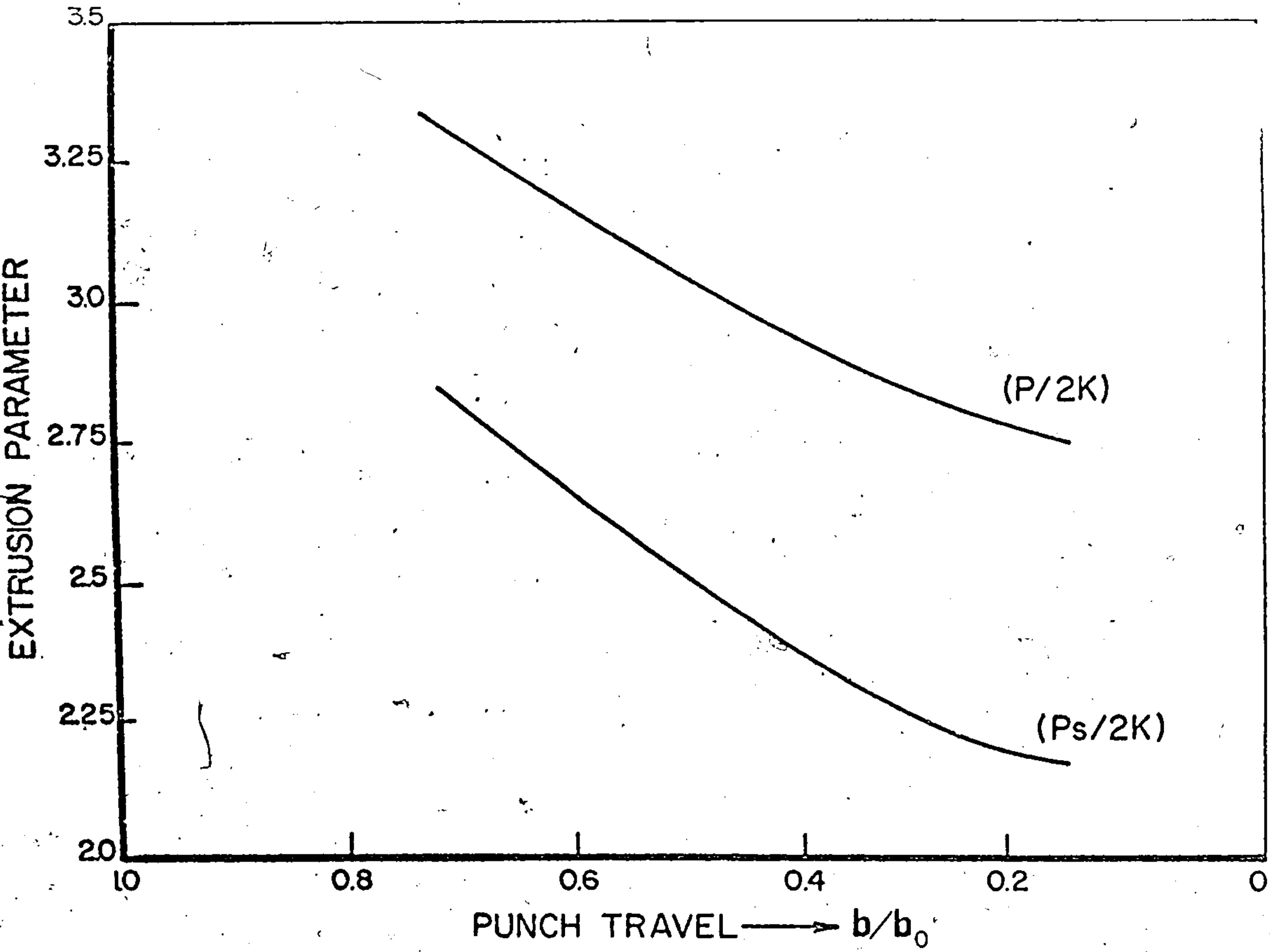

Fig. 6.4 Variation of the side extrusion parameter ($\bar{P}_s/2k$), and the total extrusion parameter ($\bar{P}/2k$) with billet height for rigid perfectly plastic material.

If a von Mises yield criterion is adopted, then the plane strain yield stress in zone II is,

$$2k = \frac{2}{\sqrt{3}}\,\sigma_2 = \frac{2}{\sqrt{3}}\,\sigma_1 \qquad (6\text{-}5)$$

as $\sigma_1 = \sigma_2$ for the perfectly plastic material. Equation (6–4) may then be written:–

$$\frac{\bar{P}}{2k} = \frac{A_1}{A_2}\left[\frac{\bar{P}_s}{2k} + \frac{\sqrt{3}}{2} + \frac{\bar{P}_q}{2k}\,\frac{(A_2 - A_1)}{A_1}\cos a\right] \qquad (6\text{-}6)$$

The variation of $(\bar{P}/2k)$ with billet height, b, is indicated by the curve for m=0 in Figure 6.5. For convenience, results are given in relation to an arbitrary initial billet height b_o, which is chosen so that with the given value of w_c a cup of height to diameter ratio of about 2.5 is produced. The gradual decrease in $\bar{P}$ as b becomes smaller may be attributed to the decreasing "side extrusion ratio".

6.2.2 Rate-Dependent Material

It is proposed here to use the slip-line field analysis for a rigid, perfectly plastic material to establish mean values of the strain-rate in the deforming zone for the extrusion of rate-dependent material. This follows an earlier technique used to analyze forming processes for strain-hardening materials. This technique modifies the results obtained from the slip-line field solution, with the aid of some assumptions concerning mean yield stress of the strain-hardening material [6.6] and [6.7].

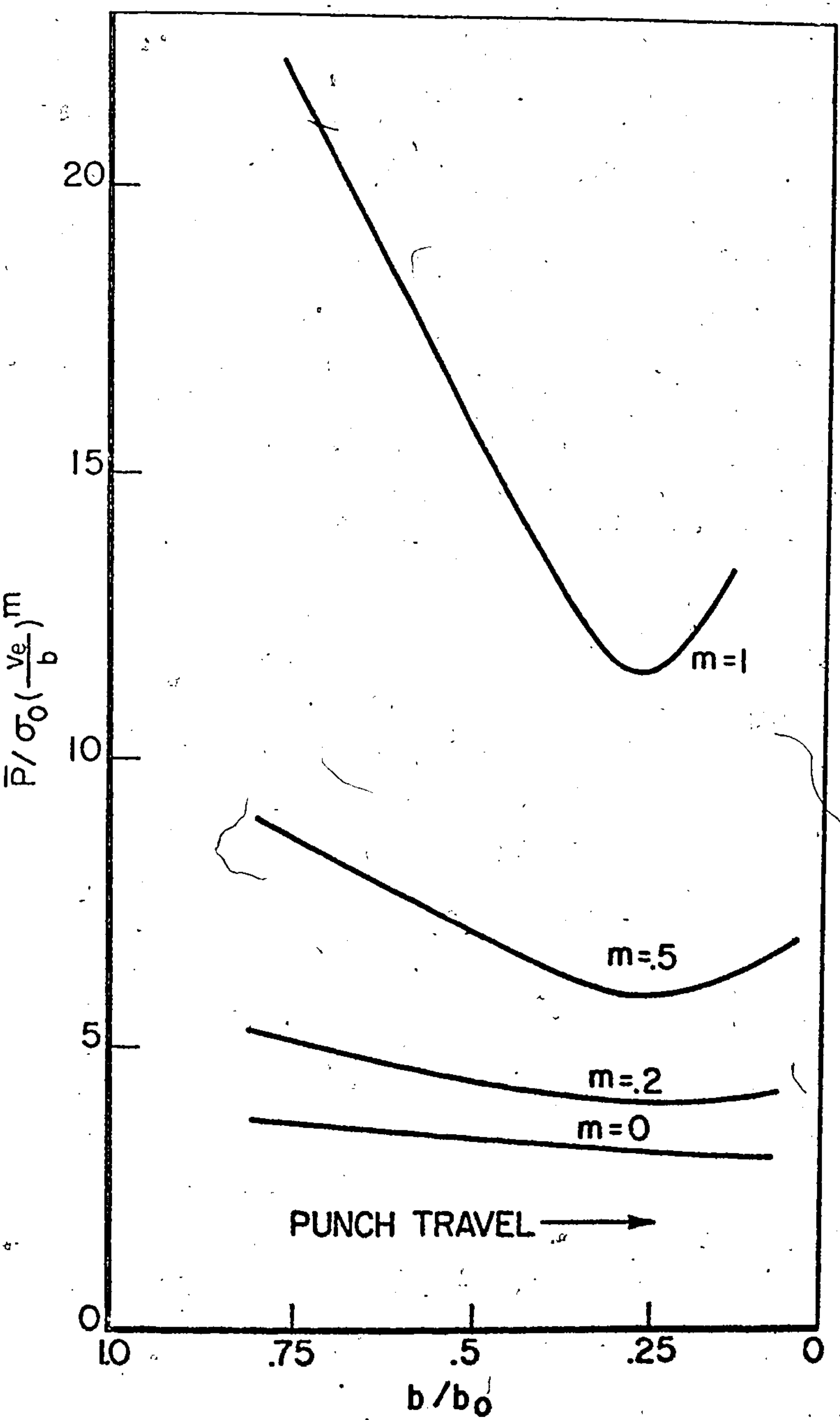

Fig. 6.5 Variation of the rate dependent extrusion parameter, $\bar{P}/\sigma_o(v_e/b)^m$, versus billet height for materials having different rate sensitivity, m.

Hill [6.13] first suggested this method for application to sheet drawing in connection with slip-line theory. His suggestion is also valid for extrusion problems and is explained briefly. If we consider an extrusion process without frictional boundaries then the work done by the extrusion force is consumed solely as plastic work done on the material. It can be shown that the average total plastic work which is absorbed by a material element of unit volume passing through the deformation zone is equal to $\bar{P}$ where $\bar{P}$ denotes the mean steady extrusion pressure. For a rigid perfectly plastic material, the work done per unit volume is also equal to Y $\int d\varepsilon_e$, where $\int d\varepsilon_e$ is the equivalent strain and Y the flow stress; therefore we can define a mean equivalent strain for the extrusion process as

$$(\int d\varepsilon_e)_m = \bar{P}/Y \qquad (6\text{-}7)$$

It must be assumed that the mean value of the equivalent total strain of any rate-sensitive material does not differ from that of the rigid perfectly plastic material. Furthermore we suppose that the extrusion is being carried out under identical geometrical and frictional conditions. Therefore in the extrusion zone II, the effective strain may be expressed by

$$(\int d\varepsilon_e)_2 = \frac{\bar{P}_s}{2k} \qquad (6\text{-}8)$$

which is obtained from the slip-line field. The rate at which material passes through this zone is not easily ascertained as the volume of zone II decreases continuously with b. If we consider however that the container is fixed in space, then the volume of material in the cup wall, IV, which passes a fixed point in the container in unit time is

$$\dot{V} = A_2 v_e \tag{6-9}$$

At any instant, the volume of the deformation zone II, denoted by V_2, may be obtained from the slip-line field, so that the time taken for unit volume to pass through zone II is

$$t = \frac{V_2}{\dot{V}} \tag{6-10}$$

The "mean effective strain-rate" in II is therefore,

$$(\dot{\varepsilon}_e)_2 = \frac{(\int d\varepsilon_e)_2}{t} = \frac{\bar{P}_s}{2k} \frac{\dot{V}}{V_2} \tag{6-11}$$

From equation (6-1), the "mean effective flow stress" in II is

$$\sigma_2 = \sigma_o \left\{ \frac{\bar{P}_s}{2k} \frac{\dot{V}}{V_2} \right\}^m \tag{6-12}$$

The strain-rate in the homogeneous compression zone I is

$$\dot{\varepsilon}_1 = \frac{v_e}{b} \tag{6-13}$$

so that the uniaxial flow stress, from equation (6-1) is,

$$\sigma_1 = \sigma_o \left(\frac{v_e}{b}\right)^m \tag{6-14}$$

The equilibrium equation (6-6) may now be re-written for the rate-dependent case, bearing in mind that the effective flow stresses in zones I and II are different; namely,

$$\bar{P}A_2 = A_1 \; [\; \{ \frac{\bar{P}_s}{2k} + \frac{\bar{P}_q}{2k} \cos\alpha \; (\frac{A_2 - A_1}{A_1}) \} \; \frac{2}{\sqrt{3}} \sigma_2 + \sigma_1] \qquad (6\text{-}15)$$

It is convenient to introduce a factor ϕ defined as

$$\frac{\sigma_2}{\sigma_1} = [\frac{(\dot{\varepsilon}_e)_2}{(\dot{\varepsilon}_e)_1}]^m = \phi^m \qquad (6\text{-}16)$$

It may be shown from equations (6-9), (6-12) and (6-14) that

$$\phi = \frac{\bar{P}_s}{2k} \cdot \frac{A_2 b}{V_2} \qquad (6\text{-}17)$$

and this can be determined completely from the slip-line field without reference to material behaviour. It is thus a non-dimensional geometric property of the particular extrusion process.

Using this factor, equation (6-15) can be written as

$$\frac{\bar{P}}{\sigma_o \; (v_e/b)^m} = \frac{A_1}{A_2} \; \{ \frac{2}{\sqrt{3}} \; \phi^m \; [\frac{\bar{P}_s}{2k} + \frac{\bar{P}_q}{2k} \cos\alpha \frac{(A_2 - A_1)}{A_1}] + 1 \} \qquad (6\text{-}18)$$

The right hand side of equation (6-18) depends only on the geometry of the extrusion and the rate-sensitivity index, m. The variation of $\bar{P}/\sigma_o$ $(v_e/b)^m$ with b for different values of m is shown in Figure 6.5.

The denominator on the left hand side of equation (6-18) clearly corresponds to the familiar 2k in rate-independent extrusion although it is only an indirect indication of material strength. If at some strain-rate other than unity, materials have the same flow stress but different rate-sensitivities, m, then the value of σ_0 will be different for each material; thus the fact that the $\bar{P}/\sigma_0(v_e/b)^m$ parameter in Figure 6.5 is higher for materials with higher m, does not mean that these materials will require a higher extrusion pressure $\bar{P}$ at all strain-rates.

The manner in which the absolute extrusion pressure varies during the process can be determined from a diagram such as Figure 6.6. If the punch speed is constant, the denominator of the extrusion parameter $\bar{P}/\sigma_0 (v_e/b_0)^m$ is constant; these curves apply to the particular case in which b_0/w_c is about 13.0. It may be seen that while the extrusion pressure continually falls during the stroke for the perfectly plastic material, m=0, the effect is very different for viscous materials and for m=1, the pressure rises rapidly as b becomes small.

The majority of industrial superplastic alloys will have a rate-sensitivity in the range $0.2 < m \leq 0.5$. In the middle section of the punch travel, Figure 6.6 indicates that the punch load would remain reasonably constant for constant speed extrusion. This suggests a "steady-state" in the extrusion of these alloys, however it will be appreciated that this steady-state is more apparent than real. It results from the countervailing effects

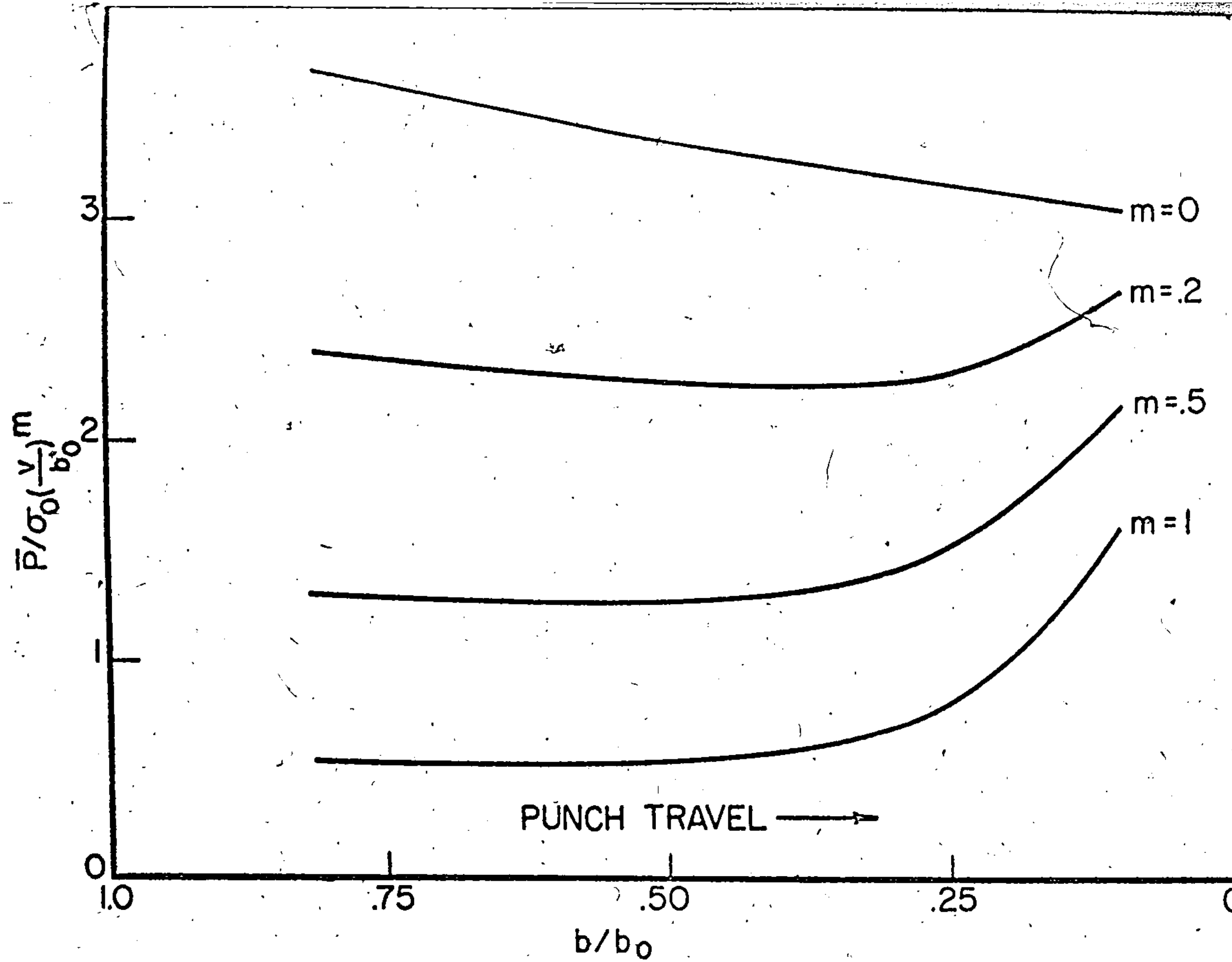

Fig. 6.6 Variation of non-dimensional extrusion pressure with billet height for materials with different values of m.

of a reduction in the $\bar{P}/2k$ ratio for perfectly plastic materials, m=0, and an increase in the quantity $\sigma_o\ (v_e/b)^m$ for rate-dependent materials as b decreases. Even though this is not a true "steady-state" we consider it as such in investigating other variables in the process such as tool geometry and reduction. The subsequent analyses are therefore performed only for values of $b/b_o = 0.42$.

(a) Effect of Punch Profile Geometry

Two further geometries were investigated. In one the area A_1 in Figure 6.2 was the same but the chamfer angle, α, increased to 45°. A slip-line field was constructed for $b/b_o = 0.42$ and this is shown in Figure 6.7. In the other case a flat bottomed punch with a sharp corner was considered; the slip-line field for this is shown in Figure 6.8. (For the square cornered punch, $(A_2 - A_1)$ is zero). The extrusion parameter, $\bar{P}/\ \sigma_o(v_e\ /b)^m$, was calculated for these cases using equation (6-18) and the results are presented in Figure 6.9. The actual punch shapes are shown in Figure 6.10. It is interesting to observe from Figure 6.9 that while the corner geometry makes very little difference for perfectly plastic materials, m=0, it becomes increasingly more important as the rate-sensitivity increases. From this limited investigation a corner angle of between 30° and 45° would appear to result in the lowest value of required pressure.

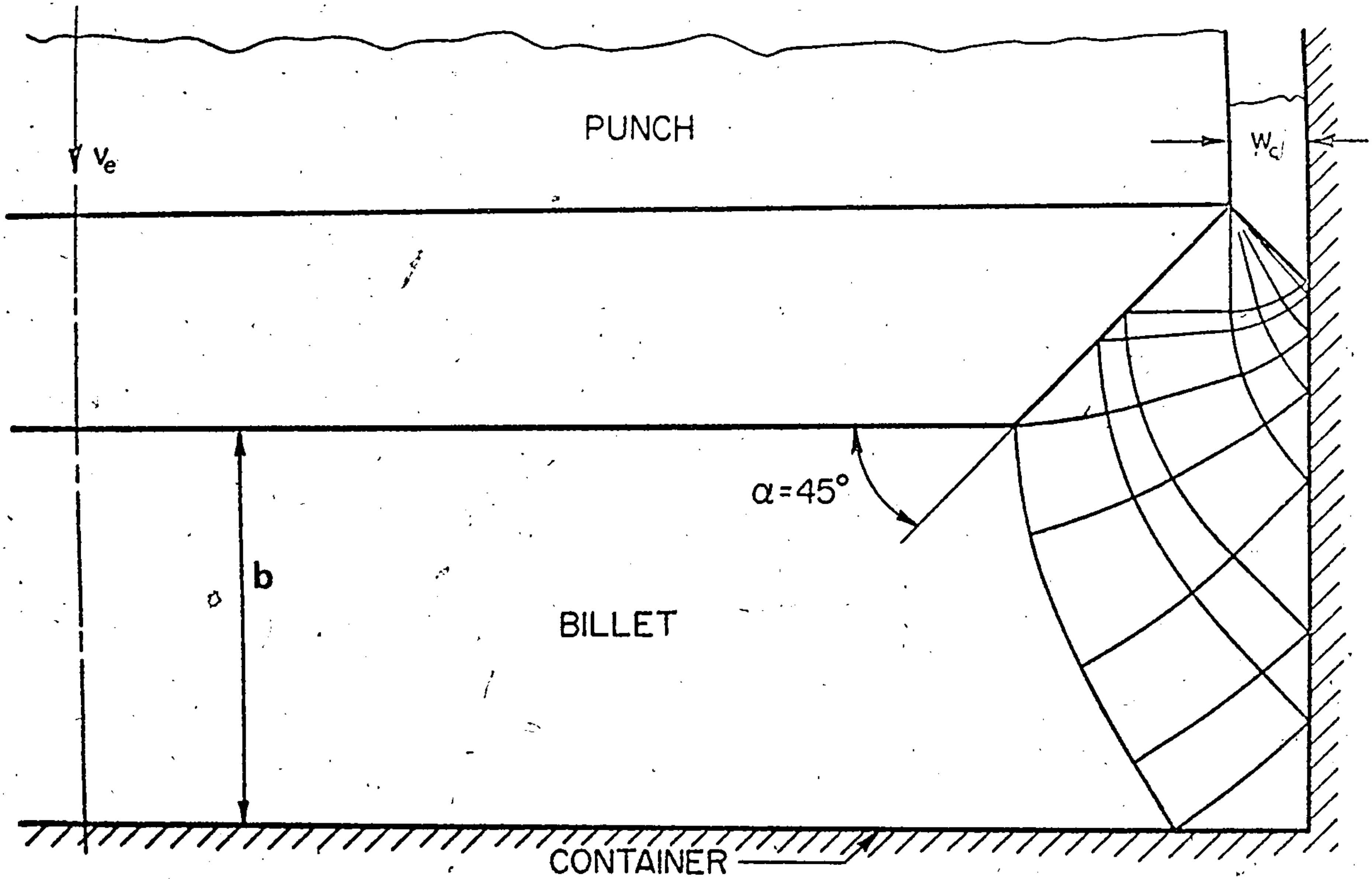

Fig. 6.7 Slip line field for the process in Zone II for a 45° punch chamfer. The ratio of billet height to wall thickness is $b/w_c \approx 5.4$.

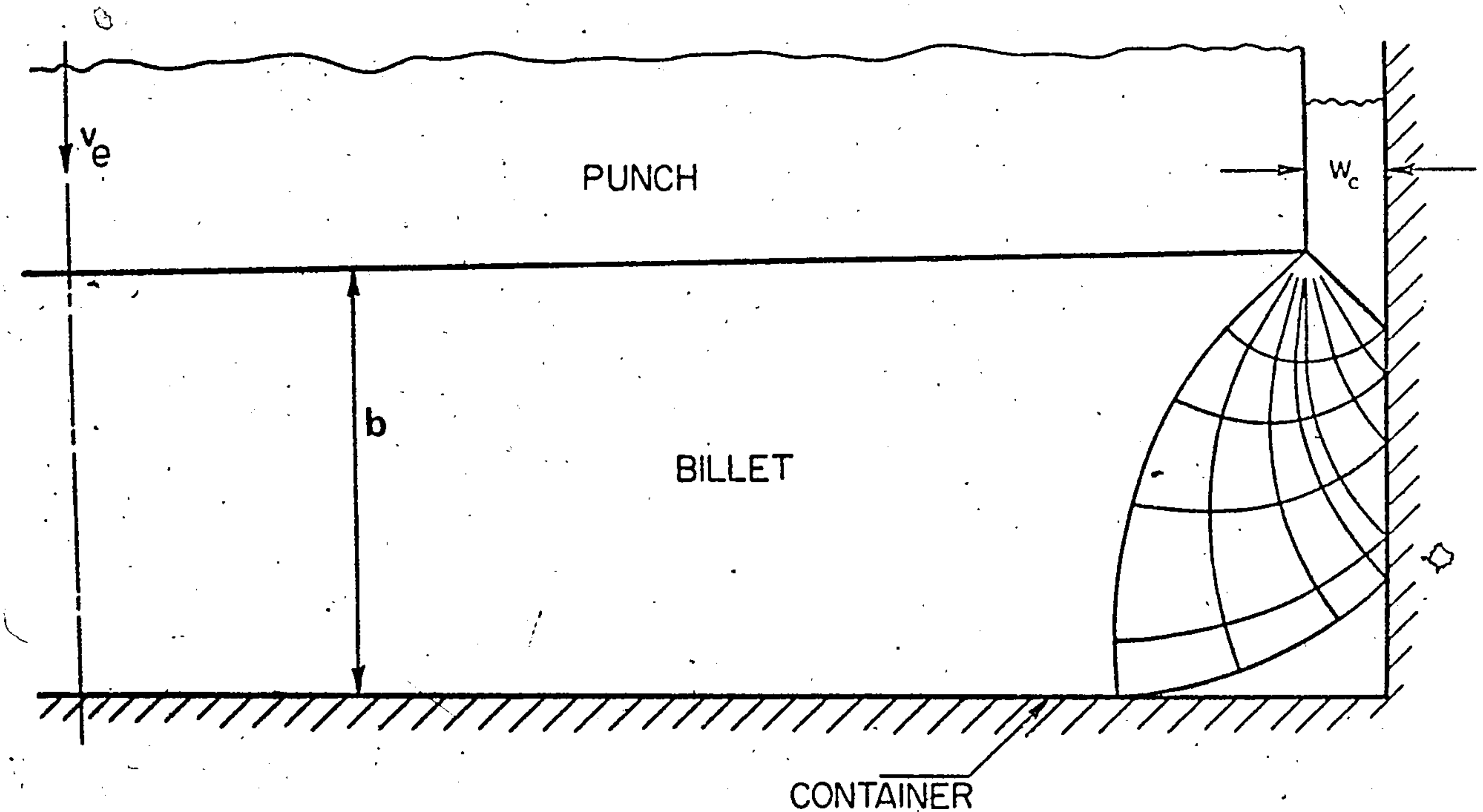

Fig. 6.8 Slip line field for the process in Zone II for a sharp cornered punch; $b/w_c \simeq 5.4$.

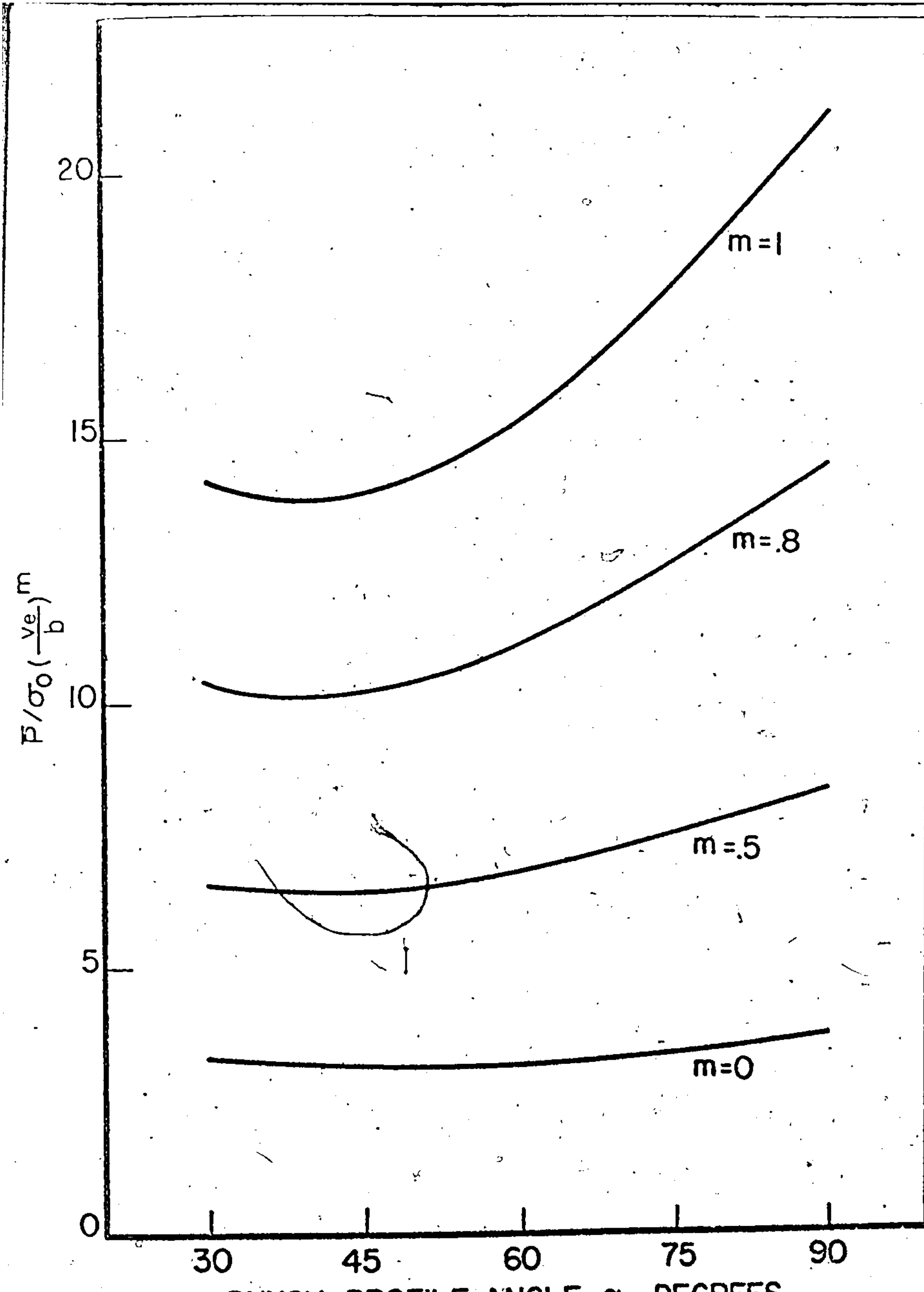

Fig. 6.9 Diagram showing the variation of the extrusion parameter, $P/\sigma_o(v_e/b)^m$, for different punch chamfer angles. The ratio of billet height to wall thickness in all cases is $b/w_c = 5.4$.

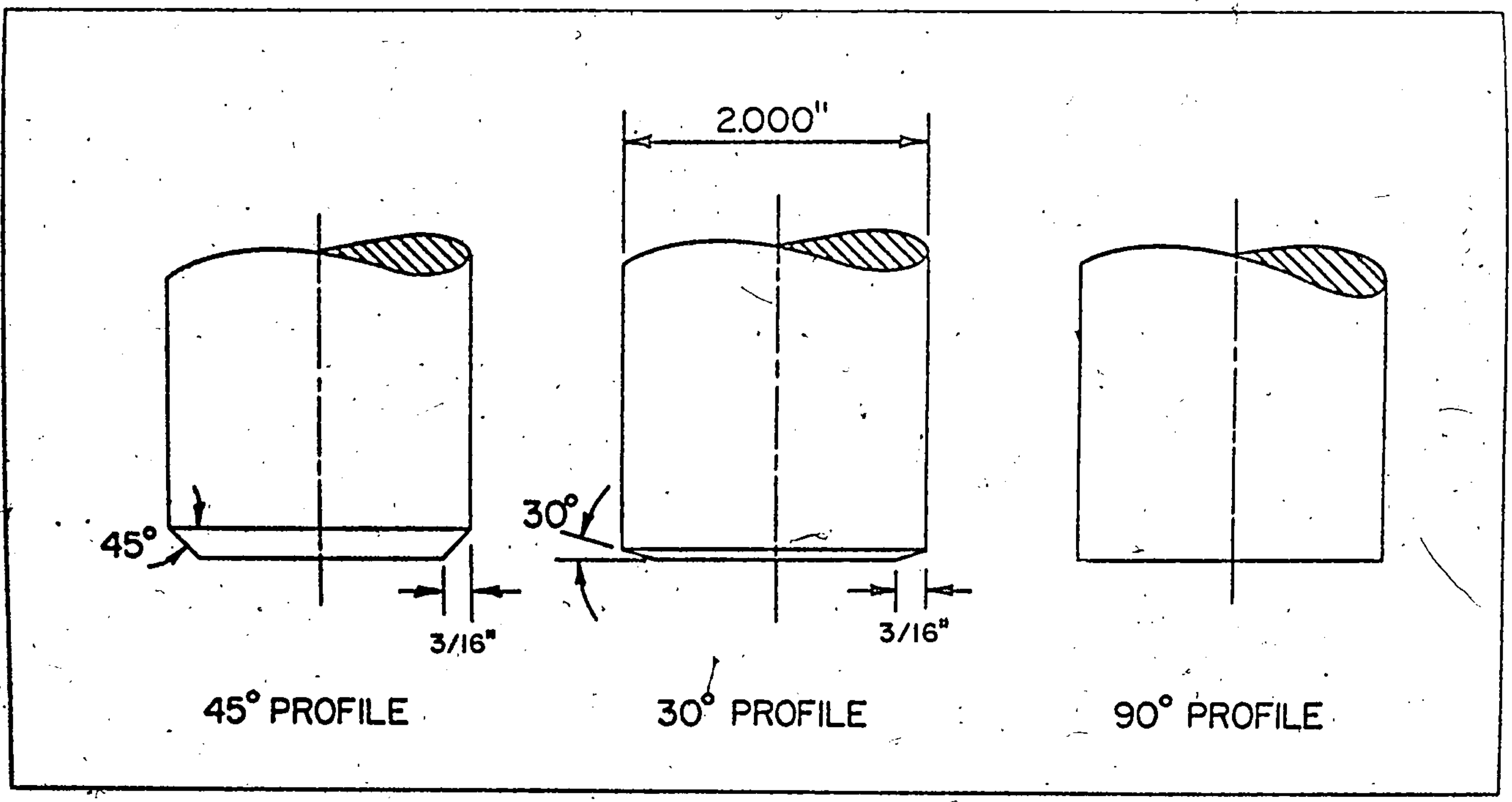

Fig. 6.10 Actual punch shapes for the cases considered in Fig. 6.9.

(b) Effect of Extrusion Ratio.

The slip-line field shown in Figure 6.11 was constructed for an extrusion ratio of 20 using a 45° punch corner angle. In this work, changes in extrusion ratio were achieved by changing the diameter of the container. The shape of the punch was not altered. The extrusion parameter, $\bar{P}/\sigma_o\,(v_e/b)^m$, is compared in Figure 6.12 with that obtained in the previous case, Figure 6.9. The increase in extrusion pressure is greater for rate-sensitive materials than for perfectly plastic ones and this is due to the increase in effective flow stress with increasing reduction.

6.3 Experimental Work on Reverse-Superplastic Extrusion

In the experiments performed by Jain and referred to in the introduction, zinc-aluminum alloy was backward-extruded at 250°C to form cups of about 2 inch diameter as shown in Figure 6.1. The extrusion billets were machined from a continuously cast rod of eutectoid composition. The material was tested in both the superplastic state and the as-cast state. To obtain a superplastic microstructure the material was soaked for 6 - 8 hours in a furnace heated to 340°C and then quenched in ice-cold water for about 30 seconds. This procedure of heat treatment is found to yield the best superplastic microstructure [6.15]. Figure 6.13 shows the microstructures typical of both as-cast and superplastic specimens.

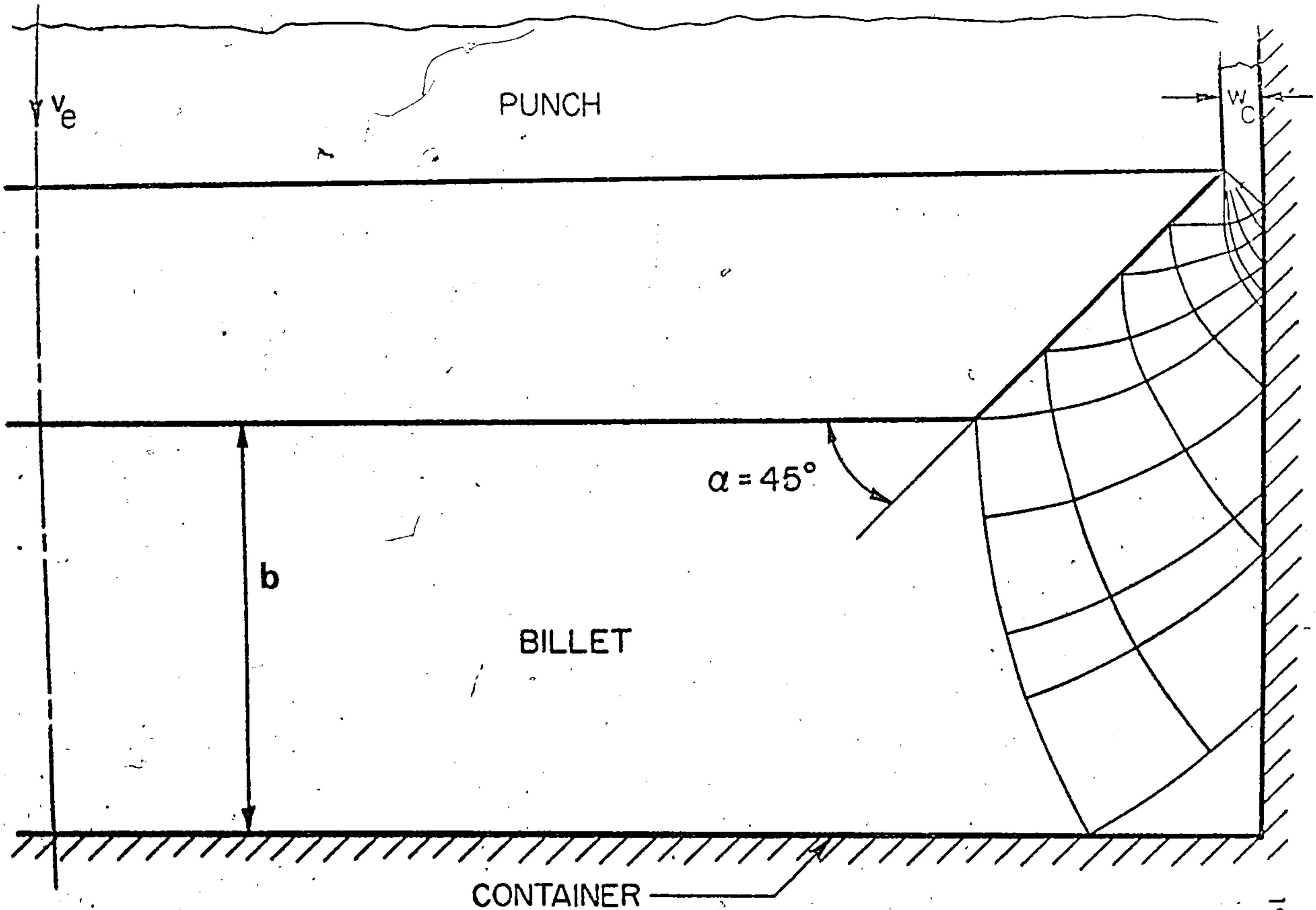

Fig. 6.11 Slip line field for the process in Zone II for a 45° punch chamfer. The ratio of billet height to wall thickness is $b/w_c \approx 11.0$.

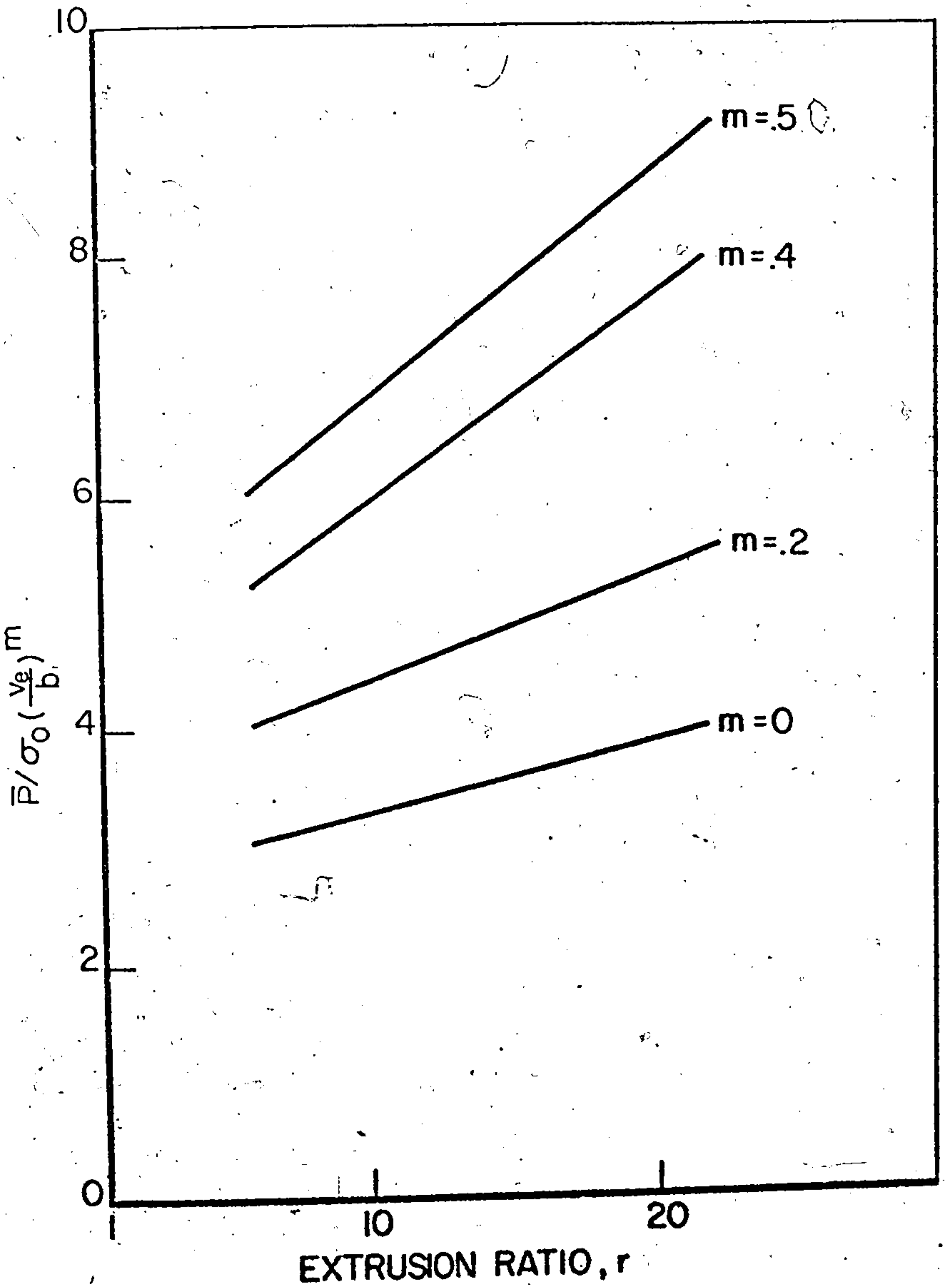

Fig. 6.12 Diagram showing the variation of the extrusion parameter, $\bar{P}/\sigma_o(v_e/b)^m$, with extrusion ratio for different values of m. The billet height is the same as in Fig. 6.7, (α = 45°).

(A) SUPERPLASTIC

(B) AS-CAST

FIG. 6.13 - MICROSTRUCTURE OF ZINC-ALUMINUM EUTECTOID ALLOY (X 1600)

6.3.1 Determination of Material Parameters in Compression.

Compression tests were performed by the author to determine the average properties of both the superplastic and the as-cast material. Compression specimens of 0.5 inch diameter and 0.75 inch height were machined to a good surface finish. Six grooves, .01 inch deep were turned in the ends of the specimens to facilitate the retention of a lubricant during the test [6.14]. Both the superplastic and the as-cast materials were tested at a temperature of 250°C.

A schematic diagram of the equipment used to conduct the compression test is shown in Figure 6.14. It consists of a base which is heated by means of a disc heater. The test billet is placed between two platens of hardened ground steel and the whole assembly is located inside a hollow aluminum cylinder to ensure a uniform temperature around the billet. Two insulating discs of asbestos were placed between the top platen and the ram of the testing machine. The rig was wrapped with asbestos cloth to reduce heat loss.

(a) Compression test procedure

The equipment was assembled without the test specimen and placed between the cross-heads of an Instron machine. The equipment was then heated up to about 220°C and the test specimen, cleaned and coated with lubricant, was placed between the platens. A slight load was applied to squeeze out superfluous lubricant. The load was then removed and the temperature increased to 250°C. During the test, the temperature was kept at 250° ± 3.0°C.

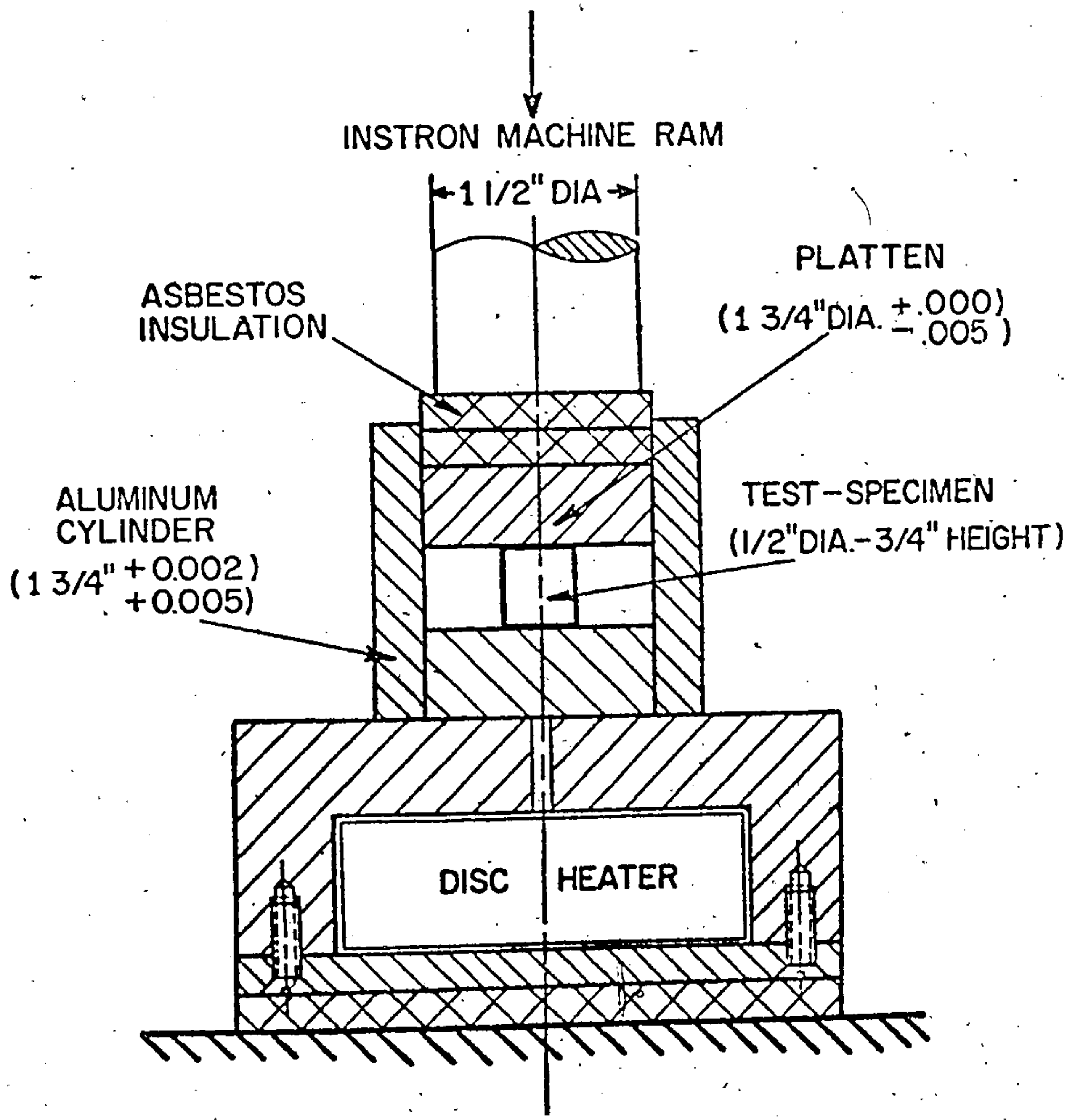

Fig. 6.14 Diagram of the equipment used to conduct compression tests on Zn-Al eutectoid alloy at 250°C.

The test was carried out at a constant cross-head speed and the specimen was compressed to 95% of its original height. The test was then interrupted to measure the diameter and height of the specimen. It was found that no significant barrelling had occurred at this stage. The specimen was then replaced between the platens and compressed, at the same previous speed and temperature, to 70% of its original height. The test was not continued beyond this point because of the increased barrelling of the specimen. Both the as-cast and superplastic alloys were tested at various cross head speeds in the range of 0.005 - 2.0 inch per minute.

(b) Compression test results

The stress-strain rate characteristics of the superplastic and as-cast materials are presented in Figure 6.15. The solid lines correspond to the average stress-strain rate properties of the two materials at a strain value of about 0.05 while the dotted line corresponds to strain value of about 0.35.

The true stress-true strain properties of both materials are given in Figure 6.15. For the superplastic material, Figure 6.16(a), the flow stress remains constant with increasing strain and hence the material could be considered as non-strain hardening [2.19] and [4.1]. However, the

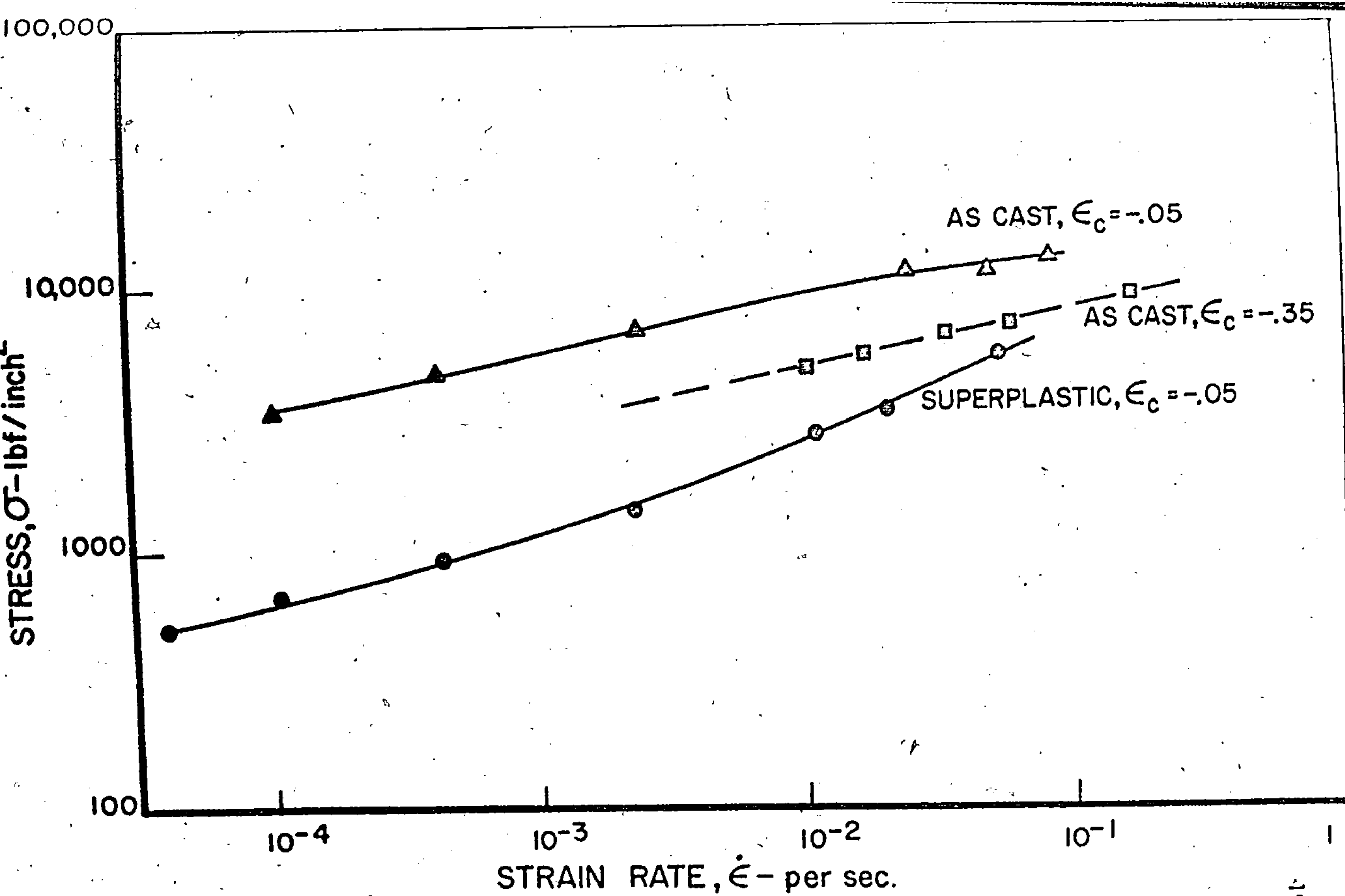

Fig. 6.15 Stress, strain-rate characteristic of Zn-Al eutectoid alloy at 250°C.

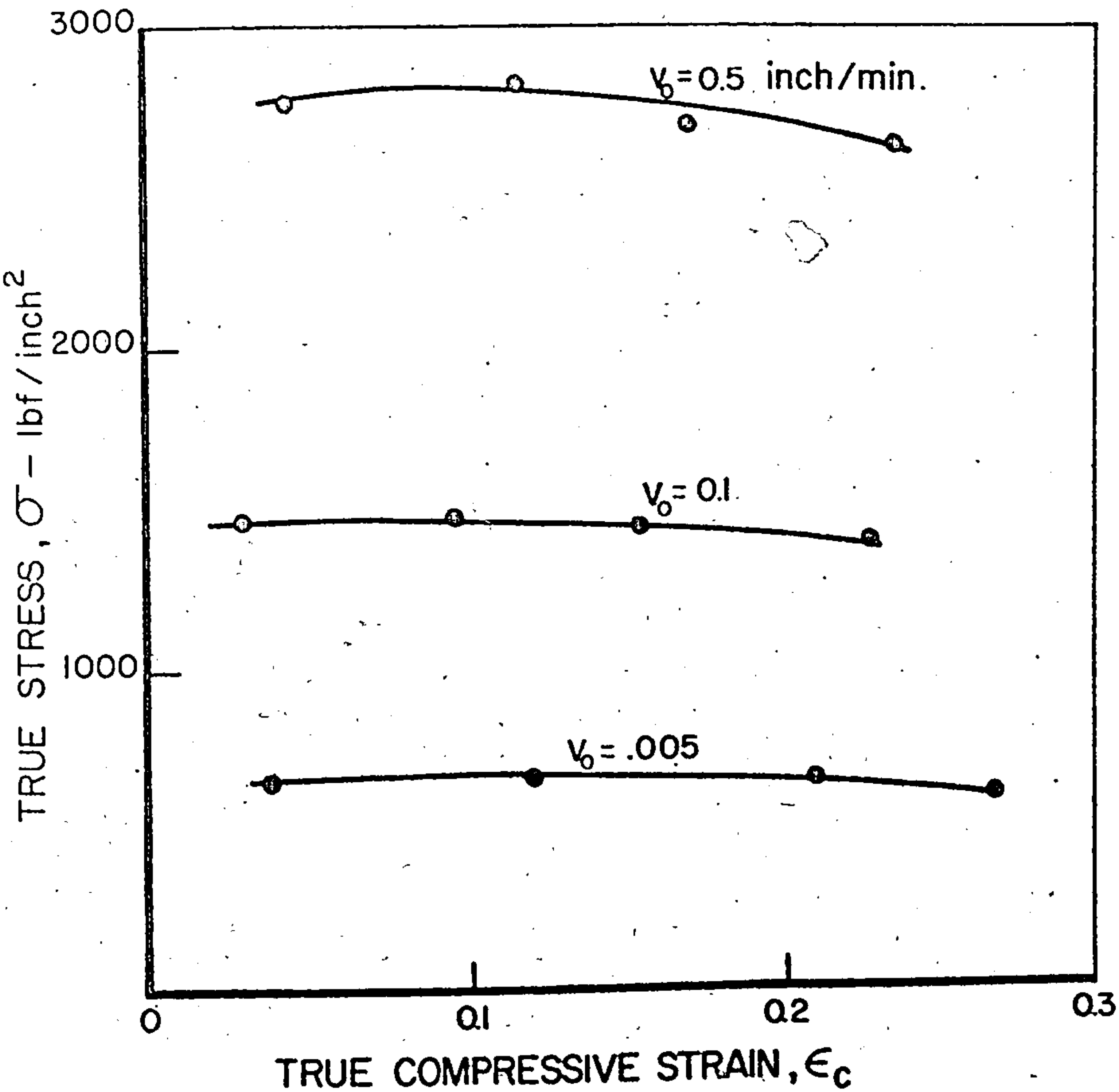

Fig. 6.16(a) Stress, strain characteristic of superplastic Zn-Al tested in compression at different cross-head speeds at 250°C.

stress-strain behaviour of the as-cast material as shown in Figure 6.6(b), indicates that strain-softening occurs during the early stages of the compression test. This has been observed by other investigators and may be attributed to changes in the microstructure during deformation. For the zinc-aluminum alloy considered in these tests, it was found that the grain size becomes finer after deformation [6.15]. Fortunately, the flow stress of the test as-cast material reaches a steady value at strains of about $\varepsilon = 0.35$. Consequently, the dotted line in Figure 6.15 represents the steady state stress, strain-rate characteristics of the as-cast material. Subsequently this $\sigma/\dot{\varepsilon}$ characteristic is used in interpreting the experimental extrusion data of the same material.

In the, strain-rate range, $5.0 \quad 10^{-4} < \dot{\varepsilon} < 1.5 \quad 10^{-1}$ per second, it was found that the empirical relation, equation (6-1) fits the material behaviour reasonably well. The values of the material parameters obtained by the least square fitting method are given in Table 6-I

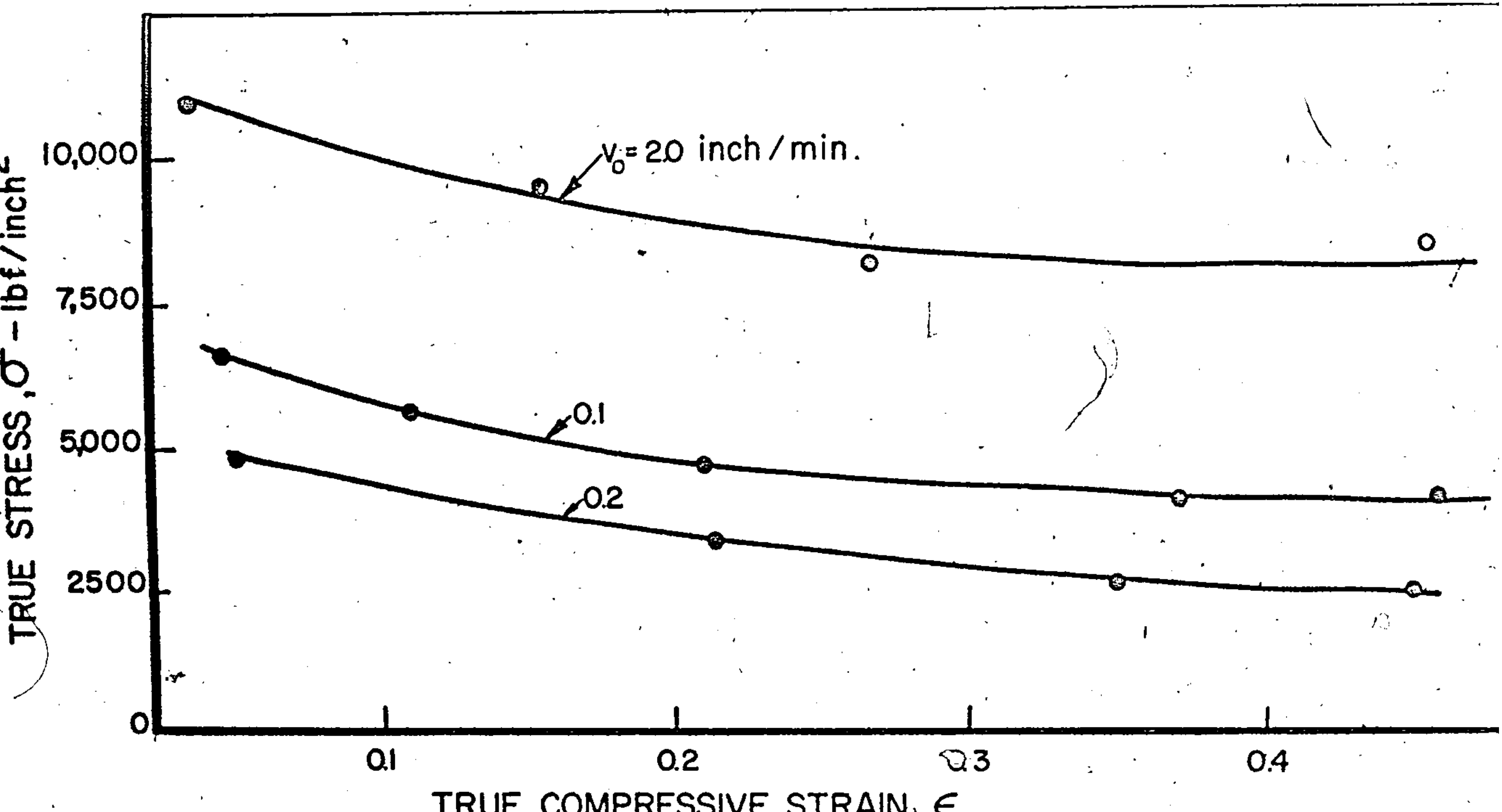

Fig. 6.16(b) Stress, strain characteristic of as-cast Zn-Al tested in compression at different cross-head speeds at 250°C.

TABLE 6-1: Material Parameters

Material Condition	σ_o $lb_f \cdot inch^{-2} \cdot sec^m$	m
As-cast $\varepsilon = -.35$	13,550	0.184
Superplastic $\varepsilon = -.05$	13,580	0.360

6.3.2 Inverse-Extrusion Experiments

The experiments described in this section were performed by K.K. Jain and described in extenso in his thesis, Ref. [6.15]. The author assisted Mr. Jain in some of these experiments and the technique is briefly recapitulated here.

(a) Extrusion equipment and test procedure

Inverse-extrusion experiments were performed on zinc-aluminum eutecloid alloy in both the as-cast state and superplastic state.

The extrusion rig assembly shown in Figure 6.17 consists essentially of a four piece-split die and a die bottom resting in a cavity in the die holder. The guide which is bolted down on the die holder, serves the dual purpose of guiding the punch and locating the die. The die was heated by means of four cylindrical cartridge heaters inserted in equally spaced holes drilled in the die holder. A detailed description of the various parts of the rig may be found in Reference [6.15].

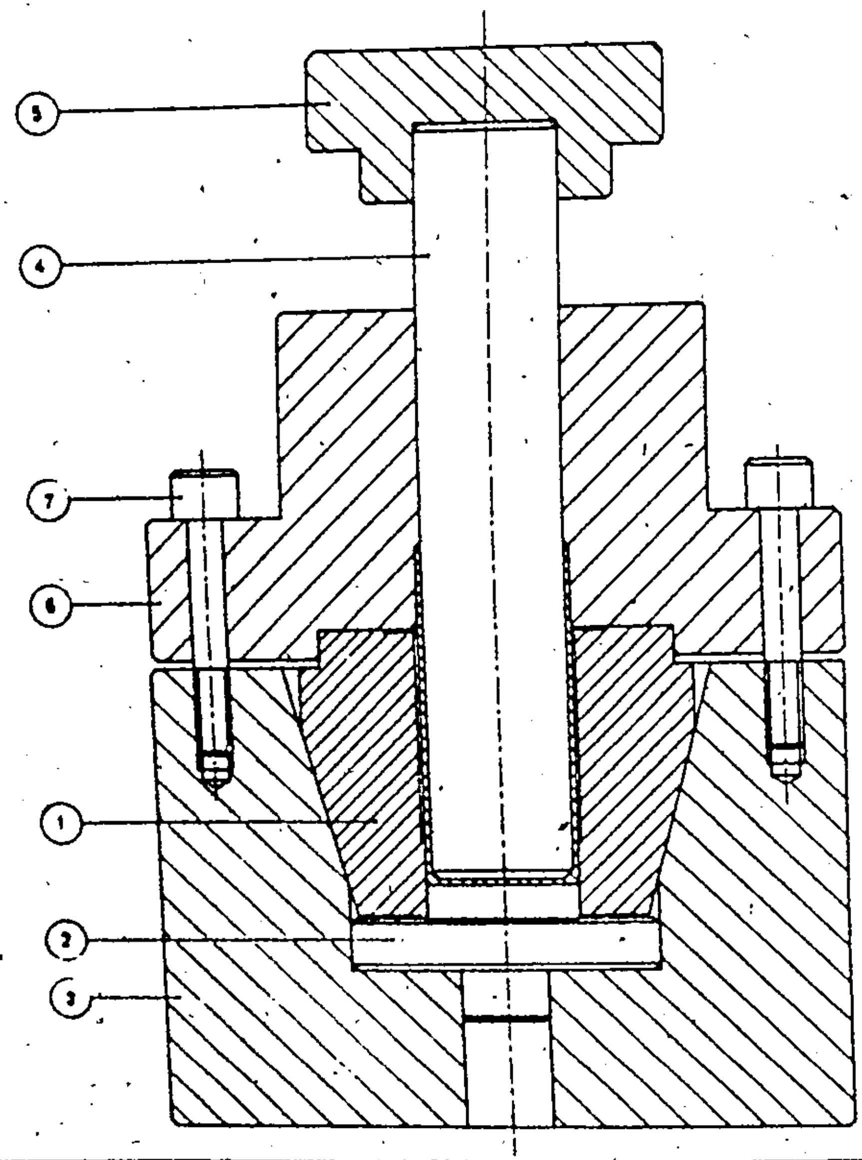

7	Socket Screw	8	M S	Std
6	Guide	1	M.S.	P 0007
5	Cap	1	M.S	P 0006
4	Punch	1	Hard.Stock	P 0005
3	Die Holder	1	M S	P 0004
2	Die Bottom	1	M S	P 0003
1	Split Die	1	M S	P 0002
No	Nomenclature	Off	Material	Drg No.
Backward Extrusion Rig				Drg No P 0001
K.K.Jain				June 1, 1971
Mech Engg Dept				McMaster University
Hamilton				ONTARIO

Fig. 6.17 Reverse-extrusion Rig [Ref. 6.15].

The extrusion test was started by assembling the rig without the test specimen, and heating it to about 220°C. The guide and the ram were then removed and the die, die bottom and ram were thoroughly lubricated with heavy duty gear box oil. A lubricated specimen was placed in the die and the guide was positioned and bolted down to the die holder. The temperature was increased and during the test the heat was regulated so that the die temperature, as measured by inserted thermo-couples, remained constant at 250°C $\pm$ 2.0. The ram travel during the extrusion test was recorded by means of a dial indicator at equal intervals of time.

(b) Experimental results

The extrusion experiments were carried out under constant load condition within the range 15,000 - 100,000 lb_f. A typical displacement-time diagram is shown in Figure 6.18. The extrusion process proceeded in three distinct stages. The first stage is a non-steady state during which the billet is compressed to fill out the die until flow is induced. Once flow is established, extrusion proceeds at an almost steady rate and, hence constant pressure. This apparent steady-state region was observed in most experiments; the punch velocity was determined from the gradients of

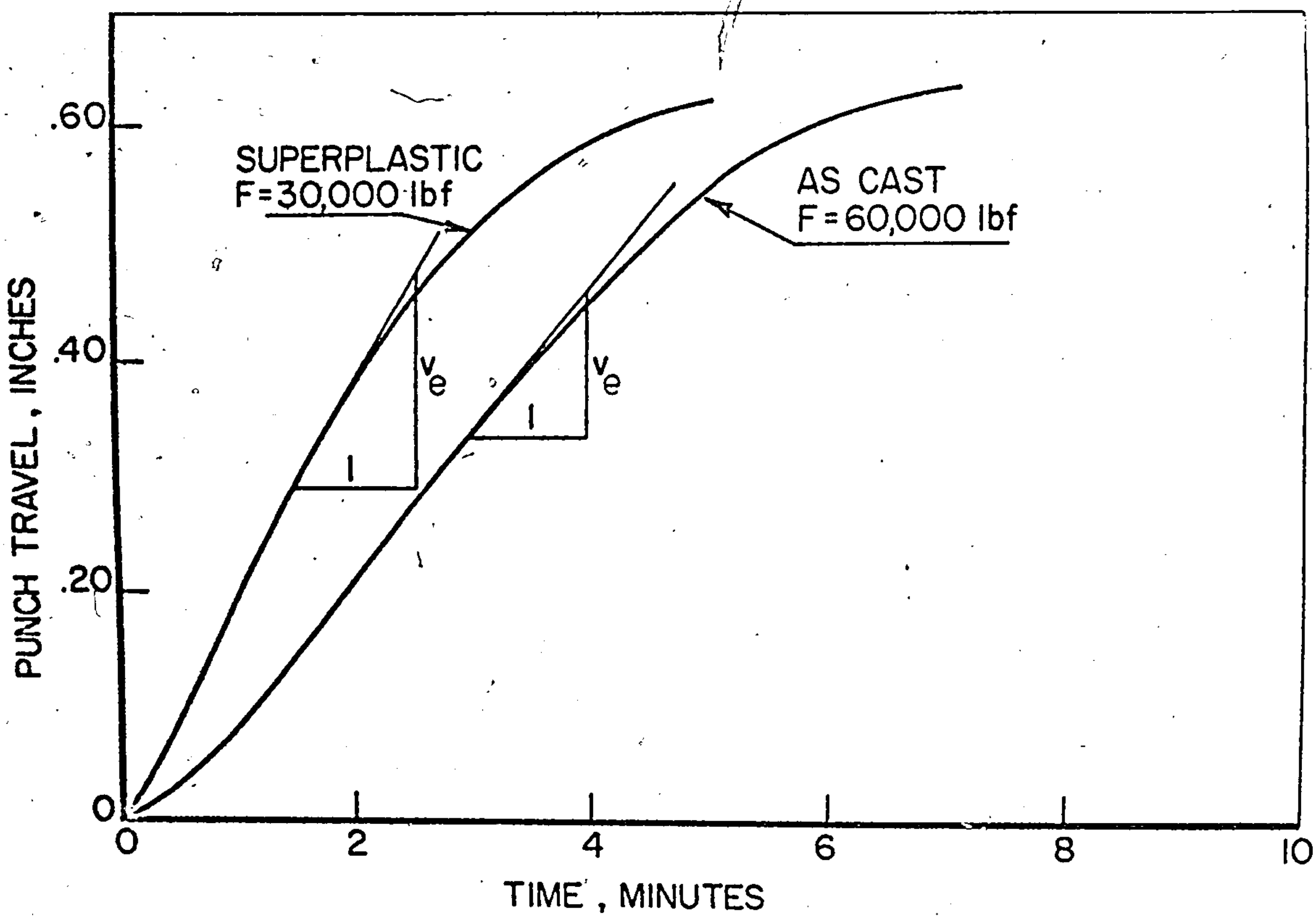

Fig. 6.18 Punch displacement versus time for constant force extrusion of superplastic and as-cast zinc-aluminum alloy at 250°C. (r = 8.3, α = 45°).

these curves as shown in Figure 6.18. Near the end of the extrusion process the speed falls rapidly as the compression effects become more predominant.

Table 6.II summarizes the load-velocity characteristics of the extrusion experiments conducted on the as-cast and superplastic material at an extrusion ratio of 8.3. It should be noted that the extrusion of the as-cast alloy was practically impossible at loads less than 30,000 lbf. Also extrusion experiments at loads higher than 100,000 lbf occurred at speed too high to record with sufficient accuracy and are consequently not listed in Table 6.II. Table 6.III gives the results of extrusion experiments for two different extrusion ratios; namely 8.3 and 20 with a ram chamfer angle of 45°.

Load	Steady-State Ram Velocity v_e inch per min					
F, lbf	90° RAM		45° RAM		30° RAM	
	As-Cast	Superplastic	As-Cast	Superplastic	As-Cast	Superplastic
15,000		.0145		.019		
20,000		.019				.0285
30,000		.042	.018	.180		
40,000						.285
50,000			.070	0.800	.030	.550
60,000	.063		.112	1.280	.063	
70,000	.110		.320		.185	
90,000	.210				.490	
100,000			.900			

TABLE 6.II: Extrusion speeds and levels, (extrusion ratio 8.3) for different ram profiles

TABLE 6.III: Extrusion speeds and loads for different extrusion ratios (45° Ram profile)

Load F, lbf	Steady-State Ram Velocity v_e inch/min.			
	r = 8.3		r = 20	
	As-Cast	Superplastic	As-Cast	Superplastic
30,000	.018	.180		
50,000	.070	.800		.100
60,000	.112	1.280		
70,000	.320		.0175	.240
90,000				.700
100,000	.900		.110	
125,000			.500	

6.4 Comparison between Theoretical and Experimental Results

Equation (6-18) indicates that the punch force F for a given extrusion should increase with v_e^m where v_e is the extrusion velocity. The theoretical curve of F versus v_e in a logarithmic diagram should therefore be a straight line of slope m. The theoretical and experimental results for as-cast and superplastic billets for the two different ram profiles are plotted in this manner in Figures 6.19(a) and (b). For the two different extrusion ratios, Figures 6.20 (a) and (b) show the load-velocity logarithmic plots for a 45° ram profile.

It may be seen from these Figures that the theory tends to over-estimate the load at the low extrusion ratio and under-estimate it at the

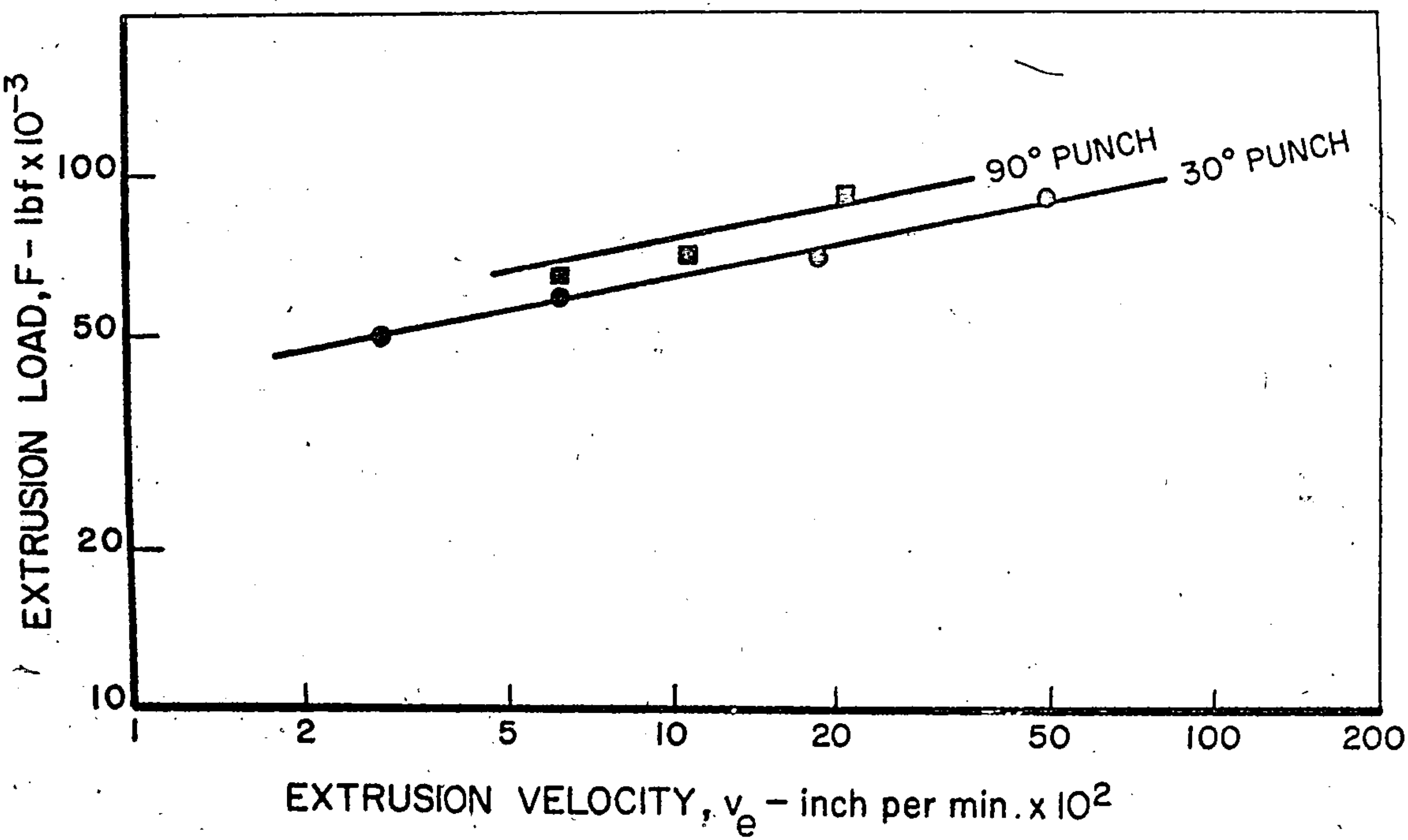

Fig. 6.19(a) Extrusion load versus extrusion velocity plotted logarithmically for as-cast Zn-Al using 90° and 30° punch profiles.

—— Theoretical curve

● ▣ Experimental data

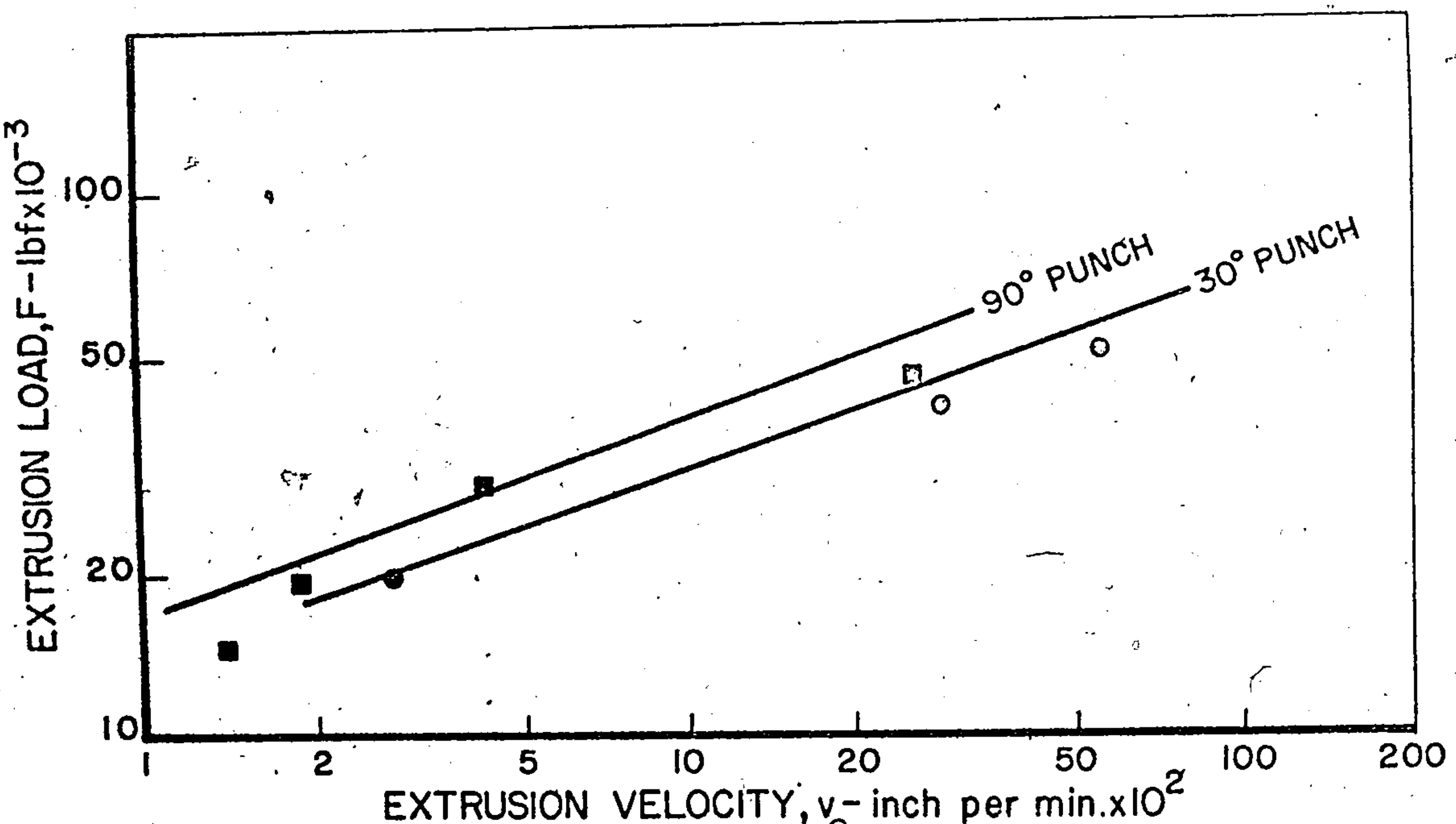

Fig. 6.19(b) Extrusion load versus extrusion velocity plotted logarithmically for superplastic Zn-Al using 90° and 30° punch profiles.

—— Theoretical curve
■ ● Experimental data

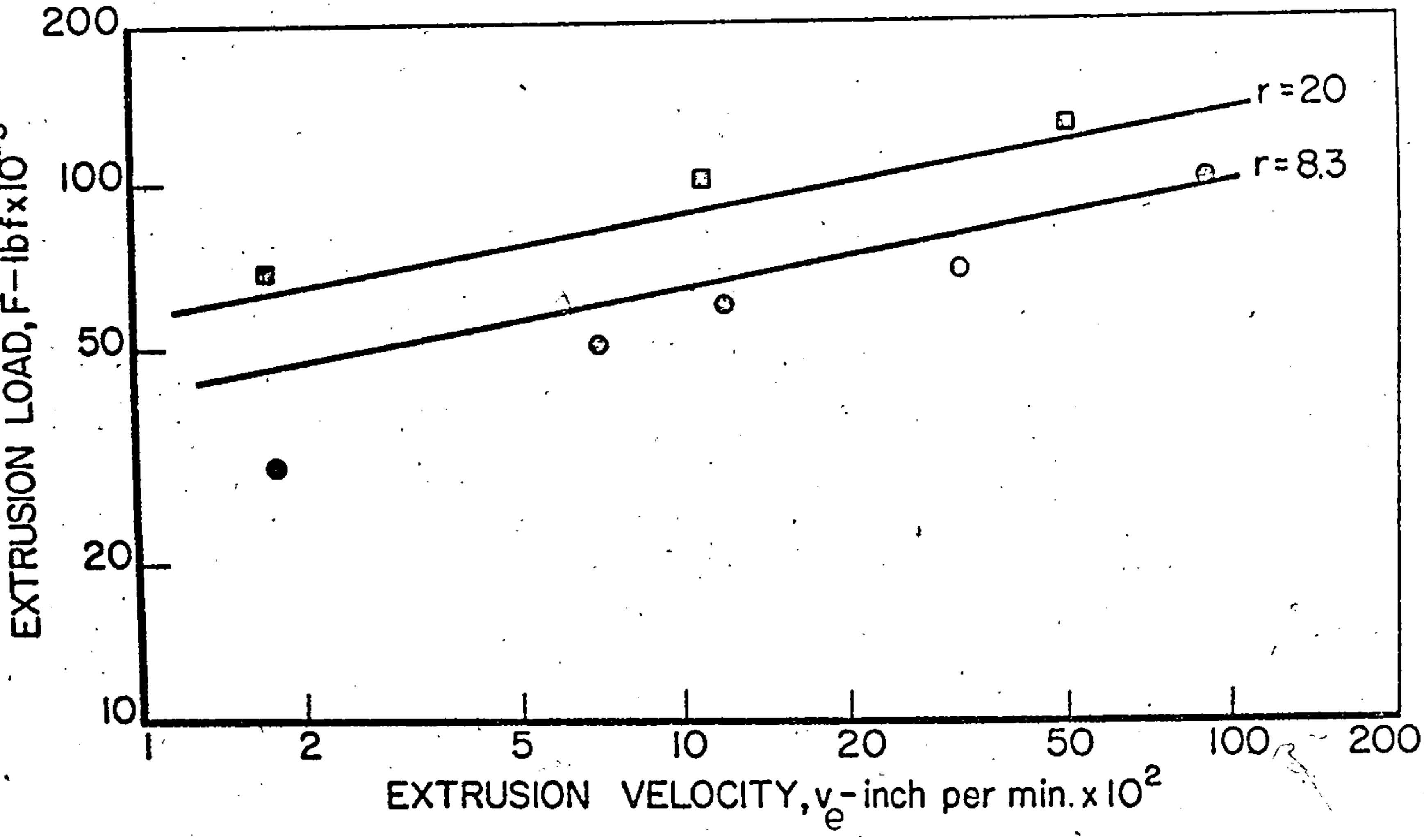

Fig. 6.20(a) Extrusion load versus extrusion velocity plotted logarithmically, for as-cast Zn-Al using a 2" diameter, 45° profile punch.

——— Theoretical curve
⊙ ⊠ Experimental data

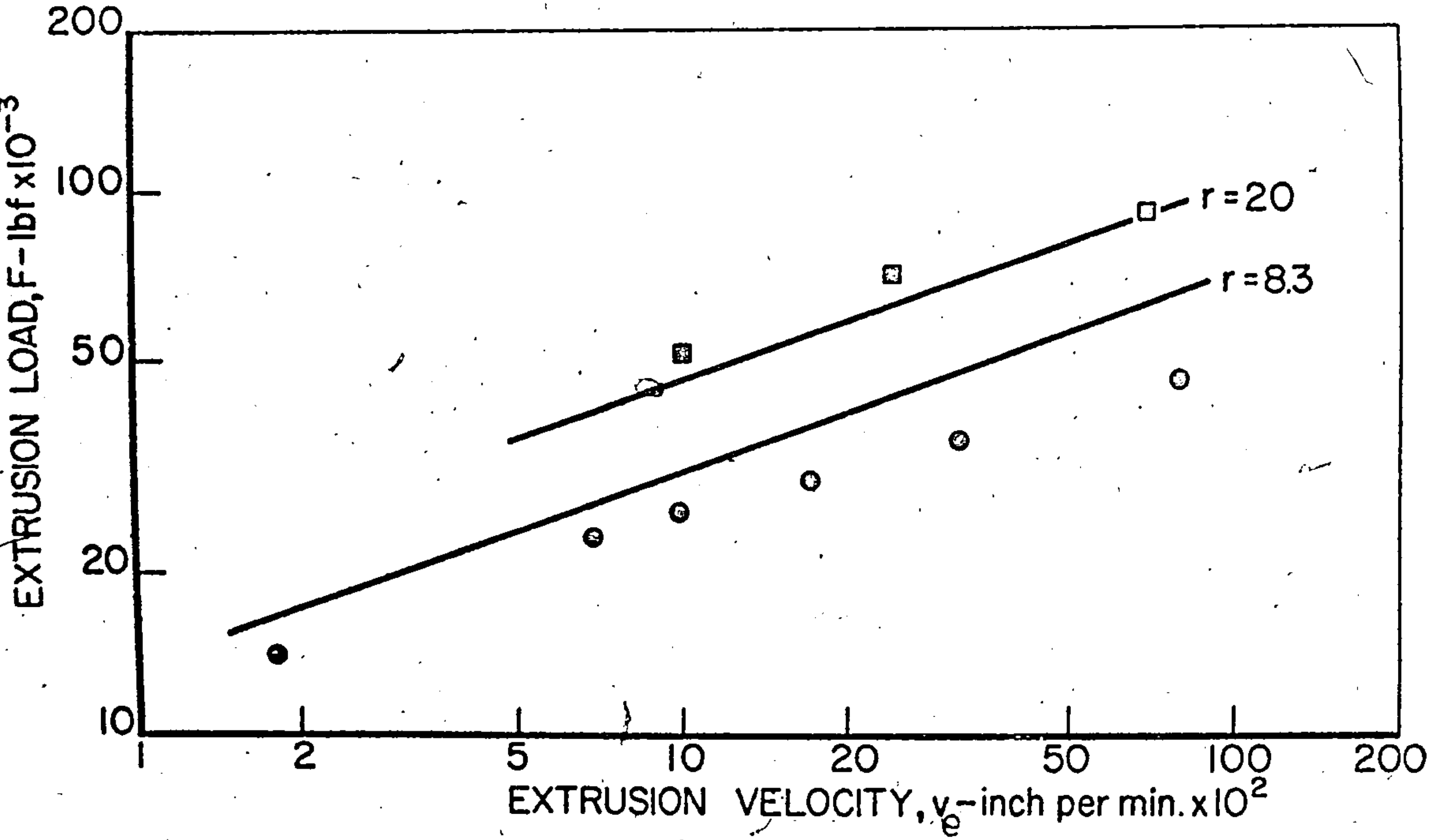

Fig. 6.20(b) Extrusion load versus extrusion velocity plotted logarithmically, for superplastic Zn-Al using a 2" diameter, 45° profile punch.

——— Theoretical curve
▣ ⊙ Experimental data

higher ratio; in all cases, however, the pressure increases with punch speed in approximately the manner predicted.

Theoretical curves similar to those in Figure 6.9 were calculated for the particular values of m in the experiments. These are presented in Figures 6.21(a) and 6.21(b) together with the experimental results. The experimental points for a particular value α in Figure 6.21 are derived from a number of tests at different speeds as in Figure 6.21. These results are for the 8.3:1 extrusion ratio and experimental pressures are generally less than predicted.

6.5 Discussion

Problems of the kind described can be solved numerically using a finite element approach and with this method of solution, rate-dependent material behaviour can be accommodated. These solutions however are frequently based on an experimentally determined velocity field [6.5] and [6.16] and it is becoming increasingly apparent that the real cost of numerical solutions of this kind is high [6.16]. On the other hand, velocity discontinuity and slip-line field methods have been successful in providing insight into a wide range of extrusion problems and the extension of these techniques to deal with strain-hardening materials has been entirely satisfactory in a practical sense even if it is an essential pragmatic rather than a rigorous approach [6.17].

The object in this work has been to explore the extension of traditional analytical methods to accommodate highly rate-sensitive materials

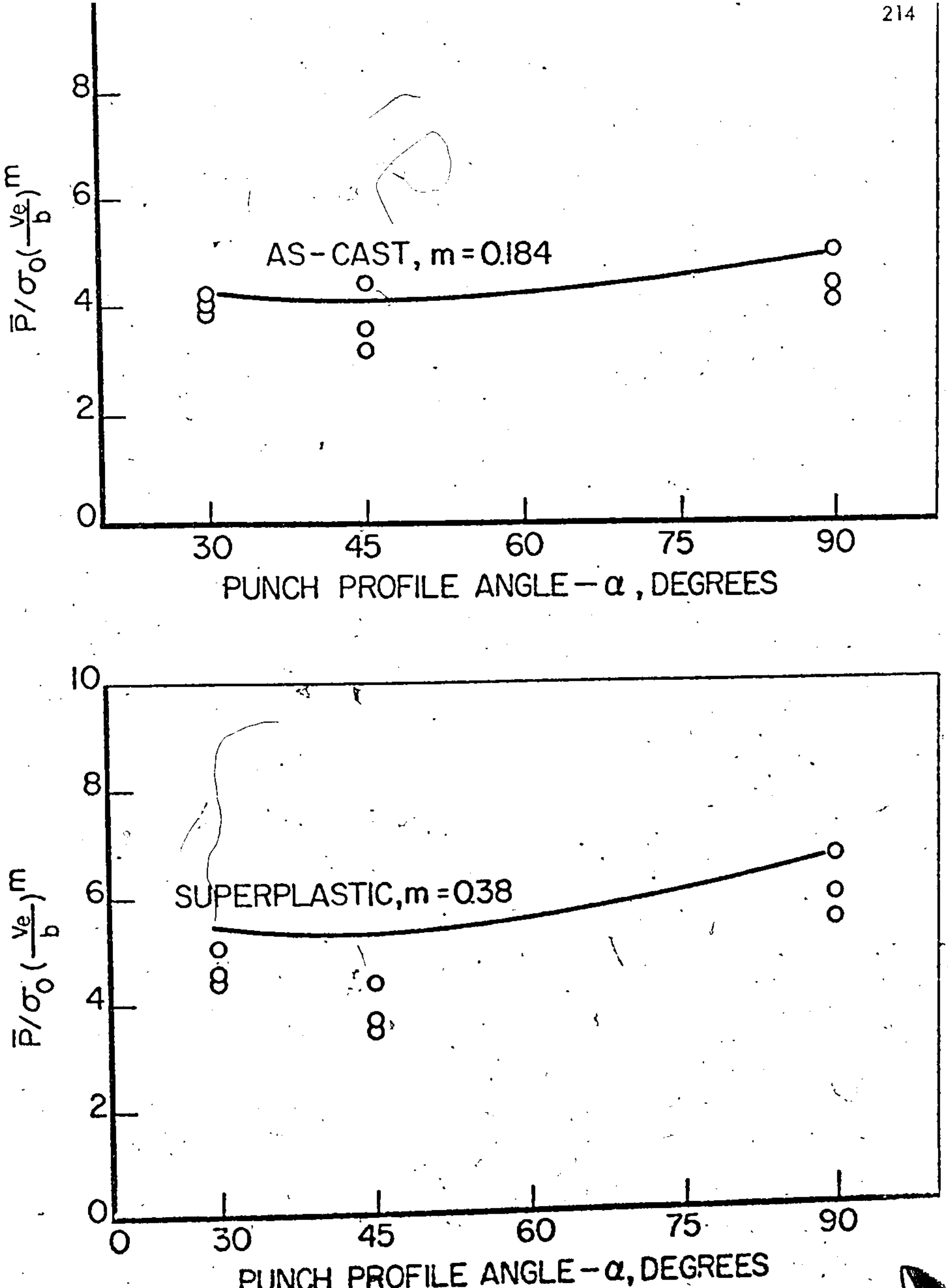

Fig. 6.21 Extrusion parameter, $\bar{P}/\sigma_o(v_e/b)^m$, versus punch angle for Zn - Al. ——— Theoretical curve , O Experimental data

such as superplastic alloys. It has been shown here that a geometric factor can be derived from the slip-line field solution which permits solutions to be obtained for materials having a non-linear viscous behaviour. The method is not rigorous in that velocity discontinuities are allowed, while intuitively one realizes these could not occur with rate-sensitive materials. The theoretical pressures are in many cases slightly above the experimental ones in spite of the fact that the process was assumed to be frictionless. This may be explained by the fact that all the proposed slip-line solutions shown in Figures 6.3, 6.7, 6.8 and 6.11 do not include an extension of the stress field into all the non-deforming regions and therefore they are incomplete. Consequently the loads determined using these fields represent an upper bound solution [6.18] and [6.19].

In correlating the extrusion experimental results with theory, one usually refers to the material behaviour as determined from compression tests. The difficulties in conducting compression tests especially at elevated temperatures are known [6.17]. Consequently, the inevitable experimental errors in the compression test result contribute to the discrepancies observed between the theoretical and experimental results

However, in the particular type of back extrusion process, this analysis has provided an explanation for the unexpected "steady-state" which was observed in extrusion of highly rate-sensitive materials; it has also shown that the rate-sensitivity of the extrusion process should be the same as that of the material. In other work, a similar conclusion is suggested for general deformation processes where the material behaviour is controlled by a thermally activated process [6.20]. The work here indicates that extrusion pressure is much more affected by punch geometry in rate-sensitive materials than in perfectly plastic ones. The fairly close agreement observed may well be fortuitous and applications of the method to more problems is required before it can be fully justified. The theoretical analysis of the effect of tooling geometry is in good agreement with the experimental results and it is anticipated that the analytical method presented can be usefully employed in the optimization of extrusion equipment design.

CHAPTER VII

CONCLUSIONS

Superplasticity is the viscous behaviour of many alloys which have an ultra-fine grain structure when they are deformed slowly at an elevated temperature. This behaviour is most dramatically displayed in a tensile test where the superplastic metal undergoes large elongations, sometimes greater than 1000%.

The overall physical manifestations of superplasticity are easily described and they are predictable. However, the microscopic deformation mechanism giving rise to this behaviour is not yet entirely clear. In this work the superplastic behaviour is viewed as one region of the overall spectrum of rate-dependent deformation of solids.

Phenomenologically it is shown that a non-linear viscous model, with certain limitations, may be employed to analyze superplastic deformation problems. It is concluded that the material parameters should be derived from a steady-state observations in uniaxial tests. The mathematical theory of secondary creep may be then used to derive a generalized non-linear viscous constitutive equation applicable to superplastic deformation under multi-axial states of stress.

This thesis presents analysis for three separate problems of superplastic deformation namely; (a) post-necking geometry in tensile-forming processes, (b) creep testing of superplastic material in sheet form and (c) reverse-extrusion of rate-dependent materials.

In tensile-forming processes of superplaslastic materials the deformation is unstable and it is shown that geometric non-uniformities develop continuously. The features of such deformation system are illustrated by the numerical analysis of initially non-uniform tensile bars and thin-walled tubes expanded by internal pressure. The material parameters used in the theoretical analysis are those for common superplastic alloys and the size of non-uniformities are typical of those which would inevitably be present in test-pieces ~~and commercially produced~~ tubes. The results of the analyses demonstrated the following:

- In tensile deformation of a tapered bar and thin walled-tube expanded by internal pressure, the non-uniformity in section is shown to increase with increasing initial non-uniformity and decreasing strain-rate sensitivity.
- Such non-uniformities of cross-sectional areas will develop continuously and be distributed along the length of the work-piece. Therefore useful products can be formed in this unstable tensile deformation régime since large overall shape changes can be achieved before the variation in thickness becomes technologically unacceptable.
- A good correlation was found between theoretical and experimental results of uniaxial tension of non-uniform superplastic zinc-aluminum strips with slight initial taper.

It is finally concluded that a non-linear viscous material model can be applied to determine the tolerances required for industrial tensile-forming processes of superplastic alloys.

In creep testing of superplastic material in sheet form, it is shown that creep data can be obtained using a test in which a strip or indeed the whole sheet is arranged as a cantilever loaded by its own weight. The results of the investigation are summarized as follows:

- The experimental results obtained from bending tests of superplastic zinc-aluminum sheets at room temperature indicate that a state of steady-state creep is achieved after a modest deflection and that this deflection rate can be easily and accurately measured using simple equipment.
- Data from bending tests can be expressed in the same form as the results of uniaxial tests. Creep data in the form of constants in Norton's creep law can be obtained from data of two bending tests but this method does not appear to give reliable results.
- A stress, strain-rate curve can be obtained from a number of bending tests by identifying the skeletal point for the beam. (The skeletal point is defined as the only point in the structure where the stress and the strain-rate can be obtained explicitly from the beam configuration, loading system and measured end deflection rate without knowing the exact values of the material parameters in creep).

- Comparison of the stress, strain-rate creep curves obtained from bending and tensile creep tests at room temperature indicates a significant difference between the two. This may be due to difficiencies in the complex creep theory used to correlate the two results rather than attributing the discrepancy entirely to defects in either test method.
- The bending test can be performed in short time using simple measuring equipment. The results indicate that it is a valid and economical test for superplastic sheet material and it appears that a test of this type may be suitable for quality control creep testing.

It is likely that further experiments would validate the method for other classes of material and the theory can readily be extended to cover tests in which higher stress levels are obtained by adding external loading. Developments of this kind could lead to substantial reduction in the cost of performing routine creep tests.

In bulk forming of superplastic material the load requirements are highly dependent on the forming speed. One process of this class is the reverse-extrusion of superplastic material used to manufacture thin-walled cups. In the present work the traditional analytical methods such as the slip-line field solutions have been extended to accommodate rate-sensitive materials. It is shown that:

- The deformation volume and the effective strain-rate identified by the slip-line field solutions, developed for the deformation at the edge of a cylindrical billet, were incorporated to define a geometric factor which permits the extrusion pressure to be determined for a non-linear viscous material.

- In the particular type of reverse-extrusion process, the analysis provided an explanation for the unexpected "steady-state" which was observed in extrusion of rate-dependent material.
- It is found that the extrusion load increases with punch speed with rate sensitivity approximately equal to that of the material when tested in compression.
- The average reverse-extrusion pressure was much more affected by punch geometry in rate-sensitive materials than in perfectly plastic ones. The theoretical analysis of tooling is in good agreement with the experimental results.

The method of analysis appears to have generality beyond the particular process considered and may be used to optimize extrusion equipment design.

REFERENCES

[1.1] Rosenhain, W., Haughton, U.K. and Bingham, K.E., J. Inst. Metals, 23 (1920), 261.

[1.2] Pearson, C.E., J. Inst. Metals, 54 (1934), 111.

[1.3] Bochvar, A.A. and Sviderskaia, Z - A., Izv. Akad. Nauk, U.S.S.R., 9 (1945), 821.

[1.4] Presnyakov, A.A. and Chervyakova, Fiz. Metal, Metaloved, 8 (1959), 114.

[1.5] Presnyakov, A.A. and Starekova, G.V., Fiz. Metal, Metaloved, 12 (1961), 873.

[1.6] Underwood, E.E., J. of Metals, 14 (1962), 914.

[1.7] Backofen, W.A., Turner, I.R. and Avery, D.H., Trans. A.S.M., 57 (1964), 980.

[1.8] Avery, D.H. and Backofen, W.A., Trans. A.S.M., 58 (1965), 551.

[1.9] Holt, D.L. and Backofen, W.A., Trans.A.S.M., 59 (1966), 755.

[1.10] Oelschlagel, D. and Veiss W., Trans. A.S.M., 58 (1966), 143.

[1.11] Johnson, R.H. and Sykes, E.C., Nature, 209 (1966), 192.

[1.12] Taraldsen, A., Material prufung, 6 (1964), 189.

[1.13] Duncan, J.L., "Superplasticity: The behaviour and Uses of Ultra-Fine Grain Alloys", Invited Lecture, International Symposium on Foundations of Plasticity, Polish Academy of Sciences, Warsaw, (1972).

[1.14] Packer, C.M. and Sherby, O.D., Trans. A.S.M., 60 (1967), 21.

[1.15] Petch, N.J., J.I.S.I., 174 (1953), 25.

[1.16] Nazifi, H. and Pearce, R., Int. J. Mech. Sci., 12 (1970), 513.

[1.17] Martin, P.J. and Backofen, W.A., Trans. A.S.M., 60 (1967), 352.

[1.18] Backofen, W.A., Azzarto, F.J., Murty, G.S. and Zehr, S.W., "Ductility", A.S.M. (Cleveland), (1968), 279.

[1.19] Nuttall, K. and Nicholson, R.B., Phil. Mag., 17 (1968), 1087.

[1.20] Taplin, D.M.R., Rama Rao, P. and Rao, V.V.P.K., Silver Jubilee Conference, Indian Institute of Metals, Delhi, Feb. 1972.

[1.21] Gervais E., Chollet, P. and Ranger R., Conference of Metallurgists, Hamilton, Ont., 1970.

[1.22] Comfield, G.C. and Johnson, R.H., Int. J. Mech. Sci., 12 (1970), 479.

[1.23] Al-Naib, T.Y.M. and Duncan, J.L., Int. J. Mech. Sci., 12 (1970), 463.

[1.24] Hubert, J.F. and Kay, R.C., Design Eng. Conference, ASME, April (1971).

[1.25] Johnson, R.H., Design Engineering, March (1969).

[1.26] Pearce, R. and Swanson, C.J., Sheet Metal Industries, July (1970).

[1.27] Saller, R.A. and Duncan, J.L., J. Inst. Met., 99 (1971), 173.

[1.28] Duncan, J.L., Shapiro, E., Crane, J. and Taplin, D.M.R., "Applications of Solid Mechanics" Symposium, U. of Waterloo, Waterloo, Ont., June (1970).

[2.1] Zehr, S.W. and Backofen, W.A., A.S.M., 61 (1968), 300.

[2.2] Ashby, M.F., Scripta Met. 3 (1969), 837.

[2.3] Karim, A., Scripta Met. 3 (1969), 887.

[2.4] Burton, B., Scripta Met. 5 (1971), 669.

[2.5] Johnson, R.H., Met. Rev., 146 (1970), 115.

[2.6] Lee, D., Acta Met. 17 (1969), 1057.

[2.7] Alden, T.H., Acta Met. 15 (1967), 468.

[2.8] Holt, D.L., Trans. A.I.M.E., 242 (1968), 25.

[2.9] Orawan, E., Reports Prog. Phys., 12 (1948-49), 185.

[2.10] Gifkins, R.C., J. Inst. Metals, 95 (1967), 373.

[2.11] Jonas, J.J., Sellars, C.M. and W.J. McG. Tegcert, Met. Rev., 14 (1969), I, 130.

[2.12] Hayden, H.W., Floreen, S. and Goodell, P.D., Metallurgical Trans., 3 (1972), 833.

[2.13] Ball, A. and Hutchinson, M.M., Metal Sci. J., 3 (1969), 1.

[2.14] Packer, C.M., Johnson, R.H. and Sherby, O.D., Trans. Met. Soc. A.I.M.E., 242 (1968), 2485.

[2.15] Drucker, D.C., "Introduction to Mechanics of Deformable Bodies", McGraw Hill, N.Y. (1967).

[2.16] Nuttal, K., Int. J. Mech. Sci., 13 (1971), 83.

[2.17] Dunlop, G.L. and Taplin, D.M.R., Journal of Materials Science, 7 (1912), 84.

[2.18] Nicholson, R.B., Inst. of Metallurgists Review Course Ser.2 No. 3, Eastbourne, U.K., October (1969).

[2.19] Baudelet, B. and Suery, M., Journal of Materials Science 7 (1972), 512.

[2.20] Newbury, D.E. and Joy, D.C., Scripta Metallurgical 4 (1970), 825.

[2.21] Watts, B.M. and Stowell, M.J., J. Materials Science, 6 (1971), 228.

[2.22] Herriott, G., Suéry, M. and Baudelet B., Scripta Metallurgica, 6 (1972), 657.

[2.23] Odqvist, F.K., "Mathematical Theory of Creep and Creep Rapture", Oxford University Press, (1966) .

[2.24] Dunlop, G.L. and Taplin, D.M.R., The Journal of the Australian Inst. of Metals, 16 No.4 (1971).

[2.25] Naziri, H. and Pearce, R., J. Inst. Metals, 98 (1970).

[2.26] Fields, D.S. Jr. and Stewart, T.J., Int. J. Mech. Sci., 13 (1971), 63.

[2.27] Gibbs, G.B., Mater. Sci. Eng., 2 (1967), 269.

[2.28] Padmanbhan, K.A., and Davies, G.J., J. Mech. Phys. Solids, 18 (1970), 261.

[2.29] Nadai, A., "Theory of Flow and Fracture of Solids", Vol.I, McGraw Hill (1950).

[2.30] Siddall, J.N., "OPTISEP - Designer's Optimization Subroutines", ME/71/DSN/REP 1, McMaster University (1971).

[2.31] Johnson, A.E., Proc. Inst. Mech. Engrs. Lond., 164 (1951), 432.

[2.32] Tang, S., ASME Publication, Journal of Basic Engineering, Paper No. 71 Met - S.

[2.33] Ghosh, A. and Duncan, J.L., Int. J. Mech. Sci., 12 (1970), 499.

[2.34] Sagat, S., Blenkinsop, P. and Taplin, D.M.R., J. Inst. Metals, 100 (1972), 268.

[2.35] Roberts, G.T., M. Sc. Diss. UMIST, Manchester Univ.(1971).

[3.1] Hart, E.W., Acta Metallurgica 15 (1967), 351.

[3.2] Thomason, P.F., Int. J. Mech. Scie., 11 (1969), 481.

[3.3] Lubahn, J.D. and Sachs, G., Trans. ASME, 68 (1946),271.

[3.4] Bridgman, P., Trans ASM, 32 (1944), 553.

[3.5] Chen, W.H., Int. J. Solids Structures, 7 No.7 (1971),685.

[3.6] Nadai, A. and Manjoine, M.J., Trans. ASME 63, A77 (1941).

[3.7] Reviewed by Sokolovsky, W.W., J. Appl. Mech., 13, No.1 (1946), p. A1.

[3.8] Hoff, N.J., J. Appl. Mech., 20 (1953), 105.

[3.9] Wray, P.J., J. Appl. Phys., 41, 8 (1970), 3347.

[4.1] Ragab, A.R. and Duncan, J.L., International Symposium on Foundations of Plasticity, Polish Academy of Sciences, Warsaw (1972).

[4.2] IBM Patent No. 826620 – Canada.

[5.1] Thomsen, T.H., Holt, D. and Backofen, W., Metal Engring. Quarterly, 10, May (1970), 1.

[5.2] Superplastic Metal, The New Jersey Zinc Company.

[5.3] Hult, J.A.H., "Creep in Engineering Structures", Blaisdell Publishing Company (1966), 25.

[5.4] Marriott, D.L. and Leckie, F.A., Proc. Instn. Mech. Engrs., 178 (1963-1964), 115.

[5.5] Anderson et al, J. Mech. Engring. Sci., 5, No. 3 (1970), 238.

[6.1] Wilcox, R.J. and Witton, P.W., J. Inst. Metals, 87 (1958), 289.

[6.2] Jovane F., Shabaik, A.H. and Thomsen, E.G., Trans ASME, Journal of Eng. for Industry, August (1969), 680.

[6.3] Chandra, T. and Jonas, J., Metallurgical Transactions, 1 August (1970), 2079.

[6.4] Avitzur, B., "Metal Forming, Processes and Analysis", McGraw-Hill (1968).

[6.5] Shabaik, A. and Kobayashi, S., Trans ASME, Journal of Eng. for Industry, May (1967), 339.

[6.6] Johnson, W., J. Mech. Phys. Solids, 4, (1956), 269.

[6.7] Dodeja, L.C. and Johnson, W., J. Mech. Phys. Solids, 5, (1957), 281.

[6.8] Dipper, M., Arch F. Eisenhuettives, 20, (1949), 276.

[6.9] Kudo, H., Int. J. Mech. Sci., 1, (1960), 57.

[6.10] Thomsen, E., Journal of Applied Mechanics, June (1956), 225.

[6.11] Duncan, J.L., Johnson, W. and Ovreset, A., Applied Mechanics Convention (1966), Inst. Mech. Engr. Paper 21.

[6.12] Duncan, J.L., Johnson, W. and Ovreset, A., Annals of CIRP, Vol. XIV (1966), 89.

[6.13] Hill, R., "The Mathematical Theory of Plasticity" Oxford University Press (1960).

[6.14] Johnson, W., J. Inst. Metals, 85, (1956), 403.

[6.15] Jain, K.K., M. Eng. Thesis, Mechanical Enging Dept., McMaster Univ. (1972).

[6.16] Lee, C. and Kobayashi, S., Trans ASME, Journal of Enging for Industry, May (1971), 445.

[6.17] Johnson, W. and Mellor, P.B., "Plasticity for Mechanical Engineers", Van Nostrand-London (1970), 275.

[6.18] Johnson, W. and Kudo, H., "The Mechanics of Metal Extrusion", Manchester Univ. Press (1962).

[6.19] Johnson, W., Sowerby, R. and Haddow, J.B., "Plane-Strain Slip-Line Fields: Theory and Bibliography" Edward Arnold (Publishers) Ltd., London (1972).

[6.20] Wong, W. and Jonas, J., Trans of the Metallurgical Society of AIME, 242 (1968), 2271.

APPENDIX A-1

```
C
C      STUDY OF POST-INSTABILITY TENSILE DEFORMATION OF
C      A SLIGTHLY TAPERED TEST-PIECE OF RECTANGULAR CROSS-
C      SECTION UNDER CONSTANT LOAD. THE MATERIAL PARAMETERS
C      ARE TYPICAL OF SUPERPLASTIC ZN-AL ALLOY.
C
C
C      WO,WW UNDEFORMED AND DEFORMED WIDTH RESPECTIVELY
C      BO,BB UNDEFORMED AND DEFORMED THICKNESS RESPECTIVELY
C      LO,L UNDEFORMED AND DEFORMED LENGTH RESPECTIVELY
C      AO,AA UNDEFORMED AND DEFORMED AREA RESPECTIVELY
C      K,M SUPERPLASTIC MATERIAL PARAMETERS
C      T TIME
C      DDT TIME INCREMENT
C      E ELONGATION
C      STR STRAIN RATE
C      P1 LOAD
C
      DIMENSION AO(9), A(9), AA(9), WO(9), W(9), WS(9), WW(9),
     1BO(9),B(9),BB(9),BS(9),AU(9),AXU(9),AXT(9),
     2AXTR(9),STR(9),STRR(9),DIFD(9),DIFDA(9)
      REAL M,M1,M2,M3,K,L,LO,LS
C
C
C      CONSTANTS
      PI=4.*ATAN(1.)
      K=4100.
      M=.315
      M1=1./M
      P1=23.
      PS=P1/K
C
C      INITIAL GEOMETRY OF TAPERD TEST PIECE
      AX=.25
      LO=1.25
      READ (5,27) (WO(I),I=1,6)
      ID=6
      ID1=ID-1
      N1=1
      N2=ID
      I1=0
      IK=1
      WRITE (6,20)
      WRITE (6,21) IK
      DO 1 N=N1,N2
      THICK=.0940
      BO(N-I1)=THICK
      W(N-I1)=WO(N)
```

```
      A(N-I1)=WO(N)*BO(N-I1)
      AO(N-I1)=A(N-I1)
      WS(N-I1)=WO(N)
      BS(N-I1)=BO(N-I1)
1     CONTINUE
      N1=N2+1
      N2=N2+ID
      I1=I1+ID
      IK=IK+1
      T=.0
      DDT=20.
C
C      CALCULATION OF DEFORMED AREAS
2     DO 16 IJ=1,2
      T=T+DDT
C
C
      DO 4 J=1,ID
      IF (IJ.EQ.1) GO TO 3
      A(J)=AA(J)
3     AA(J)=(AO(J)**M1-T*M1*(PS)**M1)**M
4     CONTINUE
C
C      CALCULATION OF DEFORMED LENGTH
      U=.0
      STRT=.0
      DO 7 I=1,ID1
      AM=A(I)+A(I+1)+SQRT(A(I)*A(I+1))
      AF=AA(I)+AA(I+1)+SQRT(AA(I)*AA(I+1))
      IF (IJ.EQ.1) GO TO 5
      AU(I)=(AM/AF-1.)*AXU(I)
      AXU(I)=AXU(I)+AU(I)
      GO TO 6
5     AU(I)=(AM/AF-1.)*AX
      AXU(I)=AX+AU(I)
      STR(I)=(AU(I)/AXU(I))/DDT
6     U=U+AU(I)
      STRT=STRT+STR(I)
      STRR(I)=STR(I)/STR(1)
7     CONTINUE
C
      IF (IJ.EQ.1) GO TO 8
      L=L+U
      GO TO 9
8     L=LO+U
9     E=((L-LO)*100.)/LO
      STL=ALOG(L/LO)
      ASR=STRT/FLOAT(ID1)
C
C      CALCULATION OF DEFORMED WIDTH AND THICKNESS
      WWA=.0
      AAS=0.
      DO 10 J=1,ID
      WW(J)=WS(J)*EXP(-.5*ALOG(AO(J)/AA(J)))
```

```
      BB(J)=BS(J)*EXP(-.5*ALOG(AO(J)/AA(J)))
C
      AAS=AAS+AA(J)
      WWA=WWA+WW(J)
10    CONTINUE
      WWAV=WWA/FLOAT(ID)
      AASAV=AAS/FLOAT(ID)
      AXT(1)=.0
C
      DO 11 I=2,ID
      AXT(I)=AXT(I-1)+AXU(I-1)
      AXTR(I)=AXT(I)/L
11    CONTINUE
      IF (IJ.EQ.1) GO TO 12
      GO TO 13
12    WRITE (6,24)
      WRITE (6,18) (W(N),N=1,ID)
C
      II=1
13    ENDEX=FLOAT(II)
      IF (E.GE.90.) GO TO 14
      TI=T-4.9999*ENDEX
      IF (TI.GE.0.) GO TO 14
      GO TO 15
14    WRITE (6,17) T
      II=II+1
      WRITE (6,29)
      WRITE (6,22)
      WRITE (6,18) (AA(N),N=1,ID)
      WRITE (6,18) (WW(N),N=1,ID)
      WRITE (6,18) (BB(N),N=1,ID)
      WRITE (6,31)
      WRITE (6,18) (AXT(I),I=2,ID)
      WRITE (6,18) (AXTR(I),I=2,ID)
C
C      CALCULATION OF NON UNIFORMITY PARAMETERS
      DIFD(1)=(ABS((WW(1)-WW(6))/WWAV))*100.
      DIFD(2)=(ABS((WW(3)-WW(5))/WWAV))*100.
      DIFDA(1)=(ABS(AA(1)-AA(6))/AASAV)*100.
      DIFDA(2)=(ABS(AA(3)-AA(5))/AASAV)*100.
      WRITE (6,25) (DIFD(I),I=1,2)
      WRITE (6,26) (DIFDA(I),I=1,2)
C
C      CALCULATION OF DEFORMED UNIFORM TEST-PIECE
      AAS=AA(1)
      STS=(A(1)-AA(1))/(DDT*AA(1))
      LS=BS(1)*WS(1)*LO/AAS
      ES=(100.*(LS-LO))/LO
C
      WRITE (6,19) U,L,E
      WRITE (6,23) STL,ASR
C
```

```
      WRITE (6,28)
      WRITE (6,30) WW(1),LS,ES,STS
      WRITE (6,18) (STRR(I),I=1,ID1)
15    IF (E.GT.200.AND.N2.EQ.12) STOP
      IF (E.GE.60.) DDT=5.
      IF (E.GE.70.) DDT=2.5
16    CONTINUE
      IF (T.LT.600) GO TO 2
      STOP
C
17    FORMAT (////60X,*TIME=*,F9.3,*SECOND*///)
18    FORMAT (/5X,8F12.5/)
19    FORMAT (//2X,*STAGE EXTENSION=*,F8.6,4X,*TOTAL LENGTH=
     1 *,F10.6,4X,*ELONGATION PERCENTAGE=*,F10.6/)
20    FORMAT (1H1)
21    FORMAT (50X,*SPECIMEN NUMBER*,I2///)
22    FORMAT (/5X,* WIDTHES,THICK. AND AREAS  OF THE LOADED
     1 SPECIMEN AT.25 INCH*/)
23    FORMAT (2X,*LOGARITHMIC STRAIN=*,F8.6,5X,*AVERAGE
     1STRAIN RATE=*,F8.6//)
24    FORMAT (/5X,* WIDTHES  OF THE UNLOADED SPECIMEN AT.25
     1  INCH STEP*/)
25    FORMAT (/10X,*NON-UNIFORMITY=*,F8.4,5X,*NON-UNIFORMITY=*
     1 ,F8.4/)
26    FORMAT (/10X,*AREA NON-UNIF=*,F8.4,10X,*AREA NON-UNIF=*
     1,F8.4/)
27    FORMAT (F5.4)
28    FORMAT (/2X,*STRAIGHT SPECIMEN *)
29    FORMAT (2X,*TAPERED SPECIMEN */)
30    FORMAT (//2X,*WIDTH =*,F12.10,5X,*TOTAL LENGTH=*,F10.6,
     1*ELONGATION  PERCENTAGE=*,F12.6,3X,*STRAIN RATE=*,F8.6/)
31    FORMAT (/10X,*DEFORMED LENGTH OF ELEMENTES*/)
      END
```

APPENDIX A-2

```
C        INFLATION OF A THIN ECCENTRIC TUBE MADE OF SUPERPLASTIC
C        MATERIAL WITH CONSTANT INTERNAL PRESSURE
C
C
C
C         NOMENCLATURE
C        K,M SUPERPLASTIC MATERIAL PARAMETERS
C        TH ANGULAR DISPLASEMENT
C        UNIF NONUNIFORMITY PARAMETER OF AREA
C        PO INTERNAL PRESSURE
C        RI UNDEFORMED INSIDE RADIUS
C        RMO,RM UNDEFORMED AND DEFORMED RADII RESPECTIVELY
C        D,DD UNDEFORMED AND DEFORMED THICKNESS REPECTIVELY
C        ST STRAIN RATE
C        UNIF THICKNESS NONUNIFORMITY PARAMETER
C        TIME
C
      REAL K,M,M1,V(2),RDTH(18,2),ST(19),STR(19)
      DIMENSION RM(2,2), D(19,2), DD(19,2), DTHO(18,2), DTH(18,2)
C
C
C        CONSTANTS
      PI=4.*ATAN(1.)
      K=10000.
      M=.5
      M1=1./M
      EPS=.0001
      RMO=2.
      EC=.005
      RI=1.95
      T=.0
      VO=PI
      ERROR=.0005
      DT=25.
      PO=25.
C
C        CALCULATION OF DEFORMED THICKNESS (USING A RUNGE KUTTA
C        NUMERCIAL SOLUTION)
      DO 1 I=1,18
      DTHO(I,1)=PI/18.
1     CONTINUE
2     DO 17 IJ=1,2
      T=T+DT
      DO 13 IK=1,2
      IF (IK.EQ.1) RM(IK,IJ)=RMO+.002
      JK=1
3     DO 7 J=1,19
      THETA=J-1
```

```
      THETA=THETA*PI/18.
      IF (IK.EQ.2.AND.JK.EQ.1) RM(IK,IJ)=RMO+.06
      IF (T.EQ.25..AND.JK.GT.1) GO TO 6
      IF (T.GT.25..AND.IJ.EQ.1) GO TO 4
      IF (T.GT.25..AND.IJ.EQ.2) GO TO 5
      C1=-4.*RMO-2.*EC*(COS(THETA))
      C2=4.*(RMO*EC*COS(THETA)+RMO**2+(EC**2/4.)-RI**2)
      D(J,IJ)=(-C1-SQRT(C1**2-4.*C2))/2.
      GO TO 6
4     D(J,IJ)=DD(J,(IJ+1))
      GO TO 6
5     D(J,IJ)=DD(J,(IJ-1))
6     DDT=-DT*SQRT(3.)/2.
      PS=PO*RM(IK,IJ)/2./K
      RK1=DDT*(PS/D(J,IJ))**M1*D(J,IJ)
      DS1=D(J,IJ)+RK1
      RK2=DDT*(PS/DS1)**M1*DS1
      DS2=D(J,IJ)+RK2
      RK3=DDT*(PS/DS2)**M1*DS2
      DS3=D(J,IJ)+RK1/2.
      RK4=DDT*(PS/DS3)**M1*DS3
      RK5=(RK1+RK3)/2.
      RK=RK4+(RK5-RK4)/3.
      DD(J,IJ)=D(J,IJ)+RK
7     CONTINUE
C
C
C      CALCULATION OF DEFORMED MEAN RADIUS
      TH=.0
      DO 12 I=1,18
      IF (T.EQ.25.) RMS=2.
      IF (T.EQ.25.) GO TO 8
      IF (IK.EQ.1.AND.IJ.EQ.2) RMS=RM((IK+1),(IJ-1))
      IF (IK.EQ.1.AND.IJ.EQ.2) RMS=RM((IK+1),(IJ-1))
      IF (IK.EQ.2.AND.IJ.EQ.2) RMS=RM(IK,(IJ-1))
      IF (IK.EQ. .AND.IJ.EQ.1) RMS=RM(IK,(IJ+1))
      IF (T.GT.25..AND.IJ.EQ.2) GO TO 9
      IF (T.GT.25..AND.IJ.EQ.1) GC TO 10
C
8     DTH(I,IJ)=(D(I,IJ)+D((I+1),IJ))*RMS*DTHO(I,IJ)/(DD(I,IJ)
     1+DD((I+1),IJ))/RM(IK,IJ)
      GO TO 11
      DTH(I,IJ)=(D(I,(IJ-1))+D((I+1),(IJ-1)))*RMS*DTH(I,(IJ-1))
     1/(DD(I,(IJ-1))+DD((I+1),(IJ-1)))/RM(IK,IJ)
      GO TO 11
10    DTH(I,IJ)=(D(I,(IJ+1))+D((I+1),(IJ+1)))*RMS*DTH(I,(IJ+1))
     1/(DD(I,(IJ+1))+DD((I+1),(IJ+1)))/RM(IK,IJ)
11    TH=DTH(I,IJ)+TH
      RDTH(I,IJ)=TH*180./PI
12    CONTINUE
C
      V(IK)=TH
```

```
      IF (IK.EQ.1) GO TO 13
      RM(IK,IJ)=RM(2,IJ)-(RM(2,IJ)-RM(1,IJ))*(V(2)-VO)/(V(2)-V(1))
      RMO=RM(IK,IJ)
      DIFV=ABS((V(IK)-VO)/VO)
      JK=JK+1
      IF (DIFV.GT.ERROR) GO TO 3
13    CONTINUE
C
C      CALCULATION OF NONUNIFORMITY PARAMETER AND
C       AVERAGE STRAIN RATE
      DDA=.0
      STA=.0
      DO 14 I=1,19
      ST(I)=(D(I,IJ)-DD(I,IJ))/DT/DD(I,IJ)
      STA=ST(I)+STA
      STR(I)=ST(I)/ST(1)
      DDA=DD(I,IJ)+DDA
14    CONTINUE
      DDAV=DDA/19.
      STAV=STA/19.
      UNIF=((DD(1,IJ)-DD(19,IJ))/DDAV)*100.
C
      IF (T.EQ.25.) GO TO 15
      GO TO 16
15    WRITE (6,25)
      WRITE (6,21) (D(N,IJ),N=1,19)
16    WRITE (6,18) T
      WRITE (6,23)
      WRITE (6,19) (DD(N,IJ),N=1,19)
      WRITE (6,27) RM(2,IJ),STAV,UNIF
      WRITE (6,22)
      WRITE (6,20) (RDTH(I,IJ),I=1,18)
      WRITE (6,26)
      WRITE (6,24) (STR(I),I=1,19)
17    CONTINUE
C
      IT=T
      IF (IT.GE.150) DT=10.
      IF (T.LT.600.) GO TO 2
      STOP
C
18    FORMAT (///60X,*TIME=*,F9.3,*SECOND*/)
19    FORMAT (10X,6F18.10)
20    FORMAT (10X,6F18.4)
21    FORMAT (10X,6F18.10)
22    FORMAT (//5X,*RELATIVE ANGULAR DISPLACEMENT OF THE*,
     1*DEFORMED TUBE */)
23    FORMAT (/5X,*THICKNESS OF THE LOADED TUBE*/)
24    FORMAT (10X,6F18.10)
25    FORMAT (/5X,*THICKNESS OF THE UNLOADED TUBE*/)
26    FORMAT (//5X,*RELATIVE THICK. STRAIN RATE*/)
27    FORMAT (//3X,* DEFORMED RADIUS=*,F7.3,2X,*AVER.THICK.*,
     1*STRAIN RATE=*,F7.3,3X,*NON-UNIF.PERCENTAGE=*,F6.3/)
      END
```

APPENDIX B

This appendix contains the experimental data obtained from testing tapered tensile-strips under constant load. The material of the test-pieces was superplastic in as-received condition [4.2]. All tests were conducted at a temperature of 200°C.

DIMENSIONS OF UNDEFORMED SPECIMEN				DIMENSIONS OF DEFORMED SPECIMEN				
Width w_o	Thickness s_o	Area A_o	Distance between marked stations	Width w	Thickness s	Area A	Distance between marked stations	$\frac{\ln(w/w_o)}{\ln(s/s_o)}$
			Test-Piece No. 1					
.3946		.0371		.3346	.0733	.0245	-----	-----
.3906		.0367		.3228	.0710	.0229	.3600	.6785
.3867		.0363		.3160	.0704	.0222	.4000	.6984
.3825		.0360		.3086	.0689	.0212	.4000	.6912
.3795	.0940	.0356	.2500	.3021	.0679	.0205	.4400	.7012
.3753		.0352		.2940	.0671	.0197	.4600	.7242
.3738		.0351		.2903	.0663	.0192	.4500	.7241
.3716		.0349		.2883	.0663	.0191	.4500	.7270
.3706		.0348		-----	-----	-----	-----	-----
			Test-Piece No. 2					
.4011		.0377		.3099	.0628	.0194	-----	.6379
.3988		.0375		.3054	.0624	.0190	.4900	.6496
.3970		.0375		.3017	.0619	.0186	.4900	.6554
.3946		.0371		.2948	.0603	.0177	.5000	.6552
.3932	.0941	.0370	.2500	.2898	.0595	.0172	.5200	.6656
.3911		.368		.2859	.0592	.0169	.5500	.6761
.3904		.0367		.2837	.0584	.0165	.5500	.6693
.3899		.0366		.2840	.0589	.0167	-----	.6764
.3894		.0366		.2865	.0592	.0169	-----	.6621

Dimensions in inches

DIMENSIONS OF UNDEFORMED SPECIMEN				DIMENSIONS OF DEFORMED SPECIMEN				
Width w_o	Thickness s_o	Area A_o	Distance between marked stations	Width w	Thickness s	Area A	Distance between marked stations	$\frac{\ell n(w/w_o)}{\ell n(s/s_o)}$
			Test-Piece No. 3					
.3996		.0378		.3461	.0761	.0765	-----	.6775
.3936		.0372		.3395	.0762	.0258	.3500	.6801
.3895		.0368		.3322	.0754	.0250	.3400	,6982
.3850		.0364		.3261	.0742	.0241	.3600	.6806
.3809	.0947	.0360	.2500	.3196	.0731	.0233	.4000	.6775
.3768		.0356		.3131	.0724	.0226	.3000	.6898
.3737		.0353		.3084	.0718	.0221	.3950	.6936
.3708		.0351		.3031	.0703	.0213	.4000	.6765
.3676		.0348		.2991	.0690	.2063	-----	-----
			Test-Piece No. 4					
.3872		.0364		.3492	.0812	.0283	-----	.7056
.3841		.0361		.3470	.0812	.0281	.3200	.6938
.3822		.0359		.3444	.0811	.0279	.3200	.7056
.3798		.0357		.3419	.0809	.0276	.3220	.7004
.3780	.0940	.0355	.2500	.3401	.0804	.0273	.3230	.6760
.3765		.0354		.3370	.0801	.0269	.3260	.6927
.3750		.0352		.3350	.0797	.0269	.3270	.6710
.3740		.0351		.3837	.0793	.0264	.3270	.6710
.3720		.0350		.3314	.0792	.0262	.3350	.6750

Dimensions in inches

DIMENSIONS OF UNDEFORMED SPECIMEN				DIMENSIONS OF DEFORMED SPECIMEN				
Width w_o	Thickness s_o	Area A_o	Distance between marked stations	Width w	Thickness s	Area A	Distance between marked stations	$\frac{\ln(w/w_o)}{\ln(s/s_o)}$
			Test-Piece No.5					
.3892		.0363		.3342	.0750	.0250	-----	.6944
.3864		.0360		.3285	.0737	.0242	.3600	.6852
.3840		.0358		.3225	.0725	.0233	.3770	.6890
.3815		.0356		.3182	.0718	.0228	.3820	.6898
.3795	.0934	.0354	.2500	.3139	.0704	.0221	.3920	.6713
.3777		.0352		.3084	.0698	.0215	.4000	.6959
.3750		.0350		.3035	.0689	.0209	.420	.6953
.3731		.0348		.2984	.0676	.0201	.4209	.6910
.3710		.0346		.2972	.0673	.0200	.4345	.6767
			Test-Piece No.6					
.4020		.0380		.3176	.0697	.0221	-----	.7716
.3951		.0373		.3091	.0684	.0211	.4500	.7570
.3916		.0370		.3031	.0672	.0203	.4400	.7490
.3873		.0366		.2947	.0656	.0193	.4700	.7966
.3839	.0946	.0362	.2500	.2835	.0634	.0179	.5200	.7532
.3793		.0356		.2755	.0620	.0170	.5250	.7580
.3754		.0355		.2647	.0586	.0155	.5600	.7290
.3716		.0351		.2547	.0575	.0146	.5950	.7590
.3670		.0347		.2467	.0559	.0138	-----	.7549

Dimensions in inches

DIMENSIONS OF UNDEFORMED SPECIMEN				DIMENSIONS OF DEFORMED SPECIMEN				
Width w_o	Thickness s_o	Area A_o	Distance between marked stations	Width w	Thickness s	Area A	Distance between marked stations	$\frac{\ln(w/w_o)}{\ln(s/s_o)}$
			Test-Piece No. 7					
.3954		.0370		.3247	.0712	.0231	-----	.7203
.3914		.0366		.3151	.0691	.0217	.3900	.7143
.3876		.0363		.3058	.0672	.0205	.4350	.7151
.3839		.0360		.2971	.0651	.0193	.4500	.7059
.3799	.0936	.0355	.2500	.2887	.0632	.0182	.4800	.6990
.3768		.0352		.2809	.0611	.0171	.5200	.6890
.3744		.0350		.2760	.0598	.0165	.5200	.6808
.3722		.0348		.2733	.0591	.0161	.5350	.6714
.3689		.0345		-----	-----	-----	-----	-----
			Test-Piece No. 8					
.4013		.0380		.3510	.0793	.0278	-----	.7546
.3969		.0375		.3437	.0777	.0267	.3400	.7284
.3903		.0369		.3340	.0763	.0255	.3500	.7210
.3850		.0364		.3240	.0751	.0243	.3600	.7438
.3794	.0947	.0359	.2500	.3143	.0732	.0230	.3800	.7310
.3737		.0353		.3052	.0714	.0218	.4100	.7170
.3684		.0348		.2956	.0703	.0208	.4150	.7389
.3632		.0343		.2878	.0681	.0195	.4300	.7057
.3581		.0339		.2825	.0670	.0189	.4400	.6353

Dimensions in inches

DIMENSIONS OF UNDEFORMED SPECIMEN				DIMENSIONS OF DEFORMED SPECIMEN				
Width w_o	Thickness s_o	Area A_o	Distance between marked stations	Width w	Thickness s	Area A	Distance between marked stations	$\frac{\ell n(w/w_o)}{\ell n\ (s/s_o)}$
			Test-Piece No. 9					
.3982		.0373		.3077	.0645	.0198	-----	.6899
.3960		.0371		.3034	.0635	.0192	.4690	.6828
.3933		.0369		.2873	.0624	.0185	.4808	.6865
.3909		.0366		.2887	.0604	.0174	.4992	.6885
.3887	.0938	.0364	.2500	.2770	.0572	.0158	.5533	.6849
.3862		.0362		.2649	.0541	.0143	.5946	.6850
.3846		.0360		.2550	.0514	.0131	.6510	.7160
.8828		.0359		.2394	.0480	.0115	.7186	.7006
.3791		.0355		.2227	.0435	.0096	.8500	.7958
			Test-Piece No. 10					
.4013		.0380		.3343	.0726	.0242	-----	.6874
.3969		.0375		.3258	.0714	.0232	.4100	.6989
.3903		.0369		.3144	.0694	.0218	.4300	.6957
.3850		.0364		.3208	.0671	.0215	.4600	.5295
.3794	.0947	.0359	.2500	.2903	.0644	.0186	.5100	.6941
.3737		.0353		.2780	.0618	.0171	.5300	.6931
.3684		.0348		.2640	.0588	.0155	.5400	.6992
.3632		.0349		.2520	.0560	.0141	.5700	.6957
.3581		.0339		.2456	.0543	.0133	.6400	.6780

Dimensions in inches

DIMENSIONS OF UNDEFORMED SPECIMEN				DIMENSIONS OF DEFORMED SPECIMEN				
Width w_o	Thickness s_o	Area A_o	Distance between marked stations	Width w	Thickness s	Area A	Distance between marked stations	$\frac{\ell n(w/w_o)}{\ell n(s/s_o)}$
			Test-Piece No. 11					
.3899		.03665		.3199	.0701	.0223	-----	.6746
.3869		.03637		.3140	.0691	.0216	.4100	.6783
.3844		.0361		.3100	.0687	.0212	.4150	.6860
.3818		.0358		.3080	.0680	.0209	.4200	.6635
.3796	.0940	.0357	.2500	.3050	.0674	.0205	.4250	.6577
.3770		.0354		.3017	.0670	.0202	.4300	.6580
.3753		.0352		.2989	.0660	.0197	.435	.6436
.3740		.0351		.2913	.0643	.0187	.4400	.6581
.3716		.0349		.2852	.0629	.0179	.4742	.6587
			Test-Piece No. 12					
.3982		.0373		.3450	.0774	.0267	-----	.7462
.3960		.0371		.3424	.0769	.0263	.3250	.7320
.3933		.0369		.3390	.0764	.0259	.3515	.7240
.3909		.0366		.3341	.0753	.0251	.3590	.7147
.3881	.0938	.0364	.2500	.3285	.0738	.0242	.3707	.7017
.3862		.0362		.3218	.0724	.0233	.3750	.7044
.3846		.0360		.3169	.0713	.0226	.3920	.7059
.3828		.0359		.3107	.0697	.0216	.4005	.7027
.3791		.0355		.3030	.0681	.0206	.4230	.6997

Dimensions in inches

DIMENSIONS OF UNDEFORMED SPECIMEN				DIMENSIONS OF DEFORMED SPECIMEN				
Width w_o	Thickness s_o	Area A_o	Distance between marked stations	Width w	Thickness s	Area A	Distance between marked stations	$\frac{\ln(w/w_o)}{\ln(s/s_o)}$
			Test-Piece No. 13					
.3982		.0373		.3022	.0629	.0190	-----	.6903
.3960		.03714		.2977	.0617	.0183	.5000	.6811
.3933		.369		.2913	.0601	.0175	.5100	.6744
.3909		.0366		.2789	.0574	.0160	.5400	.6873
.3887	.0938	.0364	.2500	.2650	.0531	.0140	.6000	.6732
.3862		.0362		.2500	.0489	.0122	.6700	.6676
.3846		.0360		.2360	.0456	.0107	.7650	.6771
.3828		.0359		.2140	.0400	.0085	.9000	.6182
.3791		.0355		-----	-----	-----	-----	-----
			Test-Piece No. 14					
.4019		.0380		.3265	.0714	.0233	-----	.7384
.3957		.0374		.3182	.0699	.0223	.4150	.7203
.3902		.0369		.3066	.0679	.0208	.4300	.7270
.3845		.0363		.2951	.0654	.0193	.4600	.7168
.3790	.0946	.0358	.2500	.2844	.0633	.0180	.4800	.7147
.3725		.0352		.2709	.0604	.0164	.5400	.7698
.3674		.0347		.2580	.0574	.0148	.5800	.7075
.3623		.0342		.2451	.0544	.0133	.5800	.70632
.3565		.0337		.2314	.0504	.0116	.6900	.6863

Dimensions in inches

APPENDIX C

In plane strain deformation of an isotropic rigid perfectly plastic material, the stresses are given by the well known Hencky relations [6.19],

$$P + 2k\,\psi = C_1$$

$$P - 2k\,\psi = C_2 \qquad \text{(C-1)}$$

These equations are equivalent to the equilibrium equations for a material obeying Von-Mises yield criterion. The solution of the problem as given by equations (C-1) and the boundary conditions are often represented by a network of orthogonal lines known as α and β slip-lines. Figure C-1 shows the stresses on a small curvilinear element bounded by slip-lines. It is essential to distinguish between the two families of slip-lines, and the convention adopted here is that when the α - and β-lines form a right-handed co-ordinate system of axes, then the line of action of the algebraically greatest principal stress, lies in the first and third quadrants. The anti-clockwise rotation, ψ, of the α-line from the chosen x-direction is taken as positive.

In some problems there will be sufficient boundary conditions involving only the stresses, to give a solution. Such problems are known as "statically determinate" and the velocities can be calculated afterwards. In other problems the boundary conditions will involve both stresses and velocities and a solution can be only obtained by considering the stress and the velocity equations (Geiringer equations [6.19]), together.

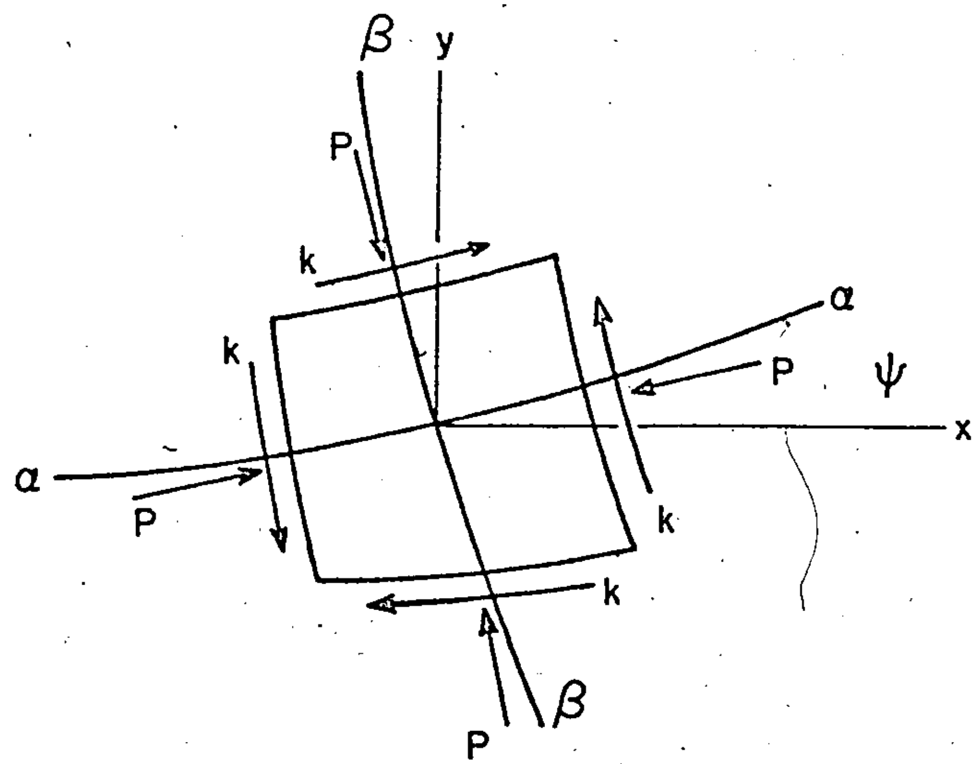

Fig. C.1 Stresses on a small curvilinear element of a slip-line field.

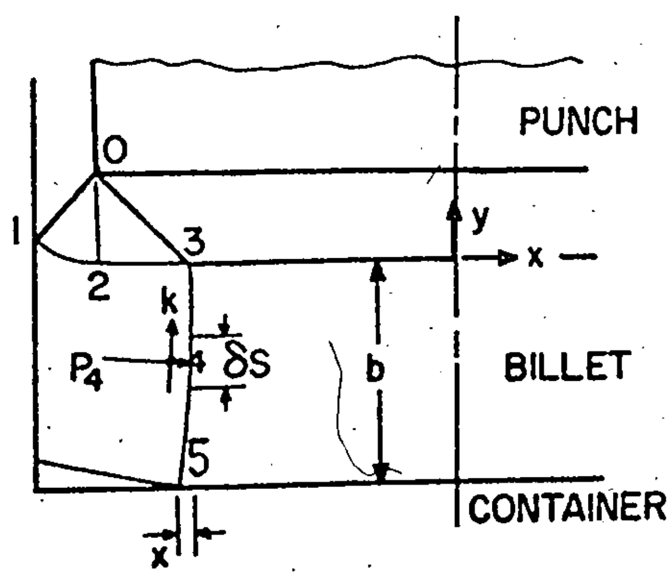

Fig. C.2 Schematic diagram for the calculation of the average pressure acting on a slip-line.

In the present analysis, the problem is statically determinate and the slip-line field solutions are obtained and shown in Figures.

A schematic diagram of a slip-line field solution is shown in Figure C·2. The average non-dimensional lateral pressure $\bar{P}_s/2k$ which acts on the slip-line 3-5 is obtained as follows.

Let δ_s be an elemental length of the slip-line 3-5; the stresses on δ_s are shown in Figure C·2. The horizontal force on δ_s is

$$\delta F = (k \sin \psi + P_4 \cos \psi) \qquad \text{(C-2)}$$

and thus $\quad F = k \int \sin \psi \, ds + P_4 \int \cos \psi \, ds \qquad$ (C-3)

or $\quad F = k \int dx + \int P_4 \, dy$ over the α-line 3-5.

Now $\quad P_4 = P_3 + 2k \psi \qquad$ (C-4)

where ψ is the magnitude of the rotation from 3 to 4 and hence

$$F = kx + 2k \left(\frac{P_3}{2k}\right) \int dy + 2k \int \psi \, dy \qquad \text{(C-5)}$$

therefore $\quad \dfrac{\bar{P}_s}{2k} = \dfrac{(F/h)}{2k} = (2 I + x)/2h + (P_3 / 2k) \qquad$ (C-6)

where $\quad I = \Sigma\psi \, \Delta y \quad$ which can be evaluated using Figure C·2. The dimensions x and h can be measured directly from the slip-line field solution.

In order to calculate the pressure P_3 in equation (C-6), Hencky equation (C-1) are employed. Since the total force on the extruded material above the α-slip line 0-1 is zero, it can be shown that $P_{0-1} = k$. In moving from point 1 to point 2 on β slip line, a positive rotation of angle; say $\frac{\pi}{4}$ is described, hence from equation (C-1)

$$P_{2-3} = P_{0-1} + 2k \left(\frac{\pi}{4} \right)$$

Therefore the pressure at point 3 is given by

$$\frac{P_3}{2k} = \left(\frac{1}{2} + \frac{\pi}{4} \right) = 1.285 \qquad \text{(C-7)}$$

The mean vertical pressure acting on the punch noze 0-3 is easily calculated from the equilibrium of the metal triangle 0-2-3.